CONTINUOUS LOW DOSE RATE IRRADIATION OF THE RAT BRAIN

Jitesh Madhoo

Thesis presented for the Degree of

DOCTOR OF PHILOSOPHY

in the Department of Radiation Oncology

UNIVERSITY OF CAPE TOWN

1999

To Ba and my dearest Anjali

and

to the memory of Bapujee

CONTENTS

ABSTRACT

The reported median survival time for patients who are diagnosed with high grade astrocytomas and who undergo postoperative radiotherapy is of the order of 24 to 40 weeks. The course of radiotherapy administered to these patients takes up a considerable portion of their expected survival time. Therefore, any means of reducing the treatment time may contribute to an enhanced quality of life for these patients.

A potentially useful method for the reduction of the treatment time may be achieved with the use of continuous low dose rate external beam radiotherapy, where the treatment is administered over a 12 to 24 hour period. A relationship between fractionated and continuous low dose rate irradiation has been reported for skin, however, no such relationship has been reported for the brain. Low dose rate protocols that are equivalent in effect to fractionated (conventional) protocols can be derived using the linear quadratic theory, provided that quantitative radiobiological data for normal tissue (brain) is known. Thus, the aim of the current study is to test the radiation tolerance of the rat brain to low dose rate and fractionated radiation in order to establish the values for the parameters of the linear quadratic model.

Male Wag/Rij rats aged between six and eight weeks and weighing between 180 and 210 grams were used in these experiments. All irradiations were performed using an Eldorado 6 ^{60}Co unit irradiating vertically downwards at an SSD of 80 cm and a field size of 40 cm by 40 cm. The rats were positioned on their sides in the centre of the radiation field under 8 cm thick lead shielding blocks with the appropriate cut-outs. As only the area between the eye and the ear was to be irradiated, positioning of the rats below the cut-outs in the lead shielding blocks was critical. However, consistency in positioning was achieved with the use of perspex restraining jigs. In this manner, two rats were irradiated simultaneously. The dose distribution across the cut-outs in the lead shielding blocks was found to be uniform using film densitometry. The dosimetry to check the dose rates and to calculate the required thickness of the lead plates to provide the low dose rates for irradiations was performed using a Farmer 2570 secondary standard dosemeter. For the low dose rate experiments, a continuous inhalation anaesthesia method, using Halothane and oxygen, was used. For the fractionated experiments, a custom made anaesthetic bag, also using Halothane and oxygen, was used. The radiation protocols that were used in the current study were, a) 10 fractions in 12 days, with total doses of 40, 47, 54, 60, 64, 68 and 72 Gy, b) a low dose rate of 0.04 Gy.min^{-1} with total doses of 31, 35, 39, 41, 47, 57 and 65 Gy, c) a low dose rate of 0.05 Gy.min^{-1} with total doses of 30, 34, 37, 40, 47, 55 and 60 Gy, and d) a low dose rate of 0.07 Gy.min^{-1} with total dose of 30, 33, 36, 38, 44, 48 and 57 Gy. All rats were killed

after an observation period of one year and perfused with 10% phosphate buffered formalin. The brains of the rats were removed and prepared for histology. Coronal sections of the rat brains cut at the level of the optic chiasma were prepared and stained with either luxol blue cresyl violet or luxol blue haematoxylin and eosin. A limited number of sections were stained with martius scarlet blue for fibrin, von Kossa's stain for calcium and glial fibrillary acidic protein stain for gliosis. The histological areas of the rat brain that were scored for reactions to radiation included the *alveus hippocampi*, the *capsula interna*, the *capsula interna pars retrolenticularis*, the choroid plexus, the *cingulum*, the ependymal cells, the *fasiculus medialis prosencephali*, the *fimbria hippocampus*, the *gyrus dentatus*, the *hippocampus*, the *nucleus lateralis*, the *nucleus lateralis habenulae*, the *nucleus lateralis thalami*, the *radiatio corporis callosi*, the *stria terminalis*, the *sulcus hippocampi*, the *truncus corporis callosi* and the *ventriculus lateralis*. Dose response curves were constructed using the incidence data by probit analysis and the ED_{50} values were obtained. The parameters of the linear quadratic model using the incomplete repair model of Thames (1985) were obtained from the ED_{50} values using Dale's (1985) graphical method.

Histological examination of the brain tissue sections indicated radiation induced changes in all the structures examined with the possible exception of the *nucleus lateralis* and the *fasiculus medialis prosencephali*. The nature of the changes were similar for each of the radiation schedules used. However, the incidence of a particular change was variable in each dose group within one dose rate group and between dose rate schedules. The major histological changes that were observed included necrosis, vessel dilation, oedema, the presence of free iron, red blood cell congested vessels, haemorrhage, the presence of histiocytes and the presence of free calcium. White matter necrosis was the most severe late effect of radiation that was observed, and the *fimbria hippocampus* was the most compromised area in the rat brain. Less common changes that were observed included disruption of the myelin fibres, pyknotic nuclei and hyalinisation of the choroid plexus. Only the data from the dose response curves for necrosis of the *fimbria hippocampus* and the *radiatio corporis callosi* could be used to determine the radiobiological parameters of the linear quadratic model. The α/β ratios for necrosis of the the *fimbria hippocampus* and the *radiatio corporis callosi* for the protracted irradiation yielded values of 6.2 and 54.5 Gy respectively. When the biologically equivalent doses for necrosis from the low dose rate studies were set equal to those for the fractionated study, the relationship held true only when the α/β ratios in the fractionated protocol were 4.1 Gy and 23.2 Gy.

The current study indicates that the prospect of achieving a better quality of life for patients with high grade astrocytomas by alteration of the conventional (fractionated) radiation protocols to that of a low dose rate protocol does not appear to be a

straightforward matter. This is evident from the finding that the different α/β ratios that were derived for the FH and the RCC in the rats may suggest that the ratios are radiation schedule dependent. This discrepancy in the α/β ratios may also suggest that it may not be possible to predict low dose rate protocols for brain irradiation which are equivalent to fractionated protocols using the linear quadratic model.

ACKNOWLEDGEMENTS

I wish to express my sincere gratitude to the following people who have assisted me during the course of this study:

- Professor V. Levin, for initiating this project.
- My supervisors, Professor G. Blekkenhorst, for being more than a supervisor by giving me much professional, technical, psychological support and encouragement, and Dr R. Bowen, for placing the resources of his department at my disposal.
- Mrs. P. Dowman, who taught me the histological skills required to perform the histology for this project.
- Professor M. Henneberg and Mrs L. Downing, for permitting me to use the postgraduate histology laboratory to cut and prepare my histological sections.
- Mrs A. Smith, Mrs E. Norval, Ms I. de Faria Leal and Ms L. Thompson, for their unconditional assistance with staining of the histological slides.
- Dr A. Hunter, Dr A. Hendrikse and Mrs. F. Rahbeeni for their criticisms, suggestions and advice.
- Dr S. Verhaart, for assistance with the interpretation of the various histological reactions, in addition to Professor K. Cooper, Dr. P. King Dr C. Wright and Dr M. Sur.
- The staff of the Medical Physics department of Groote Schuur Hospital for their assistance with the dosimetry required for this study.
- Mr S. Sokanyile for assistance with the care and maintenance of the rats.
- Mr M. Lanesman and Mr G. Hall for photographing and developing the numerous photomicrographs used in this thesis.

My sincere thanks to Ms J. Ambral for keeping Anjali on the other side of the line while this thesis was being typed.

Finally, I would like to thank Roshan for his encouragement and support and Norma for her forbearance.

ABBREVIATIONS

AH	-	*alveus hippocampi*
C	-	*cingulum*
Ca	-	Calcium deposits
CAI	-	*capsula interna*
CAIR	-	*capsula interna pars retrolenticularis*
CNS	-	Central nervous system
CP	-	Choroid plexus
CRE	-	Cumulative radiation effect
D	-	Disruption of fibres
DV	-	Dilated vessels
EC	-	Ependymal cells
ED_{50}	-	Effective dose to produce an effect in 50% of the animals
Fe	-	Iron deposits
FH	-	*fimbria hippocampus*
FMP	-	*fasiculus medialis prosencephali*
GD	-	*gyrus dentatus*
GFAP	-	Glial fibrillary acidic protein
Gy	-	Gray
H	-	Hyalinisation
HA	-	Haemorrhage
HI	-	*hippocampus*
LBCR	-	Luxol blue cresyl violet
LBHE	-	Luxol blue haematoxylin and eosin
LQ	-	Linear quadratic
MSB	-	Martius scarlet blue
N	-	Necrosis
NL	-	*nucleus lateralis*

NLH	-	*nucleus lateralis habenulae*
NLT	-	*nucleus lateralis thalami*
NSD	-	Nominal standard dose
O	-	Oedema
P	-	Pyknotic nuclei
PT	-	Partial tolerance
RBC	-	Red blood cell congested vessels
RCC	-	*radiatio corporis callosi*
SE	-	Standard error
SH	-	*sulcus hippocampi*
SSD	-	Source to skin distance
ST	-	*stria terminalis*
TBV	-	Thickened blood vessel wall
TCC	-	*truncus corporis callosi*
TDF	-	Time-dose-fractionation
V	-	Vacuolation
VL	-	*ventriculus lateralis*

CHAPTER 1:

INTRODUCTION: BRAIN TUMOURS AND RADIOTHERAPY

Patients who present with a high-grade astrocytoma may display any combination of the following clinical symptoms and signs, namely, changes in personality, headache, gastrointestinal disorders such as vomiting and nausea, epileptic seizures and changes in psychomotor functions [Levin et al., 1997; Nelson et al., 1993]. These symptoms and signs may be produced primarily by two mechanisms, a) the 'mass effect' and increased intracranial pressure, which is due to either the tumour or the tumour and the surrounding oedema, and b) by infiltration, destruction and compression of the normal brain tissue [Levin et al., 1997; Nelson et al., 1993].

The diagnostic tests that these patients may be subjected to could include any of the following, a) neurologic and physical examinations, b) funduscopic examination, c) visual field examination, c) magnetic resonance imaging, d) computerised tomography scanning, e) skull x-rays, f) electroencephalograms, g) cerebral angiography, h) lumbar puncture and i) cerebrospinal fluid analysis [Levin et al., 1997; Nelson et al., 1993].

On being diagnosed as having a high-grade astrocytoma (anaplastic astrocytoma or glioblastoma multiforme), patients generally undergo surgery followed by a course of radiotherapy. Patients who do receive post-operative radiotherapy have a median survival ranging anywhere from 24 weeks to 40 weeks [Kristiansen et al., 1981; Salazar et al., 1979; Walker et al., 1978]. From the time of diagnosis to completion of the course of radiotherapy, between six to eight weeks would have lapsed. What this implies for the patient is that a significant proportion of their expected life-span is spent coming to hospital to receive their radiotherapy.

There is consensus in the literature that post-operative radiotherapy has a role in increasing the survival time for these patients although the prognosis is still very poor [Andersen, 1978; Kristiansen et al., 1981; Salazar et al., 1979; Sheline, 1977; Walker et al., 1978].

Due to the poor prognosis of these patients, any reduction in the length of time that a patient with a high-grade astrocytoma needs to spend in either coming to or being in hospital would result in an improved quality of life for the patient. This would imply that these patients would then have more time available to spend with their families and friends at home. In the South African context, this is especially important. Many patients from the rural areas who need to be treated at specialist radiotherapy centres

may have to travel for many hours or even days to reach the hospital. They are obliged to stay in the city, usually in hospital, whilst they are treated, usually without support from relatives or friends, and then travel home on completion of their treatment. If the time that patients have to spend away from home can be reduced in any way, it justifies the claim to an improved quality of life for these patients. Additionally, due to the shorter stay in hospital the cost to the state health service would be reduced. The question then arises as to what may be done to alter the standard or conventional protocols to achieve the goal of effectively reducing the time that the patient spends in or at the hospital to receive radiotherapy.

One method that has the potential of achieving this goal is by altering the radiation protocol in such a manner that the time that the patient needs to be in or at hospital is reduced. However, it is important that a result be achieved which is similar to or better than the current protocols employed.

Radiation tolerance of the brain may be increased by decreasing the fraction size, and increasing both the number of fractions and the overall treatment time [Cohen and Creditor, 1981, 1983a; Hornsey et al., 1981a; Kim and Fayos, 1981; Levin et al., 1997; McCunniff and Liang, 1989; Pezner and Archambeau, 1981]. Sheline et al. (1980) in a review and reanalysis of the literature on the adverse effects of therapeutic irradiation on the brain, found that there was an obvious trend in which the longer the time or greater the number of fractions, the larger the dose associated with necrosis, a late radiation effect. In the same paper it was also stated that the number of fractions is more important for central nervous system necrosis. Cohen and Creditor (1981, 1983a, 1983b) have shown that by increasing the number of fractions and likewise the time to deliver the fractions, one can increase the total dose tolerated by the spinal cord and the brain. This implies that in order to irradiate the brain with a high dose, a large number of fractions must be employed. Furthermore, Cohen and Creditor (1983b) have shown that the tolerance dose for normal tissue stroma increases with protracted treatment to such an extent that tumour control may be achieved without exceeding the tolerance dose of the normal tissue stroma. Walker et al. (1978) have stated that the ultimate brain tolerance will be for an infinite number of infinitely small fractions. A similar statement by White and Hornsey (1978) was made with regards to the spinal cord. All of these conditions are suitably met with the use of continuous low dose rate irradiation as Hall (1988, 1994) states that an infinite number of infinitely small fractions can be achieved by the use of continuous low dose rate irradiation.

Turesson and Notter (1979a, 1979b, 1979c) have shown that there is a relationship between fractionated irradiation and continuous low dose rate irradiation for skin. No such equivalent relationship has been determined for brain. The aim of this thesis was

therefore to establish or obtain an understanding of the histological reactions of the CNS to low dose rate irradiation when compared to a fractionated schedule.

It is envisaged that the results of this study could be extended to patient treatment, in that patients would receive continuous low dose rate radiotherapy over a 12 to 24 hour period, that is, overnight, rather than fractionated treatment over six weeks. This would mean that in addition to an improvement in the quality of life, more patients could be treated with limited resources, yielding a cost benefit.

CHAPTER 2:

CENTRAL NERVOUS SYSTEM (CNS) AND CNS TUMOURS

This chapter briefly describes the human central nervous system (CNS) with regard to its cellular composition. In addition, we also briefly discuss malignant gliomas with regards to their incidence, treatment and prognosis. For detailed information regarding the physiology and anatomy of the CNS the reader is referred to the textbook, "The Human Nervous System: An Anatomical Viewpoint" by ML Barr.

2.1. BASIC STRUCTURE OF THE CENTRAL NERVOUS SYSTEM [Barr, 1979; Junqueira & Carneiro, 1980]

The CNS comprises the brain and spinal cord, both being composed of grey matter and white matter. The grey matter is composed of the cell bodies of neurons whereas the white matter is composed of the long processes of neurons. Both grey and white matter contain neuroglial cells and blood capillaries. The neuroglia have an important role in the normal functioning of the nervous system. Neuroglial cells are classified as: i) astrocytes, ii) oligodendrocytes, iii) microglial cells, and iv) ependymal cells.

The astrocytes and oligodendrocytes are collectively referred to as macroglia.

The Astrocytes

Astrocytes are the largest of the neuroglia, possessing numerous long processes. Astrocytes are present in profusion throughout the grey and the white matter of the brain. Astrocytes are considered to provide a structural and supporting network for the CNS. They are also responsible for attaching the neurons to their blood vessels.

The Oligodendrocytes

Oligodendrocytes have fewer and much shorter processes than those of the other neuroglial cells and are much smaller than astrocytes. They are found in both grey and white matter, with predominance in the white matter, and are responsible for the formation of myelin sheaths in the CNS.

The Microglial cells

Microglial cells are present in both grey and white matter but are not as numerous as the macroglial cells. The microglial cells function as macrophages of the CNS.

The Ependymal cells

Ependymal cells are found lining the ventricles of the brain and the central canal of the spinal cord. Since they are ciliated cells their function is thought to pertain to the circulation of cerebrospinal fluid in the ventricles and spinal canal.

2.2 TUMOURS OF THE CENTRAL NERVOUS SYSTEM

Gliomas (which include glioblastoma multiforme, anaplastic astrocytoma, astrocytoma, oligodendroglioma, ependymoma, and mixed astrocytoma-oligodendroglioma and astrocytoma-ependymoma tumours) can be considered to be the largest group of all brain tumours [Levin et al., 1989; McDonald et al., 1983; Ransohoff et al., 1991]. Those considered to be malignant or of a high grade are associated with the worst prognosis as is evident in Table 2.1 [Fike et al., 1988; Levin et al., 1989; McDonald et al., 1983; Nelson et al., 1993; Packer, 1991; Ransohoff et al., 1991; Schoenberg, 1991; Young et al., 1991;].

Table 2.1: Estimated survival for the more common brain tumours [Levin et al., 1997].

		% Survival	
		5-year	**10-year**
Astrocytoma:	Grade I (cerebellar)	90-100	85-100
	Grade I (all sites)	50-60	30-40
	Grade II	16-46	8-15
	Grade III	10-30	0-10
	Grade IV	0-10	0-1

Classification / Grading

The classification of astrocytomas can either be based on the presumed cell of origin or the degree of malignancy [Levin et al., 1989]. There are essentially two grading systems for astrocytomas, the four grade Kernohan system and the three grade Bailey-Cushing system [Nelson et al., 1993] modified by Daumas-Duport et al. (1988). Briefly, the Kernohan system can be divided into low grade or benign gliomas (grades I and II) and high grade or malignant gliomas (grades III and IV). The Bailey-Cushing system divides gliomas into astrocytomas that are low grade or benign, anaplastic astrocytoma and glioblastoma multiforme.

The histological classification of brain tumours seems to be well standardised, however, this is not entirely acceptable to all experts [Garcia, 1991; Salazar et al., 1979; Sheline, 1977].

Prognosis

Prognosis may be determined according to a number of factors, of which age of the patient at presentation, the patients' functional neurologic status which is assessed with the aid of the Karnofsky scale [Karnofsky et al., 1948] and the amount of residual tumour post surgery are considered as being the most important [Ransohoff et al., 1991].

That postoperative radiotherapy increases the median survival of patients with malignant gliomas, when compared to surgery alone has been documented by many studies [Chang et al., 1983; Gehan & Walker, 1977; Marks, 1991; Salazar et al., 1979; Walker et al., 1978; Walker et al., 1979]. This is illustrated by the differences in median survival for surgery alone compared to postoperative radiotherapy.

The median survival for glioblastoma multiforme after surgery only is three to six months [Chang et al., 1983; Davis, 1989; Kristiansen et al., 1981; Nelson et al., 1985; Nelson et al., 1986; Nelson et al., 1988; Nelson et al., 1993; Sheline, 1977; Sheline, 1990; Walker et al., 1978]. For glioblastoma multiforme with postoperative radiotherapy, the median survival is 8 to 11 months [Chang et al., 1983; Davis, 1989; Kristiansen et al., 1981; Nelson et al., 1985; Nelson et al., 1986; Nelson et al., 1988; Nelson et al., 1993; Sheline, 1977; Sheline, 1990; Walker et al., 1978].

At present, even though there have been advances in neurosurgery, radiotherapy and chemotherapy, the increase in survival time for patients diagnosed with malignant glioma has been minimal [McDonald et al., 1983; Packer, 1991; Schoenberg, 1991; Young et al., 1991;]. Packer (1991) suggested that the failure of neuropathologists

to agree on a single grading system has resulted in there being no determination of histological features on prognosis in these patients [Garcia, 1991; Green et al., 1983].

Treatment

There has not been much change in the treatment of high grade gliomas over the last decade [Lee et al., 1991; Levin et al., 1997; Nelson et al., 1993]. Curative radiotherapy for malignant brain tumours is limited by normal CNS tissue tolerance. The destruction of these tumours unfortunately requires relatively high doses (greater than 70 Gy) [Salazar et al., 1979], which invariably exceeds the CNS tolerance. The approximate threshold doses for CNS injury, namely necrosis, are illustrated in Table 2.2.

Table 2.2: Approximate threshold doses for brain necrosis [Sheline et al., 1980; Levin et al., 1997].

Number of fractions	Total dose (Gy)
10	35
35	60
60	76

Current protocols for the treatment of high-grade astrocytomas may be summarised as follows: a total dose of 50 to 60 Gy given as a fractionated schedule of 25 to 30 fractions. Treatment is given as five fractions per week, excluding weekends, with the dose per fraction being of the order of 1.8 to 2.0 Gy [Andersen, 1978; Fike et al., 1988; McCunniff & Liang, 1989; Salazar et al., 1979; Sheline, 1977; Walker et al., 1978]. These doses are used with a general acceptance of a 5% risk for brain necrosis [Levin et al., 1989; McDonald et al., 1983; Nelson et al., 1993].

CHAPTER 3:

IONISING RADIATION AND THE NORMAL RAT BRAIN

The CNS displays reactions to radiation which become evident at varying time intervals ranging from a few months to years post-irradiation. The occurrence of these reactions is dependent on the total dose administered and most importantly on the number of fractions in which the total dose was given [Cohen and Creditor, 1981, 1983a; Hornsey et al., 1981a; Kim and Fayos, 1981; McCunniff and Liang, 1989; Pezner and Archambeau, 1981; Sheline et al., 1980; Schultheiss et al., 1995].

The cervical spinal cord reactions to irradiation in humans have been shown to be similar to those of the CNS in rodents [Hopewell and Wright, 1970; Hornsey et al., 1981a; Norman and O'Kusky, 1986; Moustafa and Hopewell, 1980; Rogers et al., 1982; van der Kogel et al., 1982]. Thus, the rat CNS is considered to be a good model for inferences to the human CNS in terms of its reactions to radiation exposure In this chapter the reactions of the rat CNS to radiation are discussed.

3.1 RADIATION MYELOPATHY IN THE RAT

Paralysis, ataxia or changes in gait are examples of functional endpoints used in experiments to investigate radiation myelopathy.

Assher and Anson (1962) observed no abnormalities at nine months post-irradiation after single exposures of x-rays (220 kV) totaling 1000 R, 2000 R or 3000 R. However, rats that were hypertensive displayed changes in gait, ataxia, paraplegia and sudden death for the same observation period and total doses. This work was supported by the later work of Hopewell and Wright (1970).

Hubbard and Hopewell (1979) observed that a 40 Gy single dose of x-rays (250 kV) to the cervical spinal cord resulted in paralysis at five to six months post-irradiation. Using single doses of 23, 25 and 27 Gy x-rays (250 kV) to the cervical spinal cord, Hornsey et al. (1990) found that ataxia developed at 179, 155 and 146 days respectively. In an earlier study Hornsey et al. (1981a) observed that a 20 Gy single dose of x-rays (250 kV) did not produce myelopathy at one year post-irradiation.

van der Kogel and Barendsen's (1974) results for doses of radiation using x-rays (300 kV) and neutrons (15 MeV) to produce paralysis within one year post-irradiation are displayed in Table 3.1. These results were supported by the later work of van der Kogel et al. (1982). Generally, these results support the observations of the other investigators though the single fraction dose does contradict the results of Hornsey et al. (1981a).

Table 3.1: Doses of radiation and the number of fractions that will produce paralysis in rats within one year post-irradiation [van der Kogel and Barendsen, 1974; van der Kogel, et al., 1982].

Type of radiation	Total dose (Gy)	Number of fractions
x-rays	20	1
	30	2
	40	5
	67.5	15
	80	20
Neutrons	16.5	1
	22.5	5

3.2 HISTOLOGICAL CHANGES RESULTING FROM RADIATION

There are only a few articles which specifically discuss the histological changes observed in the rat brain following radiation. In order to orientate the reader, Figure 3.1 illustrates the structures in the rat brain investigated in this study.

Rat brain general

It has been observed that the histopathological findings of post-irradiation necrosis have generally been limited to the white matter of the CNS [Burger et al., 1979; Burger and Boyko, 1991; Rubin et al., 1994; Schultheiss et al., 1995; van der Kogel, 1986]

Hopewell (1974) found constrictions in blood vessels, after a single exposure of 3000 R x-rays to the brain, which was due to damaged endothelial cells. These vessel occlusions were expected to influence vascular function [Hopewell, 1983; Hopewell et al., 1986].

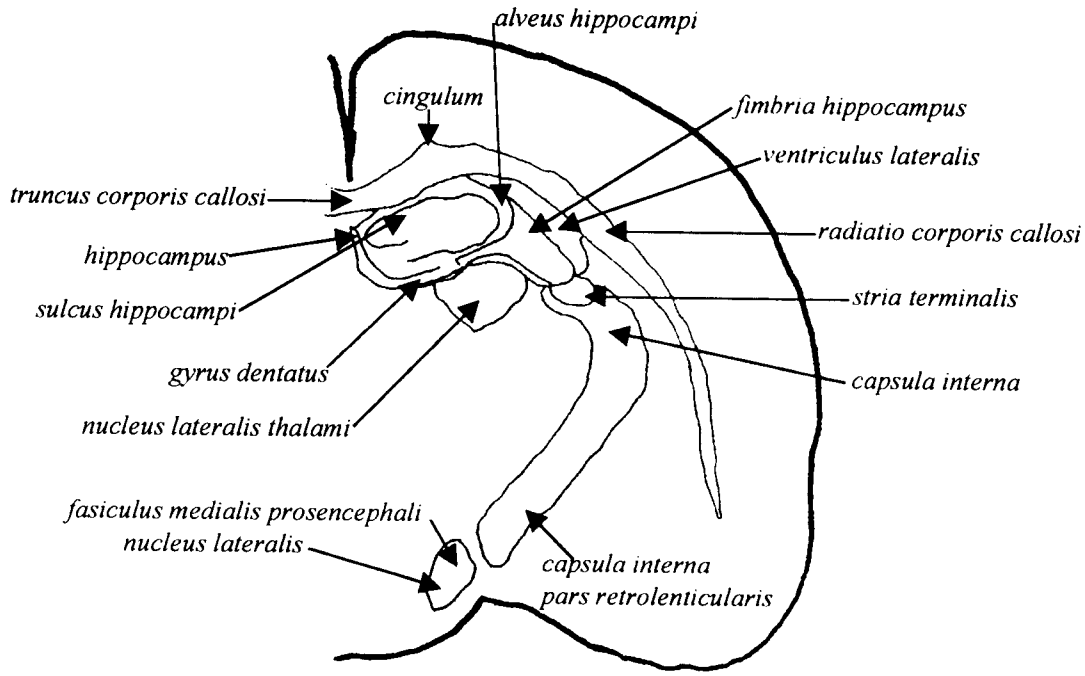

Figure 3.1 Histological sites examined in the rat brain. The *choroid plexus* and *ependymal cells* are found in and attached to the lining of the *ventriculus lateralis* respectively [Albe-Fessard et al., 1966; de Groot, 1967; König and Klippel, 1963; Pellegrino et al., 1978].

The caudate nucleus

Reinhold and Hopewell (1980) observed marked vascular changes after an x-ray (300 kV) dose of 20 Gy. A 25 Gy dose of x-rays (200 kV) resulted in focal gross vascular abnormalities in which the size and shape of the blood vessels was severely altered [Plotnikova et al., 1988].

The cerebral cortex

Abnormal astrocytes were found in the cerebral cortex after an x-ray exposure of 4000 R [Hopewell and Wright, 1970].

A 20 Gy dose of x-rays (200 kV) resulted in a reduction in the number of vessel cross-sections at 26 weeks and this reduction was found to be less marked for x-ray doses of 25 and 30 Gy [Wilkinson, et al., 1986]. However, Moustafa and Hopewell (1980) stated that the cerebral hemispheres rarely experienced vascular damage after a dose of 20 Gy. These authors did however find a

significant increase in the blood flow of the cerebral hemispheres after 20 Gy. On the other hand, Reinhold and Hopewell (1980) observed that the grey matter of the superficial cortex did not display any vascular changes after an x-ray dose of 20 Gy. Hopewell et al. (1978) found significant vascularity changes in the cortex at nine months after an x-ray dose of 20 Gy. This was due to an increase in the number of vessels which had a diameter of more than 8 micrometres. Rogers et al. (1982) found that rats surviving for longer than 200 days post-irradiation displayed telangiectasia accompanied by microhaemorrhage.

The cervical spinal cord

Asscher and Anson (1962) found no abnormalities in the cervical spinal cord of normotensive rats with x-ray (220 kV) exposures of 1000 to 3000 R after an observation period of 270 days. Fibrinoid necrosis of the spinal artery with peripheral inflammation and multiple focal vascular necrosis was observed at 25 days post-irradiation in hypertensive rats after an exposure of 1000 R. An exposure of 2000 R in hypertensive rats resulted in multiple focal acute vascular necrosis with the white matter displaying numerous holes (*status spongiosus)* with thrombosed vessels. Hypertensive rats exposed to 3000 R displayed vascular necrosis between 43 to 70 days.

At six months, van der Kogel and Barendsen (1974) observed necrosis of the dorsal and lateral columns of the white matter after an x-ray (300 kV) dose of 35 Gy. The grey matter however had a normal appearance. Myers et al. (1986) also found necrosis in the dorsal horn at 5.5 months after an x-ray dose of 24.5 Gy. The reactions to radiation were characterised by generalised oedema, cellular reactions, vessels with swollen perivascular spaces and neurons undergoing ischaemic necrosis.

The choroid plexus

Hopewell and Wright (1970) found vascular lesions in 50% of rats that had received an x-ray exposure of 2000 R. The endothelial cells in the choroid plexus were found to be more sensitive to radiation than the epithelial cells in the choroid plexus [Calvo et al., 1986]. This was true for the dose range of 17.5 – 25 Gy x-rays (250 kV). The post-irradiation decrease in endothelial cells was dose related as opposed to the epithelial cells which did not display any marked decreases for the same doses of radiation [Calvo et al., 1986; Calvo et al., 1987].

Atrophy of the smooth muscle cells in the arterioles of the choroid plexus was found to be dose related by Hopewell (1987). Hopewell et al. (1986) reported

that smooth muscle cell atrophy was seen at nine to12 months post-irradiation after doses of 22.5 and 25 Gy x-rays (250 kV).

At one year post-irradiation, Hopewell et al. (1986) described basement membrane thickening after x-ray doses of 17.5 to 25 Gy. Calvo et al. (1987) observed late radiation damage of the choroid plexus at one year post-irradiation after an x-ray dose of 22.5 or 25 Gy. The late radiation damage observed by Calvo et al. (1987) comprised degeneration of the tunica media of the arterioles, thickening of the basement membrane, thrombosis and fibrosis, and supported the earlier work of Calvo et al. (1986).

The corpus callosum

A 25 Gy dose of x-rays (200 kV) produced necrotic areas in the corpus callosum in addition to gross vascular abnormalities [Plotnikova et al., 1988]. Calvo et al. 1988 found that the effective x-ray (250 kV) dose to produce necrosis in the corpus callosum at 39 and 52 weeks was 23.2 and 28.2 Gy respectively. Hopewell and Wright (1970) found the complete destruction and appearance of large cystic spaces after x-ray exposures of 3000 R or 4000 R.

Cytoplasmic changes

Cotran et al. (1989) makes mention of the following cytoplasmic changes that may be observed following radiation damage to the CNS, namely, cytoplasmic swelling, mitochondrial distortion, and degeneration of the endoplasmic reticulum. Similar changes were observed by Maisin (1974) using electron microscopy.

The fimbria

Necrosis of the fimbria was found to develop earlier than that in the internal capsule and corpus callosum [Hopewell, 1987; Rogers et al., 1982]. Necrosis was seen at 51 and 36 weeks after x-ray doses of 22.5 and 25 Gy respectively [Hopewell, 1987]. These observations are supported by the later work of Calvo et al. (1988) who found that the effective x-ray (250 kV) dose to produce necrosis in the fimbria in 50% of the animals at 39 and 52 weeks was 23.8 and 22.5 Gy respectively. These authors also concluded that the development of necrosis in the fimbria was dose related. Bearing this in mind, necrosis was also seen at nine months after an x-ray exposure of 4000 R [Hopewell and Wright, 1970].

No necrosis was seen at 86 weeks after a dose of 20 Gy [Hopewell, 1987; Hopewell et al., 1987]. This observation was supported by the work of Reinhold et al. (1990) who observed that an x-ray dose of 20 Gy did not result in any

demyelination. Reinhold et al. (1990) also devised the "Tissue Injury Unit" scoring system which took account of the following four histological changes, namely, astrocyte enlargement, endothelial cell enlargement, blood vessel thickening and blood vessel dilation. These changes are similar to those discussed by Hopewell (1987). The results of Reinhold et al. (1990) showed that after x-ray doses of 20, 22.5 and 25 Gy the latent periods were 51, 35 and 32.5 weeks respectively. These results were similar to the observations of Calvo et al., (1988). Additional histological changes were observed by Calvo et al. (1988) and Hopewell (1987) which comprised the appearance of groups or pairs of endothelial cell nuclei, the presence of perivascular oedema, and hypertrophy of astrocytes.

Fibrinoid necrosis of the small arteries or arterioles was the most frequent observation in terms of damage to the blood vessels and this lesion was deemed to be present whenever there was any necrosis present [Rogers et al., 1982]. Calvo et al. (1988) observed that at 13, 26 and 39 weeks after irradiation with 22.5 or 25 Gy and at 26 weeks with 20 Gy, a significant drop in the density of blood vessels was evident. These authors did not make any correction for change in vessel diameter which was stated as being significantly increased at 26 weeks after a dose of 22.5 Gy.

The gyrus dentatus

Hopewell and Wright (1970) observed necrosis of the gyrus dentatus which extended from the fimbria at nine months after x-ray exposure of 4000 R.

The hippocampus

Necrosis of the hippocampus, which extended from the fimbria, was observed at nine months post irradiation after an x-ray exposure of 4000 R [Hopewell and Wright, 1970].

The hypothalamus and thalamus

Necrosis was observed in these areas at 10.5 months after an x-ray exposure of 4000 R by Hopewell and Wright (1970). The same radiation dose resulted in hyaline thickening being observed at 15 months post-irradiation. Thrombosed blood vessels and haemorrhagic foci around small dilated blood vessels were also reported. Calcium containing basophilic bodies were also found to cause occlusion of the blood vessels.

The internal capsule

Necrosis of the internal capsule was seen at nine months post irradiation after an x-ray exposure of 4000 R [Hopewell and Wright, 1970]. It was also reported that after exposures of 3000 and 4000 R the internal capsule generally displayed either large areas of necrosis or was completely destroyed. Calvo et al. (1988) found that the effective x-ray dose to produce necrosis in the internal capsule at 39 and 52 weeks was 24.1 and 26.4 Gy respectively.

The lateral ventricles

There are no reports of observations in terms of histological changes in the lateral ventricles following radiation exposure. However, changes were reported in the surrounding structures. A 20 Gy dose of x-rays resulted in marked vascular changes in the surrounding structures [Reinhold and Hopewell, 1980]. Plotnikova et al. (1988) found that a dose of 25 Gy x-rays (200 kV) resulted in extensive necrotic areas which were localised near the walls of the lateral ventricles.

The optic nerve and chiasma

Hopewell and Wright (1970) observed complete necrosis in these structures in 25% of their animals after x-ray exposures of 3000 and 4000 R.

The subependymal plate

The normal subependymal plate has a high nuclear density [Hopewell and Wright, 1970]. An x-ray exposure of either 3000 or 4000 R resulted in the subependymal plate being absent and the subependymal plate close to the lateral ventricles was found to be almost anuclear [Hopewell and Wright, 1970]. Exposures of 1000 and 2000 R did not result in a decrease in the nuclear density of the supependymal plate.

Hopewell and Cavanagh (1972) found that the mitotic activity of the subependymal plate was dose-dependent following exposures to x-rays (220 kV) between 200 and 4000 R. This was also confirmed by the later work of Hornsey et al. (1981). Hopewell and Cavanagh (1972) found that there was a rapid decrease in the mitotic counts within 24 hours after the exposure. At day 14 post-irradiation the mitotic counts appeared to be that of the normal subependymal plate. After exposures of 200 and 2000 R there was recovery to normal nuclear density in one month and three months respectively. An exposure of 4000 R showed no recovery at six months.

Chauser et al. (1977) found that x-ray (250 kV) doses up to 10 Gy resulted in recovery towards normal cell numbers by 30 days. This may be compared to

doses of 15 Gy or greater, that resulted in a constant decrease in the cell numbers with time after irradiation. A sharp decrease in the number of cells was found after two to four days irrespective of the dose of radiation. Rogers et al. (1982) concluded that the subependymal plate in every irradiated rat was devoid of cells after doses in the range of 20 to 42.5 Gy.

3.3 WHITE MATTER NECROSIS – CELLULAR BASIS

A great deal of debate has taken place to identify the primary target for radiation damage in the CNS. Two theories have been put forward in order to identify the critical target cells. The 'glial' hypothesis [Chauser et al., 1977; Myers et al., 1986; Reinhold et al., 1984; Schultheiss et al., 1988; Withers et al., 1980; Yaes and Kalend, 1988] which implicates the oligodendrocytes and the 'vascular' hypothesis [Chauser et al., 1977; Myers et al., 1986; Reinhold et al., 1984; Yaes and Kalend, 1988] which implicates the vascular endothelium as the critical target.

Spinal cord - Glial cells as the primary radiation target

Hubbard and Hopewell (1979) performing autoradiography in the normal unirradiated rat cervical spinal cord observed that there was a greater turnover of glial cells in the white matter than in the grey matter. Examining the neuroglia of the cervical spinal cord after a single dose of 40 Gy (250 kV x-rays) they observed a) that at three months post-irradiation there was a marked decrease in the neuroglia of the cervical spinal cord which continued into the fourth month, and b) that white matter necrosis was present at four months post-irradiation. These observations lead them to conclude that radiation induced white matter necrosis was due to a loss of neuroglia, which was substantiated by their observation that the oligodendrocyte population of the cervical spinal cord showed the greatest deficiency just prior to the development of white matter necrosis. This was probably the most conclusive evidence, at that time, indicating that the oligodendrocytes may be the primary target cell in the development of white matter necrosis. These observations were supported by those of van der Kogel et al. (1982) and supported the earlier findings of van der Kogel and Barendsen (1974).

Radiation induced white matter necrosis without nerve root degeneration was observed at five to six months post-irradiation by van der Kogel et al. (1982) with the oligodendrocyte considered the target cell.

van der Kogel and Barendsen (1974) using myelopathy as an endpoint in rats exposed to x-rays (300 kV), found that single doses up to 20 Gy produced no functional damage (palpable muscle atrophy or impaired use of hind legs) when compared to doses of 22 Gy or greater at which functional damage became evident with a latent period of four months. When they examined the white matter necrosis in the cervical spinal cord, they found that the grey matter and the nerve roots appeared to be relatively normal, leading them to also conclude that the oligodendrocyte is the critical cell due to it being radiosensitive.
Schultheiss et al. (1988) in their analysis concluded that the 'glial' hypothesis for white matter necrosis is more complex than the sudden loss of a critical number of oligodendrocytes. This was supported by the earlier work of Schultheiss et al. (1984) and Reinhold et al. (1984).
However, Myers et al. (1986) expressed the view that radiation damage to oligodendrocytes alone was not likely to cause white matter necrosis.

Brain – Glial cells as the primary radiation target

Calvo et al. (1988) observed that there was no reduction in numbers in the astrocyte population prior to the onset of necrosis. These authors also found no significant changes in the number of oligodendrocytes after irradiation. They did however mention that the number of oligodendrocytes around areas of necrosis did display variation.

Plotnikova et al. (1988) stated that the damage to glial cells after moderate doses of radiation may play a certain role in the development of brain necrotic damage. This view was supported by the observations of Reinhold et al. (1990) who observed that necrosis was highly correlated with demyelination.

Hornsey et al. (1981a) stated that white matter necrosis observed at five to ten months post-irradiation was associated with the loss of the reproductive ability of the neuroglial cells in the subependymal plate. The x-ray (250 kV) doses used in this study ranged from 20 Gy to 150 Gy and included single doses and various fractionated regimes. This view supported the earlier observations of Chauser et al. (1977).

Spinal cord – Vascular cells as the primary target

Hornsey et al. (1990) concluded that vascular effects were important in the development of necrosis in the cervical spinal cord. This was in view of the delayed onset of ataxia as a result of the irradiated rats having vasoactive drugs

administered to them. van der Kogel et al. (1982) considered the vascular endothelium as the target cell for late delayed radiation damage.
Myers et al. (1986) concluded that white matter necrosis may be due to infarction. However, van der Kogel and Barendsen (1974) stated that it was difficult to explain the damage seen in nerve roots or white matter on the basis of change to blood vessels in the absence of damage to the grey matter.

Brain – Vascular cells as the primary target

Calvo et al. (1988) found a decrease in the vascular density which was said to be similar to the decrease in the number of endothelial cells. These authors also stated that the exact relationship between the loss of endothelial cells and white matter parenchymal necrosis remains unclear even though their results suggest that there may be a direct relationship between endothelial cell loss and loss of capillaries. This loss of capillaries could in turn result in ischaemic necrosis. These observations supported the earlier work of Calvo et al. (1986). The most frequent observation in terms of damage to the blood vessels was fibrinoid necrosis of the small arteries or arterioles [Rogers et al., 1982]. This lesion was deemed to be present whenever there was any necrosis. Necrosis was said to be preceded by changes in the vasculature by Hopewell (1987). This view was supported by the work of Calvo et al. (1987), Hopewell (1987), Hopewell et al. (1986), Hopewell et al. (1987), Hopewell and Wright (1970), Hornsey et al. (1981b), and Plotnikova et al. (1984).

Radiation of the microvasculature

Plotnikova et al. (1984) suggested that damage to the microcirculation may be the cause of late radiation injury in the rat brain. The work performed by van der Kogel et al. (1995) using the process of boron neutron capture which facilitated the selective irradiation of the microvasculature, specifically the endothelial cells, proved conclusively that damage to the vascular endothelial cells is the primary event leading to white matter necrosis.

CHAPTER 4:

THE LINEAR QUADRATIC (LQ) EQUATION AND PROTRACTED IRRADIATION

4.1 INTRODUCTION

Dose rate, dose fractionation and treatment time all influence tolerance doses to ionising radiation of various normal tissues to varying extents. Quantitation of the influence of these factors is important for the practice of clinical radiotherapy, as it will allow modification of radiation dose prescription to achieve equivalent (iso-effective) clinical end-points.

The "cube-root" dependence of tolerance dose (D_{tol}) on total treatment time T, namely $D_{tol} = kT^{1/3}$ was the earliest proposed isoeffect relationship, and was used by Strandqvist (1944) to show that isoeffect curves for various endpoints in human skin (necrosis, cure of skin carcinoma, wet and dry desquamation and erythema) had a slope of approximately 0.33. All treatments were given as three or five fractions per week, which implies that the overall time T includes also the number of fractions in the "cube-root" formulation.

Later studies showed that it was important to separate the number of fractions and overall treatment time [Fowler et al., 1963]. Hence, the "nominal standard dose" (NSD) formula was introduced by Ellis (1968, 1969) where

$$\text{Total Tolerance Dose} = (\text{NSD}) T^{0.11} N^{0.24} \qquad \textbf{Equation 1}$$

This was based on clinical observations of tolerance of connective tissue to radiotherapy.

From the NSD formulation, the concepts of partial tolerance (PT), time-dose-fractionation factors (TDF) and cumulative radiation effect (CRE) evolved, which simplified the application of the NSD formula for everyday clinical use, and to include also the effect of low dose rate irradiation [Kirk et al., 1971; Kirk et al., 1972; Orton, 1974; Orton and Ellis, 1973].

4.2 LIMITATIONS OF NSD, TDF AND CRE

The NSD system is based ultimately on skin reaction data. Therefore, although early effects, i.e., those occurring from within days to about eight weeks after radiation, can be reasonably well predicted, the same is not true for late effects occurring from six months to several years after radiation of tissue other than skin and mucosa [Berry et al., 1974; Fowler, 1971; Peters and Withers, 1980].

Fowler (1989) has summarised other weaknesses in the NSD formulism, which include:

(a) that the late damage that occurs with large fractions is not predicted,

(b) there is insufficient importance or weighting attached to fractions size,

(c) the exponent of the time factor ($T^{0.11}$) initially suggests a large increase in isoeffect dose followed by a slower increase. Radiation studies of tissues show no initial increase followed later by a rapid rise as a faster accumulation of clonogens occurs, and

(d) because the relationship between time and dose per fraction is incorrect, the time factor for tumours and early reacting tissue is underestimated, and that for late reacting tissues is overestimated.

In spite of these shortfalls, some clinicians still make use of the NSD formulism to adjust radiotherapy schedules, perhaps because of the availability of simple conversion tables. However, it is worth noting that in most clinical situations, changes in dosage are generally minor. As long as changes in the radiotherapy protocols are kept small, then almost any mathematical formula which predicts increased tolerance doses with increasing fractionation (N) and overall time (T) would be satisfactory over small ranges of N and T [Thames and Hendry, 1987].

4.3 THE LINEAR QUADRATIC EQUATION

The observed frequency of various effects resulting from x- or γ-irradiation of mammalian cells is not a simple linear function of dose. At doses in excess of a few Gy, damage accumulation contributes significantly to the induction of any particular effect [Barendsen, 1982]. Thus, in order to analyse the effects, at least, a linear and quadratic term may be involved. Then, the frequency of effect

as a function of dose may be represented by $F(D) = \alpha D + \beta D^2$ where α and β are constants depending on the effects and conditions of exposure to dose D [Barendsen, 1982].

Functional cell survival (S), i.e., probability of cells showing no effect as a result of radiation, may be given by

$$S = \frac{S(D)}{S(0)} = \exp - (\alpha D + \beta D^2) \qquad \textbf{Equation 2}$$

where S(D) is survival after dose D, and S(0) is survival after zero dose.

Although this equation is representative of any one of a number of biophysical/mechanistic processes, it may be usefully considered as representing two processes, each of which may lead to cell death. In the first process, one radiation event damages two critical sites in the cell simultaneously, resulting in cell death (so-called "α-kill"). In the second process, two sites are damaged by separate radiation events. The damage may cooperate to result in cell death (so-called "β-kill"). Because α and β indicate the relative importance of each of the two processes, the $^{\alpha}/_{\beta}$ ratio then becomes of importance because its value is characteristic of a particular tissue or cell type.

The linear quadratic formula (Equation 2) has been found to provide good fit to experimental data on chromosome aberrations, mutations, tumour induction and cell reproductive death [Barendsen, 1978; Barendsen, 1979; Brown, 1977; Cox et al., 1977; Fertil and Malaise, 1981; Lloyd et al., 1976] and indeed is now the model of choice to describe cell survival curves.

However, the curve described by Equation 1 is continuously bending, without a final straight portion as is seen experimentally when survival curves are determined to surviving fractions of less than 10^{-2}. If the use of the linear quadratic formulation is restricted to survival fractions between 1.0 and 0.1, and to doses used in daily radiotherapy schedules, the model is an excellent representation of the data.

4.4 THE LINEAR QUADRATIC AND TISSUE RESPONSE PREDICTION

The linear quadratic equation allows prediction of doses required to achieve specific clinical end points in radiotherapy. In the clinical setting and *in vivo*

experiments, the effect of radiation is usually measured in terms of organ function. Organ function is proportional to the number of functional cells remaining in an irradiated organ at a particular time after irradiation, and is generally not proportional to clonogenic cell number. Clearly, the tolerance of tissues to radiation is determined by the proportion of remaining functional cells, and will be described by the dose response curves for organ function.

The linear quadratic model has now been accepted as having wider validity in fractionated and low dose rate radiotherapy than the NSD formula and its derivatives [Hall, 1994]. Although the LQ model can be used to compare and predict the effect of different radiotherapy regimens, the model must not be used to the exclusion of clinical experience and judgement.

4.5 THE LINEAR QUADRATIC EQUATION AND A QUANTITATIVE DESCRIPTION OF FRACTIONATION AND PROTRACTED RADIATION EFFECTS

Several authors have shown how the linear quadratic formula can be used to calculate effective doses in radiotherapy, and how kinetic parameters can be obtained using isoeffective protocols [Barendsen, 1982; Dale, 1985; Hall, 1994; Thames et al., 1982]. A summary of important concepts and equations relevant to the work presented in this thesis is presented below.

The biological effect (E) in irradiated tissues is related to the surviving fraction of target cells thus

$$E = \alpha D + \beta D^2 \qquad \textbf{Equation 3}$$

where α and β are constants and D is the dose of radiation.

For n fractions of dose d, the biological effect is given by

$$E = n(\alpha d + \beta d^2) \qquad \textbf{Equation 4}$$

Then,

$$\frac{E}{\alpha} = nd\left(1 + \frac{d}{\alpha/\beta}\right) \qquad \textbf{Equation 5}$$

The quantity $\left(1 + \frac{d}{\alpha/\beta}\right)$ has been termed the Relative Effectiveness (RE) by Barendsen (1982).

Because $nd = D$, the total dose,

$$\frac{E}{\alpha} = \textit{Total Dose} \times \textit{Relative Effectiveness} \qquad \textbf{Equation 6}$$

that is,

$$\frac{E}{\alpha} = D\left(1 + \frac{d}{\alpha/\beta}\right) \qquad \textbf{Equation 7}$$

The quantity $\frac{E}{\alpha}$ is known as the Biologically Effective Dose (BED) [Fowler, 1989], the Extrapolated Tolerance Dose (ETD) or Extrapolated Response Dose (ERD) [Barendsen, 1982].

For protracted irradiation at a constant dose rate R,

$$RT = D \qquad \textbf{Equation 8}$$

where T is overall time and D is the total dose.

Then,

$$RE_{\text{Protracted}} = 1 + \frac{2R}{\mu}\left(\frac{1}{\alpha/\beta}\right)\left\{1 - \frac{1}{\mu T}\left[1 - \exp(-\mu T)\right]\right\} \qquad \textbf{Equation 9}$$

where μ is the repair time constant for repair of sub-lethal damage (produced by single target hits) [Dale, 1985].

Equation 9 may be written as

$$(RE)_{\text{Protracted}} = 1 + \frac{KR}{\left(\alpha/\beta\right)} \qquad \textbf{Equation 10}$$

where $$K = \frac{2}{\mu}\left\{1 - \frac{1}{\mu T}\left[1 - \exp(-\mu T)\right]\right\}$$

Because *BED* = *Total Dose* x *Relative Effectiveness*, then for protracted radiation,

$$BED = D\left[1 + \frac{KR}{\left(\alpha/\beta\right)}\right] \qquad \textbf{Equation 11}$$

Then, $$\frac{1}{D} = \frac{1}{BED} + \frac{KR}{BED\left(\alpha/\beta\right)} \qquad \textbf{Equation 12}$$

Equation 12 offers a graphical method to analyse for μ and $^{\alpha}/_{\beta}$. For a number of isoeffective radiation regimes, a plot of KR against $^{1}/_{D}$ will yield a straight line, provided that an appropriate value of μ is chosen. The $^{\alpha}/_{\beta}$ value is given by the intercept on the KR axis, that is, when $^{1}/_{D}=0$.

The graphical method is a two-step method and allows an indirect method of determining the $^{\alpha}/_{\beta}$ ratio and μ, the repair constant. It has been argued [Pop et al., 1997] that the direct analysis of Thames et al. (1986) is mathematically more appropriate to ascertain the values of these two parameters.

4.6 THE LINEAR QUADRATIC EQUATION AND A TIME FACTOR

Clonogenic cell repopulation in normal tissues and tumours that occur during the course of radiation treatment may have an effect on treatment outcome. For this reason several authors have incorporated a time factor into the linear quadratic formalism [Dale, 1989; Fowler, 1989; Travis and Tucker, 1987]. However, in the case of late reacting tissues, proliferation is slow and will not occur to any appreciable extent during a course of radiation. No time factor then needs to be included [Fowler, 1989]. In the analyses presented in this thesis involving the linear quadratic formalism, because the organ of interest was the brain which is a late responding organ, no time factor was therefore incorporated.

CHAPTER 5:

MATERIALS AND METHODS

This chapter describes the procedures that were used in each of the experimental protocols. The method for rat brain perfusion at one year post-irradiation is also described in addition to the removal of the rats' brains. The process of preparing the brains for histology is also described as well as the staining protocols that were used.

5.1 ANIMALS

Male Wag/Rij rats between six to eight weeks of age and weighing between 180 – 210 grams were used in these experiments. The rats were bred both in the University of Cape Town Medical School's and at the Radiobiology Department's animal units.

The rats were housed in the Radiobiology Department's animal unit for two weeks prior to irradiation and for the entire observation period after irradiation. Their diet consisted of Epol rat cubes (Atlas Feeds, Wynberg, South Africa) and tap water *ad libitum*. The temperature of the animal unit was maintained at 22 ± 1 °C. The lighting in the animal unit was set to mimic a 12 hour day – 12 hour night cycle.

Prior to irradiation four rats were housed per cage, the dimensions of which were 47 cm by 27 cm by 11 cm. On completion of the irradiation, only two rats were housed per cage, and inspected daily except weekends. The animals were weighed on a daily basis for one month, then weekly for five months, followed by monthly weighing until the animals were killed.

5.2 IRRADIATIONS

All radiations were performed with an Eldorado 6 ^{60}Co unit with a fixed head and irradiating vertically downwards. All radiations were with the bottom of the base plate of the rat holding device or jig (described below) at 80 cm from the source (that is, a source to surface distance (SSD) of 80 cm). Full backscatter

was provided by 20 wooden blocks (40 cm by 40 cm by 2.2 cm) positioned underneath the base plate of the rat jig.

The ^{60}Co unit was equipped with a cast-lead collimator to give a fixed 40 cm by 40 cm field at an SSD of 80 cm. The 40 cm by 40 cm field was not uniform because of casting irregularities in the lead collimator. However, it was found that there was less than 2% variation in the dose across a 10 cm by 10 cm area at the centre of the 40 cm by 40 cm field.

All brain irradiations were performed using a 5.14 cm^2 field as defined by the shape of lead shielding blocks (see below) within this 10 cm by 10 cm area.

5.3 RADIATION SET-UP

It was required to irradiate only the rat brain, that is, an area between the eye and the ear, as shown in Figure 5.1. Based on the external features of the rat head, Figure 5.2 illustrates the gross anatomical areas of the rat brain that would be included in the radiation field used for the present study. Lead blocks 30 cm long, 10 cm wide and 8 cm thick with a 2 cm diameter semicircular cut-out, as shown in Figure 5.1, were placed above the jig holding the rat (Figure 5.3 below). Rats lying on their sides were positioned such that apart from the area to be irradiated under the cut-out, the remainder of the rat body was shielded by lead. The 8 cm thickness of lead represents 7.27 half-value layers for ^{60}Co, so that whole body dose was less than 0.8% of the dose administered to the brain.

Throughout the study, two rats were irradiated simultaneously, with shielding blocks placed side by side as shown in Figure 5.1. The blocks were placed 5 cm above the base plate of the jigs using 5 cm by 6.8 cm by 2 cm perspex blocks. The centre of the two cut-outs and the intersecting point midway between the two shielding blocks was placed at the centre of the irradiation field, as shown in Figure 5.1.

For the fractionated study, because of the short duration of each fraction, the rats were not restrained in the jig when positioned underneath the lead shielding blocks. Perspex supports for the anaesthetic bag allowed the positioning of the rat's head at the same height above the base plate as that for the low dose rate irradiations, where the rats were positioned with the jig.

5.4 RAT HOLDING DEVICE (JIG)

The rat jig was constructed of perspex and designed in such a manner that the rats were held lying on their sides and is illustrated in Figure 5.3.

The upper incisors of anaesthetised rats were put into the hole in the hinged plate, which is detailed in Figure 5.4. This plate was adjusted by tightening the nut sufficiently to ensure stable positioning of the head of the rat, with care taken that breathing was unrestricted.

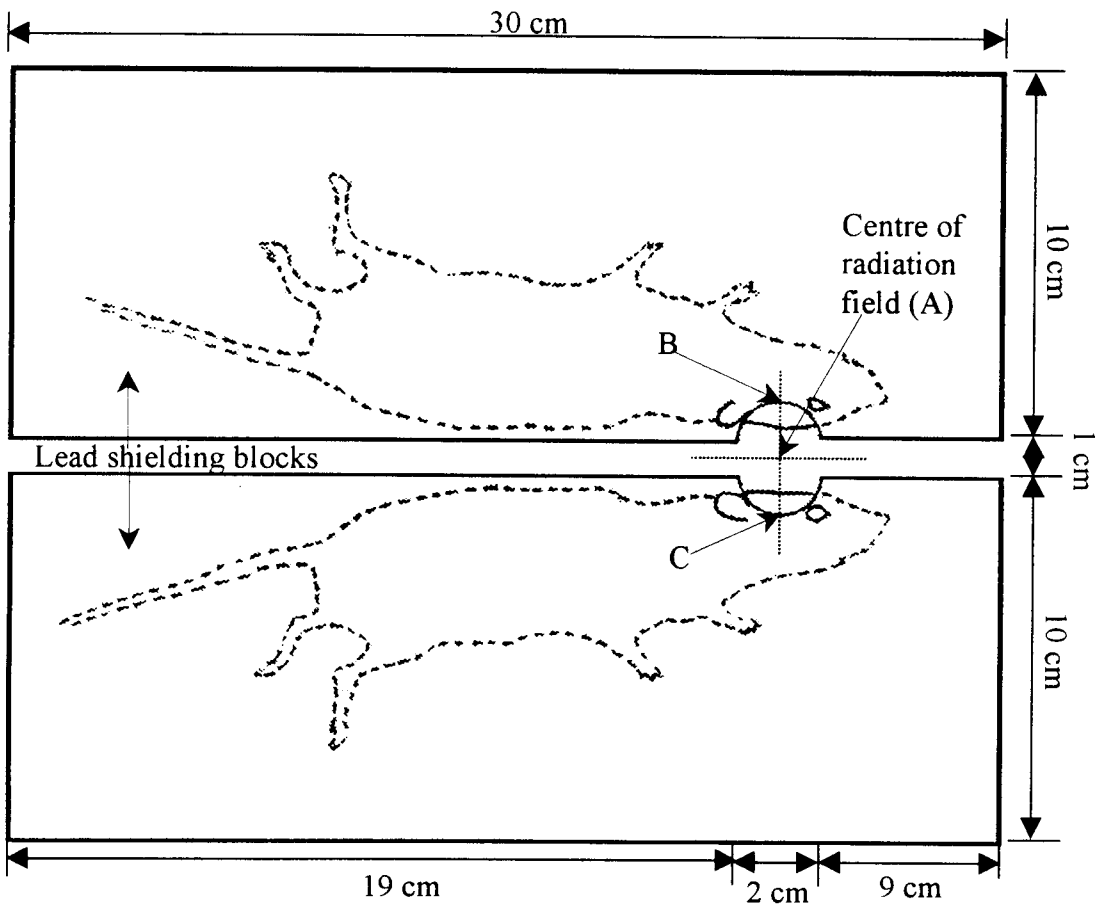

Figure 5.1 Lead shielding blocks and positioning of rats for ^{60}Co irradiation. Thickness of blocks was 8 cm. The rat holding jigs have been omitted from the diagram to preserve clarity. Points A, B and C correspond to those shown in Figure 6.2.

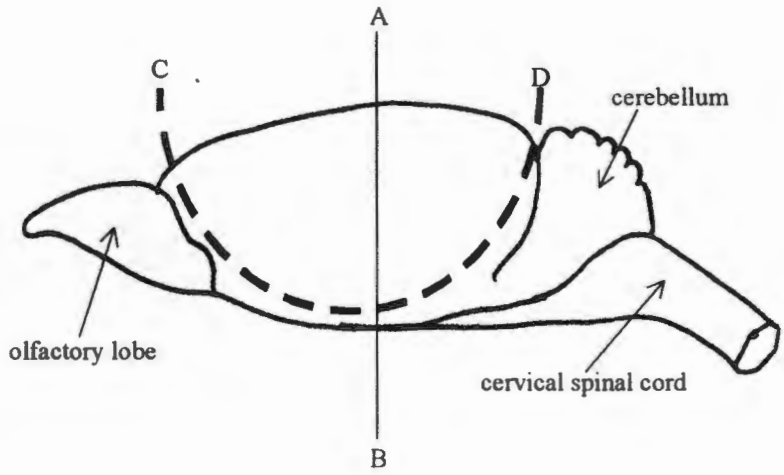

Figure 5.2 Lateral view of the gross anatomy of the rat brain after the skull has been removed. Line AB represents the level of the optic chiasma. Arc CD represents the area of the rat brain in the radiation field [Albe-Fessard et al., 1966; Calvo et al., 1987; Chauser et al., 1977; de Groot, 1967; Hopewell and Wright, 1970; Hornsey et al., 1981a; König and Klippel, 1963; Pelligrino et al., 1978; Plotnikova et al., 1984; Reinhold and Hopewell, 1980; Rogers et al., 1982].

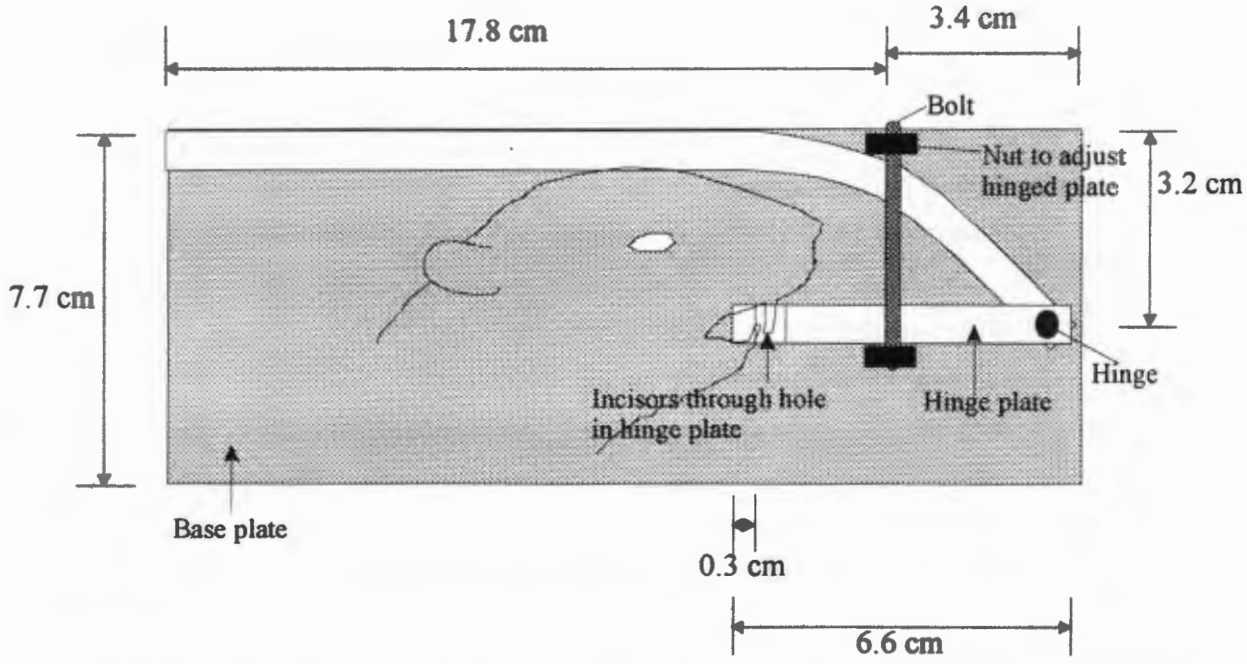

Figure 5.3 Rat holding jig for rat brain irradiation with ^{60}Co gamma irradiation. The height of the jig was 4.0 cm.

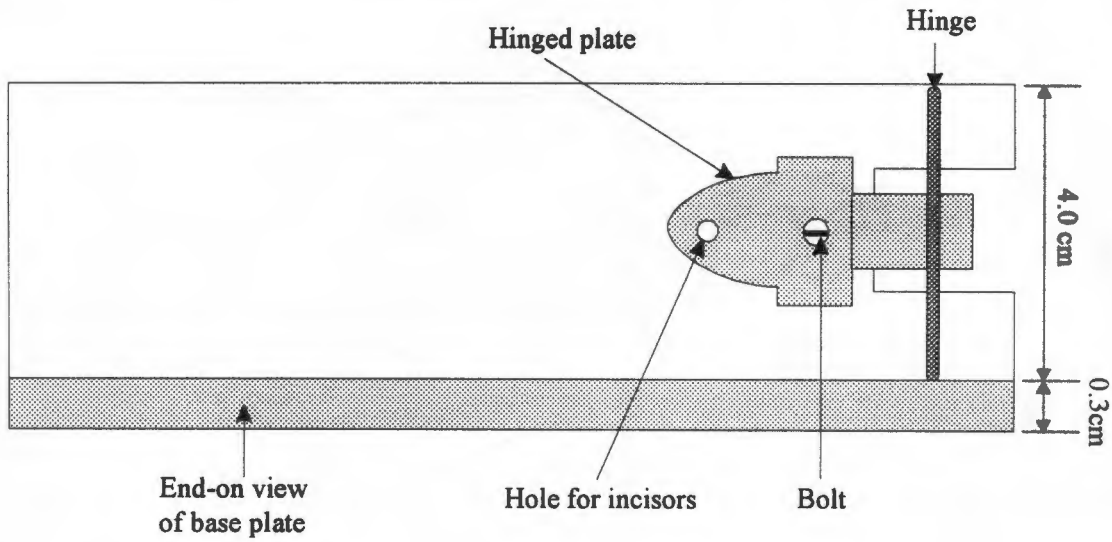

Figure 5.4 Detail of rat jig showing hinged bottom plate.

5.5 DOSIMETRY

Dosimetry was performed with the lead shielding blocks in the same position as for rat brain irradiation, i.e. 5 cm above the base plate and with the cut-outs around the centre of the radiation field.

Dose uniformity assessment

The dose uniformity in the brain irradiation field, that is, the field defined by the cut-outs in the lead shielding blocks and the area between the two cut-outs, was determined using film densitometry. Film (Kodak (U.S.A.) X-O mat diagnostic film) was placed under the lead blocks which were 5 cm above the base plate without the jig in place and exposed to ^{60}Co radiation for 0.4 minutes. After development in a Kodak (U.S.A.) RP X-O mat processor, films were analysed with a Therados 2 Densitometer.

Dose measurement – ionisation chamber

Dose measurements in the field defined by the cut-outs and the area between the cut-outs were made using a Farmer 2570 secondary standard dosemeter with the ionisation chamber (0.6 cm^3) placed at various positions in the brain irradiation field. These positions were a) on the base plate without the jig, that is, in the position of the film used for dose uniformity measurement, b) in a wax rat

phantom which had a hole in the position of the brain, and c) in a rat that had been perfused with phosphate buffered formalin, also having a hole in the position of the brain. The measurements with the wax rat and perfused rat phantoms were made such that the positioning of the phantoms was exactly that which would have been obtained if the phantoms had been placed in the rat holding jig. The ionisation chamber was exposed to radiation for one minute and the exposure reading recorded. All the readings from the Farmer ionisation chamber were manipulated to obtain an answer in Gy as follows:

Dose (Gy) = *R* x (*PT*) x (*QF*) x (*ATCF*) [Johns and Cunningham, 1969]

where R is the exposure reading, PT the pressure and temperature correction factor, QF the correction factor for the instrument, and ATCF the air tissue correction factor.

Filter thickness for low dose rate irradiation

In addition to investigating the effect of fractionated high dose rate (0.50 to 0.75 Gy min^{-1}) conventional radiation, the present investigation was also designed to investigate the effect of three low dose rate irradiations in the brain, that is, nominally 0.04, 0.05 and 0.07 Gy min^{-1}. In order to achieve these low dose rates, lead filters of different thicknesses were placed in a holder immediately below the collimator of the Eldorado ^{60}Co unit.

The thickness of the lead filters required to achieve the low dose rates was calculated using the dose rate as measured using the ionisation chamber in the perfused rat under the lead shielding blocks in the position of the brain irradiation field.

The thickness of lead filters required were calculated as follows:

$$D_r = D_o e^{-\left(\frac{(\ln 2)x}{HVL}\right)}$$

where D_r is the required dose rate, D_o the current dose rate, e the base of the natural logarithm, x the thickness of the lead filter, and HVL the half-value-layer for ^{60}Co was 1.1 cm.

The lead filter plates were machined to the correct thickness in the mechanical workshop of the Department of Medical Physics.

Dose Measurements in presence of lead filter plates

Dose measurements as discussed in the above sections using the ionisation chamber were repeated with each of the three lead filters in place.

5.6 RAT ANAESTHESIA

All radiations of rat brains took place whilst the rats were anaesthetised. The initial anaesthesia was induced by placing the animal in a 5000 ml glass beaker into which 0.5 ml Halothane (May and Baker, South Africa) had been aliquoted. A fine wire mesh was positioned 2 cm from the bottom of the beaker, and the top of the beaker was tightly covered with a polythene sheet. When the rat had succumbed to the anaesthetic, it was removed from the beaker. It was then positioned for radiation with an anesthetic bag (see below) over its snout for the fractionated irradiation or in the jig in the continuous inhalation anaesthesia set-up [Ang et al., 1982; van der Kogel, 1979] for the low dose rate radiation (see below).

The anaesthetic bag

The anaesthetic bag consisted of a plastic bag of dimensions 19 by 21 cm with the open end tapering over a distance of 7 cm onto a tube of 4 cm length with an inside diameter of 2.2 cm as illustrated in Figure 5.5. This tube fitted snugly when placed over the rat's snout.

Each bag contained 20 g of calcium chloride, and 0.3 ml of Halothane was injected into the bag with a glass syringe. Medical oxygen was blown into the bag, which was sealed with a stopper made of a pliable resin material (Prestik® Bostik, South Africa). When the anaesthetic bag was removed from the rats' snouts on completion of irradiation, they regained consciousness almost immediately.

Continuous inhalation anaesthesia for low dose rate irradiations

Anaesthetised rats were placed in the holding jig which was positioned under the shielding blocks in the radiation field so that only the area between the eye and ear was below the semi-circular cut-out. A plastic sheet was draped over the jig and lead shielding blocks.

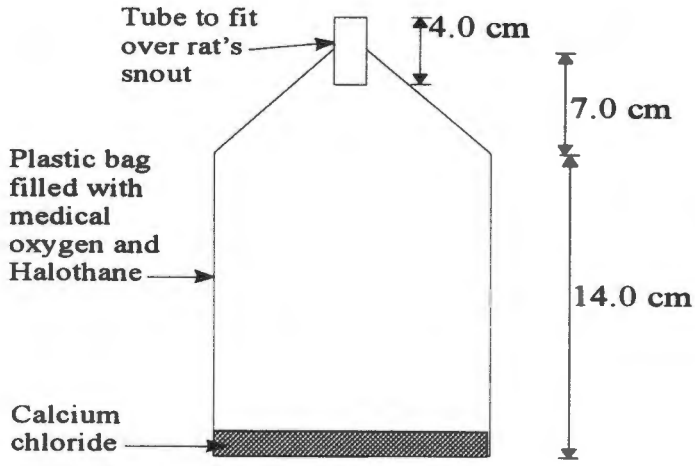

Figure 5.5 Illustration of the plastic anaesthetic bag.

This was not taped or affixed to the wooden backscatter boards. Oxygen (medical grade, AFROX, Epping, South Africa) at 2 $l.min^{-1}$ was piped into a Fluotec vaporizer filled with Halothane (May and Baker, South Africa). The gas was then warmed to 37 °C and humidified with an MiCH Humidity Center (Allied Health Products, St. Louis, U.S.A.), and the anaesthetic gas was passed under the plastic drape. In order to remove the anaesthetic gas, one end of a plastic pipe of diameter 1 cm, was placed under the plastic drape with the other end connected to an extraction pump (Air-Shields Dia-Pump, Narco Scientific, Ireland). The exhaust gas from the pump was fed via a duct to the outside of the building. The set-up for maintenance of anaesthesia whilst irradiating at low dose rates is shown in Figure 5.6.

A portable 30 cm electric fan was placed in the room housing the ^{60}Co unit to ensure continuous circulation of air in the room.

The Fluotec vaporizer was set initially to deliver a gas containing 1% Halothane, but after two hours was adjusted to 0.5% Halothane.

Checks were made every hour during the low dose rate irradiations to see that the Halothane levels were adequate and that the rats had not aroused or moved. On the completion of irradiation, the rats were fully aroused and moving about in their housing cages within two to five minutes after being removed from the anaesthetic set-up. The rats were caged and housed in the Radiobiology Department animal unit.

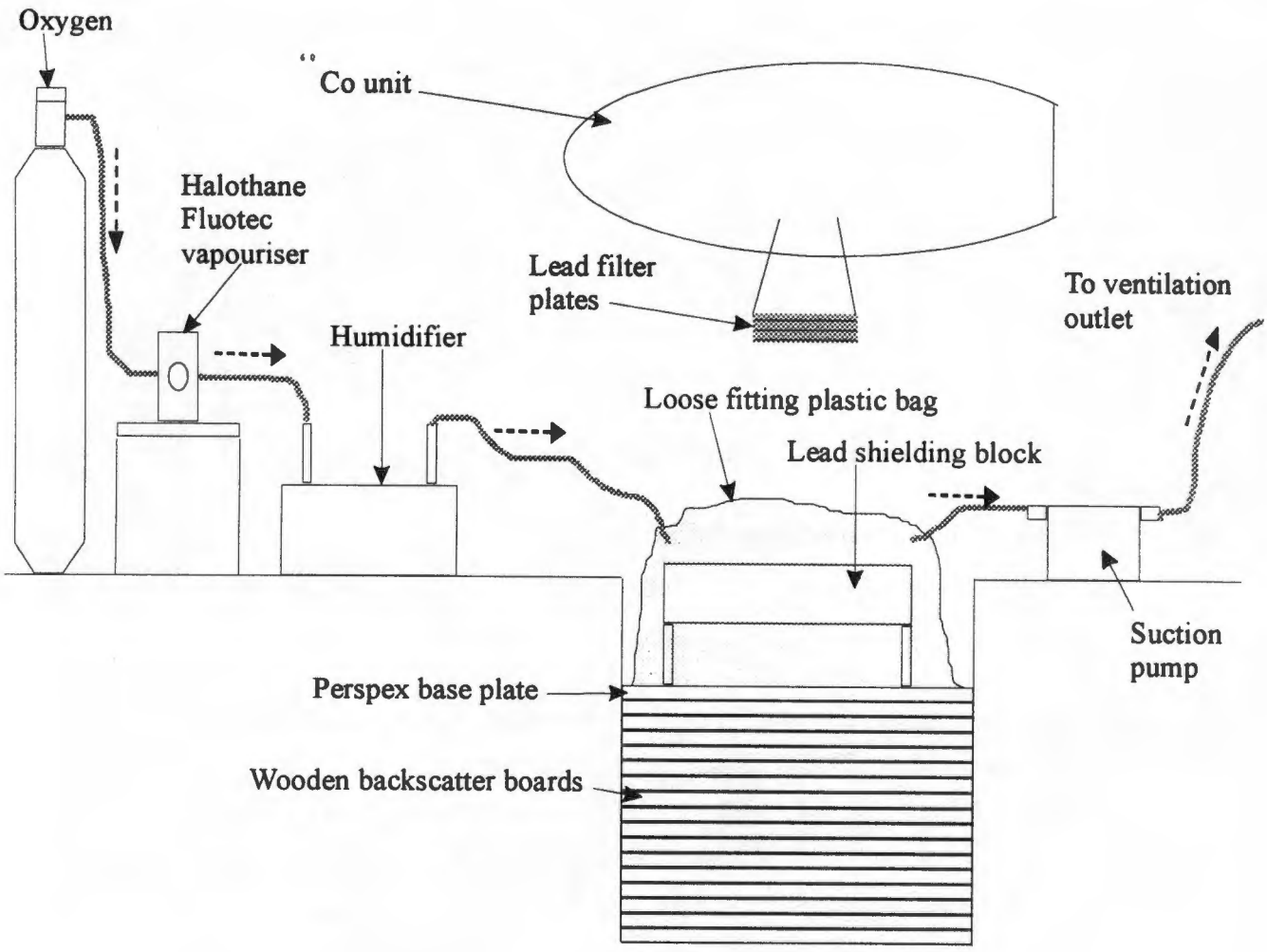

Figure 5.6 Illustration of the set-up for maintenance of anaesthesia and low dose rate irradiation. The dashed arrows indicate the flow of the anaesthetic gas.

5.7 DETERMINATION OF OXYGEN LEVELS UNDER THE PLASTIC DRAPE DURING CONTINUOUS ANAESTHESIA

Prolonged exposure to 100% oxygen may be toxic to the rat. For this reason, experiments were conducted where the rats were anaesthetised and positioned as for irradiation, and the oxygen in the vicinity of the snout (within 7 cm) was monitored using a Marcent (U.S.A.) oxygen monitor.

5.8 RADIATION PROTOCOLS

Irradiation of rat brains was conducted in two series. In both series, irradiations were either fractionated (10 fractions in 12 days) or administered continuously at low dose rates (0.04, 0.05 and 0.07 Gy min^{-1}).

In the first (earlier) series of experiments the total doses administered were found to be too low to yield a range of responses where incidences could be adequately analysed. For this reason the second (later) series of irradiations were performed, when brains were irradiated to a higher total dose.

The experimental radiation protocol is detailed in Table 5.1, which includes information regarding the experimental series.

5.9 PERFUSION OF RATS' BRAINS WITH PHOSPHATE BUFFERED FORMALIN

Anaesthesia was induced in the rats by placing them in a 5 *l* beaker containing 0.5 ml Halothane as described in section 5.6. Perfusion of the rats was performed at one-year post irradiation to the date plus minus seven days. One rat was perfused at a time and the procedures that were adhered to are detailed below. The rat was removed from the beaker and positioned supine on a cork board. All four limbs of the rat were lightly strapped with masking tape to the cork board. This board, together with the rat, was placed into a perspex tray which facilitated collection of the draining blood and perfusion fluid. Anaesthesia was maintained by means of the anaesthetic bag as discussed in section 5.6. An incision was made on the abdomen, beneath the diaphragm, to expose the abdominal muscle layer which was incised to expose the abdominal cavity and viscera. On locating the descending aorta, a fine surgical clamp was applied in close proximity to the diaphragm. Immediately after applying the clamp, the diaphragm was incised exposing the viscera of the thoracic cavity. The heart was located and the left ventricle was catheterised with an 18 gauge Jelco needle and sheath. The needle was then withdrawn and the sheath was attached to a normal saline drip for approximately one minute after which the line was switched to a 10% phosphate buffered formalin solution.

Table 5.1 Experimental protocols used in rat brain irradiation. Experimental series 1 and 2 refer to the earlier and later experiments respectively.

Dose rate (Gy min^{-1})	Total dose (Gy)	Number of rats irradiated	Experimental series	Fraction size (Gy)	Number of fractions
0.04	31	6	1		
	35	6	1		
	39	6	1		
	41	6	1		
	47	6	2		
	57	7	2		
	65	6	2		
0.05	30	6	1		
	34	6	1		
	37	6	1		
	40	6	1		
	47	6	2		
	55	6	2		
	60	6	2		
0.07	30	6	1		
	33	6	1		
	36	6	1		
	38	6	1		
	44	6	2		
	48	6	2		
	57	6	2		
Fractionated 0.50 – 0.75	40	6	1	4.0	10
	47	6	1	4.7	10
	54	6	1	5.4	10
	60	6	1	6.0	10
	64	7	2	6.4	10
	68	6	2	6.8	10
	72	7	2	7.2	10

The bags containing the perfusate were at a height of 1.5 m above the rat. The right atrium of the heart was then incised to provide a drain for the perfusion solution. One litre of perfusate was used for each rat. This procedure resulted in the death of the rat.

On completion of the perfusion the rat's head was severed using a scalpel and the skin and hair were removed. The intact skull was stored in a 10% phosphate buffered formalin solution for one to two months before any attempt was made to remove the brain.

To remove the intact brain, a sagittal cut using a fine hacksaw blade was made in the midline of the skull. Care was taken not to damage the brain when sawing through the skull. The two halves of the skull were pried apart using a pair of fine surgical clamps. The brain was then carefully removed and stored in a 10% phosphate buffered formalin solution for six weeks.

5.10 UNEXPECTED DEATHS

In the experiments, there were instances where some animals died unexpectedly. Upon discovery of a dead rat, an attempt was made to preserve the brain. This proved to be difficult because invariably the rat's body had started to decompose or the other rat in the cage may have eaten it. As these rats could not be perfused, the head was severed, the overlying skin was removed and the intact skull was stored in a 10% phosphate buffered formalin solution. Attempts at removing the intact brain were difficult because the brains were soft and jelly-like. In those rats where the brains were removed, invariably, on attempting to transfer the wax sections to a glass slide by flotation in a water bath, the sections disintegrated. Therefore, histological specimens from the dead animals were not included in the analysis.

5.11 HISTOLOGY

The rats brains were prepared one at a time in order to minimise the imposition of any damage to the gross structure of the brains. At the level of the optic chiasma (Figure 5.2) a coronal section was made by hand with the aid of a razor which resulted in two sections of the rat brain, namely, a frontal and caudal section.

The two sections of the brain were then prepared for further processing. This entailed placing each half into a plastic separator dish and putting it through a dehydration process using a processing machine (Shandon Tissue Processing Machine (Histokinette)) and is described in more detail in the Appendix. The dehydration process entailed soaking the brains in a number of different concentrations of absolute alcohol for varying times. The final soaking was in xylene which completed the dehydration process. On completion of the dehydration process, each half of the brain was placed in a plastic frame and wax was poured to prepare a cutting block. Then, with the aid of a sledge type microtome (Reichert-Jung (Germany)), sections were prepared that were approximately 6 microns thick. The sections were transferred to albuminised microscope slides by flotation in a water bath. These sections were then stained using either the Luxol Blue Cresyl Violet (LBCV) stain or the Luxol Blue Haematoxylin and Eosin (LBHE) stain.

Specific staining for fibrin (Martius Scarlet Blue stain), for calcium deposition (von Kossa's stain) and for gliosis (Glial Fibrillary Acidic Protein (GFAP)) were performed only on a selection of slides due to cost restrictions. The methods for the various staining procedures are detailed in the Appendix.

5.12 SCORING / OBSERVATIONS

The histological observations for the areas of interest were assessed using a Nikon microscope using the 10 by 4 magnification for gross microscopy. For more detailed microscopy, higher levels of magnification was used. The end reaction that was assessed in this study was the incidence of necrosis in any of the structures of interest. The main area of interest was the *fimbria hippocampus* as this was the area of the rat brain that has been investigated by most brain researchers [Calvo et al., 1986, 1987, 1988; Hopewell, 1974, 1987; Hopewell and Cavanagh, 1972; Hopewell and Wright, 1970; Hopewell et al., 1986, 1987; Reinhold and Hopewell, 1980; Reinhold et al., 1984, 1990].

Additional observations were made which included the following areas, namely, *alveus hippocampi*, *capsula interna*, *capsula interna pars retrolenticularis*, choroid plexus, *cingulum*, the ependymal cells, *fasiculus medialis prosencephali*, *gyrus dendatus*, *hippocampus*, *nucleus lateralis*, *nucleus lateralis habenulae*, *nucleus lateralis thalami*, *radiatio corporis callosi*, *stria terminalis*, *sulcus hippocampi*, *truncus corporis callosi* and *ventriculus lateralis*.

5.13 DOSE RESPONSE RELATIONSHIPS

Dose response curves were constructed using incidence data by probit analysis and ED_{50} values were obtained. The ED_{50} value is the dose required to produce a response in 50% of the number of experimental subjects.

CHAPTER 6:

RESULTS

6.1 ANIMAL WEIGHTS

The relative change in the mean weight of untreated (control) rats and those receiving the lowest and highest dose within each experimental group (0.04, 0.05 and 0.07 Gy min^{-1} and 10 fractions in 12 days) for the one year observation period are shown in Figure 6.1.

No significant difference in weight gain was observed between the untreated group, the lowest dose group, and the highest dose group at each of the experimental dose rates. Also, there was no significant difference in weight gain in the rats receiving radiation at the different dose rates.

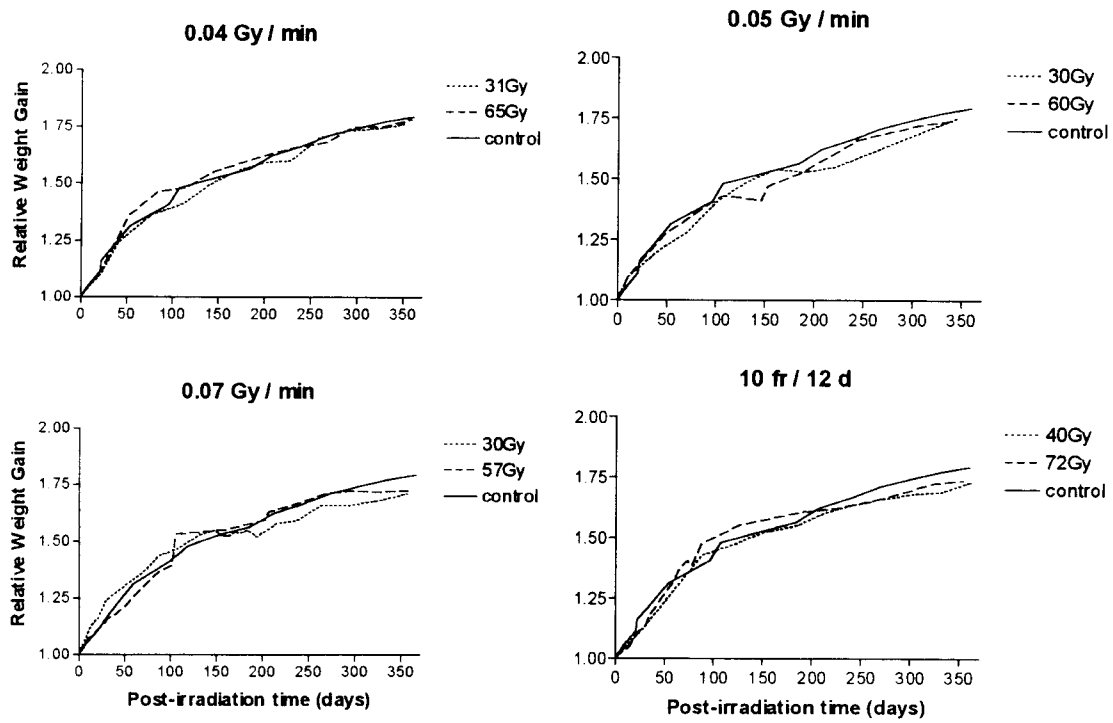

Figure 6.1 Mean weight gain over one year relative to the mean weight at the start of irradiation, for the untreated rats (controls), and those rats receiving the lowest and highest doses in each experiment. The number of rats in the control group and for the various doses of the different dose rate experiments totaled six per group. Only the 72 Gy dose group for the fractionated experiment had seven rats. Error bars are omitted for clarity.

6.2 DOSIMETRY

Dose Uniformity

A cross-plane densitometer plot across the largest axis of the brain irradiation field (obtained from film exposed to ^{60}Co with lead shielding blocks in place) is shown in Figure 6.2. Dose was found to be uniform across the field, with a sharp beam edge as defined by the lead shield.

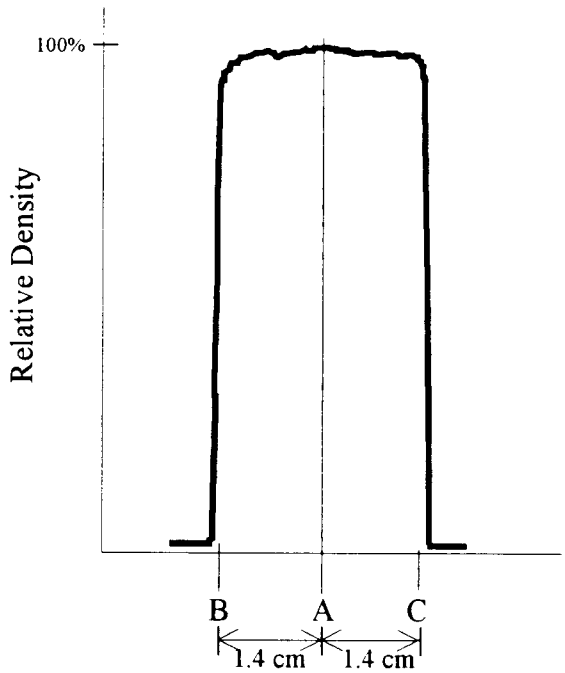

Figure 6.2 Beam profile of brain irradiation field obtained by film densitometry. Points A (centre of radiation field), B and C correspond to those in Figure 5.1.

Dose Measurements - Ionisation chamber

Mean dose rate measurements at the position of the base plate, in a wax rat phantom and in a formalin perfused rat with the ionisation chamber's build-up cap in place is given in Table 6.1. A total of five measurements in each case was made.

Measurements were made in the brain irradiation field as defined by the cut-outs in the lead shielding blocks.

The maximum difference in dose rate between any of the positions was 1%. The measurements as made in the formalin perfused rat were used for all dose calculations.

Table 6.1 Dose rate measurements in rat brain irradiation field.

Position of ionisation chamber	**Dose rate (Gy min^{-1})**
Base Plate	0.593 ± 0
Wax rat phantom	0.595 ± 0
Formalin perfused rat	0.589 ± 0.001

Dosimetry with lead filters

Examples of dose rate measurements made with lead filters in the beam are given in Table 6.2. The thickness of the lead filters was adjusted every six weeks throughout the course of the experiments, and dose rates measured after each adjustment using an ionisation chamber in a perfused rat. The dose rate was not allowed to vary by more than 5% from the nominal dose rates of 0.04, 0.05 and 0.07 Gy min^{-1}.

Table 6.2 Examples of dose rate measurements with lead beam filters.

Dose rate without filter (Gy min^{-1})	**Filter thickness (cm)**	**Dose rate with filter (Gy min^{-1})**
0.528	4.50	0.0384
0.433	3.79	0.0409
0.428	3.94	0.0390
0.539	3.94	0.0491
0.589	4.11	0.0490
0.433	3.80	0.0510
0.550	3.35	0.0695
0.428	2.87	0.0699
0.552	3.58	0.0701

6.3 DETERMINATION OF OXYGEN LEVELS UNDER THE PLASTIC DRAPE DURING CONTINUOUS ANAESTHESIA

The results of one experiment where oxygen was measured are given in Table 6.3. The highest measurement recorded in this experiment was 76.5%. This was in fact the highest oxygen measurement seen in all the experiments.

Table 6.3 Percentage oxygen under the plastic drape during continuous irradiation.

Time (min.)	Oxygen (%)	Time (min.)	Oxygen (%)	Time (min.)	Oxygen (%)
20	68.3	90	66.3	172	61.7
55	65.2	106	64.3	188	72.8
60	66.0	110	67.4	235	76.5
65	66.5	137	70.7	240	59.6
85	61.4	165	70.6	250	56.2

6.4 BEHAVIOURAL CHANGES RESULTING FROM RAT BRAIN IRRADIATION

No frank changes in gait or eating habits were observed over the twelve month post-irradiation observation period.

6.5 HISTOLOGICAL OBSERVATIONS

Histological changes in most of the brain structures examined were noted, with the most severe occurring particularly in those rats receiving the higher radiation doses in each of the dose rate experiments. The nature of the changes were similar in the groups of rats receiving radiation at 0.04, 0.05, 0.07 Gy min^{-1} or 10 fractions in 12 days. However, the incidence of a particular change was variable in each dose group within one dose rate group and between dose rate groups.

The major changes included necrosis, vessel dilation, oedema, the presence of free iron, red blood cell (RBC) congested vessels, haemorrhage, the presence of histiocytes and the presence of free calcium. In the selection of photomicrographs (Figure 6.3 to Figure 6.90) presented below, the abovementioned histological reactions are shown. Less common changes that were observed included disruption of myelin fibres, pyknotic nuclei and hyalinisation in the choroid plexus. These photomicrographs illustrate the increasing severity of the reactions with increasing dose for a particular experiment. The most compromised area was the *fimbria hippocampus* and its surrounding structures.

Low magnification observations

The *fimbria hippocampus* (FH) and its surrounding structures for a control rat brain after one year of observation are shown in Figure 6.3. Of note are the easily discernable structures and the limited presence of dilated vessels especially in the FH. The nuclei tracts of the *hippocampus* (HI), *alveus hippocampi* (AH) and the *sulcus hippocampi* (SH) are also easily observed as well as that of the *gyrus dentatus* (GD). The choroid plexus (CP) and ependymal cells (EC) lining the *ventriculus lateralis* (VL) are also easily discernable. The *radiatio coporis callosi* (RCC), *capsula interna* (CAI), *nucleus lateralis thalami* (NLT) and the *stria terminalis* (ST) are also easily recognised with very few if any dilated vessels present.

An example of the FH and its surrounding structures at a x40 magnification for each dose point in each dose rate experiment are shown in Figures 6.4 to 6.10 for the 0.04 Gy min^{-1} (31 Gy to 65 Gy) experiments, Figures 6.11 to 6.17 for the 0.05 Gy min^{-1} (30 Gy to 60 Gy) experiments, Figures 6.18 to 6.24 for the 0.07 Gy min^{-1} (30 Gy to 57 Gy) experiments, and Figures 6.25 to 6.31 for the 10 fractions in 12 days (40 Gy to 72 Gy) experiments.

Low magnification observations: 0.04 Gy min^{-1} study

Figures 6.4 (31 Gy, x40) to 6.10 (65 Gy, x40) for the 0.04 Gy min^{-1} study show an increase in disruption and destruction of the rat brain tissue as the radiation dose was increased, with the maximum tissue damage occurring at the highest doses of radiation. In general, it is also shown that as the dose of radiation was increased, the number of dilated vessels in all the visible structures also increased. However, there was also a general increase in the diameter of the dilated vessels with increasing radiation dose.

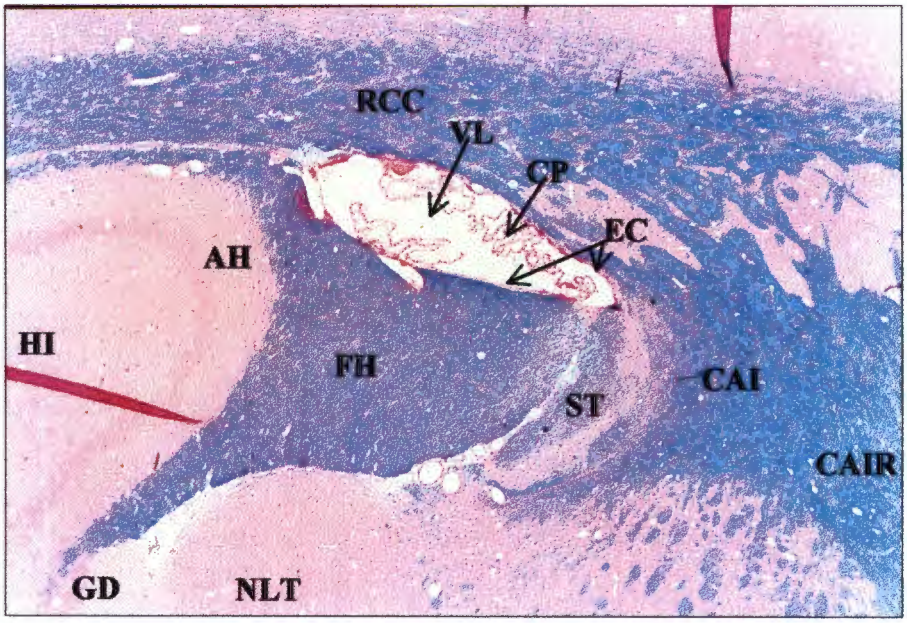

Figure 6.3 The *fimbria hippocampus* (FH) and surrounding structures of a control rat brain after one year of observation. Stained with luxol blue cressyl violet (x40). AH = *alveus hippocampi*, CAI = *capsula interna*, CAIR = *capsula interna pars retrolenticularis*, CP = choroid plexus, EC = ependymal cells, GD = *gyrus dentatus*, HI = *hippocampus*, NLT = *nucleus lateralis thalami*, RCC = *radiatio corporis callosi*, ST = *stria terminalis*, VL = *ventriculus lateralis*.

Figures 6.4 to 6.7 (31 Gy to 41 Gy) represent the first part of the present study in which no frank necrosis was observed in any of the histological areas examined. The area marked 1 in Figure 6.7 does not represent an area of necrosis but rather that of a tissue processing artifact. Figures 6.8 to 6.10 (47 Gy to 65 Gy) represent the second part of this study in which frank necrosis was easily observed. Examples of the observed necrosis are shown for the 57 Gy (Figure 6.9) and the 65 Gy (Figure 6.10) rat brains. Large dilated vessels in the FH, the HI, the NLT and the CAI after a radiation dose of 47 Gy are shown in Figure 6.8. Figure 6.9 (57 Gy) shows the almost complete necrosis of the FH with the necrosis extending into the adjacent AH, ST, CAI and NLT. Free lying red blood cells, indicative of a recent haemorrhage and calcium deposition associated with areas of necrosis are also shown in Figure 6.9. In addition, the nuclei tracts of the HI and AH are not easily distinguished. The brain tissue destruction is most severe in Figure 6.10 (65 Gy) for the 0.04 Gy min^{-1} in that there is complete necrosis of the FH, ST and CAI. The necrosis also extends into the AH and HI. Large dilated vessels are shown in all the observable structures and there is disruption of the nuclei tracts of the AH and HI.

Figure 6.4 The *fimbria hippocampus* and surrounding structures of a rat brain at one year after 31 Gy at 0.04 Gy min^{-1}. Stained with luxol blue haematoxylin and eosin (x40).

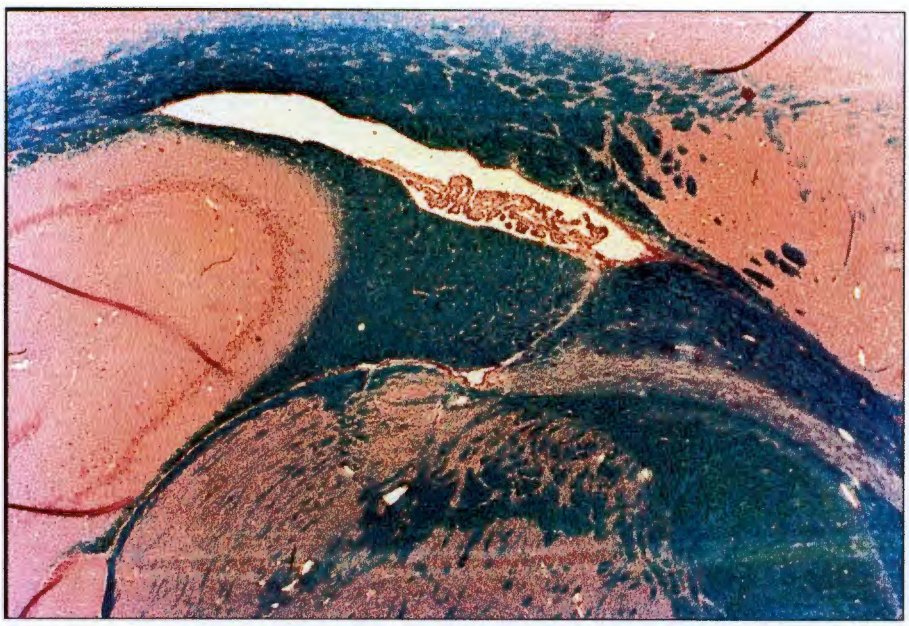

Figure 6.5 The *fimbria hippocampus* and surrounding structures of a rat brain at one year after 35 Gy at 0.04 Gy min^{-1}. Stained with luxol blue haematoxylin and eosin (x40).

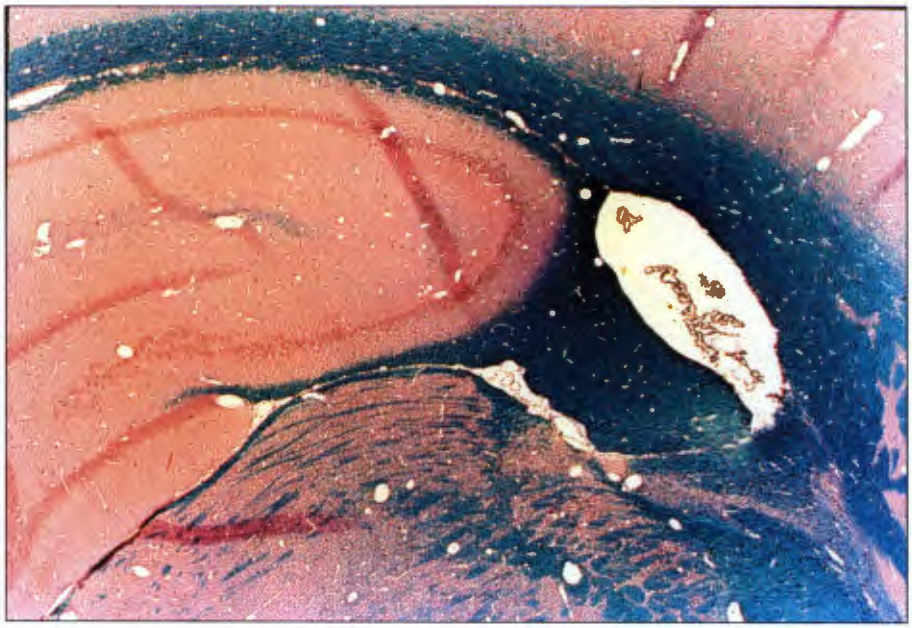

Figure 6.6 The *fimbria hippocampus* and surrounding structures of a rat brain at one year after 39 Gy at 0.04 Gy min^{-1}. Stained with luxol blue haematoxylin and eosin (x40).

Figure 6.7 The *fimbria hippocampus* and surrounding structures of a rat brain at one year after 41 Gy at 0.04 Gy min^{-1}. Stained with luxol blue haematoxylin and eosin (x40).

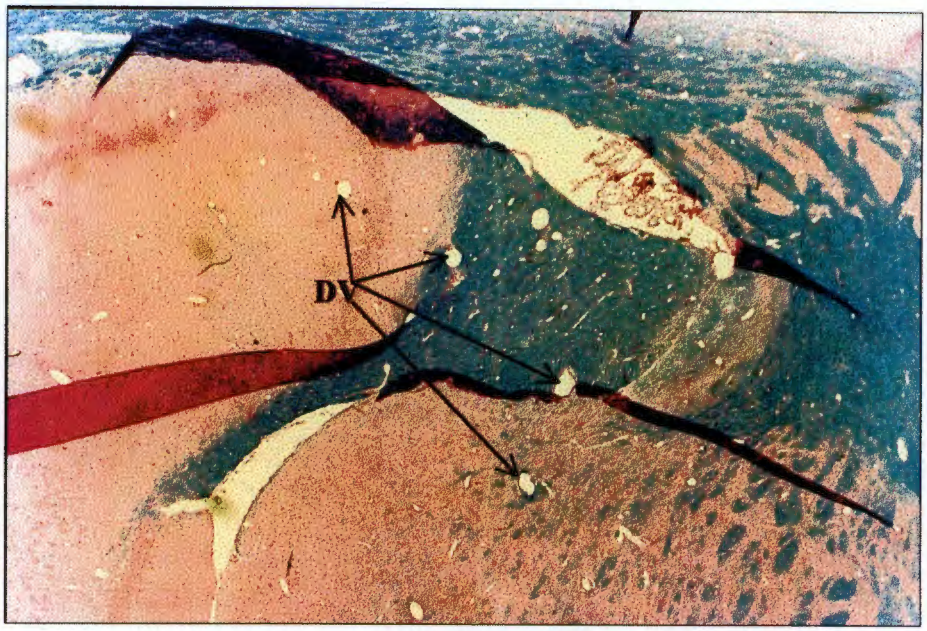

Figure 6.8 The *fimbria hippocampus* and surrounding structures of a rat brain at one year after 47 Gy at 0.04 Gy min^{-1}. Stained with luxol blue haematoxylin and eosin (x40). DV = dilated vessels.

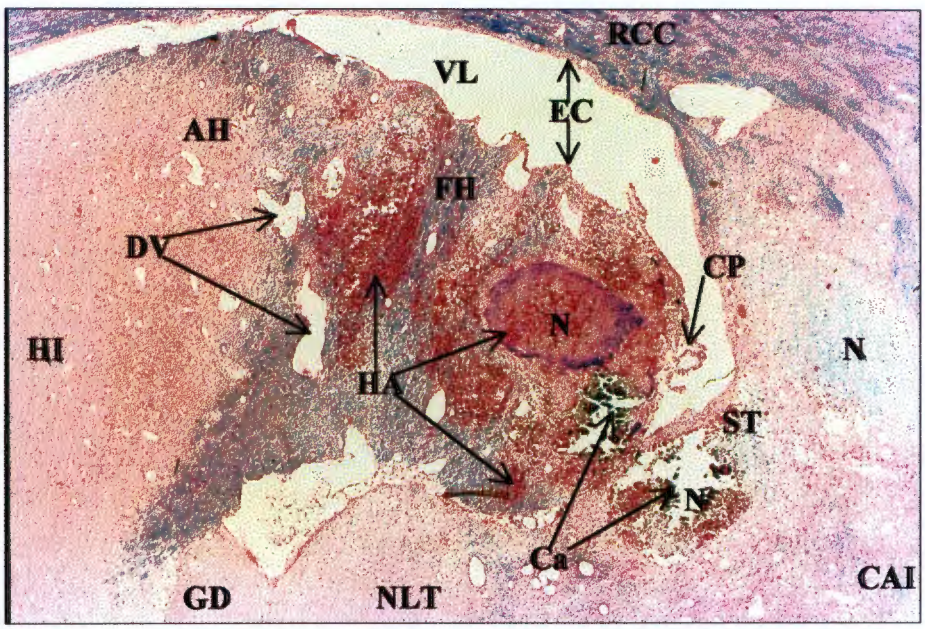

Figure 6.9 The *fimbria hippocampus* (FH) and surrounding structures of a rat brain at one year after 57 Gy at 0.04 Gy min^{-1}. Stained with luxol blue haematoxylin and eosin (x40). AH = *alveus hippocampi*, Ca = calcium deposits, CAI = *capsula interna*, CP = choroid plexus, DV = dilated vessels, EC = ependymal cells, GD = *gyrus dentatus*, HA = haemorrhage, HI = *hippocampus*, N = necrosis, NLT = *nucleus lateralis thalami*, RCC = *radiatio corporis callosi*, ST = *stria terminalis*, VL = *ventriculus lateralis*.

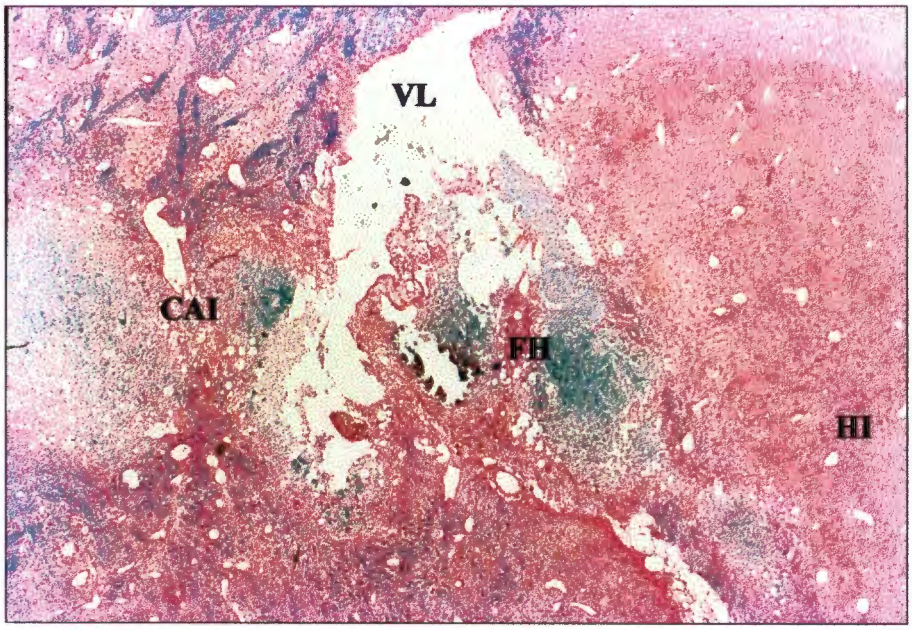

Figure 6.10 The *fimbria hippocampus* (FH) and surrounding structures of a rat brain at one year after 57 Gy at 0.04 Gy min^{-1}. Stained with luxol blue haematoxylin and eosin (x40). CAI = *capsula interna*, HI = *hippocampus*, VL = *ventriculus lateralis*.

Low magnification observations: 0.05 Gy min^{-1} study

Figures 6.11 to 6.14 (30 Gy to 40 Gy) represents the first part of the present study in which no frank necrosis was observed. Figures 6.15 to 6.17 (47 Gy to 60 Gy) represents the second part of this study and frank necrosis was easily observed. For the lower doses of radiation (30 Gy to 40 Gy) in this dose rate study the only reactions that were easily discernable were the dilated vessels. The nuclei of the HI, AH and GD are easily observed and are uniformly distributed throughout the HI. For the higher doses of radiation (47 Gy to 60 Gy) frank necrosis is easily identified and red blood cell congested blood vessels are observed at each of these dose points. An extensive area of haemorrhage is observed in Figure 6.16 (55 Gy) in the *truncus corporis callosi* (TCC) and extends into the HI and *cingulum* (C). The CP is not easily discernable in Figures 6.15 to 6.17 as it appears to be part of the necrotic debris and has dilated vessels and hyalinisation. Again, as for the 0.04 Gy min^{-1} study, the necrosis becomes more destructive and extensive with the increase in the dose of radiation.

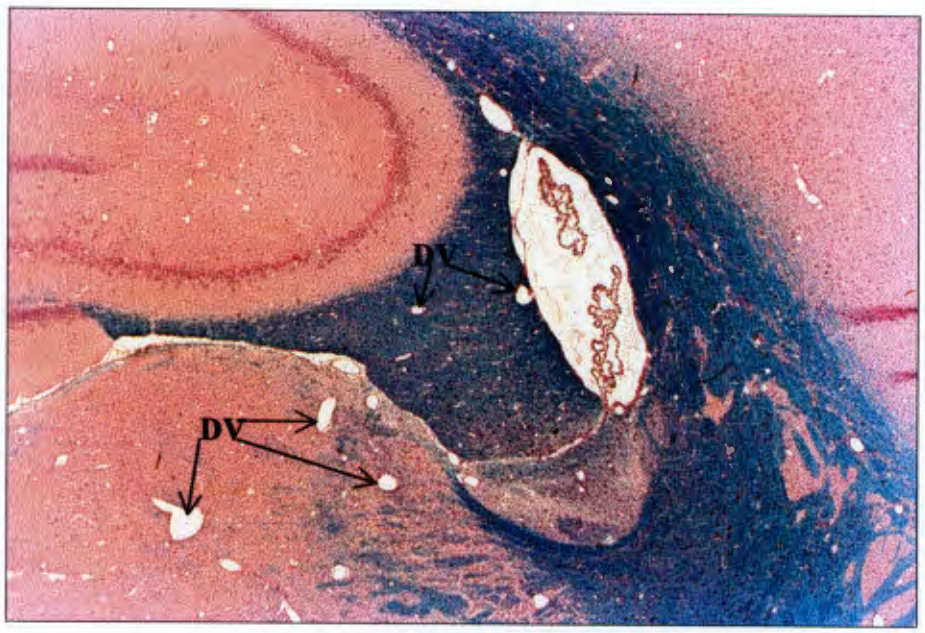

Figure 6.11 The *fimbria hippocampus* and surrounding structures of a rat brain at one year after 30 Gy at 0.05 Gy min^{-1}. Stained with luxol blue haematoxylin and eosin (x40). DV = dilated vessels.

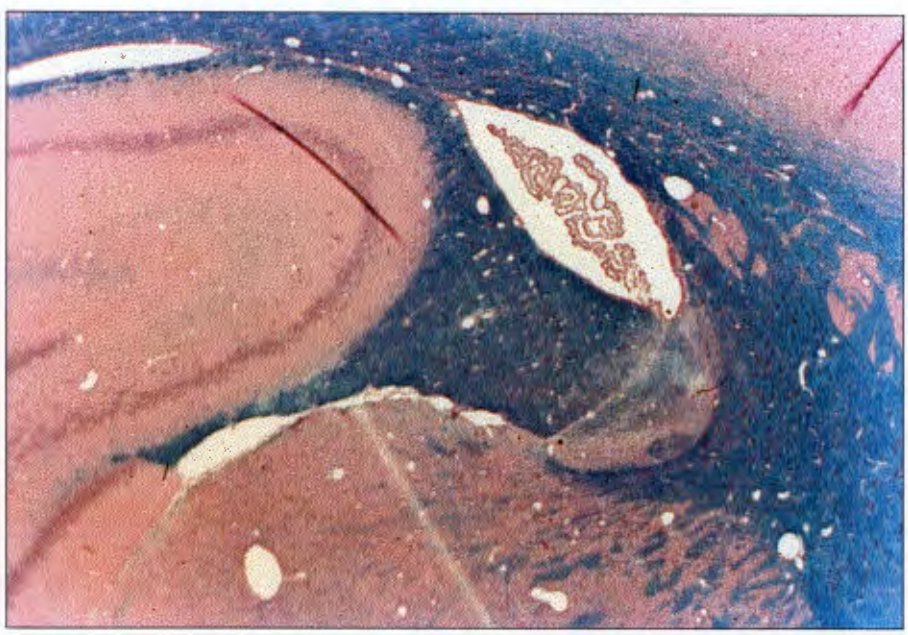

Figure 6.12 The *fimbria hippocampus* and surrounding structures of a rat brain at one year after 34 Gy at 0.05 Gy min^{-1}. Stained with luxol blue haematoxylin and eosin (x40).

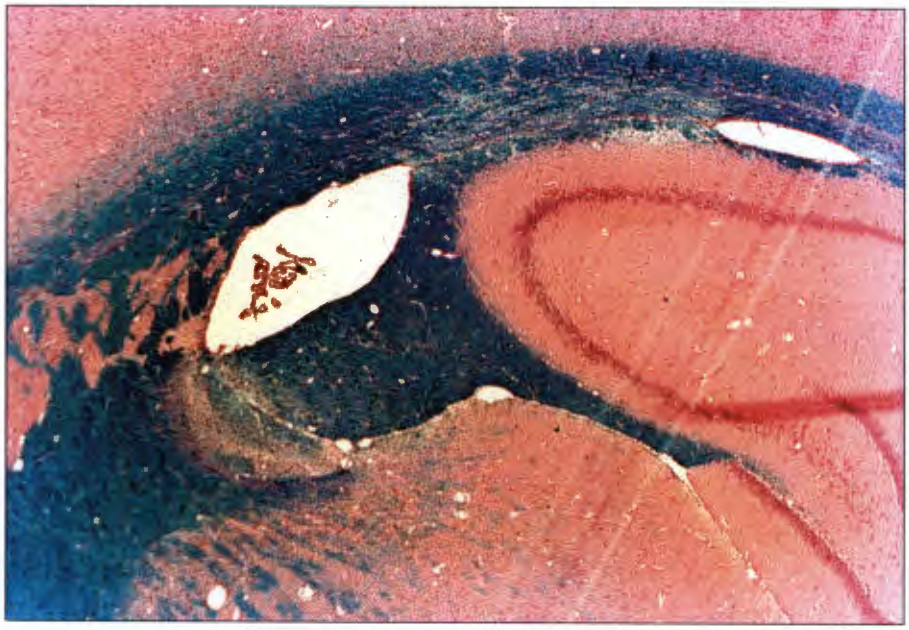

Figure 6.13 The *fimbria hippocampus* and surrounding structures of a rat brain at one year after 37 Gy at 0.05 Gy min^{-1}. Stained with luxol blue haematoxylin and eosin (x40).

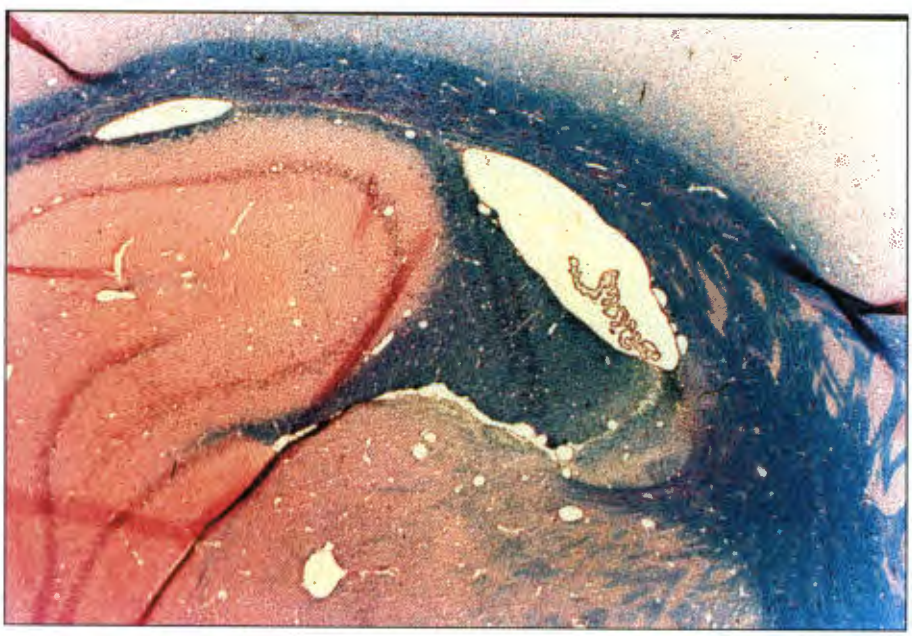

Figure 6.14 The *fimbria hippocampus* and surrounding structures of a rat brain at one year after 40 Gy at 0.05 Gy min^{-1}. Stained with luxol blue haematoxylin and eosin (x40).

Figure 6.15 The *fimbria hippocampus* and surrounding structures of a rat brain at one year after 47 Gy at 0.05 Gy min^{-1}. Stained with luxol blue haematoxylin and eosin (x40). N = necrosis, RBC = red blood cell congested vessels.

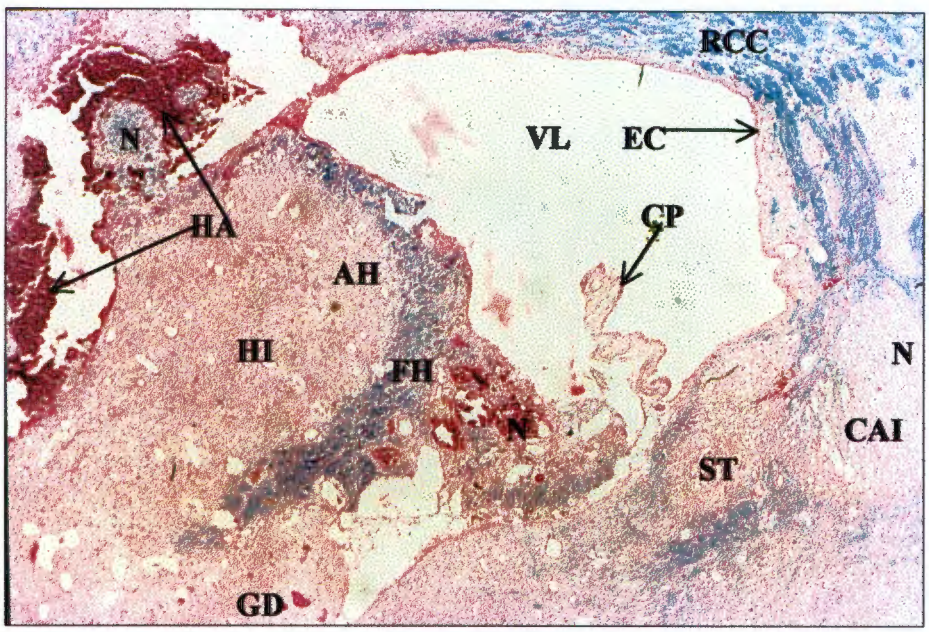

Figure 6.16 The *fimbria hippocampus* (FH) and surrounding structures of a rat brain at one year after 55 Gy at 0.05 Gy min^{-1}. Stained with luxol blue haematoxylin and eosin (x40). AH = *alveus hippocampi*, CAI = *capsula interna*, CP = choroid plexux, EC = ependymal cells, GD = *gyrus dentatus*, HA = haemorrhage, HI = hippocampus, N = necrosis, RCC = *radiatio corporis callosi*, ST = *stria terminalis*, VL = *ventriculus lateralis*.

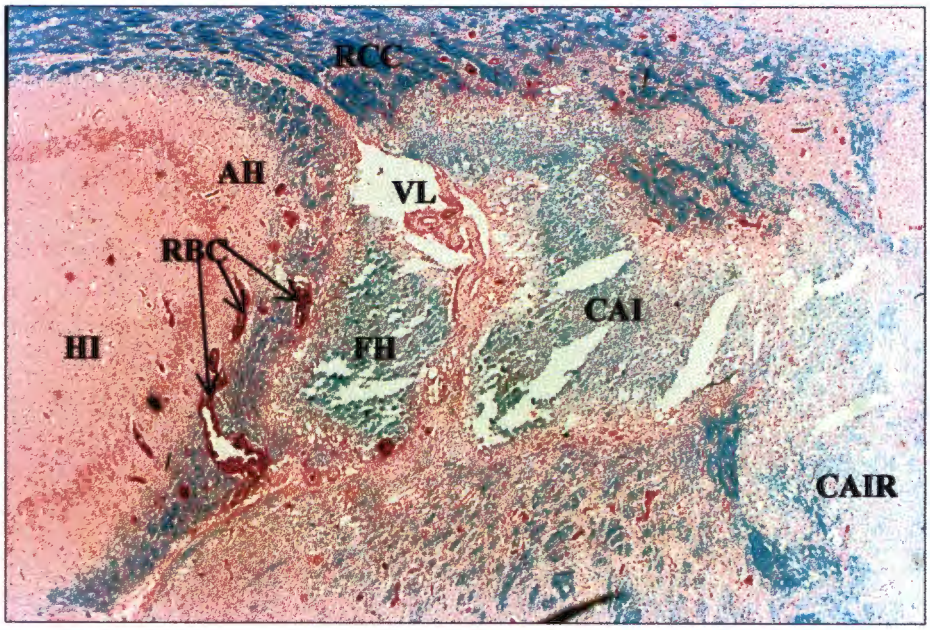

Figure 6.17 The *fimbria hippocampus* (FH) and surrounding structures of a rat brain at one year after 60 Gy at 0.05 Gy min^{-1}. Stained with luxol blue haematoxylin and eosin (x40). AH = *alveus hippocampi*, CAI = *capsula interna*, CAIR = *capsula interna pars retrolenticularis*, HI = hippocampus, RBC = red blood cell congested vessels, RCC = *radiatio corporis callosi*, VL = *ventriculus lateralis*.

Low magnification observations: 0.07 Gy min^{-1} study

Figures 6.18 to 6.21 (30 Gy to 38 Gy) are representative of the first part of this study and no necrosis observed at any of these dose points. Dilated vessels of varying diameter are observed in these figures and in general, the various histological areas of the brain are easily recognised. The nuclei tracts of the HI, AH and GD are distinct. Figures 6.22 to 6.24 (44 Gy to 57 Gy) are representative of the second part of this study and frank necrosis is observed at the higher dose points. The FH can still be distinguished in Figure 6.23 (48 Gy) even though necrosis is present. The necrosis extends into the ST, CAI and the *capsula interna pars retrolenticularis* (CAIR). Areas of calcium deposition in the necrotic areas are also observed in Figure 6.23. Figure 6.24 (57 Gy) shows complete necrosis of the FH, ST and CAI. The necrosis also extends into the AH and HI. An area of haemorrhage in the HI is also shown in Figure 6.24.

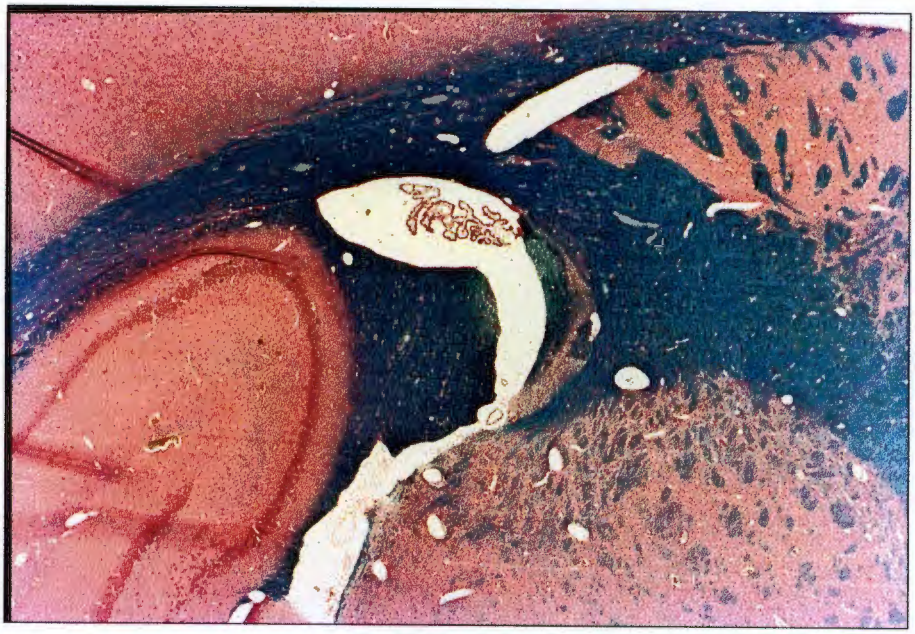

Figure 6.18 The *fimbria hippocampus* and surrounding structures of a rat brain at one year after 30 Gy at 0.07 Gy min^{-1}. Stained with luxol blue haematoxylin and eosin (x40).

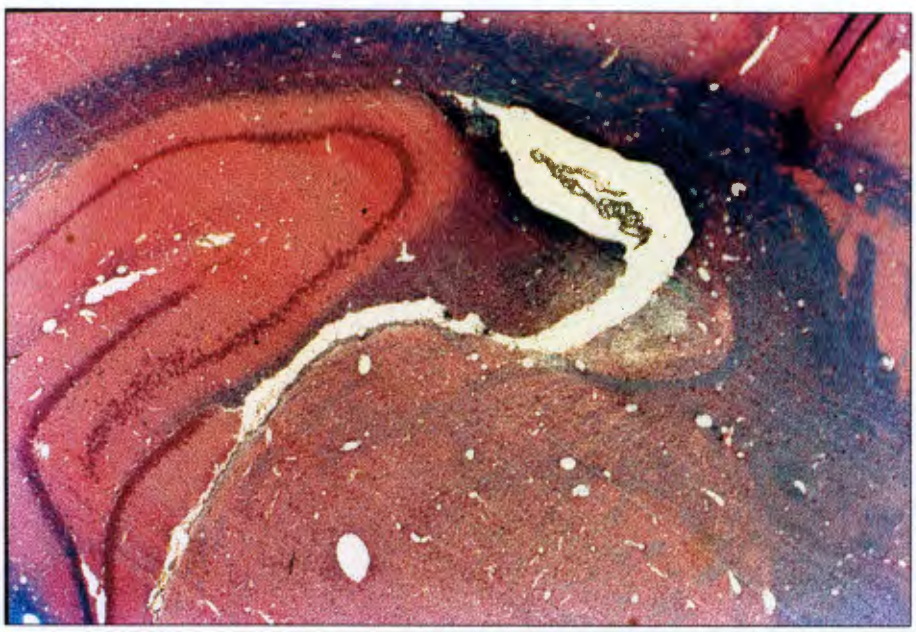

Figure 6.19 The *fimbria hippocampus* and surrounding structures of a rat brain at one year after 33 Gy at 0.07 Gy min^{-1}. Stained with luxol blue haematoxylin and eosin (x40).

Figure 6.20 The *fimbria hippocampus* and surrounding structures of a rat brain at one year after 36 Gy at 0.07 Gy min^{-1}. Stained with luxol blue haematoxylin and eosin (x40).

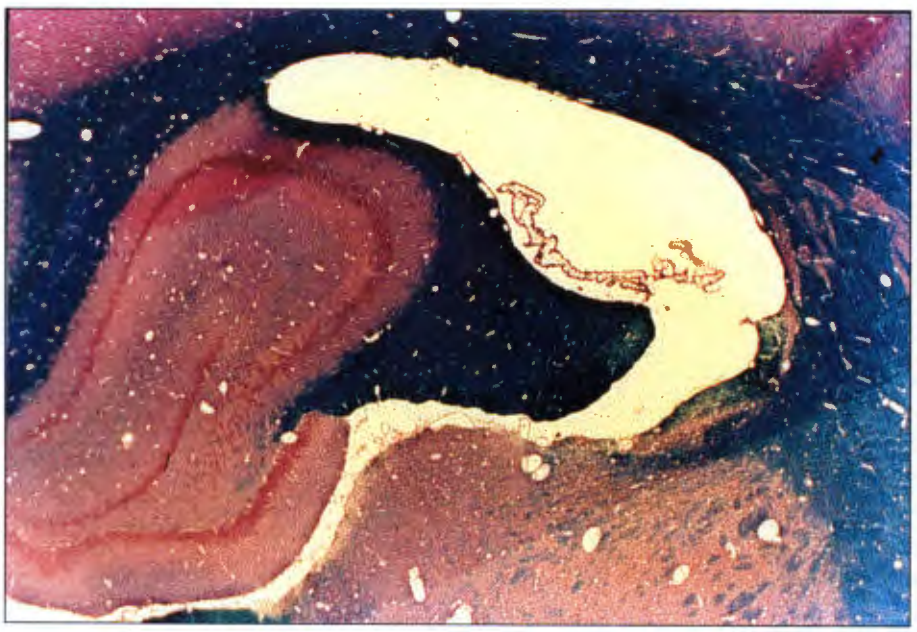

Figure 6.21 The *fimbria hippocampus* and surrounding structures of a rat brain at one year after 38 Gy at 0.07 Gy min^{-1}. Stained with luxol blue haematoxylin and eosin (x40).

Figure 6.22 The *fimbria hippocampus* and surrounding structures of a rat brain at one year after 44 Gy at 0.07 Gy min^{-1}. Stained with luxol blue haematoxylin and eosin (x40).

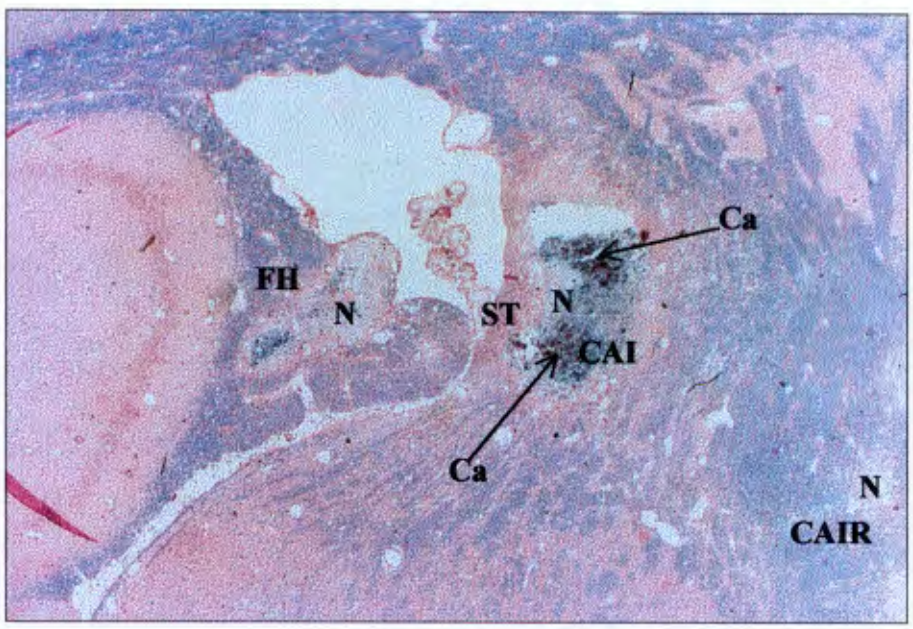

Figure 6.23 The *fimbria hippocampus* (FH) and surrounding structures of a rat brain at one year after 48 Gy at 0.07 Gy min^{-1}. Stained with luxol blue haematoxylin and eosin (x40). Ca = calcium deposition, CAI = *capsula interna*, CAIR = *capsula interna pars retrolenticularis*, N = necrosis, ST = *stria terminalis*.

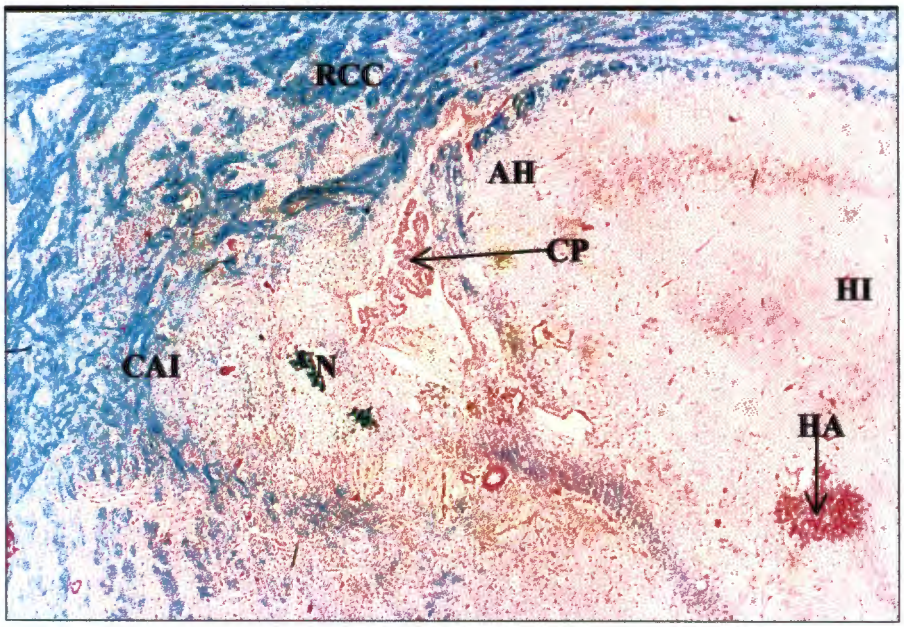

Figure 6.24 The *fimbria hippocampus* and surrounding structures of a rat brain at one year after 57 Gy at 0.07 Gy min^{-1}. Stained with luxol blue haematoxylin and eosin (x40). AH = *alveus hippocampi*, CAI = *capsula interna*, CP = choroid plexus, HA = haemorrhage, HI = *hippocampus*, N = necrosis, RCC = *radiatio corporis callosi*.

Low magnification observations: Fractionated study (10 fractions in 12 days)

Figures 6.25 to 6.28 (40 Gy to 60 Gy) represents the first part of this study and as mentioned earlier for each low dose rate experiment, no necrosis was observed at any dose point. Dilated vessels of varying diameter with no disruption of any histological structures are shown in Figures 6.25 to 6.28. Figures 6.29 to 6.31 (64 Gy to 72 Gy) representative of the second part of this study, display necrosis and tissue destruction which for the highest radiation doses extends from the FH to include the ST, CAI, CAIR, HI and AH. In Figure 6.31 (72 Gy) the tissue destruction is such that the nuclei tracts of the HI and AH are completely disrupted. The CP in Figures 6.30 (68 Gy) and 6.31 (72 Gy) appear to be part of or attached to the necrotic debris.

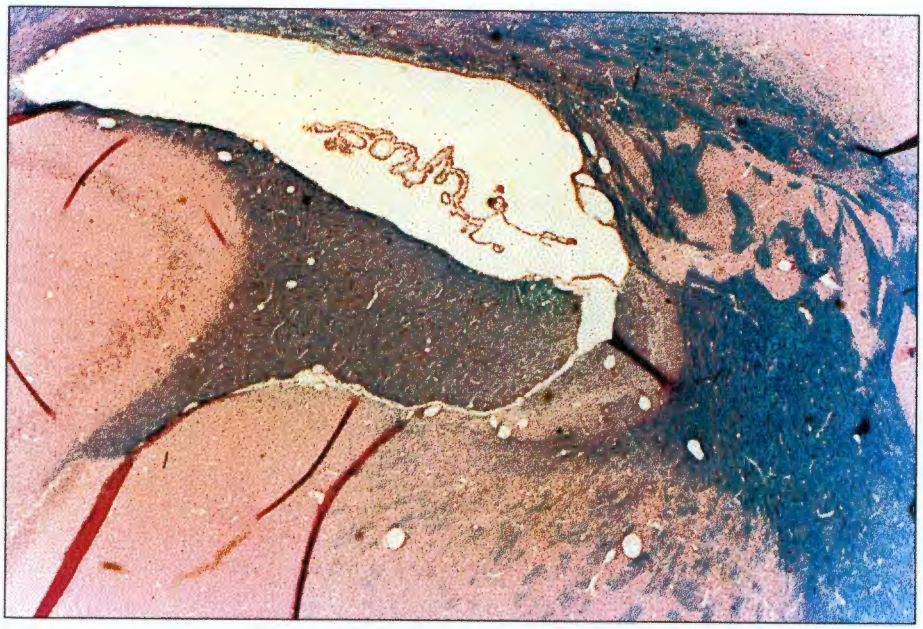

Figure 6.25 The *fimbria hippocampus* and surrounding structures of a rat brain at one year after 40 Gy (10 fractions in 12 days). Stained with luxol blue haematoxylin and eosin (x40).

Figure 6.26 The *fimbria hippocampus* and surrounding structures of a rat brain at one year after 47 Gy (10 fractions in 12 days). Stained with luxol blue haematoxylin and eosin (x40).

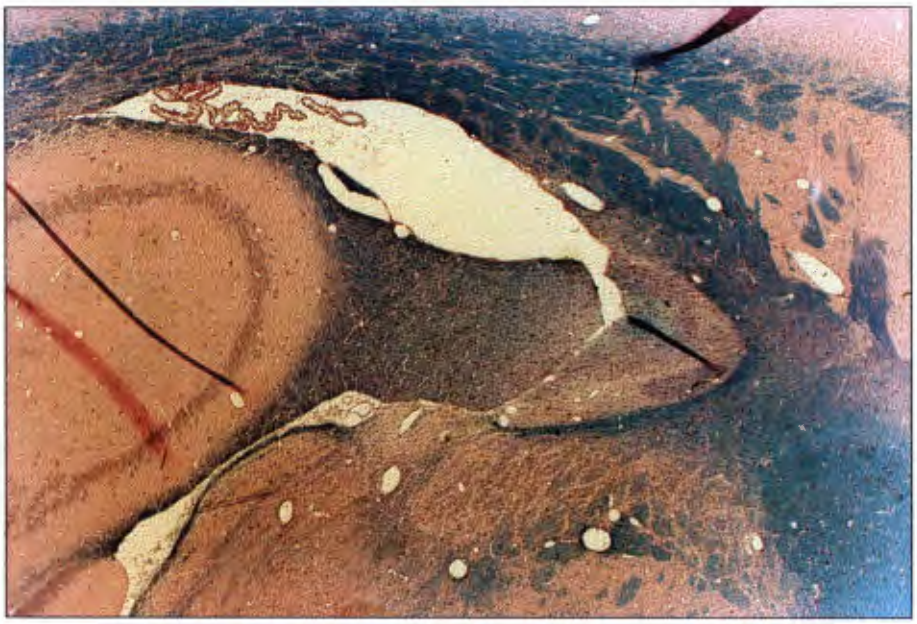

Figure 6.27 The *fimbria hippocampus* and surrounding structures of a rat brain at one year after 54 Gy (10 fractions in 12 days). Stained with luxol blue haematoxylin and eosin (x40).

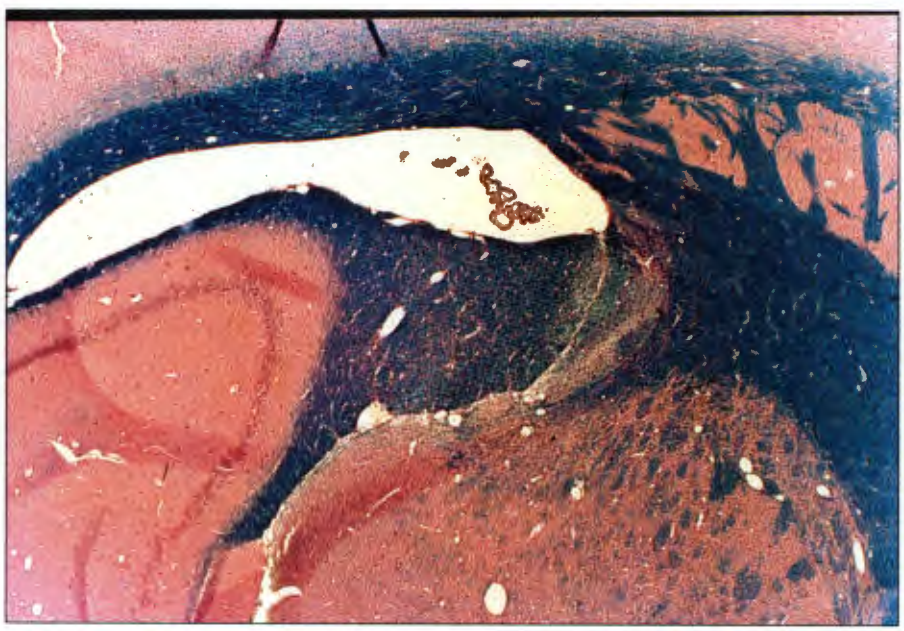

Figure 6.28 The *fimbria hippocampus* and surrounding structures of a rat brain at one year after 60 Gy (10 fractions in 12 days). Stained with luxol blue haematoxylin and eosin (x40).

Figure 6.29 The *fimbria hippocampus* and surrounding structures of a rat brain at one year after 64 Gy (10 fractions in 12 days). Stained with luxol blue haematoxylin and eosin (x40). N = necrosis.

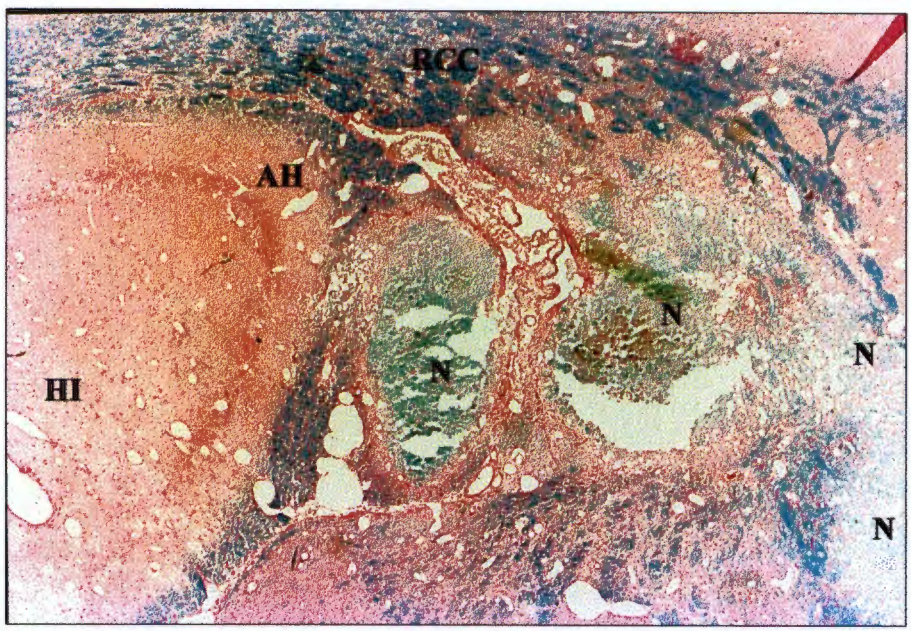

Figure 6.30 The *fimbria hippocampus* and surrounding structures of a rat brain at one year after 68 Gy (10 fractions in 12 days). Stained with luxol blue haematoxylin and eosin (x40). AH = *alveus hippocampi*, HI = hippocampus, N = necrosis, RCC = *radiatio corporis callosi*.

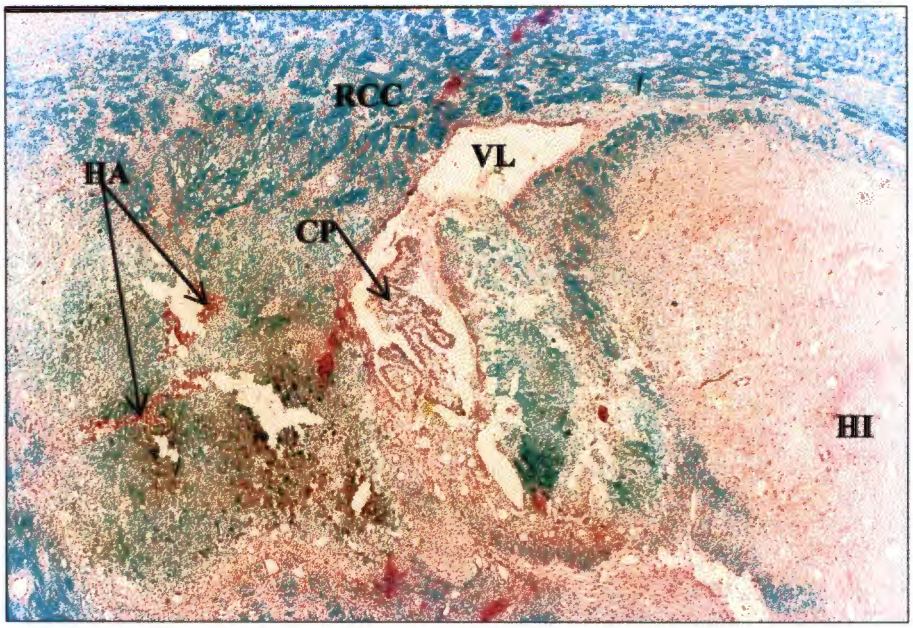

Figure 6.31 The *fimbria hippocampus* and surrounding structures of a rat brain at one year after 72 Gy (10 fractions in 12 days). Stained with luxol blue haematoxylin and eosin (x40). CP = choroid plexus, HA = haemorrhage, HI = hippocampus, RCC = *radiatio corporis callosi*, VL = *ventriculus lateralis*.

Observations at other magnifications

The FH and ST of a control rat brain at one year are shown in Figures 6.32 and 6.33 respectively. Of note is the uniform distribution of nuclei in both structures and the presence of small dilated vessels in the ST.

Numerous small dilated vessels and a few large dilated vessels are evident in the FH, ST and CAI in Figure 6.34 (47 Gy at 0.04 Gy min^{-1}). Large dilated vessels are observed in the CP. No disruption of fibres in any of the histological areas is observed other than a focus of oedema in the FH.

Figure 6.35 (47 Gy at 0.05 Gy min^{-1}) shows the partial destruction of the FH as a result of necrosis and large dilated vessels scattered throughout the FH and ST. The nuclei of the ST and FH are not uniformly distributed and the necrotic area is devoid of nuclei.

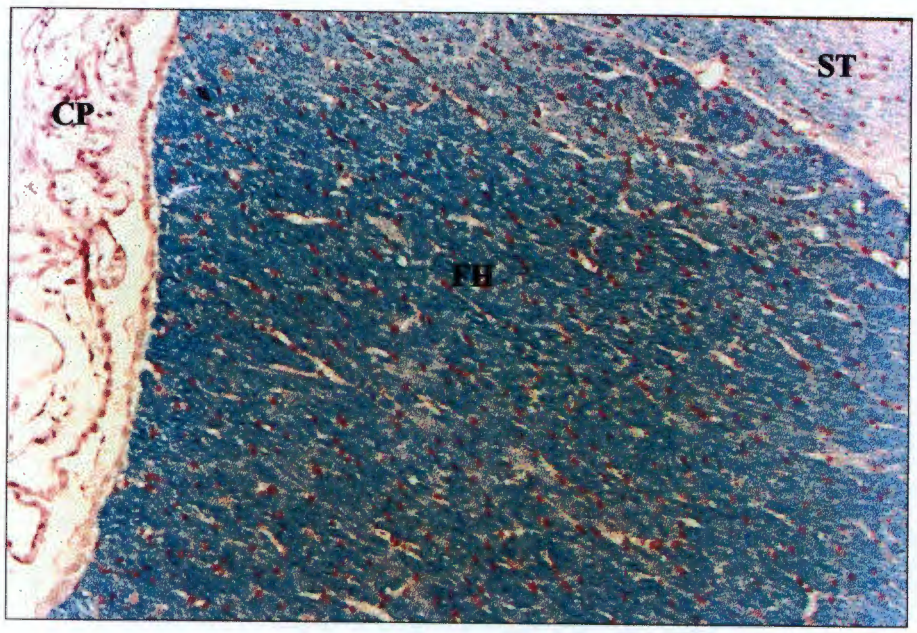

Figure 6.32 The *fimbria hippocampus*(FH) of a control rat brain after one year of observation. Stained with luxol blue haematoxylin and eosin (x250). CP = choroid plexus, ST = *stria terminalis*.

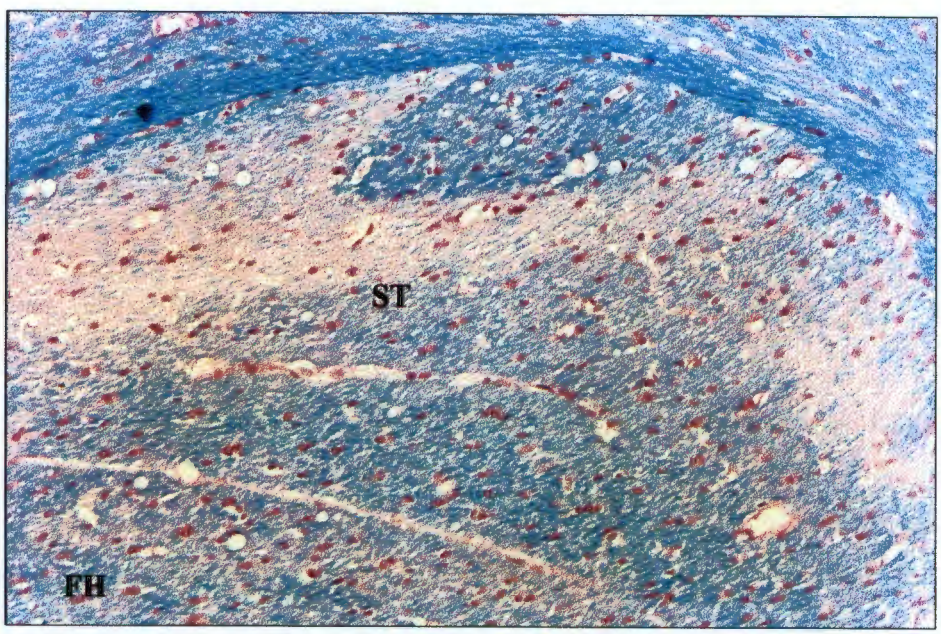

Figure 6.33 The *stria terminalis* (ST) of a control rat brain after one year of observation. Stained with luxol blue haematoxylin and eosin (x250). FH = *fimbria hippocampus*.

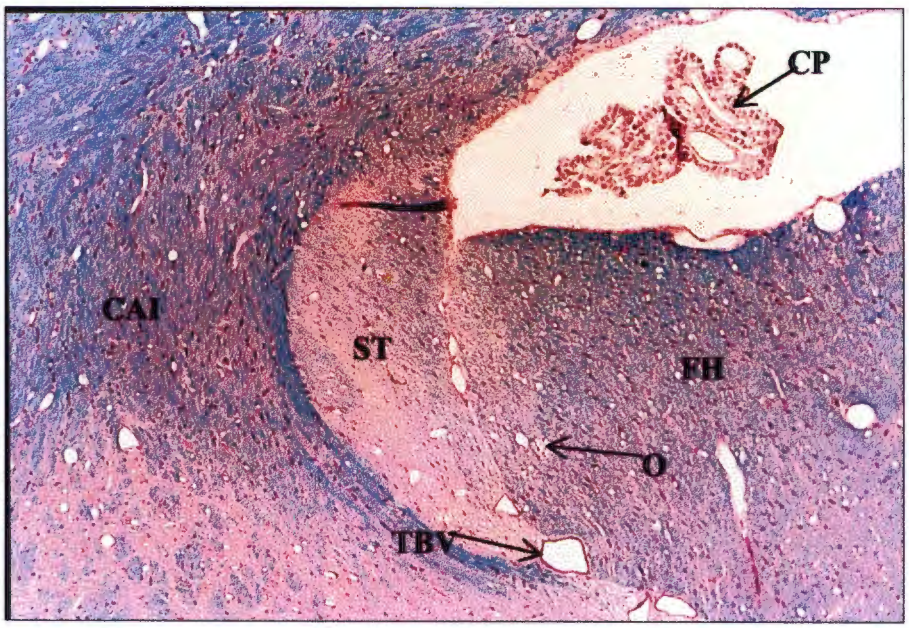

Figure 6.34 The *fimbria hippocampus* (FH) and surrounding structures of a rat brain at one year after 47 Gy at 0.04 Gy min^{-1}. Stained with luxol blue haematoxylin and eosin (x80). CAI = *capsula interna*, CP = choroid plexus, O = foci of oedema, ST = *stria terminalis*, TBV = thickened blood vessel wall.

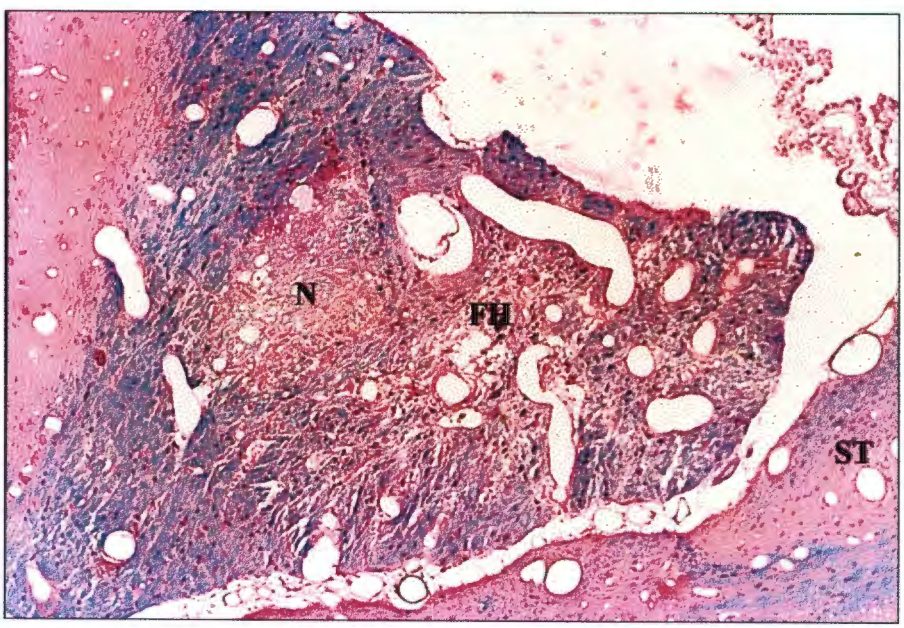

Figure 6.35 The *fimbria hippocampus* (FH) and surrounding structures of a rat brain at one year after 47 Gy at 0.05 Gy min^{-1}. Stained with luxol blue haematoxylin and eosin (x80). N = necrosis, ST = *stria terminalis*.

Figure 6.36 (55 Gy at 0.05 Gy min^{-1}) shows the complete necrosis of the FH and the necrosis extending into the ST, CAI, AH and the HI. Dilated vessels of varying diameter are distributed throughout the tissue including the CP and disruption of the nuclei tracts of the AH and HI are also shown. Figure 6.37 (55 Gy at 0.05 Gy min^{-1}) also shows complete necrosis and large areas of haemorrhages in the FH. Large dilated vessels congested with red blood cells are also observed. Free iron deposits are also observed and the cells constituting the ependymal cells (EC) and the CP are not easily distinguished.

Figure 6.38 (60 Gy at 0.05 Gy min^{-1}) shows the complete necrosis of the FH extending into the ST, CAI and AH. Large dilated vessels are observed in the CP, ST, CAI and NLT. Histiocytes in the FH are shown in Figure 6.39 (60 Gy at 0.05 Gy min^{-1}).

Figure 6.40 (44 Gy at 0.07 Gy min^{-1}) shows the partial necrosis of the FH and large dilated vessels in both the FH and ST.

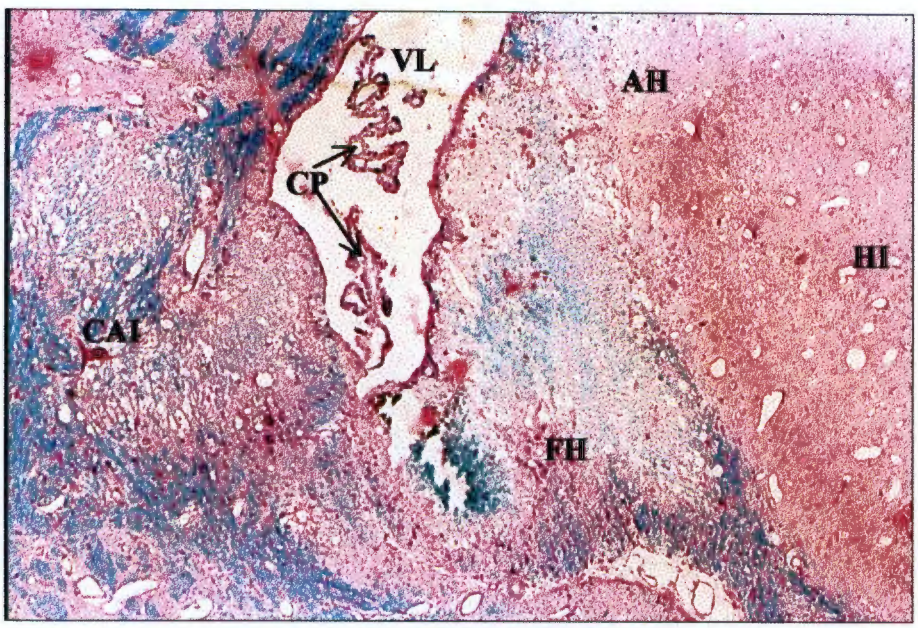

Figure 6.36 The *fimbria hippocampus* (FH) and surrounding structures of a rat brain at one year after 55 Gy given at 0.05 Gy min^{-1}. Stained with luxol blue haematoxylin and eosin (x51). AH = *alveus hippocampi*, CAI = *capsula interna*, CP = choroid plexus, HI = *hippocampus*, VL = *ventriculus lateralis*.

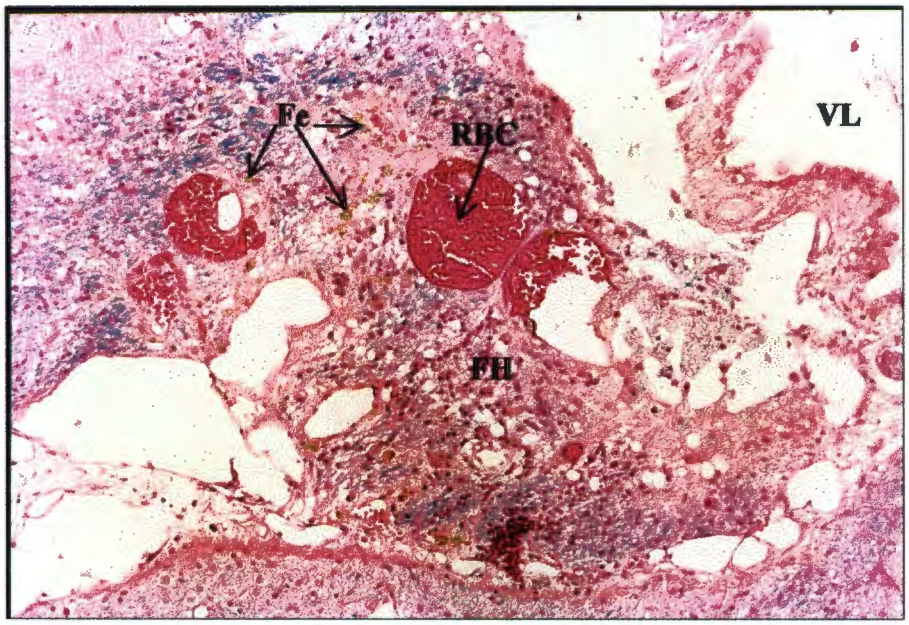

Figure 6.37 The *fimbria hippocampus* (FH) and surrounding structures of a rat brain after 55 Gy given at 0.05 Gy min^{-1}. Stained with luxol blue haematoxylin and eosin (x295). Fe = iron deposits, RBC = red blood cell congested vessels, VL = *ventriculus lateralis*.

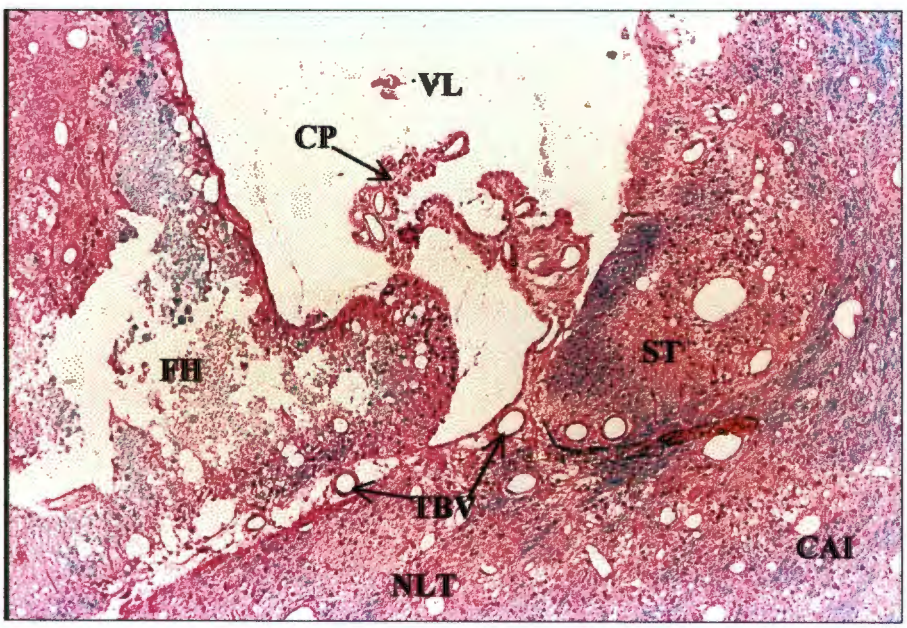

Figure 6.38 The *fimbria hippocampus* (FH) and surrounding structures of a rat brain after 60 Gy given at 0.05 Gy min^{-1}. Stained with luxol blue haematoxylin and eosin (x80). CAI = *capsula interna*, CP = choroid plexus, NLT = *nucleus lateralis thalami*, ST = *stria terminalis*, TBV = thickened blood vessel wall, VL = *ventriculus lateralis*.

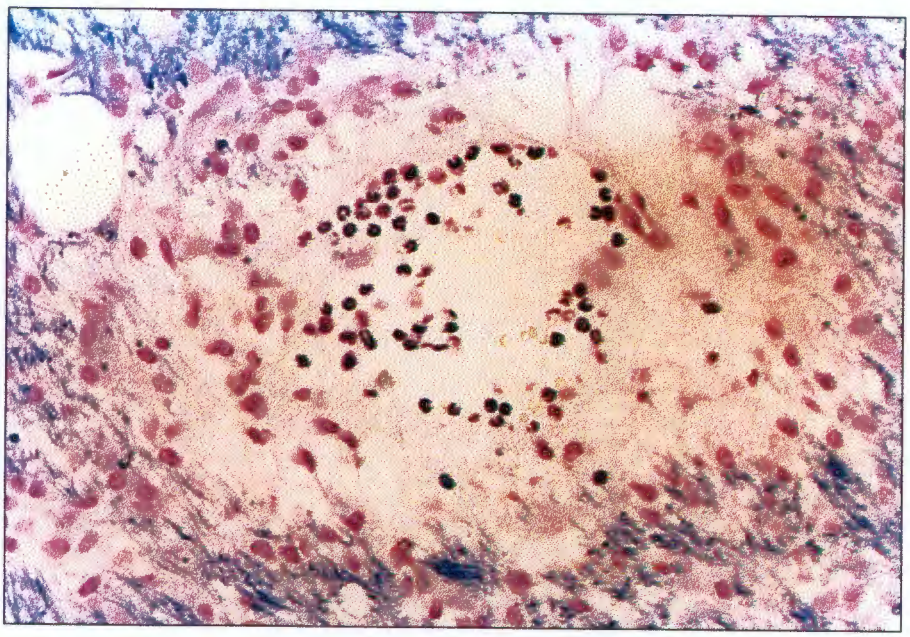

Figure 6.39 Histiocytes in the *fimbria hippocampus* of a rat brain at one year after 60 Gy given at 0.05 Gy min^{-1}. Stained with luxol blue haematoxylin and eosin (x200).

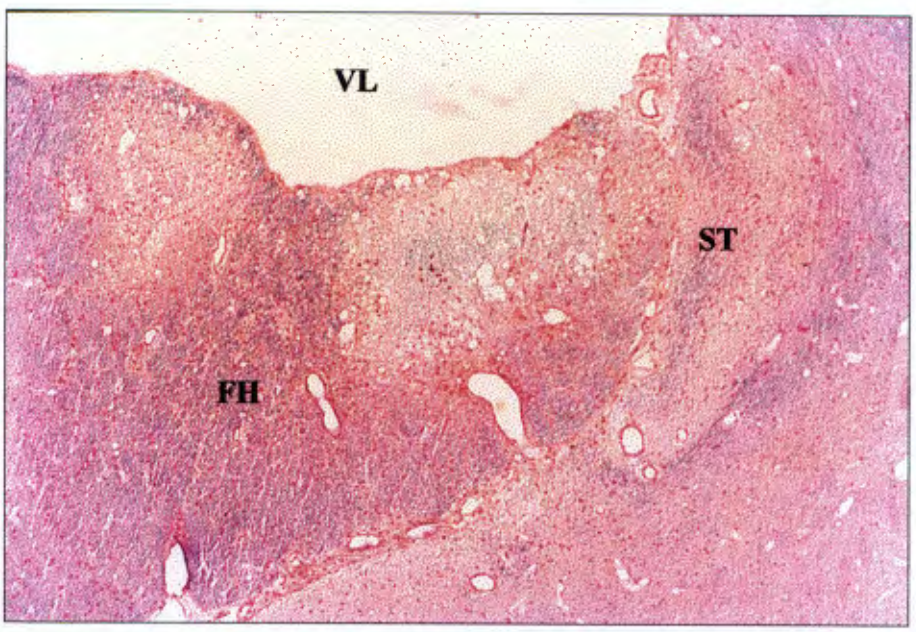

Figure 6.40 The *fimbria hippocampus* (FH) and surrounding structures of a rat brain at one year after 44 Gy given at 0.07 Gy min^{-1}. Stained with luxol blue haematoxylin and eosin (x68). ST = *stria terminalis*, VL = *ventriculus lateralis*.

Figure 6.41 shows necrosis of the FH, ST and CAI. Calcium deposition in the necrotic areas and hyalinisation in the CP is also shown. Figure 6.42 (48 Gy at 0.07 Gy min^{-1}) shows an extensive area of haemorrhage which encompasses the entire HI, AH, GD and VL. The aforementioned structures, including the CP, are not easily distinguished.

Figure 6.43 (57 Gy at 0.07 Gy min^{-1}) shows complete necrosis of the FH, ST and CAI with extension into the HI. Large dilated vessels are present throughout the tissue and a focus of haemorrhage is present at the AH–FH border. The CP shows hyalinisation and appears to be attached to the necrotic area of the FH.

Figure 6.44 (64 Gy in 10 fractions and 12 days) shows the partial necrosis of the FH with the necrosis extending into the ST and CAI. Red blood cell congested vessels are shown in the CAI, CP and AH. The nuclei tracts of the HI and AH are not easily distinguished.

Figure 6.45 (68 Gy in 10 fractions and 12 days) shows necrosis of the FH, ST and CAI. Disruption of the nuclei tracts of the AH are also shown. Large dilated vessels are distributed throughout the tissue and the CP is not discernable. The EC are not continuous and are disrupted by the large areas of necrosis.

Figure 6.46 (72 Gy in 10 fractions and 12 days) shows the complete destruction of the FH, ST and CAI as a result of necrosis. The CP shows hyalinisation and appears to be attached to the large necrotic area. Disruption of the EC lining the VL is also shown in a number of areas. Calcium deposits and haemorrhage in the necrotic areas are also shown.

Figure 6.47 shows the CAI of a control rat brain. The distribution of the fibre 'bundles' and that of the nuclei is distinctive for the CAI. Few small dilated vessels are shown.

Figure 6.48 (47 Gy at 0.04 Gy min^{-1}) shows a focus of oedema in the CAI. Dilated vessels of varying diameter are shown and the distribution of nuclei and that of the fibre 'bundles' are no different from that of a control rat brain as shown in Figure 6.47. Figure 6.49 (64 Gy in 10 fractions and 12 days) shows an area of necrosis in the CAI and the presence of red blood cell congested vessels. The CP appears to be adhering to the necrotic areas of the FH.

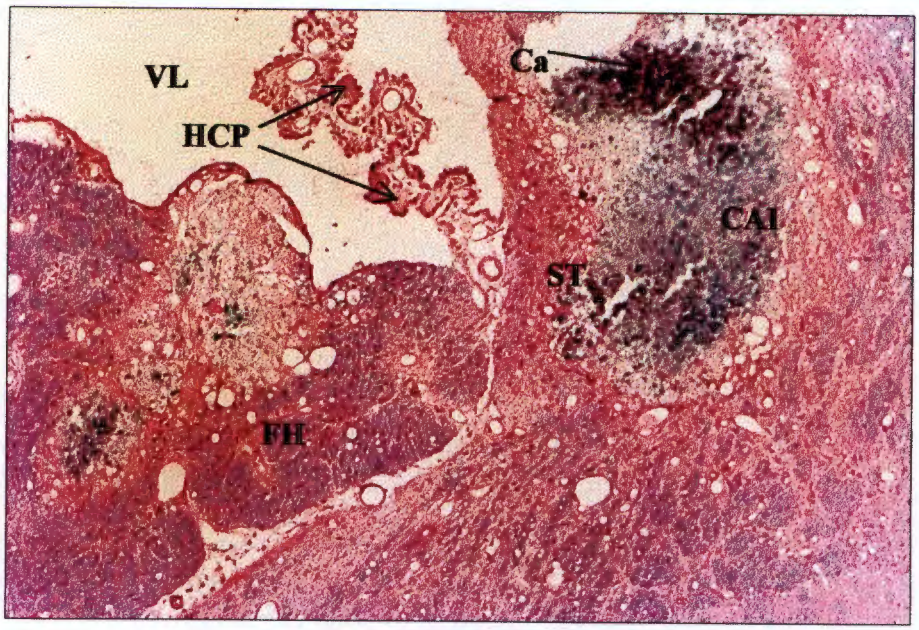

Figure 6.41 The *fimbria hippocampus* (FH) and surrounding structures of a rat brain at one year after 48 Gy given at 0.07 Gy min^{-1}. Stained with luxol blue haematoxylin and eosin (x80). Ca = calcium deposition, CAI = *capsula interna*, HCP = hyalinisation of the choroid plexus, ST = *stria terminalis*, VL = *ventriculus lateralis*.

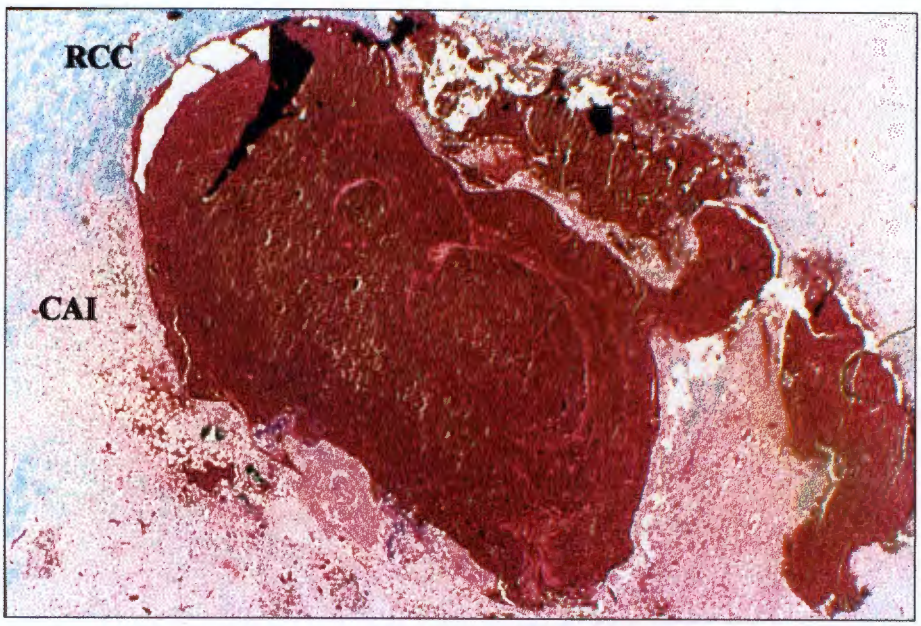

Figure 6.42 An extensive area of haemorrhage in a rat brain at one year after 48 Gy given at 0.07 Gy min^{-1}. Stained with luxol blue haematoxylin and eosin (x16). CAI = *capsula interna*, RCC = *radiatio corporis callosi*.

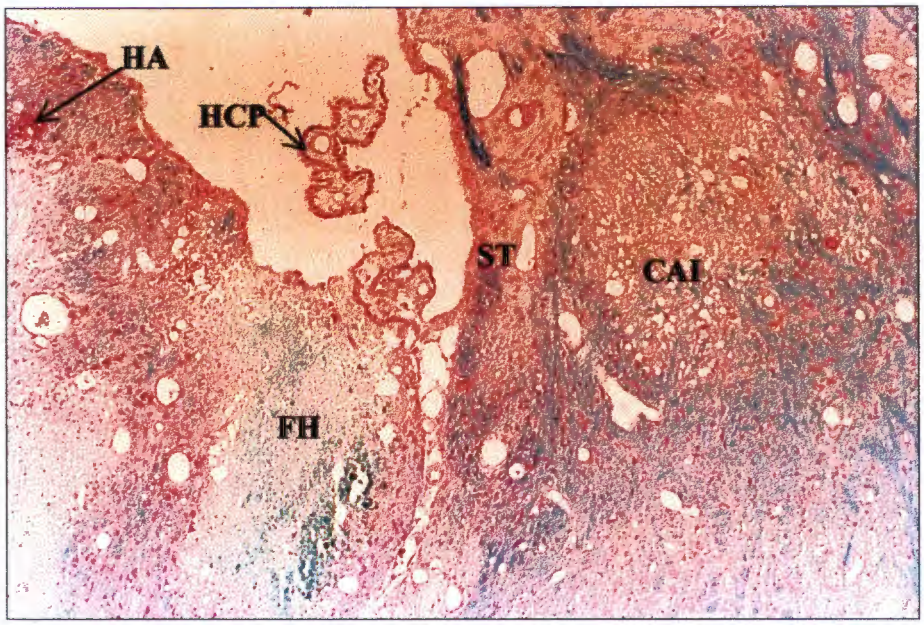

Figure 6.43 The *fimbria hippocampus* (FH) and surrounding structures of a rat brain at one year after 57 Gy given at 0.07 Gy min^{-1}. Stained with luxol blue haematoxylin and eosin (x60). CAI = *capsula interna*, HCP = hyalinisation of choroid plexus, HA = haemorrhage, ST = *stria terminalis*.

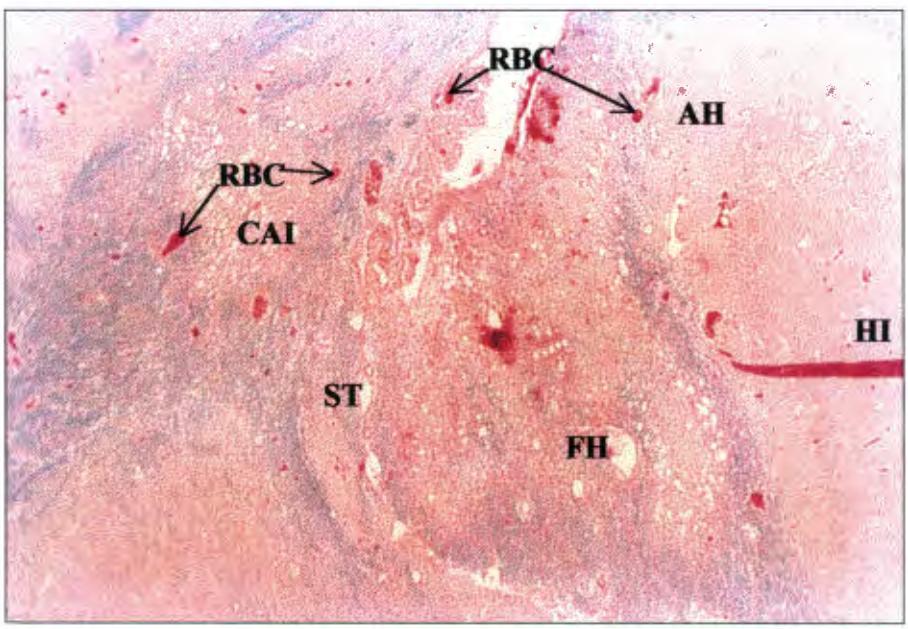

Figure 6.44 The *fimbria hippocampus* (FH) and surrounding structures of a rat brain at one year after 64 Gy (10 fractions in 12 days). Stained with luxol blue haematoxylin and eosin (x40). AH = *alveus hippocampi*, CAI = *capsula interna*, HI = *hippocampus*, RBC = red blood cell congested vessels, ST = *stria terminalis*.

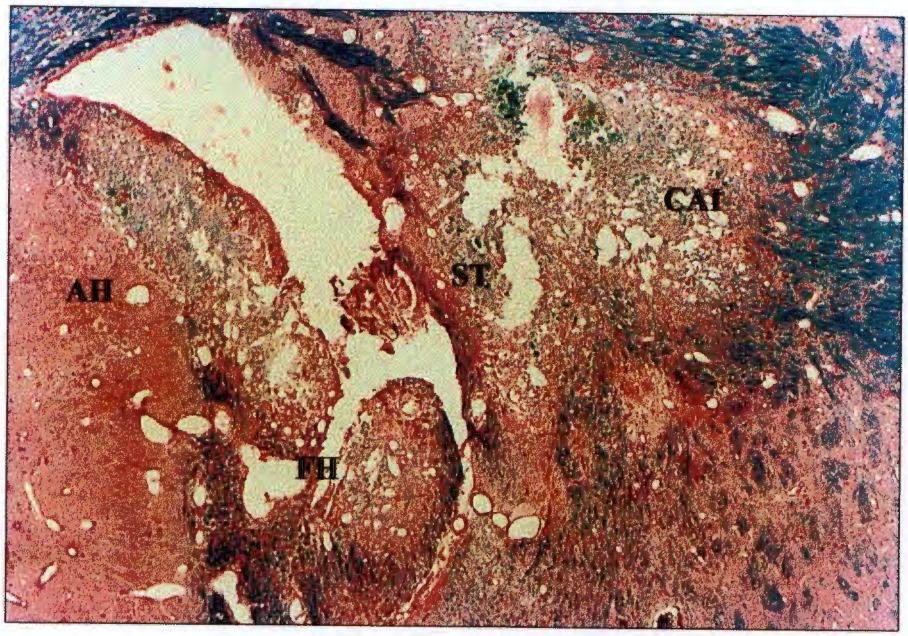

Figure 6.45 The *fimbria hippocampus* (FH) and surrounding structures of a rat brain at one year after 68 Gy (10 fractions in 12 days). Stained with luxol blue haematoxylin and eosin (x51). AH = *alveus hippocampi*, CAI = *capsula interna*, ST = *stria terminalis*.

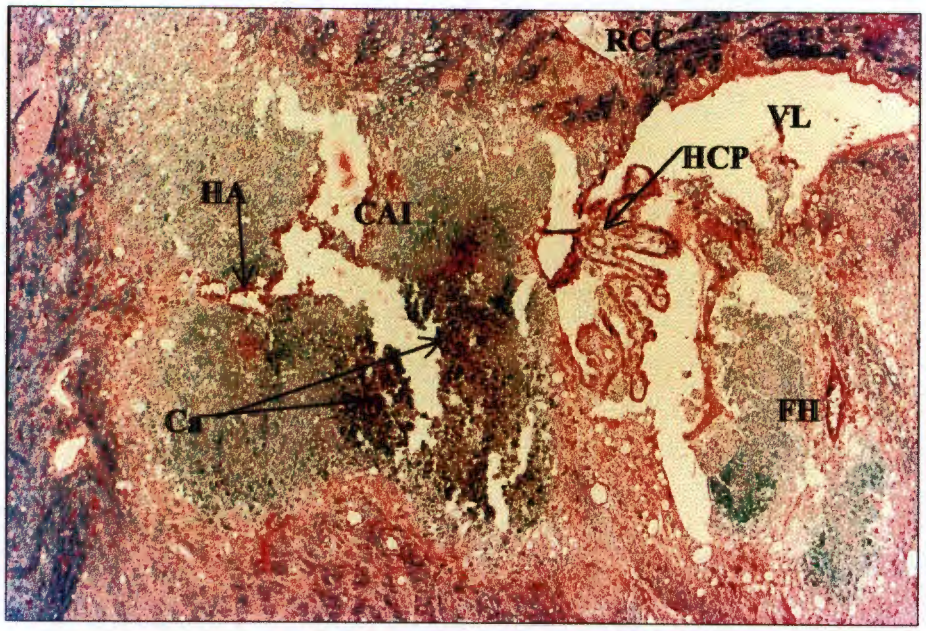

Figure 6.46 The *fimbria hippocampus* (FH) and surrounding structures of a rat brain at one year after 72 Gy (10 fractions in 12 days). Stained with luxol blue haematoxylin and eosin (x49). Ca = calcium deposition, CAI = *capsula interna*, HA = haemorrhage, HCP = hyalinisation of choroid plexus, RCC = *radiatio corporis callosi*, VL = *ventriculus lateralis*.

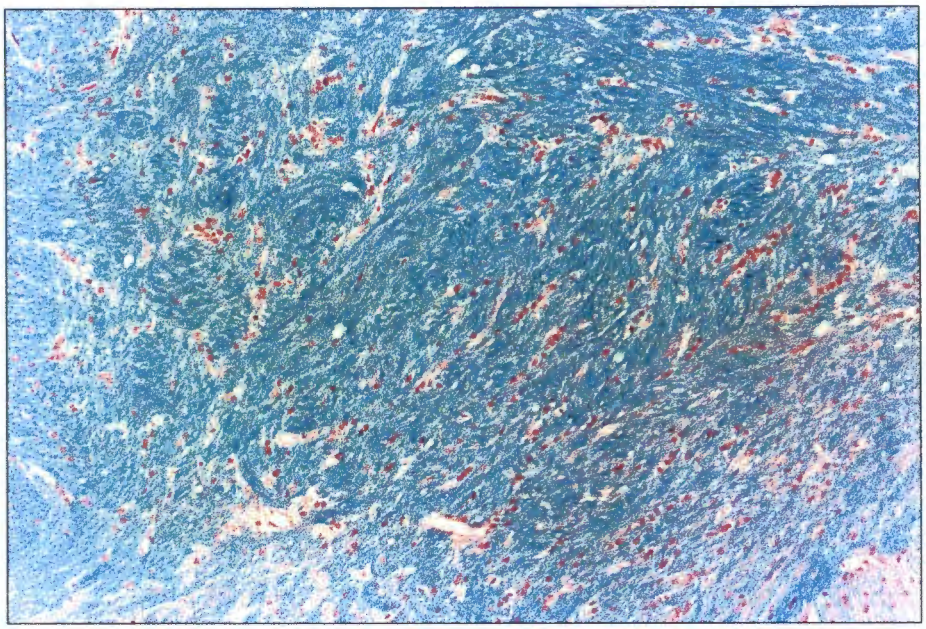

Figure 6.47 The *capsula interna* of a control rat brain after one year of observation. Stained with luxol blue haematoxylin and eosin (x320).

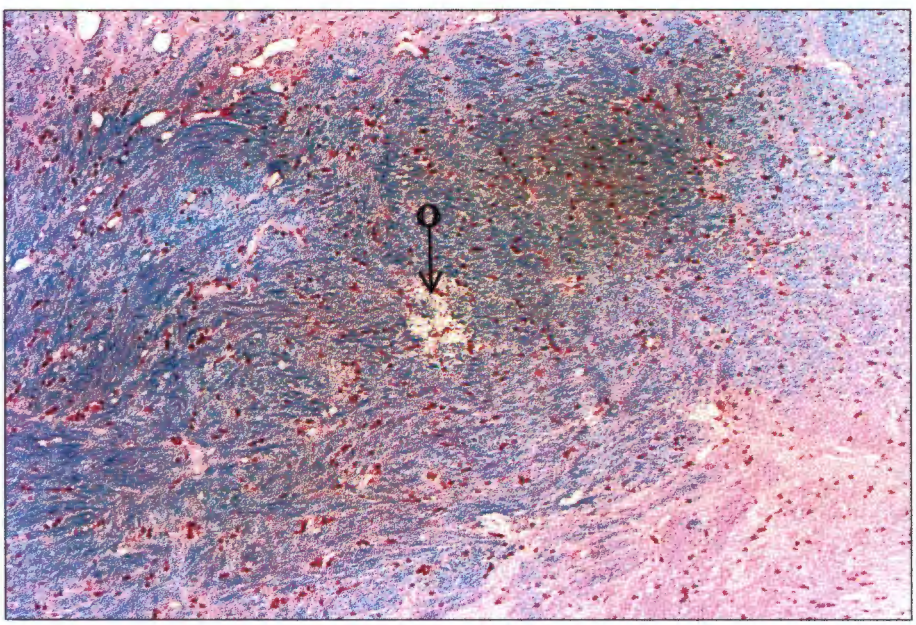

Figure 6.48 The *capsula interna* of a rat brain at one year after 47 Gy given at 0.04 Gy min^{-1}. Stained with luxol blue haematoxylin and eosin (x250). O = oedema.

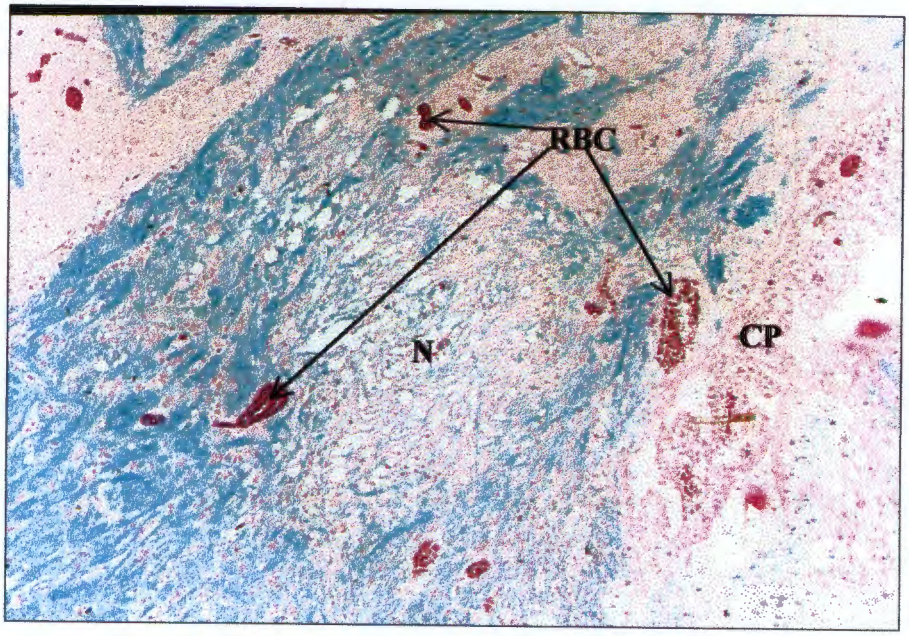

Figure 6.49 The *capsula interna* of a rat brain at one year after 64 Gy (10 fractions in 12 days). Stained with luxol blue haematoxylin and eosin (x80). CP = choroid plexus, N = necrosis, RBC = red blood cell congested vessels.

Figure 6.50 shows the CAIR of a control rat brain. The distinct bundles of myelin and the presence of small dilated vessels are noted. An area of oedema surrounding a dilated vessel in the CAIR of a rat brain is shown in Figure 6.51 (47 Gy at 0.05 Gy min^{-1}). Figures 6.52 (47 Gy at 0.05 Gy min^{-1}) and 6.53 (64 Gy in 10 fractions and 12 days) show an area of calcium deposition in the CAIR. Dilated vessels are shown in Figure 6.52 and disruption of the fibres of the CAIR are shown in Figure 6.53.

An extensive area of haemorrhage in the CAIR of a rat brain is shown in Figure 6.54 (44 Gy at 0.07 Gy min^{-1}) as is evident by the presence of numerous free lying red blood cells. Figure 6.55 (48 Gy at 0.07 Gy min^{-1}) shows the almost complete destruction of the CAIR by necrosis and the presence of numerous dilated vessels.

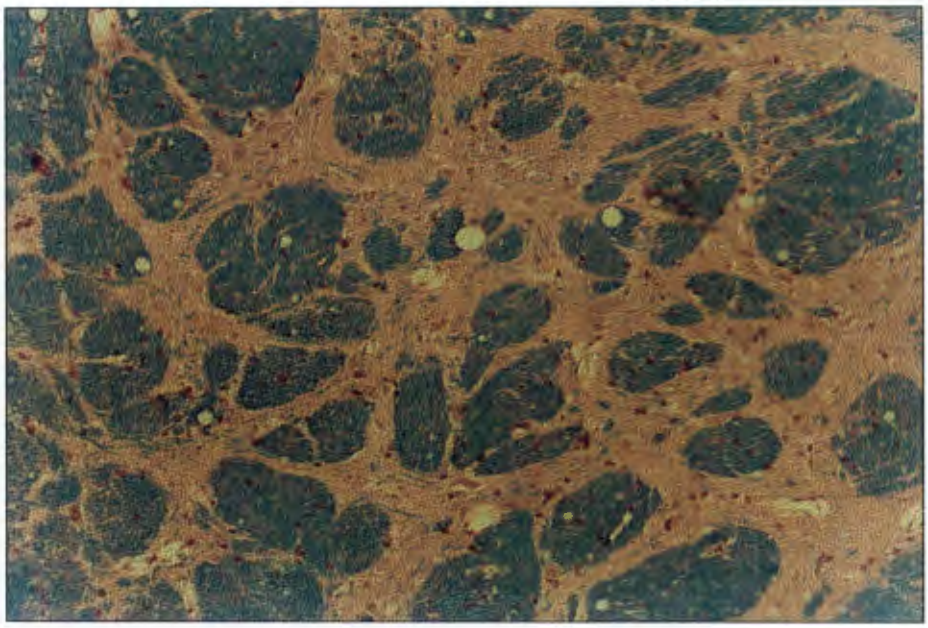

Figure 6.50 The *capsula interna pars retrolenticularis* of a control rat brain after one year of observation. Stained with luxol blue haematoxylin and eosin (x375).

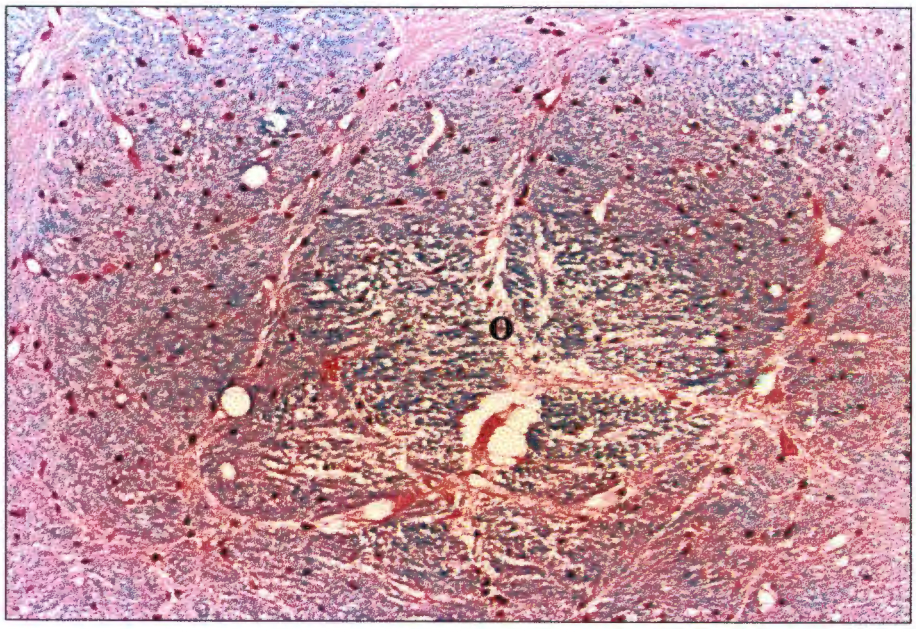

Figure 6.51 The *capsula interna pars retrolenticularis* of a rat brain at one year after 47 Gy given at 0.05 Gy min^{-1}. Stained with luxol blue haematoxylin and eosin (x500). O = oedema.

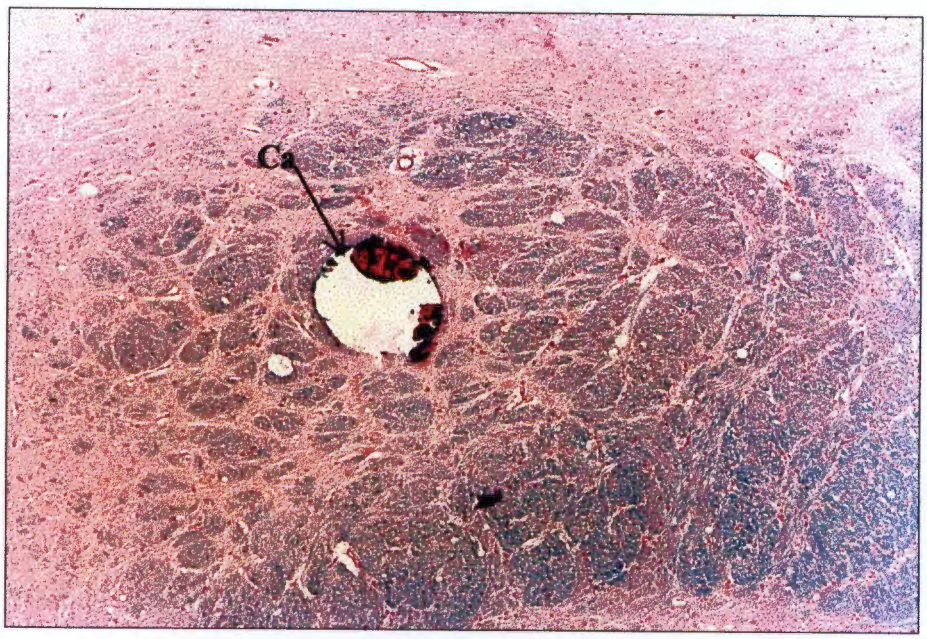

Figure 6.52 The *capsula interna pars retrolenticularis* of a rat brain at one year after 47 Gy given at 0.05 Gy min^{-1}. Stained with luxol blue haematoxlyin and eosin (x200). Ca = calcium deposition.

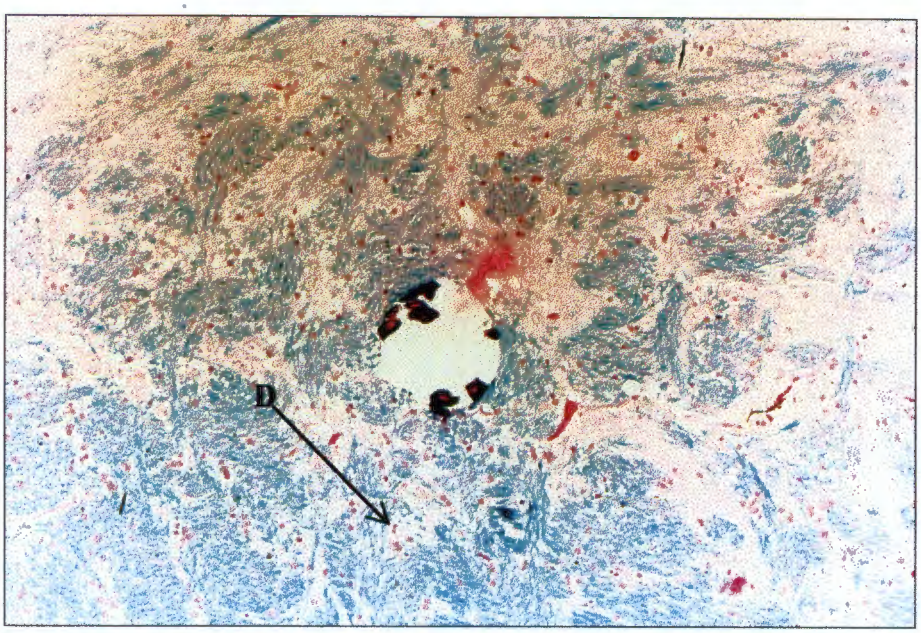

Figure 6.53 The *capsula interna pars retrolenticularis* of a rat brain at one year after 64 Gy (10 fractions in 12 days). Stained with luxol blue haematoxlyin and eosin (x275). D = disruption of fibres.

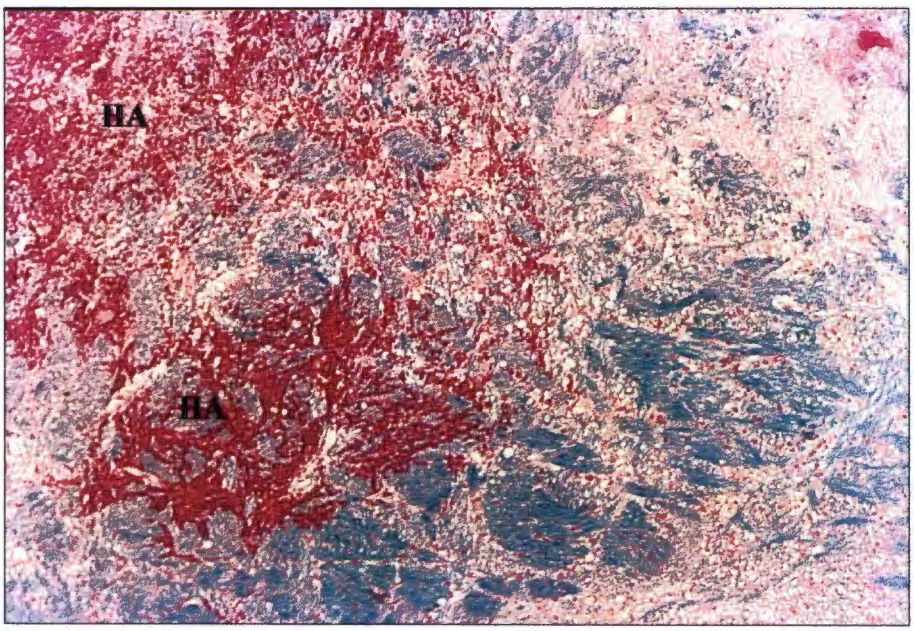

Figure 6.54 The *capsula interna pars retrolenticularis* of a rat brain at one year after 44 Gy given at 0.07 Gy min^{-1}. Stained with luxol blue haematoxlyin and eosin (x80). HA = haemorrhage.

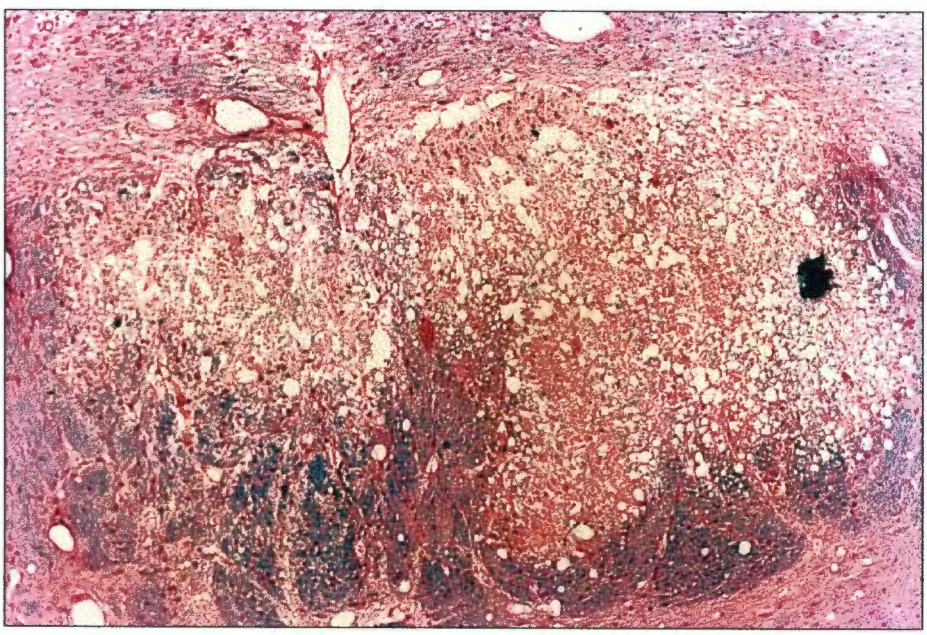

Figure 6.55 The *capsula interna pars retrolenticularis* of a rat brain at one year after 48 Gy given at 0.07 Gy min^{-1}. Stained with luxol blue haematoxylin and eosin (x80).

The C and the corpus callosum (CC) beneath the C of a control rat brain are shown in Figure 6.56. Numerous small dilated vessels are noted in both the C and in the CC. Partial necrosis of the C in addition to large dilated vessels in the C of a rat brain are shown in Figure 6.57 (44 Gy at 0.07 Gy min^{-1}) and complete disruption of the fibres of the CC due to necrosis is also shown. Figure 6.58 (55 Gy at 0.05 Gy min^{-1}) shows complete necrosis of both the C and CC in a rat brain with an extensive haemorrhage accompanying the necrosis. Large dilated vessels in the C and CC of a rat brain are shown in Figure 6.59 (64 Gy in 10 fractions and 12 days). Partial destruction of the C and complete destruction of the CC due to extensive haemorrhage are shown in Figure 6.60 (68 Gy in 10 fractions and 12 days). In addition, free iron deposits are also noted in the CC in Figure 6.60.

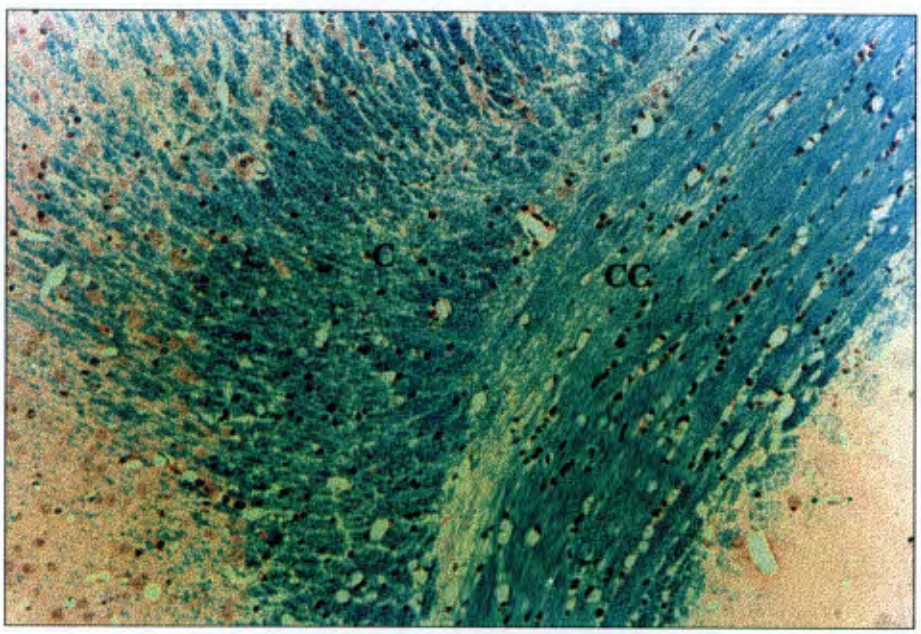

Figure 6.56 The *cingulum* (C) and corpus callosum (CC) of a control rat brain after one year of observation. Stained with luxol blue haematoxylin and eosin (x422).

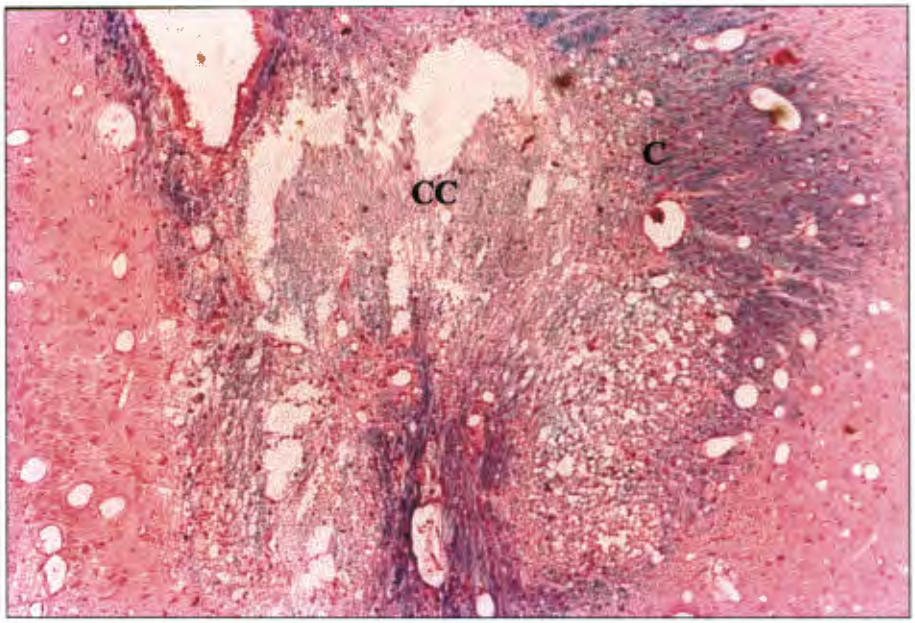

Figure 6.57 The *cingulum* (C) and corpus callosum (CC) of a rat brain at one year after 44 Gy at 0.07 Gy min^{-1}. Stained with luxol blue haematoxylin and eosin (x250).

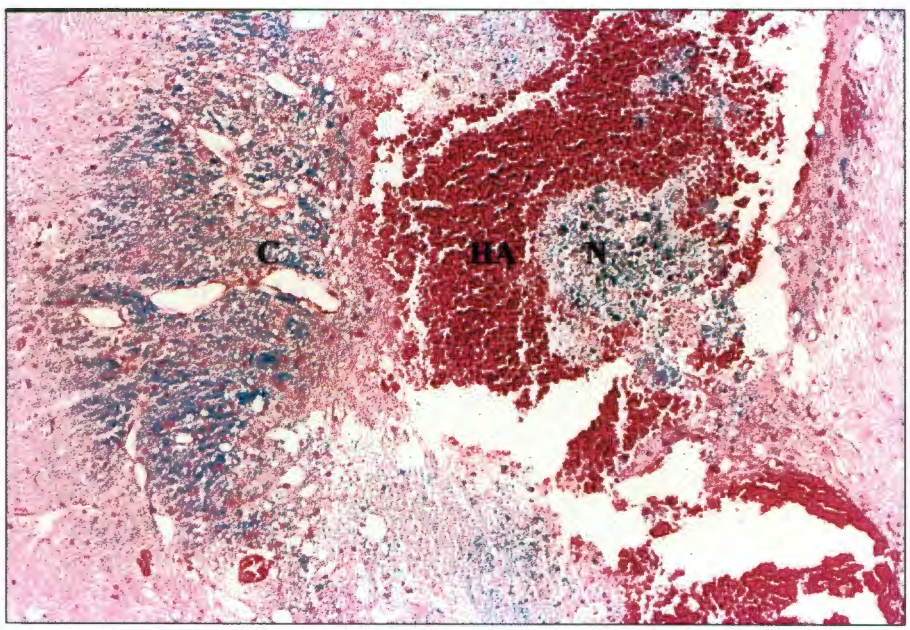

Figure 6.58 The *cingulum* (C) and corpus callosum of a rat brain at one year after 55 Gy at 0.05 Gy min^{-1}. Stained with luxol blue haematoxylin and eosin (x250). HA = haemorrhage, N = necrosis.

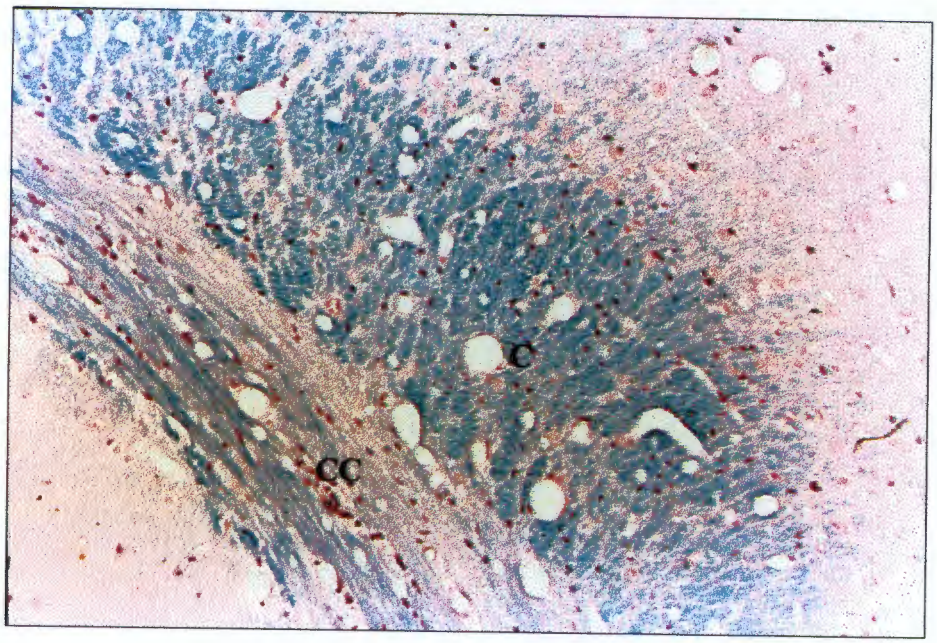

Figure 6.59 The *cingulum* (C) and corpus callosum (CC) of a rat brain at one year after 64 Gy (10 fractions in 12 days). Stained with luxol blue haematoxylin and eosin (x402).

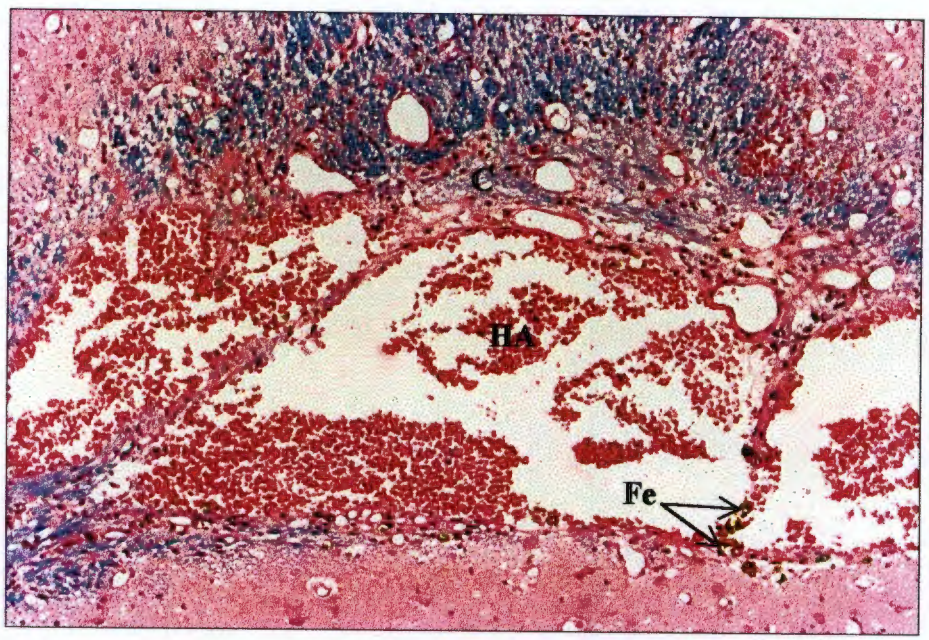

Figure 6.60 The *cingulum* (C) and corpus callosum of a rat brain at one year after 72 Gy (10 fractions in 12 days). Stained with luxol blue haematoxylin and eosin (x420). Fe = free iron deposits, HA = haemorrhage.

Figure 6.61 shows the TCC of a control rat brain. The even distribution of nuclei and fibres and the presence of numerous small dilated vessels is also shown. Necrosis of the TCC accompanied by a large haemorrhage is shown in Figure 6.62 (55 Gy at 0.05 Gy min^{-1}). The haemorrhage is shown to extend into the HI and numerous large dilated vessels are also shown in Figure 6.62. Figure 6.63 (48 Gy at 0.07 Gy min^{-1}) shows the disruption of fibres in the TCC due to necrosis, oedema and large dilated vessels. A focus of haemorrhage is also shown in Figure 6.63. Numerous dilated vessels of varying diameter are shown in the TCC in Figure 6.64 (64 Gy in 10 fractions and 12 days). Complete necrosis of the TCC is shown in Figure 6.65 (72 Gy in 10 fractions and 12 days).

The CP, VL and EC of a control rat brain at one year are shown in Figure 6.66. The nuclei of the CP are evenly distributed and a limited presence of vacuolation in the CP is also shown. Marked hyalinisation and vacuolation of the CP is shown in Figures 6.67 (47 Gy at 0.05 Gy min^{-1}) and 6.68 (55 Gy at 0.05 Gy min^{-1}). Pyknotic nuclei in the CP are also shown in Figure 6.68. Large dilated vessels congested with red blood cells in the CP are shown in Figure 6.69 (64 Gy in 10 fractions and 12 days).

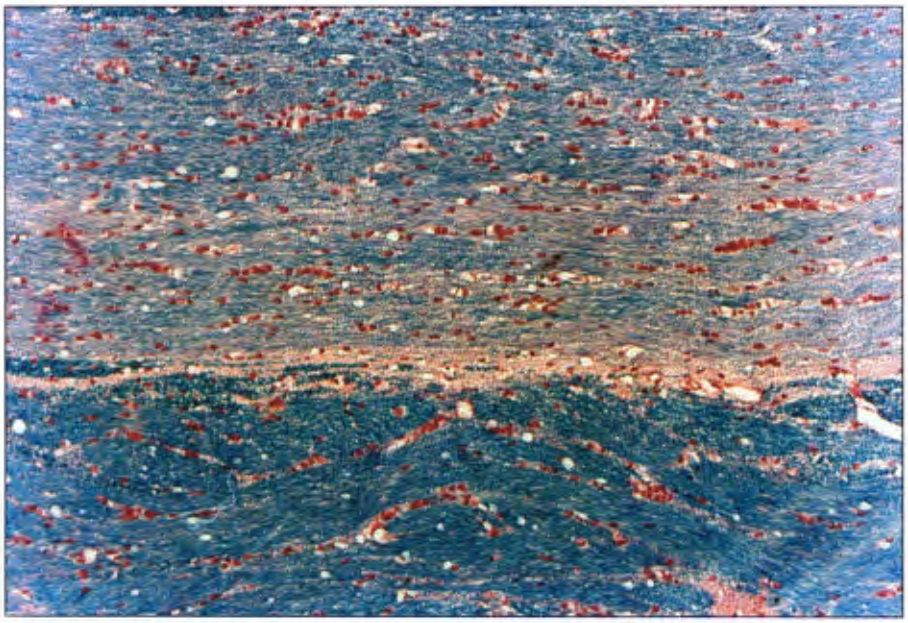

Figure 6.61 The *truncus corporis callosi* of a control rat brain after one year of observation. Stained with luxol blue haematoxylin and eosin (x400).

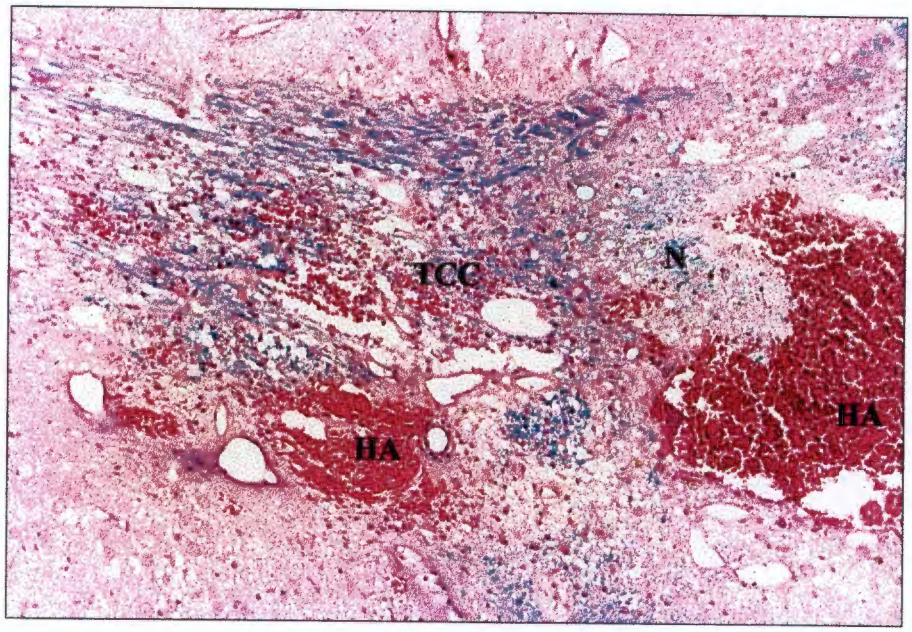

Figure 6.62 The *truncus corporis callosi* (TCC) of a rat brain at one year after 55 Gy given at 0.05 Gy min^{-1}. Stained with luxol blue haematoxlin and eosin (x275). HA = haemorrhage, N = necrosis.

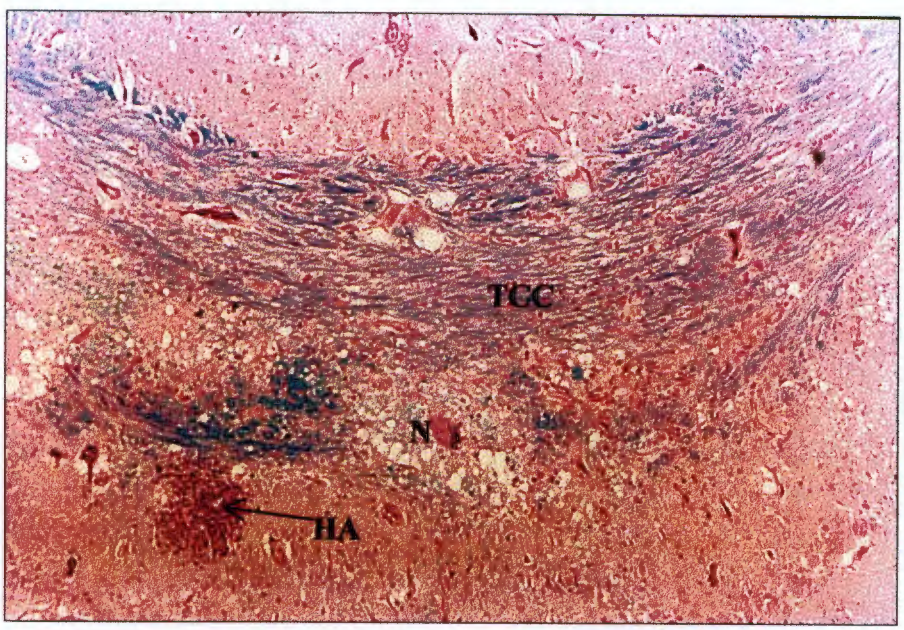

Figure 6.63 The *truncus corporis callosi* (TCC) of a rat brain at one year after 48 Gy given at 0.07 Gy min^{-1}. Stained with luxol blue haematoxlin and eosin (x199). HA = haemorrhage, N = necrosis.

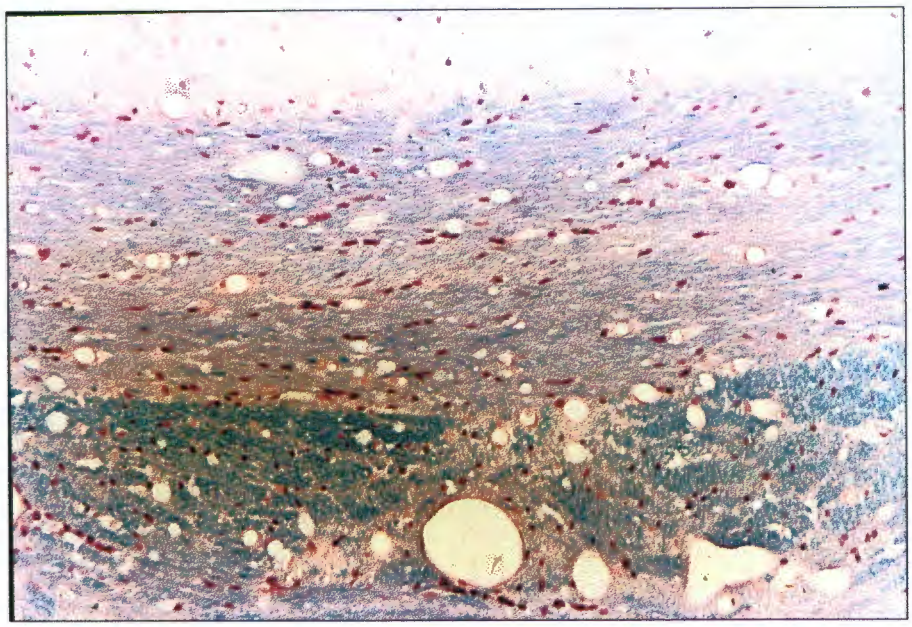

Figure 6.64 The *truncus corporis callosi* of a rat brain at one year after 64 Gy (10 fractions in 12 days). Stained with luxol blue haematoxlin and eosin (x500).

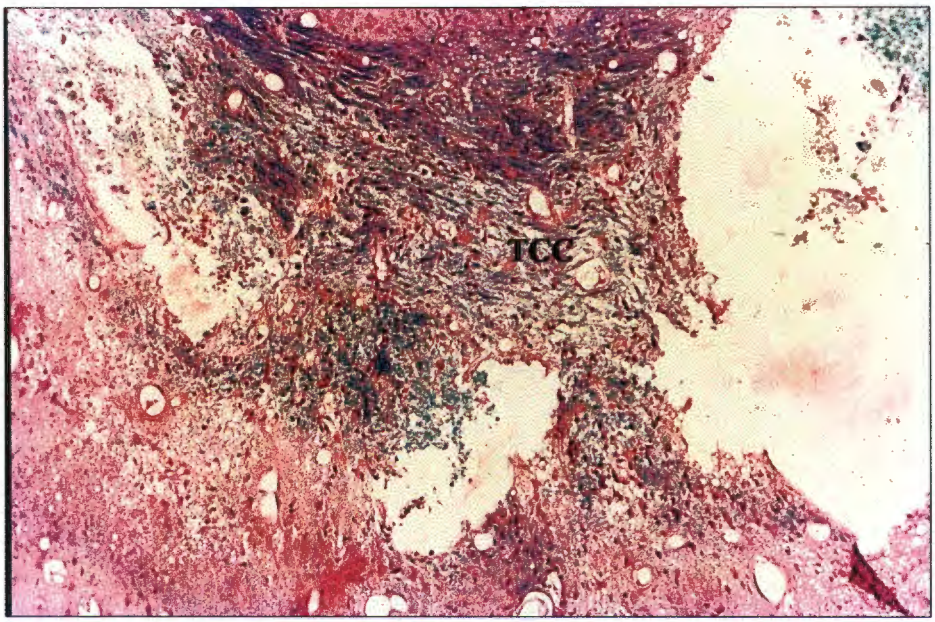

Figure 6.65 The *truncus corporis callosi* (TCC) of a rat brain at one year after 72 Gy (10 fractions in 12 days). Stained with luxol blue haematoxlin and eosin (x200).

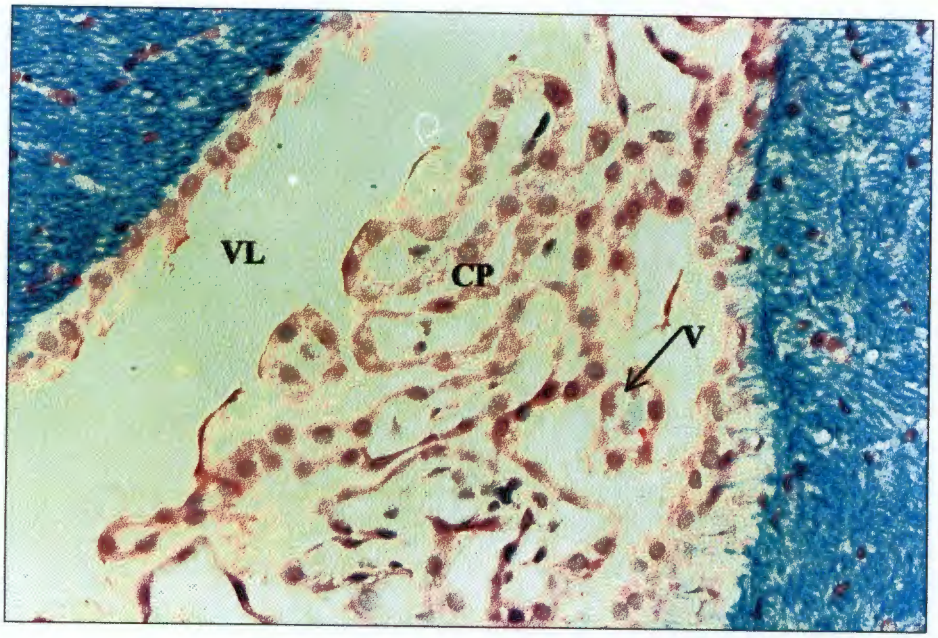

Figure 6.66 The choroid plexus (CP) of a control rat brain after one year of observation. Stained with luxol blue haematoxylin and eosin (x400). V = vacuolation, VL = *ventriculus lateralis*.

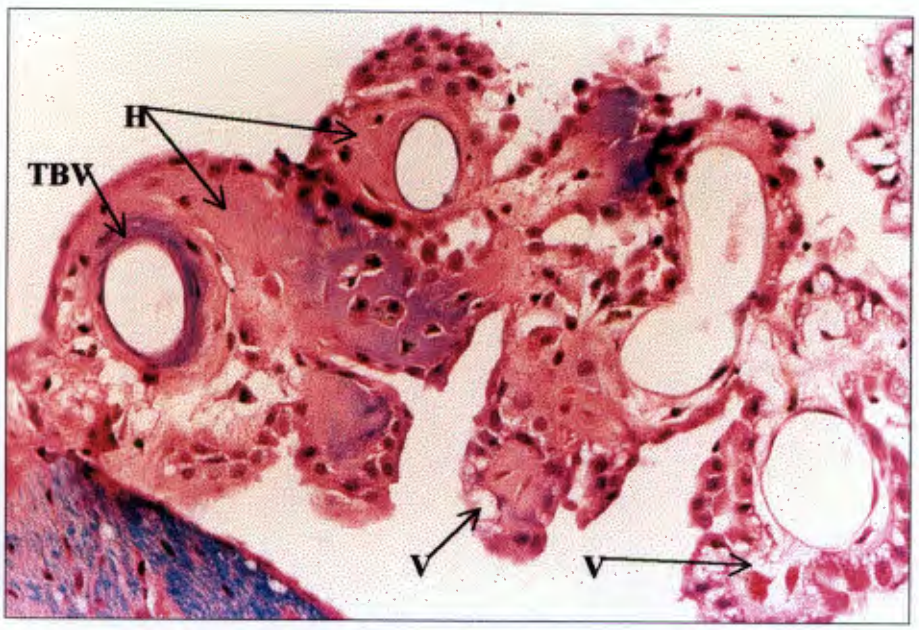

Figure 6.67 The choroid plexus of a rat brain at one year after 47 Gy given at 0.05 Gy min^{-1}. Stained with luxol blue haematoxylin and eosin (x700). H = hyalinisation, TBV = thickened blood vessel wall, V = vacuolation.

Figure 6.68 The choroid plexus of a rat brain at one year after 55 Gy given at 0.05 Gy min^{-1}. Stained with luxol blue haematoxylin and eosin (x350). H = hyalinisation, P = pyknotic nuclei, V = vacuolation.

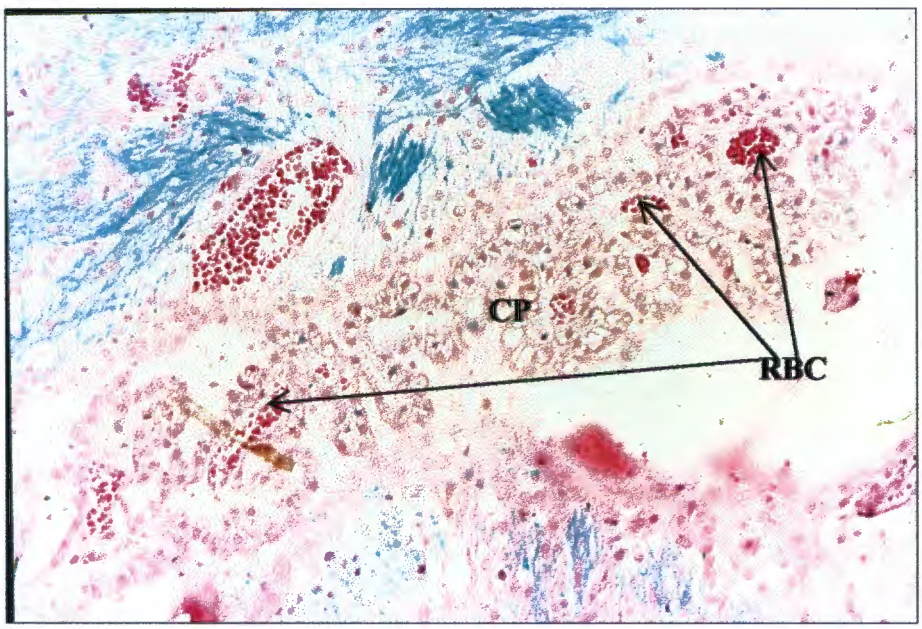

Figure 6.69 The choroid plexus (CP) of a rat brain at one year after 64 Gy (10 fractions in 12 days). Stained with luxol blue haematoxylin and eosin (x410). RBC = red blood cell congested vessels.

The RCC of a control rat brain at one year is shown in Figure 6.70. Necrosis extending from the FH and red blood cell congested vessels in the RCC are shown in Figures 6.71 (60 Gy at 0.05 Gy min^{-1}) and 6.72 (64 Gy in 10 fractions and 12 days).

The GD, with its distinctive tract of nuclei, of a control rat brain is shown in Figure 6.73. Oedematous changes in the body and nuclei tract of the GD are shown in Figure 6.74 (55 Gy at 0.05 Gy min^{-1}). Figure 6.75 (68 Gy in 10 fractions and 12 days) shows oedema restricted to the nuclei tract of the GD with a focus of haemorrhage and numerous dilated vessels in the body of the GD.

The AH, also characterised by a distinctive tract of nuclei, of a control rat brain at one year is shown in Figure 6.76. Disruption of the nuclei of the AH due to oedema, necrosis and dilated vessels is shown in Figure 6.77 (55 Gy at 0.05 Gy min^{-1}). RBC congested vessels and oedema in the AH are shown in Figure 6.78 (64 Gy in 10 fractions and 12 days).

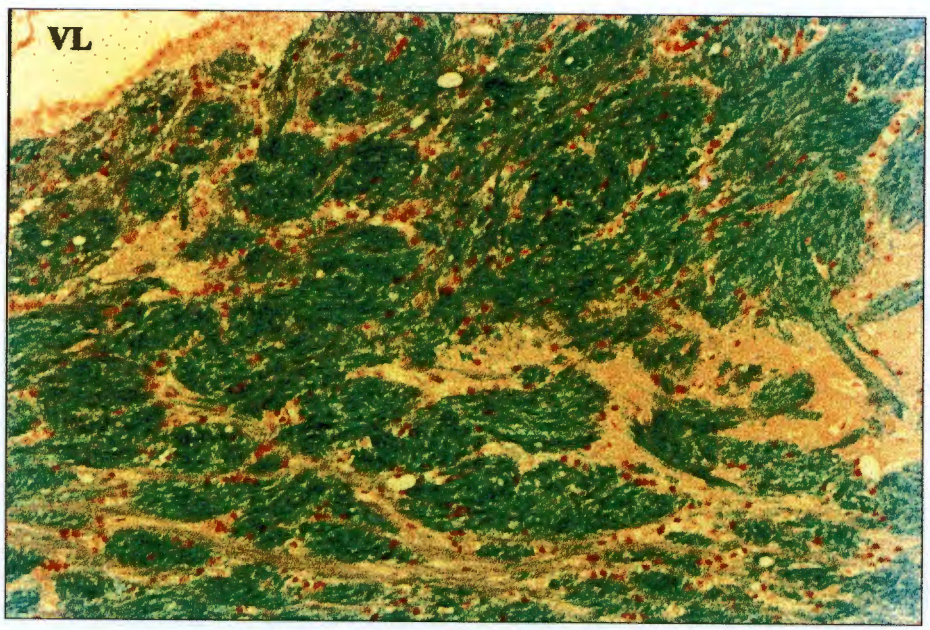

Figure 6.70 The *radiatio corporis callosi* of a control rat brain after one year of observation. Stained with luxol blue haematoxylin and eosin (x375). VL = *ventriculus lateralis*.

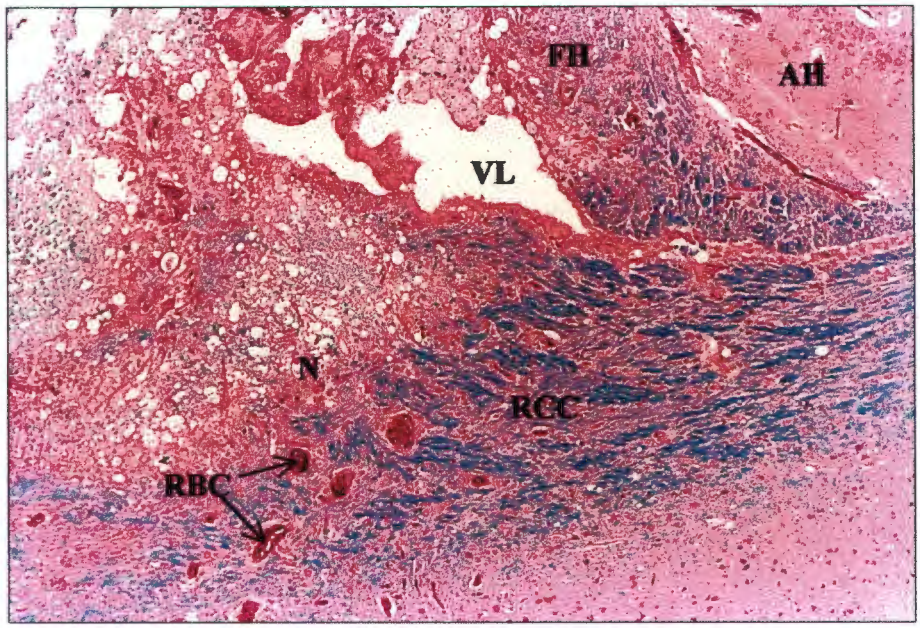

Figure 6.71 The *radiatio corporis callosi* (RCC) of a rat brain at one year after 60 Gy given at 0.05 Gy min^{-1}. Stained with luxol blue haematoxylin and eosin (x200). AH = *alveus* hippocampi, FH = *fimbria hippocampus*, N = necrosis, RBC = red blood cell congested vessels, VL = *ventriculus lateralis*.

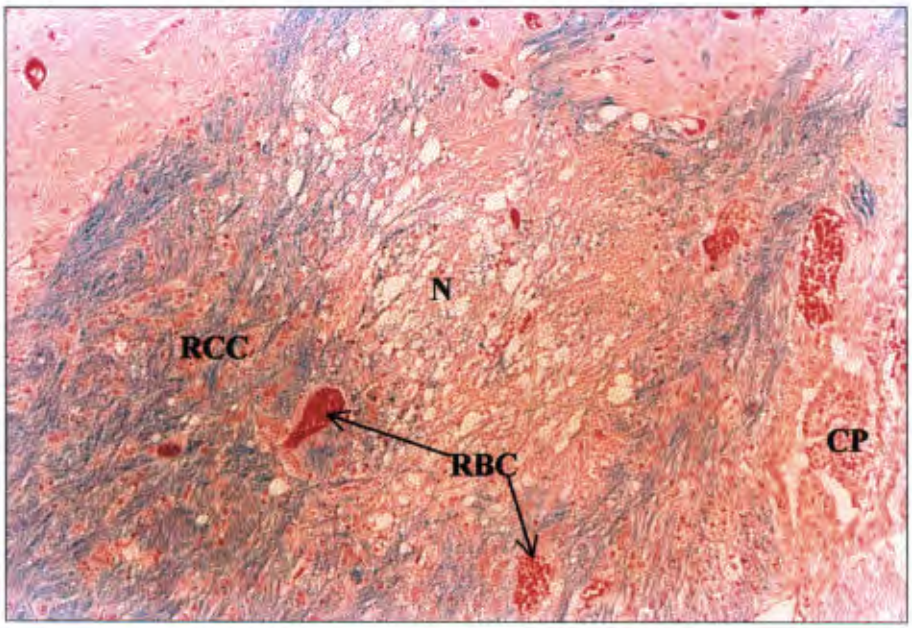

Figure 6.72 The *radiatio corporis callosi* (RCC) of a rat brain at one year after 64 Gy (10 fractions in 12 days). Stained with luxol blue haematoxylin and eosin (x250). CP = choroid plexus, N = necrosis, RBC = red blood cell congested vessels.

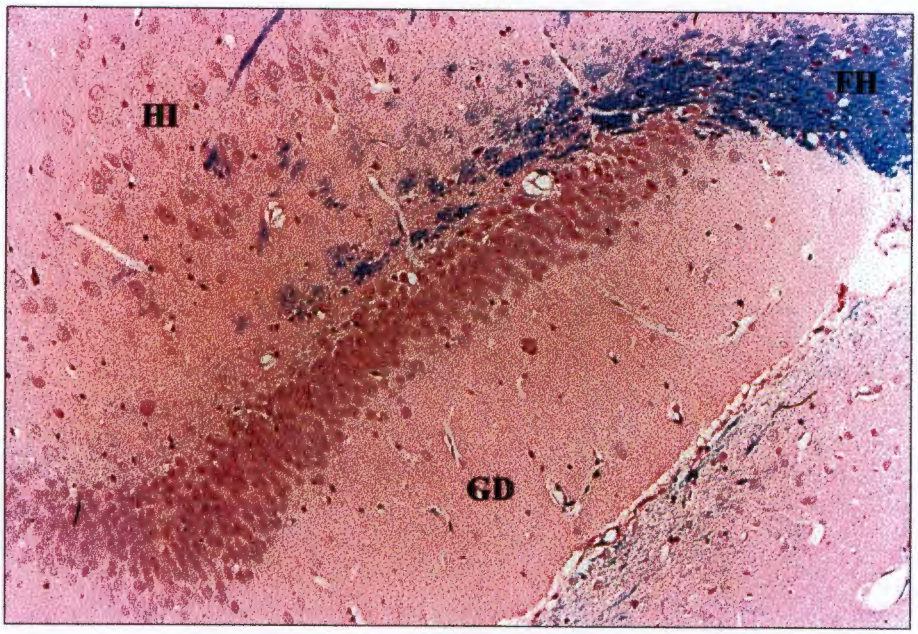

Figure 6.73 The *gyrus dentatus* (GD) of a control rat brain after one year of observation. Stained with luxol blue haematoxylin and eosin (x330). FH = *fimbria hippocampus*, HI = *hippocampus*.

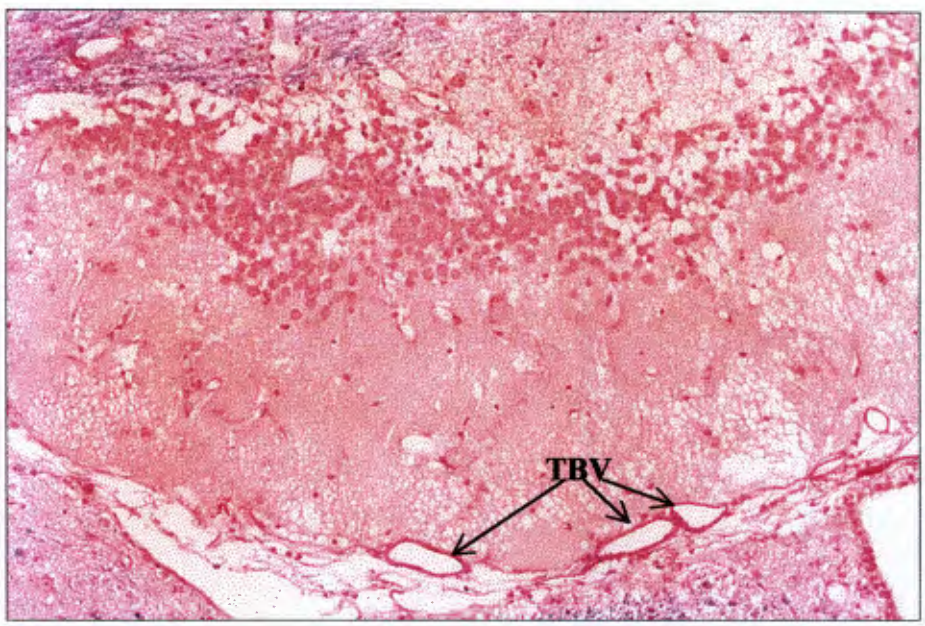

Figure 6.74 The *gyrus dentatus* (GD) of a rat brain at one year after 55 Gy given at 0.05 Gy min^{-1}. Stained with luxol blue haematoxylin and eosin (x315). FH = *fimbria hippocampus*, HI = *hippocampus*, TBV = thickened blood vessel wall.

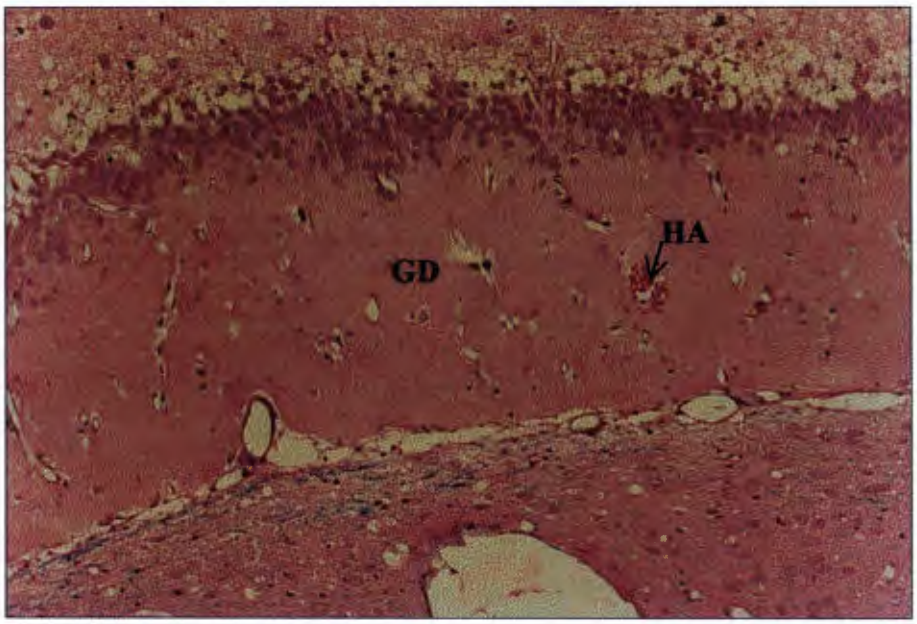

Figure 6.75 The *gyrus dentatus* (GD) of a rat brain at one year after 68 Gy (10 fractions in 12 days). Stained with luxol blue haematoxylin and eosin (x337). HA = haemorrhage.

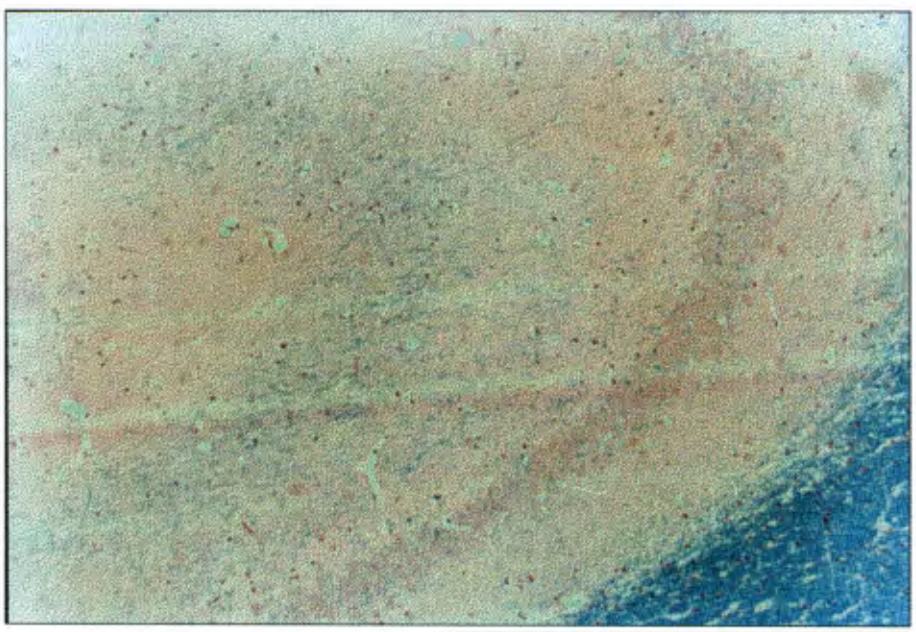

Figure 6.76 The *alveus hippocampi* of a control rat brain after one year of observation. Stained with luxol blue haematoxylin and eosin (x250).

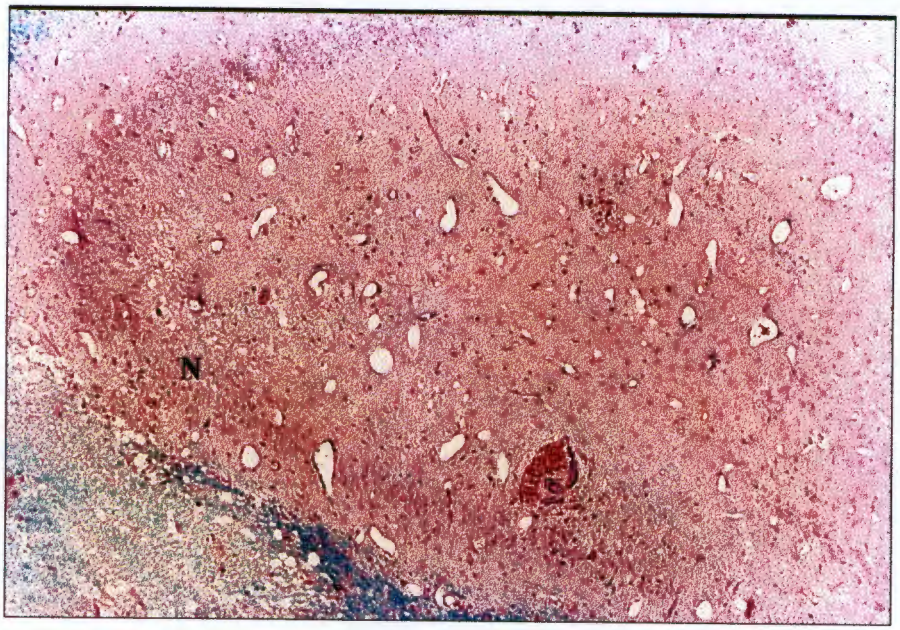

Figure 6.77 The *alveus hippocampi* of a rat brain at one year after 55 Gy given at 0.05 Gy min^{-1}. Stained with luxol blue haematoxylin and eosin (x153). N = necrosis.

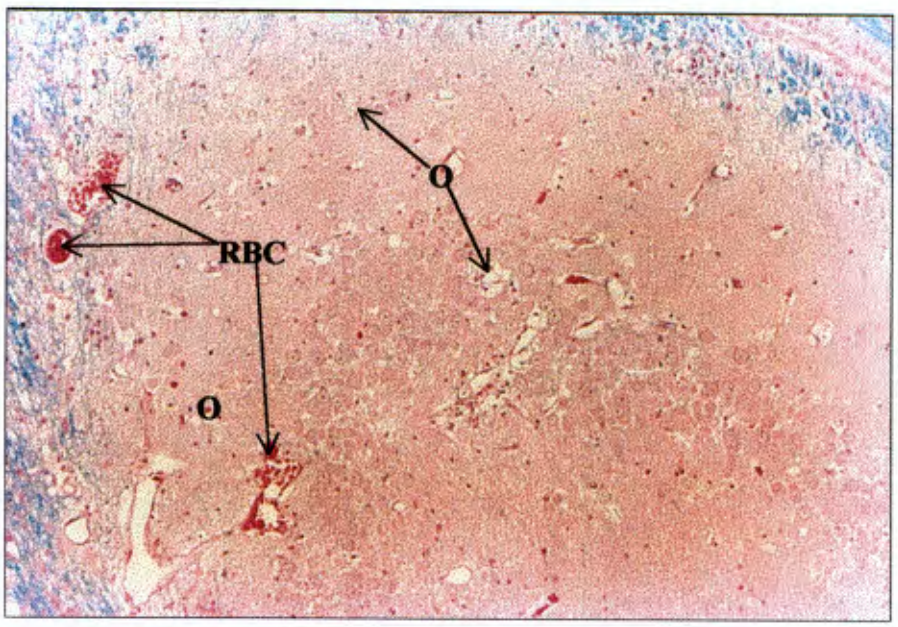

Figure 6.78 The *alveus hippocampi* of a rat brain at one year after 64 Gy (10 fractions in 12 days). Stained with luxol blue haematoxylin and eosin (x250). O = oedema, RBC = red blood cell congested vessels.

Special stains

No fibrin was seen in any of the limited histological sections of this study that were stained with the MSB stain. A control rat brain after one year of observation is shown in Figure 6.79 without any fibrin deposition. Figure 6.80 (55 Gy at 0.05 Gy min^{-1}) shows extensive areas of both haemorrhage and necrosis and Figure 6.81 (65 Gy at 0.04 Gy min^{-1}) an extensive area of necrosis without any fibrin deposition.

Calcium deposition in areas of necrosis was confirmed in a limited number of histological sections with the use of the von Kossa's stain, which stains calcium deposits black. Figure 6.82 (47 Gy at 0.04 Gy min^{-1}) shows the FH and surrounding structures with no calcium deposition in any of the structures. Figures 6.83 (57 Gy at 0.04 Gy min^{-1}) and 6.84 (72 Gy in 10 fractions and 12 days) show areas of calcium deposition in and around the necrotic areas of the FH and surrounding structures.

Figures 6.85 and 6.86 show the FH and surrounding structures of a control rat brain after one year of observation stained with the GFAP stain. A limited presence of astrocytosis and gliosis is shown in the control rat brain FH. Frank astrocytosis and gliosis are shown in Figures 6.87 (47 Gy at 0.05 Gy min^{-1}), 6.88 (60 Gy at 0.05 Gy min^{-1}), 6.89 (48 Gy at 0.07 Gy min^{-1}) and 6.90 (72 Gy in 10 fractions and 12 days).

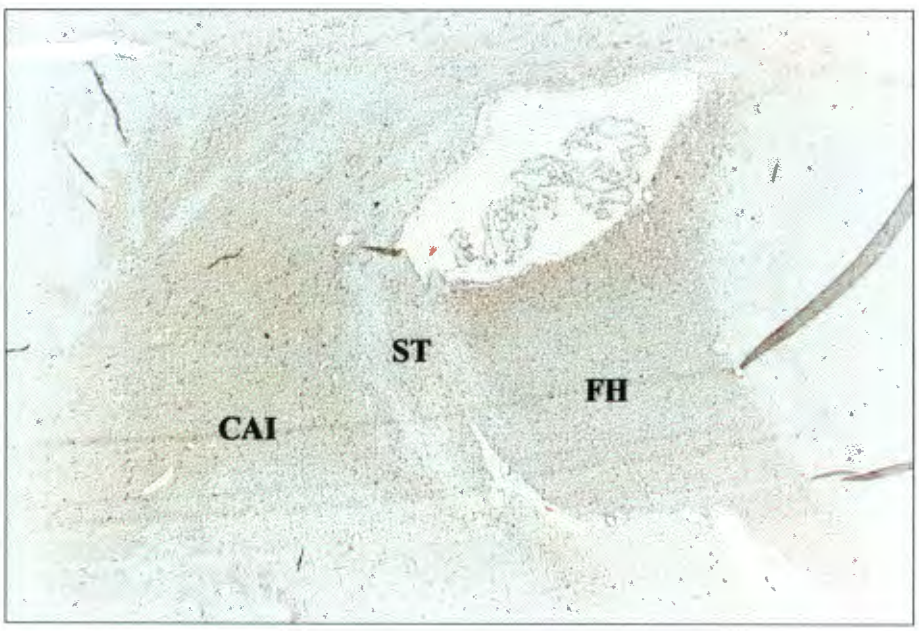

Figure 6.79 The *fimbria hippocampus* (FH) and surrounding structures of a control rat brain after one year of observation. Stained with Martius Scarlet Blue (x40). CAI = *capsula interna*, ST = *stria terminalis*.

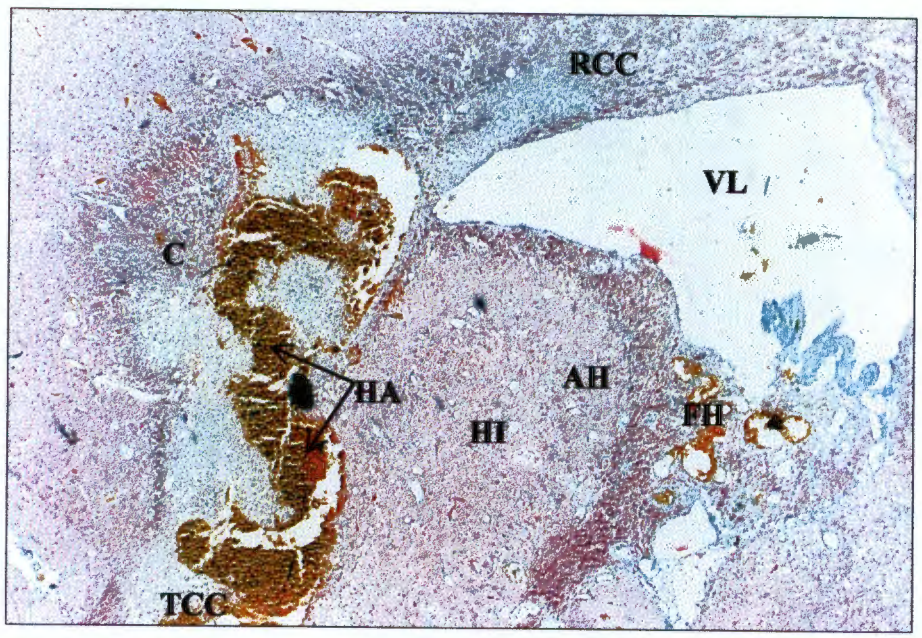

Figure 6.80 The *fimbria hippocampus* (FH) and surrounding structures of a rat brain at one year after 55 Gy at 0.05 Gy min^{-1}. Stained with Martius Scarlet Blue (x40). AH = *alveus hippocampi*, C = *cingulum*, HA = haemorrhage (stained yellow), HI = *hippocampus*, RCC = *radiatio corporis callosi*, TCC = *truncus corporis callosi*, VL = *ventriculus lateralis*.

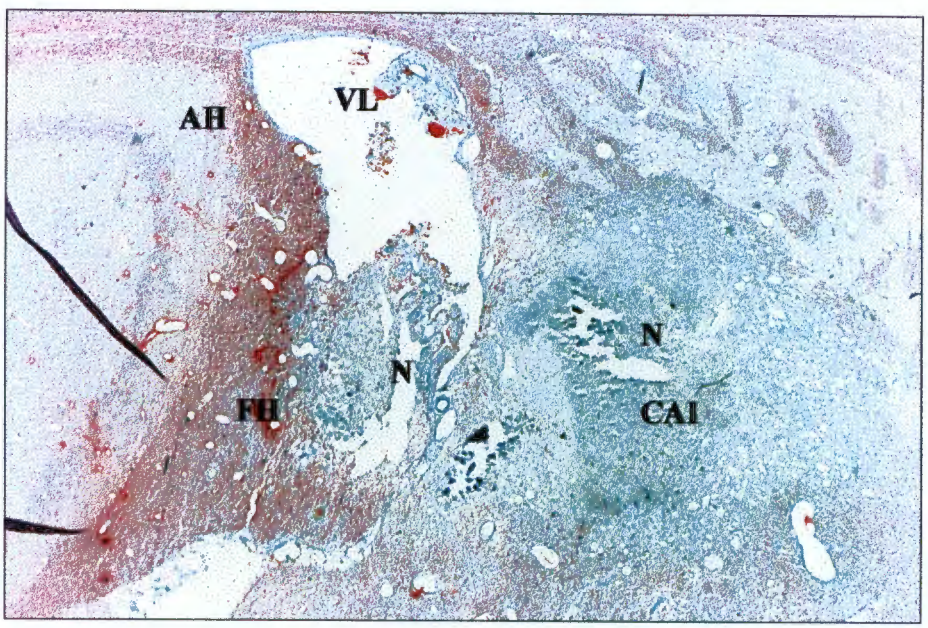

Figure 6.81 The *fimbria hippocampus* (FH) and surrounding structures of a rat brain at one year after 65 Gy at 0.04 Gy min^{-1}. Stained with Martius Scarlet Blue (x40). AH = *alveus hippocampi*, CAI = *capsula interna*, N= necrosis, VL = *ventriculus lateralis*.

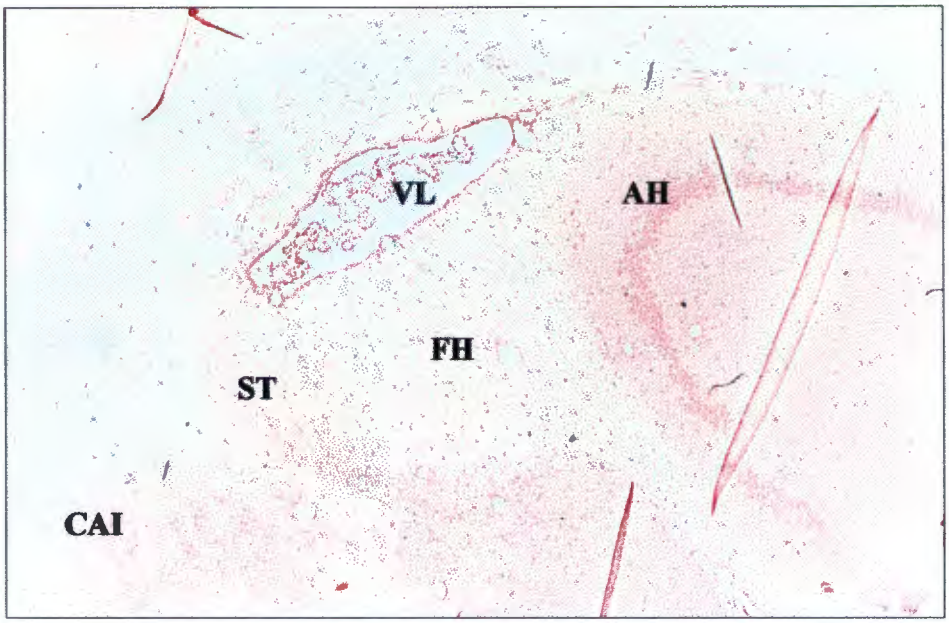

Figure 6.82 The *fimbria hippocampus* (FH) and surrounding structures of a rat brain at one year after 47 Gy at 0.04 Gy min^{-1}. Stained with von Kossa (x40). AH = *alveus hippocampi*, CAI = *capsula interna*, ST = *stria terminalis*, VL = *ventriculus lateralis*.

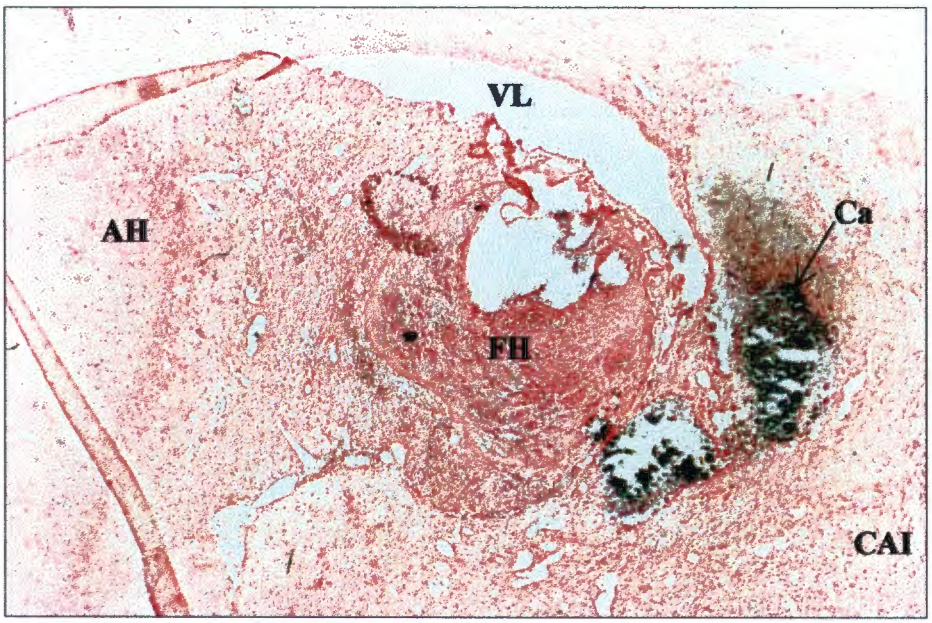

Figure 6.83 The *fimbria hippocampus* (FH) and surrounding structures of a rat brain at one year after 57 Gy at 0.04 Gy min^{-1}. Stained with von Kossa (x40). AH = *alveus hippocampi*, Ca = calcium deposits (stained black), CAI = *capsula interna*, VL = *ventriculus lateralis*.

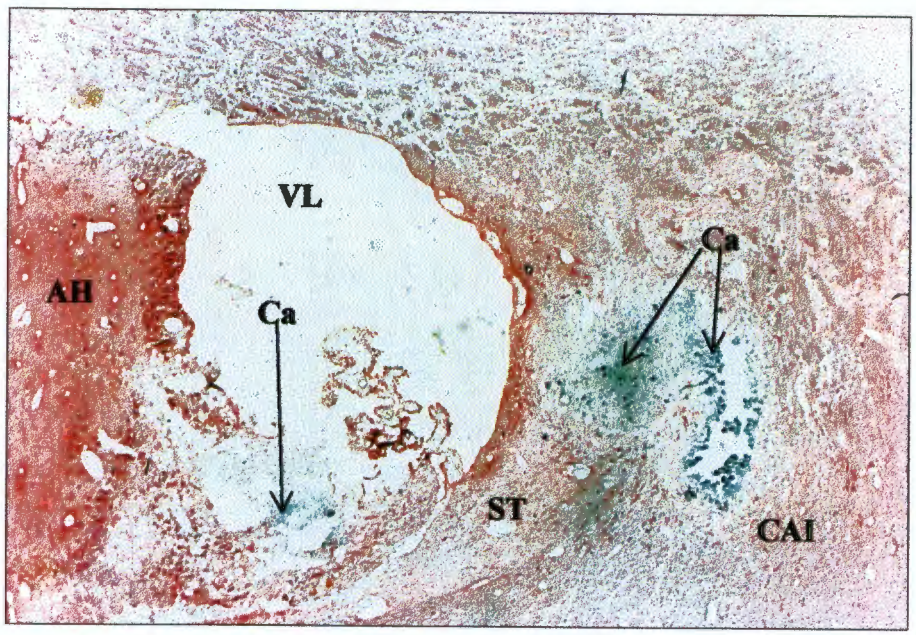

Figure 6.84 The *fimbria hippocampus* and surrounding structures of a rat brain at one year after 72 Gy (10 fractions in 12 days). Stained with von Kossa (x40). AH = *alveus hippocampi*, Ca = calcium deposits (stained black), CAI = *capsula interna*, ST = *stria terminalis*, VL = *ventriculus lateralis*.

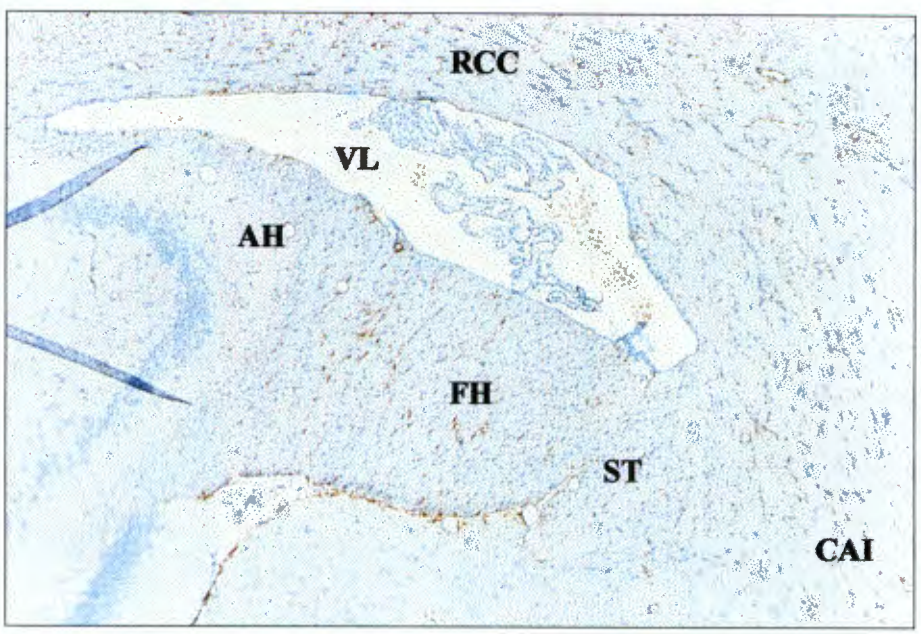

Figure 6.85 The *fimbria hippocampus* (FH) and surrounding structures of a control rat brain after one year of observation. Stained with Glial Fibrillary Acidic Protein where positive stains brown, (x40). AH = *alveus hippocampi*, CAI = *capsula interna*, RCC = *radiatio corporis callosi*, ST = *stria terminalis*, VL = *ventriculus lateralis*.

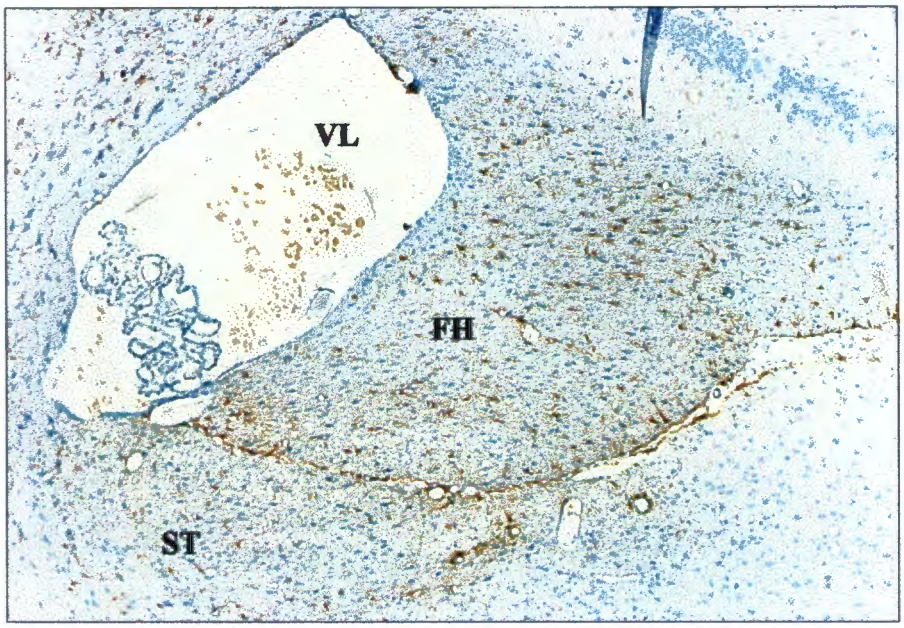

Figure 6.86 The *fimbria hippocampus* (FH) of a control rat brain after one year of observation. Stained with Glial Fibrillary Acidic Protein where positive stains brown, (x80). ST = *stria terminalis*, VL = *ventriculus lateralis*.

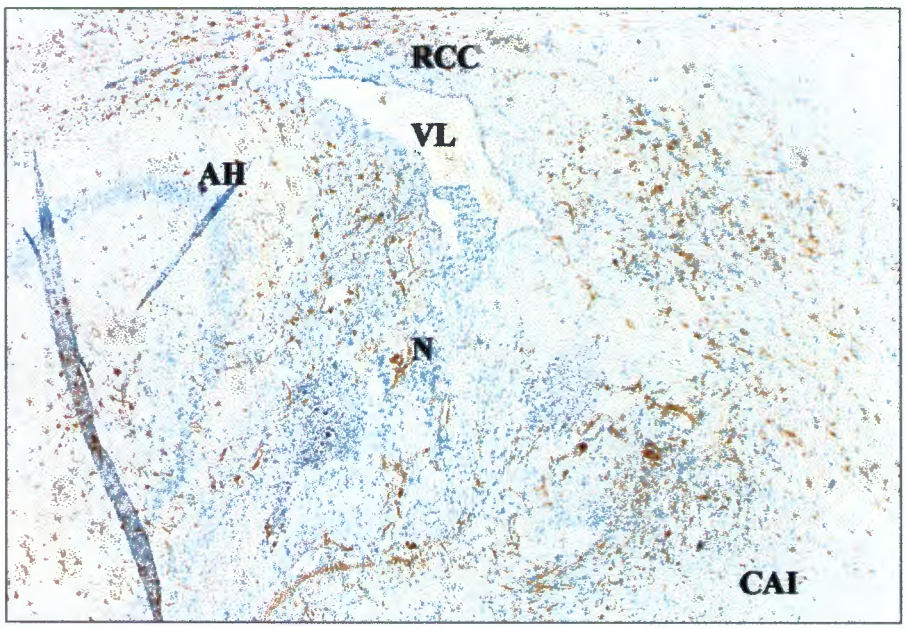

Figure 6.87 The *fimbria hippocampus* and surrounding structures of a rat brain at one year after 47 Gy at 0.05 Gy min^{-1}. Stained with Glial Fibrillary Acidic Protein where positive stains brown, (x40). AH = *alveus hippocampi*, CAI = *capsula interna*, N = necrosis, RCC = *radiatio corporis callosi*, VL = *ventriculus lateralis*.

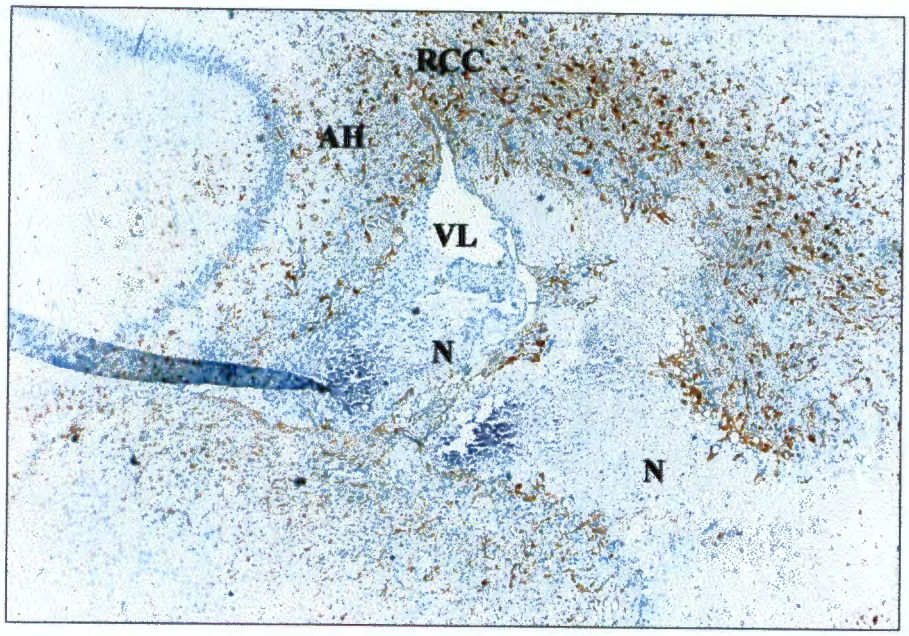

Figure 6.88 The *fimbria hippocampus* and surrounding structures of a rat brain at one year after 60 Gy at 0.05 Gy min^{-1}. Stained with Glial Fibrillary Acidic Protein where positive stains brown, (x40). AH = *alveus hippocampi*, RCC = *radiatio corporis callosi*, VL = *ventriculus lateralis*.

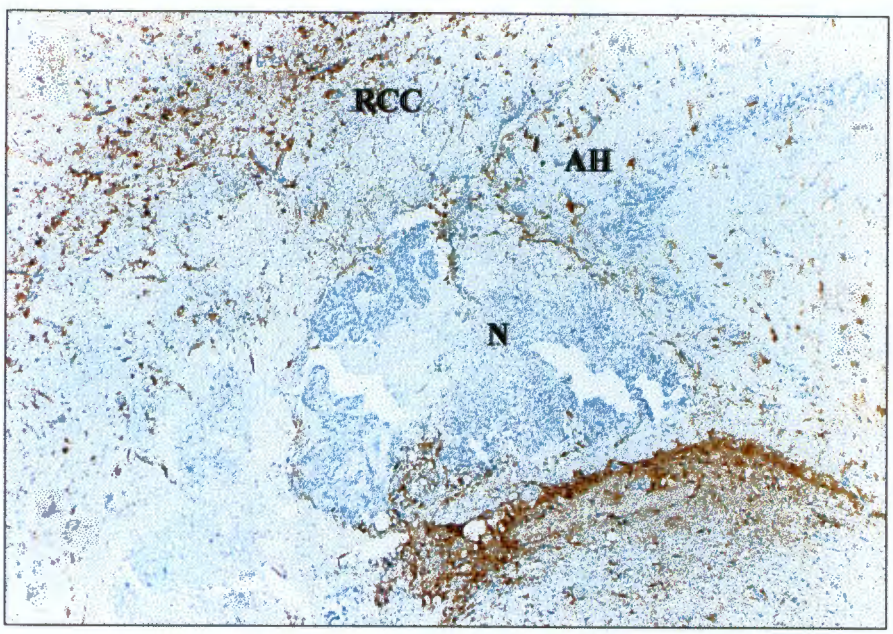

Figure 6.89 The *fimbria hippocampus* and surrounding structures of a rat brain at one year after 48 Gy at 0.07 Gy min^{-1}. Stained with Glial Fibrillary Acidic Protein where positive stains brown, (x40). AH = *alveus hippocampi*, N = necrosis, RCC = *radiatio corporis callosi*.

Figure 6.90 The *fimbria hippocampus* and surrounding structures of a rat brain at one year after 72 Gy (10 fractions in 12 days). Stained with Glial Fibrillary Acidic Protein where positive stains brown, (x15). AH = *alveus hippocampi*, CAI = *capsula* interna, N = necrosis.

6.6 HISTOLOGICAL OBSERVATION SCORES

Histological sections were examined from every single animal and incidences of changes as a result of radiation at each dose level within each experimental group and for each of the 17 sites examined is given in Tables 6.4 – 6.20.

Necrosis is a well documented late effect of radiation [Cotran et al., 1989; Ruifrok et al., 1994; Schultheiss et al., 1995; van der Kogel, 1979; van der Kogel and Barendsen, 1974] and the percentage incidences were calculated for all the doses in all the different dose rate experiments for all the sites (Tables 6.21 – 6.37). In addition, oedema was a consistent finding, the severity of which appeared to increase with dose for most of the sites and therefore the percentage incidences for oedema were also calculated (Tables 6.21 – 6.37).

Table 6.4 Incidence of histological changes in the *alveus hippocampi* of the rat brain one year after continuous protracted or fractionated ^{60}Co γ irradiation.

Radiation Protocol	Total Dose (Gy)	Number at risk	Necrosis		Blood Vessel Dilations		Oedema	Free iron	RBC congested vessels	Haemorrhage	Free calcium
			Partial	Complete	Small	Large					
0.04 Gy/min	31	5			1						
	35	5									
	39	4			1						
	41	5			4						
	47	6			1						
	57	7	6		2						
	65	6	3		1	1	1				
0.05 Gy/min	30	4									
	34	5			1		1				
	37	5			2						
	40	4			1						
	47	6	1		4						
	55	5	3		1	2	1			1	
	65	6	2		2	2		1	1		

Table 6.4 continued.

Radiation Protocol	Total Dose (Gy)	Number at risk	Necrosis		Blood Vessel Dilations		Oedema	Free iron	RBC congested vessels	Haemorrhage	Free calcium
			Partial	Complete	Small	Large					
0.07 Gy/min	30	5			5	1					
	33	4			4						
	36	5			5						
	38	5			4	1					
	44	6			4	2	2			1	
	48	6	3	1	2	1	1		2		
	57	4	2		2	2					
10 fx / 12 d	40	4			2						
	47	5			4						
	54	5			5						
	60	5			5						
	64	7	1		2	4	2		2	3	
	68	5	2		3	2	3			1	
	72	7	7			2	2				1

Table 6.5 Incidence of histological changes in the *capsula interna* of the rat brain one year after continuous protracted or fractionated ^{60}Co γ irradiation.

Radiation Protocol	Total Dose (Gy)	Number at risk	Necrosis		Blood Vessel Dilations		Oedema	Free iron	RBC congested vessels	Haemorrhage	Free calcium	Calcification of vessel walls
			Partial	Complete	Small	Large						
0.04 Gy/min	31	5			1	1						
	35	5			2							
	39	4			3	1						
	41	5			4							
	47	6			6							
	57	7	5	1	5	1						
	65	6	2	1	3	2	2					
0.05 Gy/min	30	4			3	1						
	34	5			5		1					
	37	5			4	1						
	40	4			4		1					
	47	6	2		5		2					
	55	5	2			3	4				1	1
	65	6	5	1	3	1	6					

Table 6.5 continued.

Radiation Protocol	Total Dose (Gy)	Number at risk	Necrosis		Blood Vessel Dilations		Oedema	Free iron	RBC congested vessels	Haemorrhage	Free calcium	Calcification of vessel walls
			Partial	Complete	Small	Large						
0.07 Gy/min	30	5			5		1					
	33	4			3	1	1					
	36	5			4	1						
	38	5			1	4	1					
	44	6		1	4	2	2			1		2
	48	6	4	1		3	3		1	1		
	57	4	3	1	1	2		1		1		
10 fx / 12 d	40	4			3	1						
	47	5			1	4						
	54	5			3	2						
	60	5			1	4						
	64	7	1		4	3	3					2
	68	5	2	1	2	2	5	1	2		2	
	72	7	1	2		2	7			1	7	

Table 6.6 Incidence of histological changes in the *capsula interna pars retrolenticularis* of the rat brain one year after continuous protracted or fractionated ^{60}Co γ irradiation.

Radiation Protocol	Total Dose (Gy)	Number at risk	Necrosis		Blood Vessel Dilations		Oedema	RBC congested vessels	Haemorrhage	Free calcium	Calcification of vessel walls
			Partial	Complete	Small	Large					
0.04 Gy/min	31	5			1	2					
	35	5			3						
	39	4			3	1					
	41	5			4						
	47	6			4	1	2			1	
	57	7			3	4					
	65	6			2	4	1				
0.05 Gy/min	30	4			3						
	34	5			4	1					
	37	5			3						
	40	4			4						
	47	6			4	1	1				1
	55	5			2	3	2				3
	65	6	2		4	2	5		1		2

Table 6.6 continued.

Radiation Protocol	Total Dose (Gy)	Number at risk	Necrosis		Blood Vessel Dilations		Oedema	RBC congested vessels	Haemorrhage	Free calcium	Calcification of vessel walls
			Partial	Complete	Small	Large					
0.07 Gy/min	30	5			5		2				
	33	4			3	1					
	36	5			4	1					
	38	5				5					
	44	6	1		3	3	2		1		1
	48	6	2		2	2	2	1			
	57	4			1	3	1				2
10 fx / 12 d	40	4			1	3					
	47	5				5					
	54	5			1	4	1				
	60	5			3	2					1
	64	7			5	2	1				3
	68	5			3	2	1			2	
	72	7	1		1	2			1		2

Table 6.7 Incidence of histological changes in the choroid plexus of the rat brain one year after continuous protracted or fractionated ^{60}Co γ irradiation.

Radiation Protocol	Total Dose (Gy)	Number at risk	Necrosis		Blood Vessel Dilations		Oedema	Free iron	RBC congested vessels	Vacuolation	Calcification of vessel walls
			Partial	Complete	Small	Large					
0.04 Gy/min	31	5									
	35	5				1					
	39	4									
	41	5									
	47	6			1					1	
	57	7	3				1				
	65	6									
0.05 Gy/min	30	4									
	34	5									
	37	5									
	40	4									
	47	6	1		1				1		
	55	5	2			1	1	1			
	65	6	3			4	6	1	2		

Table 6.7 continued.

Radiation Protocol	Total Dose (Gy)	Number at risk	Necrosis		Blood Vessel Dilations		Oedema	Free iron	RBC congested vessels	Vacuolation	Calcification of vessel walls
			Partial	Complete	Small	Large					
0.07 Gy/min	30	5							2		
	33	4			2	1			3		
	36	5			1	1					
	38	5				3					
	44	6	1		1	5	5	3	2		1
	48	6	3			2	4		1		
	57	4				3	4				1
10 fx / 12 d	40	4									
	47	5				1					
	54	5								5	
	60	5				3			1	5	
	64	7				6	1		3	7	
	68	5	3			2				4	
	72	7				7	2		1	7	

Table 6.8 Incidence of histological changes in the *cingulum* of the rat brain one year after continuous protracted or fractionated ^{60}Co γ irradiation.

Radiation Protocol	Total Dose (Gy)	Number at risk	Necrosis		Blood Vessel Dilations		Oedema	Free iron	RBC congested vessels	Haemorrhage	Free calcium
			Partial	Complete	Small	Large					
0.04 Gy/min	31	5			4						
	35	5									
	39	4			3						
	41	5			4	1					
	47	6									
	57	7	1	1	6	1					
	65	6	2		6		2				
0.05 Gy/min	30	4			2	1	1				
	34	5			4	1	1				
	37	5			5		2				
	40	4			3	1					
	47	6	1		5		1				
	55	5	1	1	1	4	1			1	
	65	6	1		3	3			2	1	1

Table 6.8 continued.

Radiation Protocol	Total Dose (Gy)	Number at risk	Necrosis		Blood Vessel Dilations		Oedema	Free iron	RBC congested vessels	Haemorrhage	Free calcium
			Partial	Complete	Small	Large					
0.07 Gy/min	30	5			2	3					
	33	4			3	1			1		
	36	5			4	1					
	38	5			5				1		
	44	6	2		4	1	2			1	
	48	6	2		3	1	1		1		
	57	4			2	3					
10 fx / 12 d	40	4			4						
	47	5			4	1	1				
	54	5			4	2					
	60	5			3	3	1				
	64	7	1		1	3	2		2	5	
	68	5	2		3	3	4	1	1	4	1
	72	7	2		1	2			1	1	2

Table 6.9 Incidence of histological changes in the ependymal cells of the rat brain one year after continuous protracted or fractionated ^{60}Co γ irradiation.

Radiation Protocol	Total Dose (Gy)	Number at risk	Necrosis		Blood Vessel Dilations		Mild hyperplasia
			Partial	Complete	Small	Large	
0.04 Gy/min	31	5					
	35	5					
	39	4			1		
	41	5					
	47	6					
	57	7	3				2
	65	6					3
0.05 Gy/min	30	4					
	34	5					4
	37	5					2
	40	4					
	47	6					
	55	5	2				
	65	6	4			1	

Table 6.9 continued.

Radiation Protocol	Total Dose (Gy)	Number at risk	Necrosis		Blood Vessel Dilations		Mild hyperplasia
			Partial	Complete	Small	Large	
0.07 Gy/min	30	5					
	33	4					1
	36	5					
	38	5					
	44	6	1			1	
	48	6	1			2	
	57	4	1			1	1
10 fx / 12 d	40	4				2	
	47	5			1	1	
	54	5				3	1
	60	5				2	
	64	7	1		1	1	
	68	5	3			1	
	72	7	7				

Table 6.10 Incidence of histological changes in the *fasiculus medialis prosencephali* of the rat brain one year after continuous protracted or fractionated ^{60}Co γ irradiation.

Radiation Protocol	Total Dose (Gy)	Number at risk	Necrosis		Blood Vessel Dilations		Oedema	RBC congested vessels	Haemorrhage
			Partial	Complete	Small	Large			
0.04 Gy/min	31	5			2	3			
	35	5			1				
	39	4			3				
	41	5							
	47	6			2	1			
	57	7			2	3			
	65	6			1				
0.05 Gy/min	30	4							
	34	5				1			
	37	5			1				
	40	4			3	1			
	47	6			2	1	1		
	55	5				1			
	65	6				1			

Table 6.10 continued.

Radiation Protocol	Total Dose (Gy)	Number at risk	Necrosis		Blood Vessel Dilations		Oedema	RBC congested vessels	Haemorrhage
			Partial	Complete	Small	Large			
0.07 Gy/min	30	5			3	1		1	
	33	4			2	2		1	
	36	5			4	1			
	38	5			2	2			
	44	6			4	1	1		
	48	6	1		2		2	1	1
	57	4			3				
10 fx / 12 d	40	4			1				
	47	5			3	2			
	54	5			4	1			
	60	5			4	1			
	64	7			5				
	68	5			1	2			
	72	7			7				

Table 6.11 Incidence of histological changes in the *fimbria hippocampus* of the rat brain one year after continuous protracted or fractionated ^{60}Co γ irradiation.

Radiation Protocol	Total Dose (Gy)	Number at risk	Necrosis		Blood Vessel Dilations		Oedema	Free iron	RBC congested vessels	Haemorrhage	Histiocytes	Free calcium
			Partial	Complete	Small	Large						
0.04 Gy/min	31	5				1	2					
	35	5			3							
	39	4			4							
	41	5			4							
	47	6			4	2	3					
	57	7	3	3	4	4	3					
	65	6	4	2	1	2	4		1			
0.05 Gy/min	30	4			2	2						
	34	5			3	1						
	37	5			1	4	3					
	40	4			4		2					
	47	6		2	5							
	55	5		5		3	1	1		1		
	65	6	2	3		2	3	1	1	1	1	

Table 6.11 continued.

Radiation Protocol	Total Dose (Gy)	Number at risk	Necrosis		Blood Vessel Dilations		Oedema	Free iron	RBC congested vessels	Haemorrhage	Histiocytes	Free calcium
			Partial	Complete	Small	Large						
0.07 Gy/min	30	5			3	2						
	33	4			2	2						
	36	5			5							
	38	5			3	2						
	44	6	2	3	3	2	2		1	1		
	48	6	2	4		2	2			1		
	57	4		4								
10 fx / 12 d	40	4			4							
	47	5			4	1	1	1				
	54	5			3	2						
	60	5			2	3						
	64	7	6		1	5	2		3	1		
	68	5	3	2		2	2					
	72	7		7				1				2

Table 6.12 Incidence of histological changes in the *gyrus dentatus* of the rat brain one year after continuous protracted or fractionated ^{60}Co γ irradiation.

Radiation Protocol	Total Dose (Gy)	Number at risk	Necrosis		Blood Vessel Dilations		Oedema	Free iron	RBC congested vessels	Haemorrhage	Free calcium	Histiocytes
			Partial	Complete	Small	Large						
0.04 Gy/min	31	5			2							
	35	5										
	39	4										
	41	5										
	47	6				1	2					
	57	7	3		1	2	4					
	65	6	3				3					
0.05 Gy/min	30	4					1					
	34	5					1					
	37	5					1					
	40	4					3					
	47	6			3	1	1			2		
	55	5	2		1	4	2			1		1
	65	6			3	1	2		1	1		1

Table 6.12 continued.

Radiation Protocol	Total Dose (Gy)	Number at risk	Necrosis		Blood Vessel Dilations		Oedema	Free iron	RBC congested vessels	Haemorrhage	Free calcium	Histiocytes
			Partial	Complete	Small	Large						
0.07 Gy/min	30	5			4							
	33	4			4							
	36	5			3							
	38	5			5							
	44	6			6		3		1	1		
	48	6	1	2		3	1		1			
	57	4			4		3		1	1		
10 fx / 12 d	40	4			1							
	47	5			5							
	54	5			5							
	60	5			3	2						
	64	7			3	1	3		1	1		
	68	5	1		2	3	3			1		
	72	7	1		1	2	3	1	1		1	

Table 6.13 Incidence of histological changes in the *hippocampus* of the rat brain one year after continuous protracted or fractionated ^{60}Co γ irradiation.

Radiation Protocol	Total Dose (Gy)	Number at risk	Necrosis		Blood Vessel Dilations		Oedema	Free iron	RBC congested vessels	Haemorrhage	Free calcium	Histiocytes
			Partial	Complete	Small	Large						
0.04 Gy/min	31	5			1							1
	35	5										
	39	4			1							
	41	5			2							
	47	6				1	1					
	57	7	6		3	1						
	65	6	3		2		2		1			
0.05 Gy/min	30	4										
	34	5				1	1					
	37	5										
	40	4			2							
	47	6	1		3				1			
	55	5	1	2		3	1		1			
	65	6	2		3	1	5	1	1	1	1	1

Table 6.13 continued.

Radiation Protocol	Total Dose (Gy)	Number at risk	Necrosis		Blood Vessel Dilations		Oedema	Free iron	RBC congested vessels	Haemorrhage	Free calcium	Histiocytes
			Partial	Complete	Small	Large						
0.07 Gy/min	30	5			5				1			
	33	4			4				1	1	1	
	36	5			5				2			
	38	5			5							
	44	6	1		3	2	2			2	2	
	48	6	2	1		3	1		1	1	1	1
	57	4	1			4	3			3	3	
10 fx / 12 d	40	4			3							
	47	5			5			1				
	54	5			4	1						
	60	5			4	1						
	64	7	2		3	4	4	1	2	5	5	
	68	5	3		2	3	3	1	2	2	2	
	72	7	2			7	7			2	2	

Table 6.14 Incidence of histological changes in the *nucleus lateralis* of the rat brain one year after continuous protracted or fractionated ^{60}Co γ irradiation.

Radiation Protocol	Total Dose (Gy)	Number at risk	Necrosis		Blood Vessel Dilations		Oedema	RBC congested vessels	Haemorrhage
			Partial	Complete	Small	Large			
0.04 Gy/min	31	5			2	2			
	35	5			1				
	39	4			3				
	41	5							
	47	6			2	1			
	57	7			2	3			
	65	6			1				
0.05 Gy/min	30	4							
	34	5				1			
	37	5			1				
	40	4			3	1			
	47	6			2	1	1		
	55	5				1			
	65	6				1			

Table 6.14 continued.

Radiation Protocol	Total Dose (Gy)	Number at risk	Necrosis		Blood Vessel Dilations		Oedema	RBC congested vessels	Haemorrhage
			Partial	Complete	Small	Large			
0.07 Gy/min	30	5			3	1		1	
	33	4			2	2		1	
	36	5			4	1			
	38	5			2	2			
	44	6			4	1	1		
	48	6	1		2	1	2	1	1
	57	4			3				
10 fx / 12 d	40	4			1				
	47	5			3	2			
	54	5			4	1			
	60	5			4	1			
	64	7			5				
	68	5			1	2			
	72	7			7				

Table 6.15 Incidence of histological changes in the *nucleus lateralis habenulae* of the rat brain one year after continuous protracted or fractionated ^{60}Co γ irradiation.

Radiation Protocol	Total Dose (Gy)	Number at risk	Necrosis		Blood Vessel Dilations		Oedema	Free iron	RBC congested vessels	Histiocytes
			Partial	Complete	Small	Large				
0.04 Gy/min	31	5								
	35	5								
	39	4								
	41	5			1					
	47	6			5					
	57	7			6	1				
	65	6			6		1	1		
0.05 Gy/min	30	4			3	1				
	34	5			4					
	37	5			4					
	40	4			4					
	47	6			5					
	55	5			4	1	1			
	65	6			6					1

Table 6.15 continued.

Radiation Protocol	Total Dose (Gy)	Number at risk	Necrosis		Blood Vessel Dilations		Oedema	Free iron	RBC congested vessels	Histiocytes
			Partial	Complete	Small	Large				
0.07 Gy/min	30	5			5					
	33	4			2	1			2	
	36	5			5				2	
	38	5			3	2				
	44	6			4	2	1			
	48	6			3	1				
	57	4			3	1				
10 fx / 12 d	40	4			3					
	47	5			2					
	54	5			3					
	60	5			2	2				
	64	7			7					
	68	5			5					
	72	7			2	1				

Table 6.16 Incidence of histological changes in the *nucleus lateralis thalami* of the rat brain one year after continuous protracted or fractionated ^{60}Co γ irradiation.

Radiation Protocol	Total Dose (Gy)	Number at risk	Necrosis		Blood Vessel Dilations		Oedema	Free iron	RBC congested vessels	Haemorrhage	Free calcium	Histiocytes
			Partial	Complete	Small	Large						
0.04 Gy/min	31	5			4	1						
	35	5										
	39	4			3	1						
	41	5			3	2						
	47	6			2	4						
	57	7	6		4	3						
	65	6	3		3	3	2					1
0.05 Gy/min	30	4				4						
	34	5				4						
	37	5				4	1					
	40	4				4						
	47	6	1		2	3						
	55	5	2			5			1			
	65	6	4		2	3			1			1

Table 6.16 continued.

Radiation Protocol	Total Dose (Gy)	Number at risk	Necrosis		Blood Vessel Dilations		Oedema	Free iron	RBC congested vessels	Haemorrhage	Free calcium	Histiocytes
			Partial	Complete	Small	Large						
0.07 Gy/min	30	5			5				1			
	33	4				4						
	36	5				5			1			
	38	5				5						
	44	6	2		4	2			1			
	48	6	3		2	2		1		1		
	57	4	2			4				1		
10 fx / 12 d	40	4				4						
	47	5				5						
	54	5				5						
	60	5				5	1					
	64	7			4	3	1		1			
	68	5	3		2	3					1	
	72	7	7			7					7	

Table 6.17 Incidence of histological changes in the *radiatio corporis callosi* of the rat brain one year after continuous protracted or fractionated ^{60}Co γ irradiation.

Radiation Protocol	Total Dose (Gy)	Number at risk	Necrosis		Blood Vessel Dilations		Oedema	RBC congested vessels	Haemorrhage	Free calcium
			Partial	Complete	Small	Large				
0.04 Gy/min	31	5				2				
	35	5								
	39	4			1					
	41	5			3					
	47	6			5	1				
	57	7	2		5	1				
	65	6	2		4	2	1			
0.05 Gy/min	30	4								
	34	5			5		1			
	37	5			3	2	2			
	40	4			4					
	47	6	1		5		1	1		
	55	5	1		3	1	3		1	
	65	6	3		3	2	3	1	1	

Table 6.17 continued.

Radiation Protocol	Total Dose (Gy)	Number at risk	Necrosis		Blood Vessel Dilations		Oedema	RBC congested vessels	Haemorrhage	Free calcium
			Partial	Complete	Small	Large				
0.07 Gy/min	30	5			3	1				
	33	4			3					
	36	5			4					
	38	5			4	1				
	44	6			5	1	2			
	48	6	1		3	1		1		
	57	4	1		3	1				
10 fx / 12 d	40	4			2	2				
	47	5			4	1				
	54	5			5					
	60	5			4	1				
	64	7			7		1		1	
	68	5	3		4	1	3		1	
	72	7	1		2	1	2	1	2	2

Table 6.18 Incidence of histological changes in the *stria terminalis* of the rat brain one year after continuous protracted or fractionated ^{60}Co γ irradiation.

Radiation Protocol	Total Dose (Gy)	Number at risk	Necrosis		Blood Vessel Dilations		Oedema	Free iron	RBC congested vessels	Haemorrhage	Free calcium
			Partial	Complete	Small	Large					
0.04 Gy/min	31	5			1		1				
	35	5									
	39	4			1						
	41	5			2						
	47	6	1		2	3	2			1	
	57	7	3	3	5	2	2				
	65	6	1	3	1	4	2				
0.05 Gy/min	30	4			2						
	34	5			2		1				
	37	5			4		2				
	40	4			4		2				
	47	6	2		4	1			1		
	55	5	1	2		3	1	1			
	65	6	6		3	1	1				

Table 6.18 continued.

Radiation Protocol	Total Dose (Gy)	Number at risk	Necrosis		Blood Vessel Dilations		Oedema	Free iron	RBC congested vessels	Haemorrhage	Free calcium
			Partial	Complete	Small	Large					
0.07 Gy/min	30	5			3	2	1				
	33	4			2		1				
	36	5			5		1			1	
	38	5			4	1	1				
	44	6	1	1	3	3	1		1		
	48	6	5	1		2	1		1		
	57	4	1	2		1					
10 fx / 12 d	40	4			3	1					
	47	5			3						
	54	5			4	1					
	60	5			5						
	64	7	2		3	4			1	1	
	68	5	3	1		4	2		1	1	3
	72	7		7		7				1	

Table 6.19 Incidence of histological changes in the *sulcus hippocampi* of the rat brain one year after continuous protracted or fractionated ^{60}Co γ irradiation.

Radiation Protocol	Total Dose (Gy)	Number at risk	Necrosis		Blood Vessel Dilations		Free iron	RBC congested vessels	Haemorrhage
			Partial	Complete	Small	Large			
0.04 Gy/min	31	5			4	1			
	35	5			4	1			
	39	4				4			
	41	5			3	2			
	47	6			2	3			
	57	7		1	1	2			
	65	6		1	1				
0.05 Gy/min	30	4			1	3			
	34	5			2	3			
	37	5				5			
	40	4			1	3			
	47	6			1	3			
	55	5				2			
	65	6			5			1	

Table 6.19 continued.

Radiation Protocol	Total Dose (Gy)	Number at risk	Necrosis		Blood Vessel Dilations		Free iron	RBC congested vessels	Haemorrhage
			Partial	Complete	Small	Large			
0.07 Gy/min	30	5				5		1	
	33	4				4		2	
	36	5				5			
	38	5				5			
	44	6			2	2			
	48	6	2			3		1	1
	57	4			1	2			
10 fx / 12 d	40	4				4			
	47	5				5			
	54	5				5			
	60	5			2	3			
	64	7			2	2			
	68	5			2	3	1		
	72	7	7						

Table 6.20 Incidence of histological changes in the *truncus corporis callosi* of the rat brain one year after continuous protracted or fractionated ^{60}Co γ irradiation.

Radiation Protocol	Total Dose (Gy)	Number at risk	Necrosis		Blood Vessel Dilations		Oedema	Free iron	RBC congested vessels	Haemorrhage	Free calcium
			Partial	Complete	Small	Large					
0.04 Gy/min	31	5			4	1					
	35	5									
	39	4			1						
	41	5			4	1					
	47	6			6						
	57	7	2		6	1	1				
	65	6	2		5		4				
0.05 Gy/min	30	4			4		1				
	34	5			5						
	37	5			5						
	40	4			2		3	1		1	
	47	6	1		5		3		1		
	55	5		3	1	2					
	65	6	1		6		2				

Table 6.20 continued.

Radiation Protocol	Total Dose (Gy)	Number at risk	Necrosis		Blood Vessel Dilations		Oedema	Free iron	RBC congested vessels	Haemorrhage	Free calcium
			Partial	Complete	Small	Large					
0.07 Gy/min	30	5			4						
	33	4			4		1		1		
	36	5			4	1					
	38	5			1	4					
	44	6	1	1	4	2				1	
	48	6	3		2	1	2	1	2		
	57	4	2		2	2	2			1	
10 fx / 12 d	40	4			3						
	47	5			5						
	54	5			3	2					
	60	5			3	2					
	64	7	2		2	4	2		1	2	
	68	5	2	1	1	2	3			1	1
	72	7	1	2	1		1				3

Table 6.21 Incidence of necrosis and oedema in the *alveus hippocampi* of the rat brain one year after irradiation with ^{60}Co γ rays.

Radiation Protocol	Total Dose (Gy)	Number at risk	Responders necrosis	% incidence of necrosis ± SE	Responders oedema	% incidence of oedema ± SE
0.04 Gy/min	31	5	0	0	0	0
	35	5	0	0	0	0
	39	4	0	0	0	0
	41	5	0	0	0	0
	47	6	0	0	0	0
	57	7	6	85.7 ± 13.2	0	0
	65	6	3	50 ± 20.4	1	16.6 ± 15.2
0.05 Gy/min	30	4	0	0	0	0
	34	5	0	0	1	20 ± 17.8
	37	5	0	0	0	0
	40	4	0	0	0	0
	47	6	1	16.6 ± 15.2	0	0
	55	5	3	60 ± 21.9	1	20 ± 17.8
	65	6	2	33.3 ± 19.2	0	0
0.07 Gy/min	30	5	0	0	0	0
	33	4	0	0	0	0
	36	5	0	0	0	0
	38	5	0	0	0	0
	44	6	0	0	2	33.3 ± 19.2
	48	6	4	66.6 ± 19.2	1	16.6 ± 15.2
	57	4	2	50 ± 25	0	0
10 fx / 12 d	40	4	0	0	0	0
	47	5	0	0	0	0
	54	5	0	0	0	0
	60	5	0	0	0	0
	64	7	1	14.2 ± 13.2	2	28.5 ± 17.0
	68	5	2	40 ± 21.9	3	60 ± 21.9
	72	7	7	100 ± 0	2	28.5 ± 17.0

Table 6.22 Incidence of necrosis and oedema in the *capsula interna* of the rat brain one year after irradiation with ^{60}Co γ rays.

Radiation Protocol	Total Dose (Gy)	Number at risk	Responders necrosis	% incidence of necrosis ± SE	Responders oedema	% incidence of oedema ± SE
0.04 Gy/min	31	5	0	0	0	0
	35	5	0	0	0	0
	39	4	0	0	0	0
	41	5	0	0	0	0
	47	6	0	0	0	0
	57	7	6	85.7 ± 13.2	0	0
	65	6	3	50 ± 20.4	2	33.3 ± 19.2
0.05 Gy/min	30	4	0	0	0	0
	34	5	0	0	1	20 ± 17.8
	37	5	0	0	0	0
	40	4	0	0	1	25 ± 21.6
	47	6	2	33.3 ± 19.2	2	33.3 ± 19.2
	55	5	2	40 ± 21.9	4	80 ± 17.8
	65	6	6	100 ± 0	6	100 ± 0
0.07 Gy/min	30	5	0	0	1	20 ± 17.8
	33	4	0	0	1	25 ± 21.6
	36	5	0	0	0	0
	38	5	0	0	1	20 ± 17.8
	44	6	1	16.6 ± 15.2	2	33.3 ± 19.2
	48	6	5	83.3 ± 15.2	3	50 ± 20.4
	57	4	4	100 ± 0	0	0
10 fr / 12 d	40	4	0	0	0	0
	47	5	0	0	0	0
	54	5	0	0	0	0
	60	5	0	0	0	0
	64	7	1	14.2 ± 13.2	3	42.8 ± 18.7
	68	5	3	60 ± 21.9	5	100 ± 0
	72	7	3	42.8 ± 18.7	7	100 ± 0

Table 6.23 Incidence of necrosis and oedema in the *capsula interna pars retrolenticularis* of the rat brain one year after irradiation with ^{60}Co γ rays.

Radiation Protocol	Total Dose (Gy)	Number at risk	Responders necrosis	% incidence of necrosis ± SE	Responders oedema	% incidence of oedema ± SE
0.04 Gy/min	31	5	0	0	0	0
	35	5	0	0	0	0
	39	4	0	0	0	0
	41	5	0	0	0	0
	47	6	0	0	2	33.3 ± 19.2
	57	7	0	0	0	0
	65	6	0	0	1	16.6 ± 15.2
0.05 Gy/min	30	4	0	0	0	0
	34	5	0	0	0	0
	37	5	0	0	0	0
	40	4	0	0	0	0
	47	6	0	0	1	16.6 ± 15.2
	55	5	0	0	2	40 ± 21.9
	65	6	2	33.3 ± 19.2	5	83.3 ± 15.2
0.07 Gy/min	30	5	0	0	2	40 ± 21.9
	33	4	0	0	0	0
	36	5	0	0	0	0
	38	5	0	0	0	0
	44	6	1	16.6 ± 15.2	2	33.3 ± 19.2
	48	6	2	33.3 ± 19.2	2	33.3 ± 19.2
	57	4	0	0	1	25 ± 21.6
10 fr / 12 d	40	4	0	0	0	0
	47	5	0	0	0	0
	54	5	0	0	1	20 ± 17.8
	60	5	0	0	0	0
	64	7	0	0	1	14.2 ± 13.2
	68	5	0	0	1	20 ± 17.8
	72	7	1	14.2 ± 13.2	0	0

Table 6.24 Incidence of necrosis and oedema in the choroid plexus of the rat brain one year after irradiation with ^{60}Co γ rays.

Radiation Protocol	Total Dose (Gy)	Number at risk	Responders necrosis	% incidence of necrosis ± SE	Responders oedema	% incidence of oedema ± SE
0.04 Gy/min	31	5	0	0	0	0
	35	5	0	0	0	0
	39	4	0	0	0	0
	41	5	0	0	0	0
	47	6	0	0	0	0
	57	7	3	42.8 ± 18.7	1	14.2 ± 13.2
	65	6	0	0	0	0
0.05 Gy/min	30	4	0	0	0	0
	34	5	0	0	0	0
	37	5	0	0	0	0
	40	4	0	0	0	0
	47	6	1	16.6 ± 15.2	0	0
	55	5	2	40 ± 21.9	1	20 ± 17.8
	65	6	3	50 ± 20.4	6	100 ± 0
0.07 Gy/min	30	5	0	0	0	0
	33	4	0	0	0	0
	36	5	0	0	0	0
	38	5	0	0	0	0
	44	6	1	16.6 ± 15.2	5	83.3 ± 15.2
	48	6	3	50 ± 20.4	4	66.6 ± 19.2
	57	4	0	0	4	100 ± 0
10 fr / 12 d	40	4	0	0	0	0
	47	5	0	0	0	0
	54	5	0	0	0	0
	60	5	0	0	0	0
	64	7	0	0	1	14.2 ± 13.2
	68	5	3	60 ± 21.9	0	0
	72	7	0	0	2	28.5 ± 17.0

Table 6.25 Incidence of necrosis and oedema in the *cingulum* of the rat brain one year after irradiation with ^{60}Co γ rays.

Radiation Protocol	Total Dose (Gy)	Number at risk	Responders necrosis	% incidence of necrosis ± SE	Responders oedema	% incidence of oedema ± SE
0.04 Gy/min	31	5	0	0	0	0
	35	5	0	0	0	0
	39	4	0	0	0	0
	41	5	0	0	0	0
	47	6	0	0	0	0
	57	7	2	28.5 ± 17.0	0	0
	65	6	2	33.3 ± 19.2	2	33.3 ± 19.2
0.05 Gy/min	30	4	0	0	1	25 ± 21.6
	34	5	0	0	1	20 ± 17.8
	37	5	0	0	2	40 ± 21.9
	40	4	0	0	0	0
	47	6	1	16.6 ± 15.2	1	16.6 ± 15.2
	55	5	2	40 ± 21.9	1	20 ± 17.8
	65	6	1	16.6 ± 15.2	0	0
0.07 Gy/min	30	5	0	0	0	0
	33	4	0	0	0	0
	36	5	0	0	0	0
	38	5	0	0	0	0
	44	6	2	33.3 ± 19.2	2	33.3 ± 19.2
	48	6	2	33.3 ± 19.2	1	16.6 ± 15.2
	57	4	0	0	0	0
10 fr / 12 d	40	4	0	0	0	0
	47	5	0	0	1	20 ± 17.8
	54	5	0	0	0	0
	60	5	0	0	1	20 ± 17.8
	64	7	1	14.2 ± 13.2	2	28.5 ± 17.0
	68	5	2	40 ± 21.9	4	80 ± 17.8
	72	7	2	28.5 ± 17.0	0	0

Table 6.26 Incidence of necrosis and oedema in the ependymal cells of the rat brain one year after irradiation with ^{60}Co γ rays.

Radiation Protocol	Total Dose (Gy)	Number at risk	Responders necrosis	% incidence of necrosis ± SE	Responders oedema	% incidence of oedema ± SE
0.04 Gy/min	31	5	0	0	0	0
	35	5	0	0	0	0
	39	4	0	0	0	0
	41	5	0	0	0	0
	47	6	0	0	0	0
	57	7	3	42.8 ± 18.7	0	0
	65	6	0	0	0	0
0.05 Gy/min	30	4	0	0	0	0
	34	5	0	0	0	0
	37	5	0	0	0	0
	40	4	0	0	0	0
	47	6	0	0	0	0
	55	5	2	40 ± 21.9	0	0
	65	6	4	66.6 ± 19.2	0	0
0.07 Gy/min	30	5	0	0	0	0
	33	4	0	0	0	0
	36	5	0	0	0	0
	38	5	0	0	0	0
	44	6	1	16.6 ± 15.2	0	0
	48	6	1	16.6 ± 15.2	0	0
	57	4	1	25 ± 21.6	0	0
10 fr / 12 d	40	4	0	0	0	0
	47	5	0	0	0	0
	54	5	0	0	0	0
	60	5	0	0	0	0
	64	7	1	14.2 ± 13.2	0	0
	68	5	3	60 ± 21.9	0	0
	72	7	7	100 ± 0	0	0

Table 6.27 Incidence of necrosis and oedema in the *fasiculus medialis prosencephali* of the rat brain one year after irradiation with ^{60}Co γ rays.

Radiation Protocol	Total Dose (Gy)	Number at risk	Responders necrosis	% incidence of necrosis ± SE	Responders oedema	% incidence of oedema ± SE
0.04 Gy/min	31	5	0	0	0	0
	35	5	0	0	0	0
	39	4	0	0	0	0
	41	5	0	0	0	0
	47	6	0	0	0	0
	57	7	0	0	0	0
	65	6	0	0	0	0
0.05 Gy/min	30	4	0	0	0	0
	34	5	0	0	0	0
	37	5	0	0	0	0
	40	4	0	0	0	0
	47	6	0	0	1	16.6 ± 15.2
	55	5	0	0	0	0
	65	6	0	0	0	0
0.07 Gy/min	30	5	0	0	0	0
	33	4	0	0	0	0
	36	5	0	0	0	0
	38	5	0	0	0	0
	44	6	0	0	1	16.6 ± 15.2
	48	6	1	16.6 ± 15.2	2	33.3 ± 19.20
	57	4	0	0	0	0
10 fr / 12 d	40	4	0	0	0	0
	47	5	0	0	0	0
	54	5	0	0	0	0
	60	5	0	0	0	0
	64	7	0	0	0	0
	68	5	0	0	0	0
	72	7	0	0	0	0

Table 6.28 Incidence of necrosis and oedema in the *fimbria hippocampus* of the rat brain one year after irradiation with ^{60}Co γ rays.

Radiation Protocol	Total Dose (Gy)	Number at risk	Responders necrosis	% incidence of necrosis ± SE	Responders oedema	% incidence of oedema ± SE
0.04 Gy/min	31	5	0	0	2	40 ± 21.9
	35	5	0	0	0	0
	39	4	0	0	0	0
	41	5	0	0	0	0
	47	6	0	0	3	50 ± 20.4
	57	7	6	85.7 ± 13.2	3	42.8 ± 18.7
	65	6	6	100 ± 0	4	66.6 ± 19.2
0.05 Gy/min	30	4	0	0	0	0
	34	5	0	0	0	0
	37	5	0	0	3	60 ± 21.9
	40	4	0	0	2	50 ± 25
	47	6	2	33.3 ± 19.2	0	0
	55	5	5	100 ± 0	1	20 ± 17.8
	65	6	5	83.3 ± 15.2	3	50 ± 20.4
0.07 Gy/min	30	5	0	0	0	0
	33	4	0	0	0	0
	36	5	0	0	0	0
	38	5	0	0	0	0
	44	6	5	83.3 ± 15.2	2	33.3 ± 19.2
	48	6	6	100 ± 0	2	33.3 ± 19.2
	57	4	4	100 ± 0	0	0
10 fr / 12 d	40	4	0	0	0	0
	47	5	0	0	1	20 ± 17.8
	54	5	0	0	0	0
	60	5	0	0	0	0
	64	7	6	85.7 ± 13.2	2	28.5 ± 17.0
	68	5	5	100 ± 0	2	40 ± 21.9
	72	7	7	100 ± 0	0	0

Table 6.29 Incidence of necrosis and oedema in the *gyrus dentatus* of the rat brain one year after irradiation with ^{60}Co γ rays.

Radiation Protocol	Total Dose (Gy)	Number at risk	Responders necrosis	% incidence of necrosis ± SE	Responders oedema	% incidence of oedema ± SE
0.04 Gy/min	31	5	0	0	0	0
	35	5	0	0	0	0
	39	4	0	0	0	0
	41	5	0	0	0	0
	47	6	0	0	2	33.3 ± 19.2
	57	7	3	42.8 ± 18.7	4	57.1 ± 18.7
	65	6	3	50 ± 20.4	3	50 ± 20.4
0.05 Gy/min	30	4	0	0	1	25 ± 21.6
	34	5	0	0	1	20 ± 17.8
	37	5	0	0	1	20 ± 17.8
	40	4	0	0	3	75 ± 21.6
	47	6	0	0	1	16.6 ± 15.2
	55	5	2	40 ± 21.9	2	40 ± 21.9
	65	6	0	0	2	33.3 ± 19.2
0.07 Gy/min	30	5	0	0	0	0
	33	4	0	0	0	0
	36	5	0	0	0	0
	38	5	0	0	0	0
	44	6	0	0	3	50 ± 20.4
	48	6	3	50 ± 20.4	1	16.6 ± 15.2
	57	4	0	0	3	75 ± 21.6
10 fr / 12 d	40	4	0	0	0	0
	47	5	0	0	0	0
	54	5	0	0	0	0
	60	5	0	0	0	0
	64	7	0	0	3	42.8 ± 18.7
	68	5	1	20 ± 17.8	3	60 ± 21.9
	72	7	1	14.2 ± 13.2	3	42.8 ± 18.7

Table 6.30 Incidence of necrosis and oedema in the *hippocampus* of the rat brain one year after irradiation with ^{60}Co γ rays.

Radiation Protocol	Total Dose (Gy)	Number at risk	Responders necrosis	% incidence of necrosis ± SE	Responders oedema	% incidence of oedema ± SE
0.04 Gy/min	31	5	0	0	0	0
	35	5	0	0	0	0
	39	4	0	0	0	0
	41	5	0	0	0	0
	47	6	0	0	1	16.6 ± 15.2
	57	7	6	85.7 ± 13.2	0	0
	65	6	3	50 ± 20.4	2	33.3 ± 19.2
0.05 Gy/min	30	4	0	0	0	0
	34	5	0	0	1	20 ± 17.8
	37	5	0	0	0	0
	40	4	0	0	0	0
	47	6	1	16.6 ± 15.2	0	0
	55	5	3	60 ± 21.9	1	20 ± 17.8
	65	6	2	33.3 ± 19.2	5	83.3 ± 15.2
0.07 Gy/min	30	5	0	0	0	0
	33	4	0	0	0	0
	36	5	0	0	0	0
	38	5	0	0	0	0
	44	6	1	16.6 ± 15.2	2	33.3 ± 19.2
	48	6	3	50 ± 20.4	1	16.6 ± 15.2
	57	4	1	25 ± 21.6	3	75 ± 21.6
10 fr / 12 d	40	4	0	0	0	0
	47	5	0	0	0	0
	54	5	0	0	0	0
	60	5	0	0	0	0
	64	7	2	28.5 ± 17.0	4	57.1 ± 18.7
	68	5	3	60 ± 21.9	3	60 ± 21.9
	72	7	2	28.5 ± 17.0	7	100 ± 0

Table 6.31 Incidence of necrosis and oedema in the *nucleus lateralis* of the rat brain one year after irradiation with ^{60}Co γ rays.

Radiation Protocol	Total Dose (Gy)	Number at risk	Responders necrosis	% incidence of necrosis ± SE	Responders oedema	% incidence of oedema ± SE
0.04 Gy/min	31	5	0	0	0	0
	35	5	0	0	0	0
	39	4	0	0	0	0
	41	5	0	0	0	0
	47	6	0	0	0	0
	57	7	0	0	0	0
	65	6	0	0	0	0
0.05 Gy/min	30	4	0	0	0	0
	34	5	0	0	0	0
	37	5	0	0	0	0
	40	4	0	0	0	0
	47	6	0	0	1	16.6 ± 15.2
	55	5	0	0	0	0
	65	6	0	0	0	0
0.07 Gy/min	30	5	0	0	0	0
	33	4	0	0	0	0
	36	5	0	0	0	0
	38	5	0	0	0	0
	44	6	0	0	1	16.6 ± 15.2
	48	6	1	16.6 ± 15.2	2	33.3 ± 19.2
	57	4	0	0	0	0
10 fr / 12 d	40	4	0	0	0	0
	47	5	0	0	0	0
	54	5	0	0	0	0
	60	5	0	0	0	0
	64	7	0	0	0	0
	68	5	0	0	0	0
	72	7	0	0	0	0

Table 6.32 Incidence of necrosis and oedema in the *nucleus lateralis habenulae* of the rat brain one year after irradiation with ^{60}Co γ rays.

Radiation Protocol	Total Dose (Gy)	Number at risk	Responders necrosis	% incidence of necrosis ± SE	Responders oedema	% incidence of oedema ± SE
0.04 Gy/min	31	5	0	0	0	0
	35	5	0	0	0	0
	39	4	0	0	0	0
	41	5	0	0	0	0
	47	6	0	0	0	0
	57	7	0	0	0	0
	65	6	0	0	1	16.6 ± 15.2
0.05 Gy/min	30	4	0	0	0	0
	34	5	0	0	0	0
	37	5	0	0	0	0
	40	4	0	0	0	0
	47	6	0	0	0	0
	55	5	0	0	1	20 ± 17.8
	65	6	0	0	0	0
0.07 Gy/min	30	5	0	0	0	0
	33	4	0	0	0	0
	36	5	0	0	0	0
	38	5	0	0	0	0
	44	6	0	0	1	16.6 ± 15.2
	48	6	0	0	0	0
	57	4	0	0	0	0
10 fr / 12 d	40	4	0	0	0	0
	47	5	0	0	0	0
	54	5	0	0	0	0
	60	5	0	0	0	0
	64	7	0	0	0	0
	68	5	0	0	0	0
	72	7	0	0	0	0

Table 6.33 Incidence of necrosis and oedema in the *nucleus lateralis thalami* of the rat brain one year after irradiation with ^{60}Co γ rays.

Radiation Protocol	Total Dose (Gy)	Number at risk	Responders necrosis	% incidence of necrosis ± SE	Responders oedema	% incidence of oedema ± SE
0.04 Gy/min	31	5	0	0	0	0
	35	5	0	0	0	0
	39	4	0	0	0	0
	41	5	0	0	0	0
	47	6	0	0	0	0
	57	7	6	85.7 ± 13.2	0	0
	65	6	3	50 ± 20.4	2	33.3 ± 19.2
0.05 Gy/min	30	4	0	0	0	0
	34	5	0	0	0	0
	37	5	0	0	1	20 ± 17.8
	40	4	0	0	0	0
	47	6	1	16.6 ± 15.2	0	0
	55	5	2	40 ± 21.9	0	0
	65	6	4	66.6 ± 19.2	0	0
0.07 Gy/min	30	5	0	0	0	0
	33	4	0	0	0	0
	36	5	0	0	0	0
	38	5	0	0	0	0
	44	6	2	33.3 ± 19.2	0	0
	48	6	3	50 ± 20.4	0	0
	57	4	2	50 ± 25	0	0
10 fr / 12 d	40	4	0	0	0	0
	47	5	0	0	0	0
	54	5	0	0	0	0
	60	5	0	0	1	20 ± 17.8
	64	7	0	0	1	14.2 ± 13.2
	68	5	3	60 ± 21.9	0	0
	72	7	7	100 ± 0	0	0

Table 6.34 Incidence of necrosis and oedema in the *radiatio corporis callosi* of the rat brain one year after irradiation with ^{60}Co γ rays.

Radiation Protocol	Total Dose (Gy)	Number at risk	Responders necrosis	% incidence of necrosis ± SE	Responders oedema	% incidence of oedema ± SE
0.04 Gy/min	31	5	0	0	0	0
	35	5	0	0	0	0
	39	4	0	0	0	0
	41	5	0	0	0	0
	47	6	0	0	0	0
	57	7	2	28.5 ± 17.0	0	0
	65	6	2	33.3 ± 19.2	1	16.6 ± 15.2
0.05 Gy/min	30	4	0	0	0	0
	34	5	0	0	1	20 ± 17.8
	37	5	0	0	2	40 ± 21.9
	40	4	0	0	0	0
	47	6	1	16.6 ± 15.2	1	16.6 ± 15.2
	55	5	1	20 ± 17.8	3	60 ± 21.9
	65	6	3	50 ± 20.4	3	50 ± 20.4
0.07 Gy/min	30	5	0	0	0	0
	33	4	0	0	0	0
	36	5	0	0	0	0
	38	5	0	0	0	0
	44	6	0	0	2	33.3 ± 19.2
	48	6	1	16.6 ± 15.2	0	0
	57	4	1	25 ± 21.6	0	0
10 fr / 12 d	40	4	0	0	0	0
	47	5	0	0	0	0
	54	5	0	0	0	0
	60	5	0	0	0	0
	64	7	0	0	1	14.2 ± 13.2
	68	5	3	60 ± 21.9	3	60 ± 21.9
	72	7	1	14.2 ± 13.2	2	28.5 ± 17.0

Table 6.35 Incidence of necrosis and oedema in the *stria terminalis* of the rat brain one year after irradiation with ^{60}Co γ rays.

Radiation Protocol	Total Dose (Gy)	Number at risk	Responders necrosis	% incidence of necrosis ± SE	Responders oedema	% incidence of oedema ± SE
0.04 Gy/min	31	5	0	0	1	20 ± 17.8
	35	5	0	0	0	0
	39	4	0	0	0	0
	41	5	0	0	0	0
	47	6	1	16.6 ± 15.2	2	33.3 ± 19.2
	57	7	6	85.7 ± 13.2	2	28.5 ± 17.0
	65	6	4	66.6 ± 19.2	2	33.3 ± 19.2
0.05 Gy/min	30	4	0	0	0	0
	34	5	0	0	1	20 ± 17.8
	37	5	0	0	2	40 ± 21.9
	40	4	0	0	2	50 ± 25
	47	6	2	33.3 ± 19.2	0	0
	55	5	3	60 ± 21.9	1	20 ± 17.8
	65	6	6	100 ± 0	1	16.6 ± 15.2
0.07 Gy/min	30	5	0	0	1	20 ± 17.8
	33	4	0	0	1	25 ± 21.6
	36	5	0	0	1	20 ± 17.8
	38	5	0	0	1	20 ± 17.8
	44	6	2	33.3 ± 19.2	1	16.6 ± 15.2
	48	6	6	100 ± 0	1	16.6 ± 15.2
	57	4	3	75 ± 21.6	0	0
10 fr / 12 d	40	4	0	0	0	0
	47	5	0	0	0	0
	54	5	0	0	0	0
	60	5	0	0	0	0
	64	7	2	28.5 ± 17.0	0	0
	68	5	4	80 ± 17.8	2	40 ± 21.9
	72	7	7	100 ± 0	0	0

Table 6.36 Incidence of necrosis and oedema in the *sulcus hippocampi* of the rat brain one year after irradiation with ^{60}Co γ rays.

Radiation Protocol	Total Dose (Gy)	Number at risk	Responders necrosis	% incidence of necrosis ± SE	Responders oedema	% incidence of oedema ± SE
0.04 Gy/min	31	5	0	0	0	0
	35	5	0	0	0	0
	39	4	0	0	0	0
	41	5	0	0	0	0
	47	6	0	0	0	0
	57	7	1	14.2 ± 13.2	0	0
	65	6	1	16.6 ± 15.2	0	0
0.05 Gy/min	30	4	0	0	0	0
	34	5	0	0	0	0
	37	5	0	0	0	0
	40	4	0	0	0	0
	47	6	0	0	0	0
	55	5	0	0	0	0
	65	6	0	0	0	0
0.07 Gy/min	30	5	0	0	0	0
	33	4	0	0	0	0
	36	5	0	0	0	0
	38	5	0	0	0	0
	44	6	0	0	0	0
	48	6	2	33.3 ± 19.2	0	0
	57	4	0	0	0	0
10 fr / 12 d	40	4	0	0	0	0
	47	5	0	0	0	0
	54	5	0	0	0	0
	60	5	0	0	0	0
	64	7	0	0	0	0
	68	5	0	0	0	0
	72	7	7	100 ± 0	0	0

Table 6.37 Incidence of necrosis and oedema in the *truncus corporis callosi* of the rat brain one year after irradiation with ^{60}Co γ rays.

Radiation Protocol	Total Dose (Gy)	Number at risk	Responders necrosis	% incidence of necrosis ± SE	Responders oedema	% incidence of oedema ± SE
0.04 Gy/min	31	5	0	0	0	0
	35	5	0	0	0	0
	39	4	0	0	0	0
	41	5	0	0	0	0
	47	6	0	0	0	0
	57	7	2	28.5 ± 17.0	1	14.2 ± 13.2
	65	6	2	33.3 ± 19.2	4	66.6 ± 19.2
0.05 Gy/min	30	4	0	0	1	25 ± 21.6
	34	5	0	0	0	0
	37	5	0	0	0	0
	40	4	0	0	3	75 ± 21.6
	47	6	1	16.6 ± 15.2	3	50 ± 20.4
	55	5	3	60 ± 21.9	0	0
	65	6	1	16.6 ± 15.2	2	33.3 ± 19.2
0.07 Gy/min	30	5	0	0	0	0
	33	4	0	0	1	25 ± 21.6
	36	5	0	0	0	0
	38	5	0	0	0	0
	44	6	2	33.3 ± 19.2	0	0
	48	6	3	50 ± 20.4	2	33.3 ± 19.2
	57	4	2	50 ± 25	2	50 ± 25
10 fr / 12 d	40	4	0	0	0	0
	47	5	0	0	0	0
	54	5	0	0	0	0
	60	5	0	0	0	0
	64	7	2	28.5 ± 17.0	2	28.5 ± 17.0
	68	5	3	60 ± 21.9	3	60 ± 21.9
	72	7	3	42.8 ± 18.7	1	14.2 ± 13.2

6.7 DOSE RESPONSE RELATIONSHIPS

Dose response relationships for the incidence of necrosis and oedema in the various sites in the irradiated rat brain at the three protracted dose rates and the fractionated radiation study are given in Figures 6.91 to 6.107.

In some instances because of insufficient incident data or because the end point did not occur at any of the doses, dose response curves could not be constructed.

ED_{50} values as obtained from the dose response curves are given in Table 6.38.

Comments on dose response relationships

It was observed in a number of sites that there was no increase in incidence with increasing dose. Examples of these sites were the *stria terminalis* (oedema – 0.05 and 0.07 Gy min^{-1}), the *truncus corporis callosi* (oedema - 0.05 Gy min^{-1}), the *alveus hippocampi* (oedema - 0.05 Gy min^{-1}), the *capsula interna* (oedema – 0.07 Gy min^{-1}), the *cingulum* (0.05 Gy min^{-1}), the *capsula interna pars retrolenticularis* (0.07 Gy min^{-1}) and the *nucleus lateralis thalami* (necrosis – 0.07 Gy min^{-1}).

An expected dose response, that is, an increasing incidence of an end point with increasing dose, was not seen in many of the sites especially with respect to the incidence of oedema. The normal sigmoid dose response curve was not seen with oedema, hence the oedematous response does not appear to be dose dependent.

The *fasiculus medialis prosencephali* (FMP) and the *nucleus lateralis* (NL) are histological structures which lie inferior to the FH, close to the base of the rat brain (Figure 3.1). The histological reactions of the FMP and NL are detailed in Tables 6.10 and 6.14, respectively. Dilated vessels were the most common reactions displayed in these two areas, with only one rat in the current study developing partial necrosis. A possible explanation for these reactions may be that these histological areas were in some instances partially out of the radiation field or received a lower dose if they fell into the penumbra. This in turn may imply that the dose of radiation that these two histological areas received may not be that which was prescribed and therefore account for the limited histological reactions.

Dose responses of the FNP and NL

The *fasiculus medialis prosencephali* (FMP) and the *nucleus lateralis* (NL) are histological structures which lie inferior to the FH, close to the base of the rat brain (Figure 3.1). The histological reactions for the FMP and NL are detailed in Tables 6.10 and 6.14, respectively. Only one rat in the current study developed partial necrosis and dilated vessels were the most common reactions displayed in these two areas. A possible explanation for these reactions may be that these histological areas were in some instances partially out of the radiation field or received a lower dose if they fell into the penumbra. This in turn may imply that the dose of radiation that these two histological areas received may not be that which was prescribed and therefore account for the limited histological reactions.

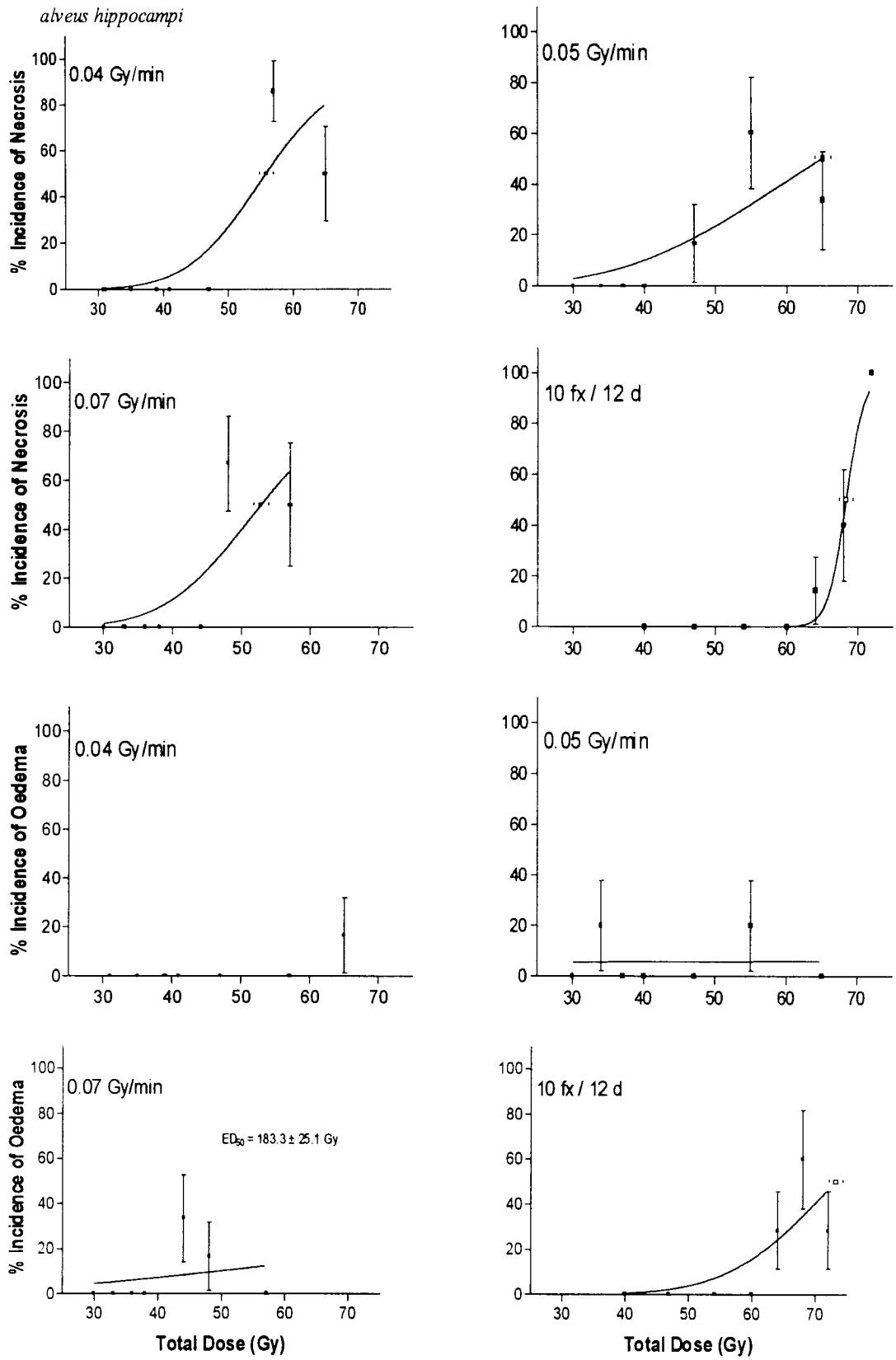

Figure 6.91 Dose related changes for incidence of necrosis and oedema in the *alveus hippocampi* one year after irradiation with ^{60}Co γ rays. Radiation was at 0.04, 0.05 and 0.07 Gy min^{-1} or 10 fractions over 12 days. Error bars indicate ± S.E.

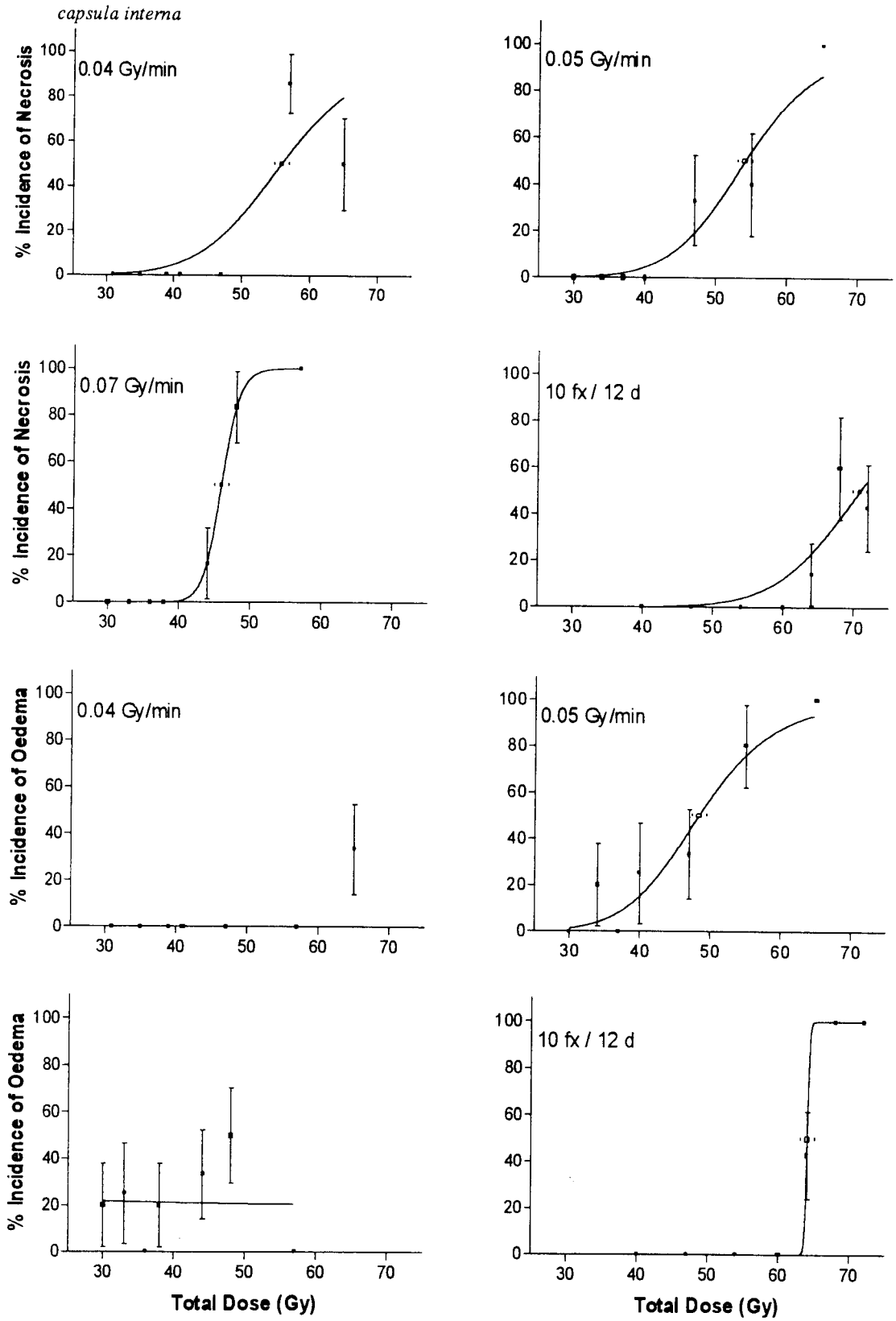

Figure 6.92 Dose related changes for incidence of necrosis and oedema in the *capsula interna* one year after irradiation with ^{60}Co γ rays. Radiation was at 0.04, 0.05 and 0.07 Gy min^{-1} or 10 fractions over 12 days. Error bars indicate ± S.E.

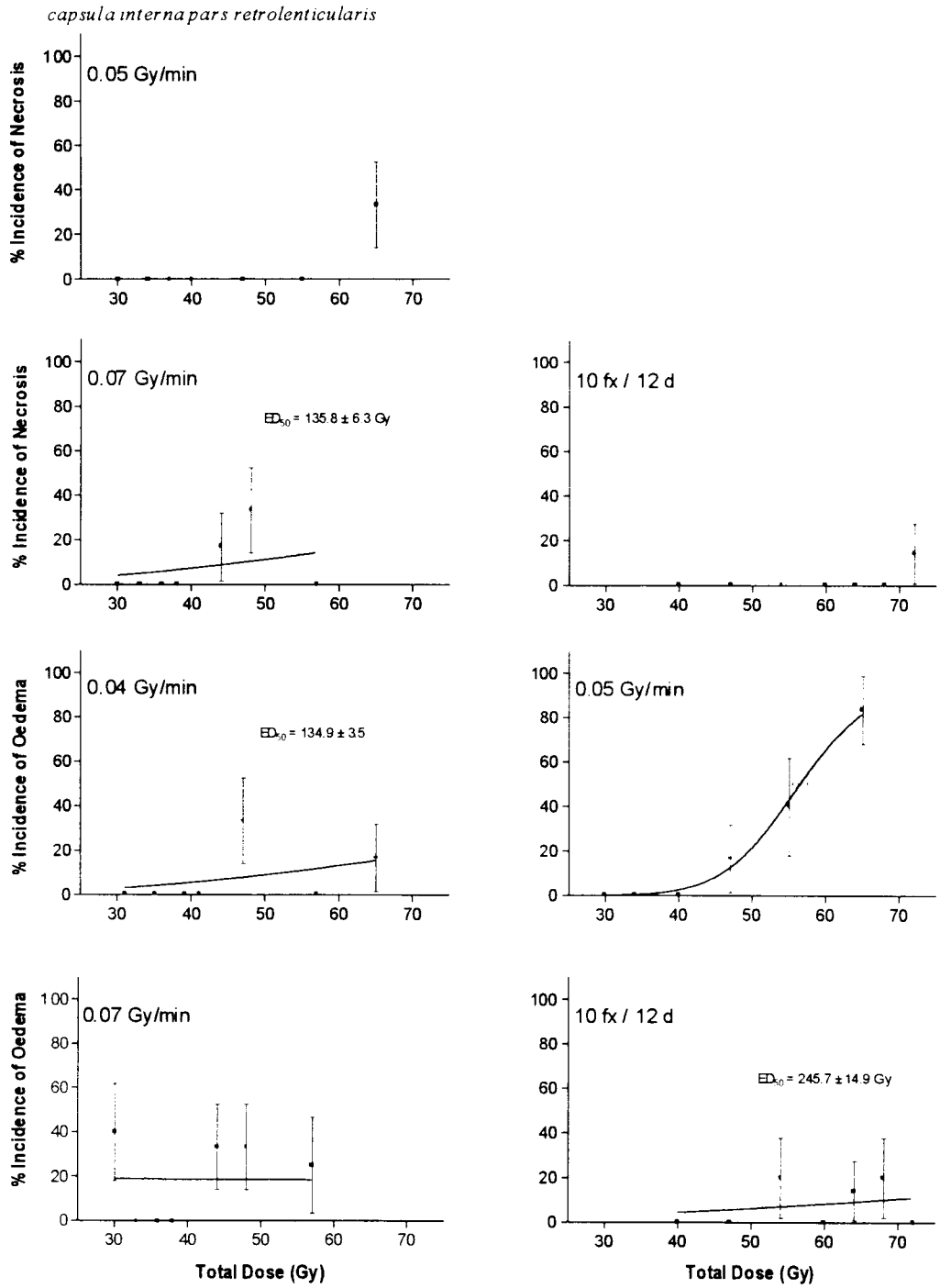

Figure 6.93 Dose related changes for incidence of necrosis and oedema in the *capsula interna pars retrolenticularis* one year after irradiation with ^{60}Co γ rays. Radiation was at 0.04, 0.05 and 0.07 Gy min^{-1} or 10 fractions over 12 days. Error bars indicate ± S.E.

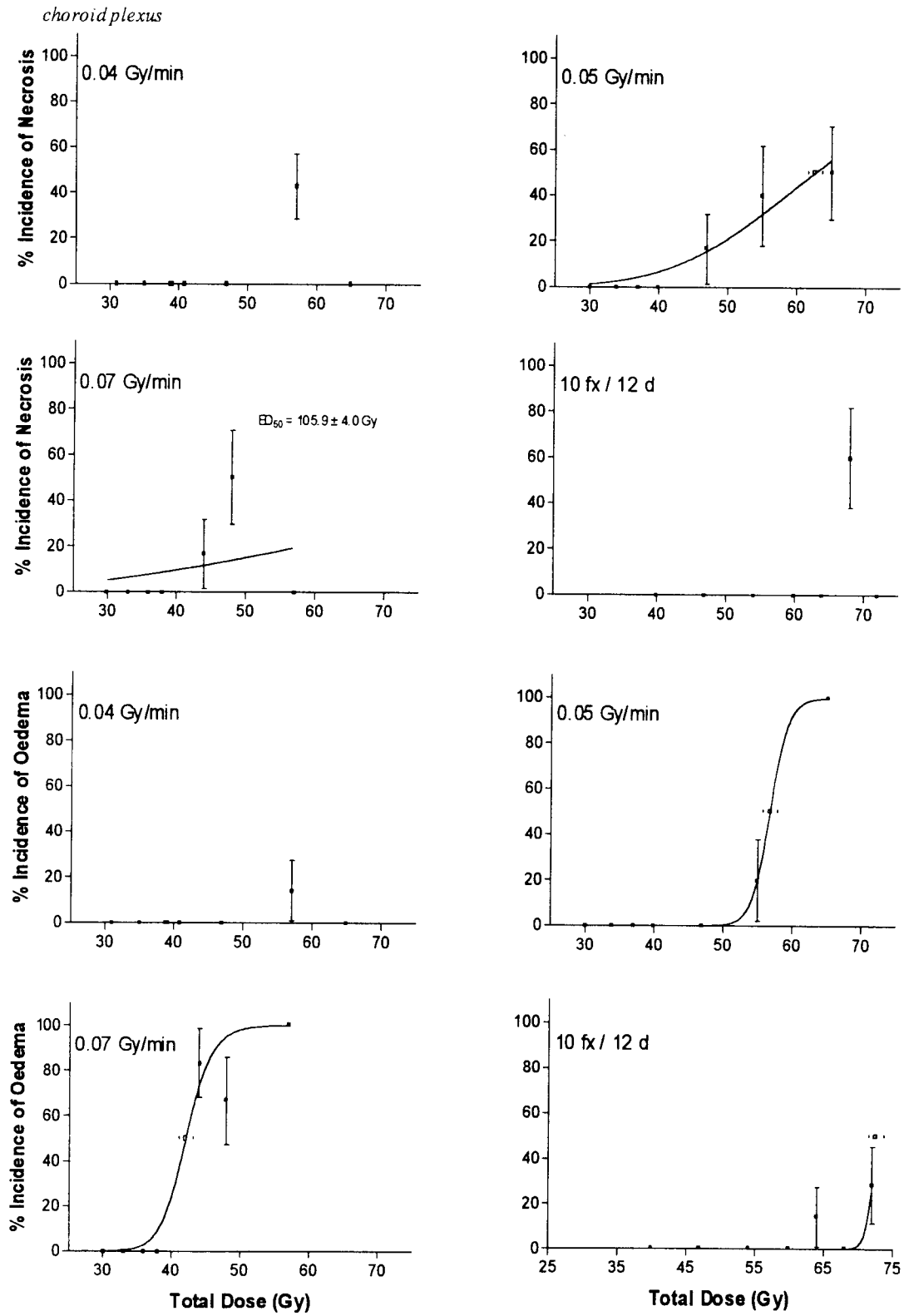

Figure 6.94 Dose related changes for incidence of necrosis and oedema in the choroid plexus one year after irradiation with ^{60}Co γ rays. Radiation was at 0.04, 0.05 and 0.07 Gy min^{-1} or 10 fractions over 12 days. Error bars indicate ± S.E.

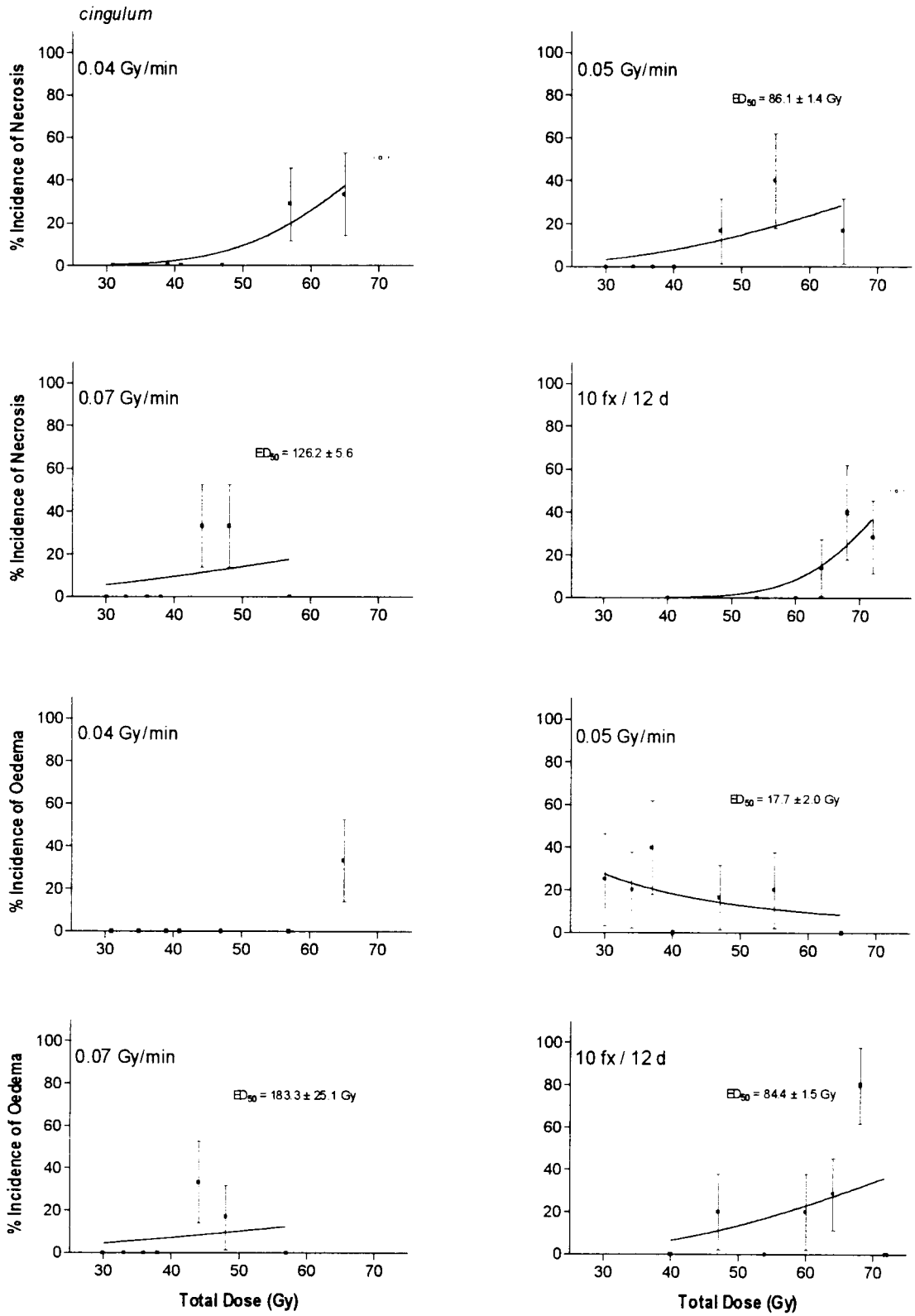

Figure 6.95 Dose related changes for incidence of necrosis and oedema in the *cingulum* one year after irradiation with ^{60}Co γ rays. Radiation was at 0.04, 0.05 and 0.07 Gy min^{-1} or 10 fractions over 12 days. Error bars indicate ± S.E.

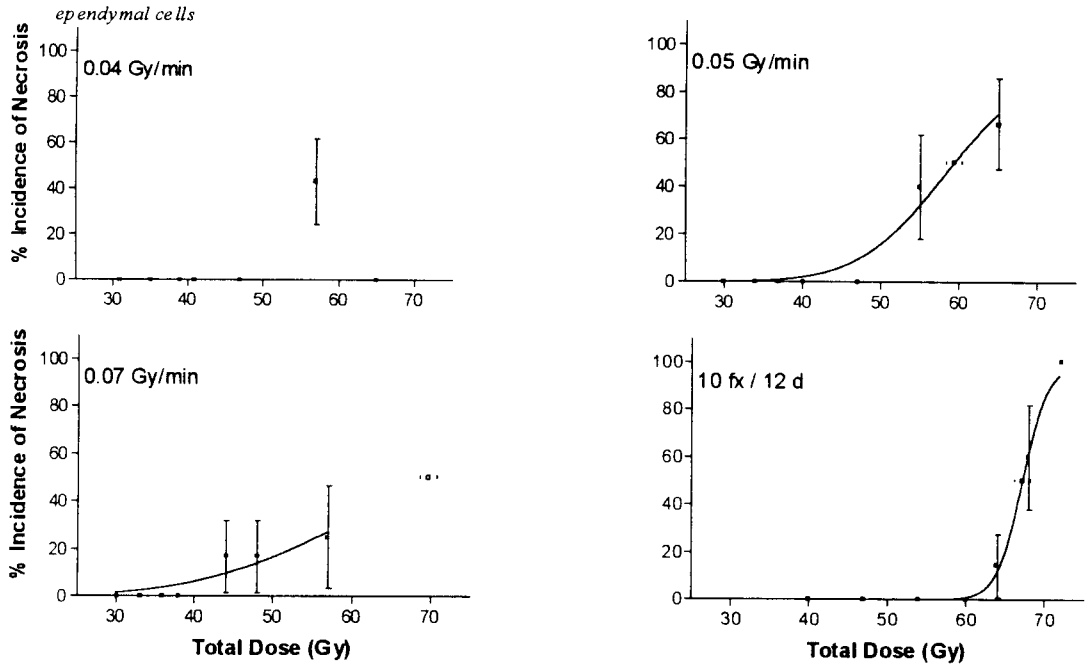

Figure 6.96 Dose related changes for incidence of necrosis in the ependymal cells one year after irradiation with ^{60}Co γ rays. Radiation was at 0.04, 0.05 and 0.07 Gy min^{-1} or 10 fractions over 12 days. Error bars indicate ± S.E.

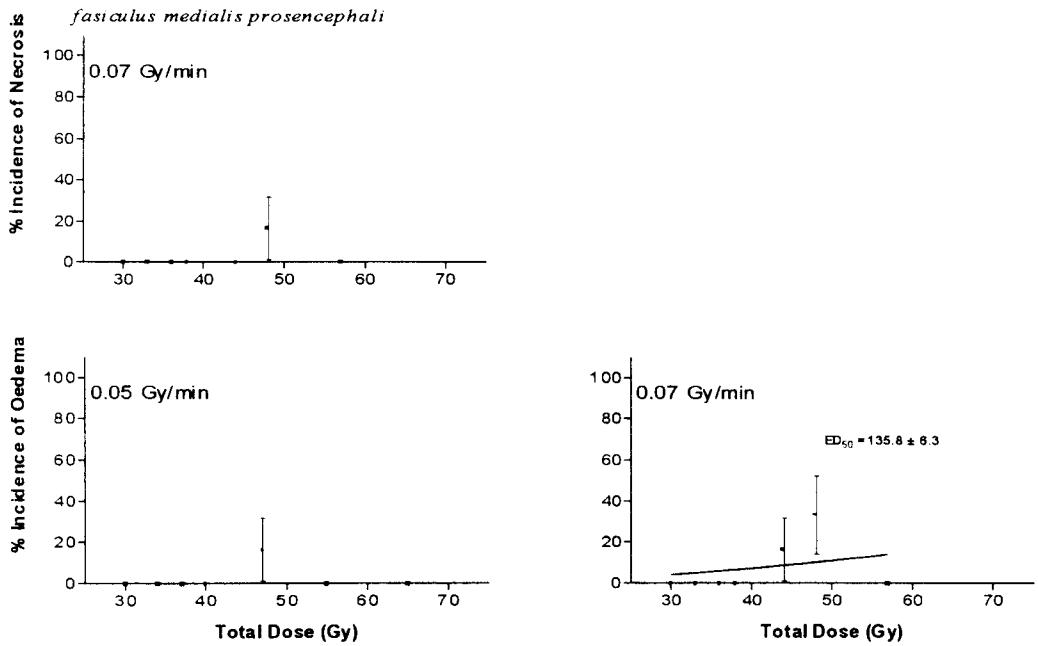

Figure 6.97 Dose related changes for incidence of necrosis and oedema in the *fasiculus medialis prosencephali* one year after irradiation with ^{60}Co γ rays. Radiation was at 0.05 and 0.07 Gy min^{-1}. Error bars indicate ± S.E.

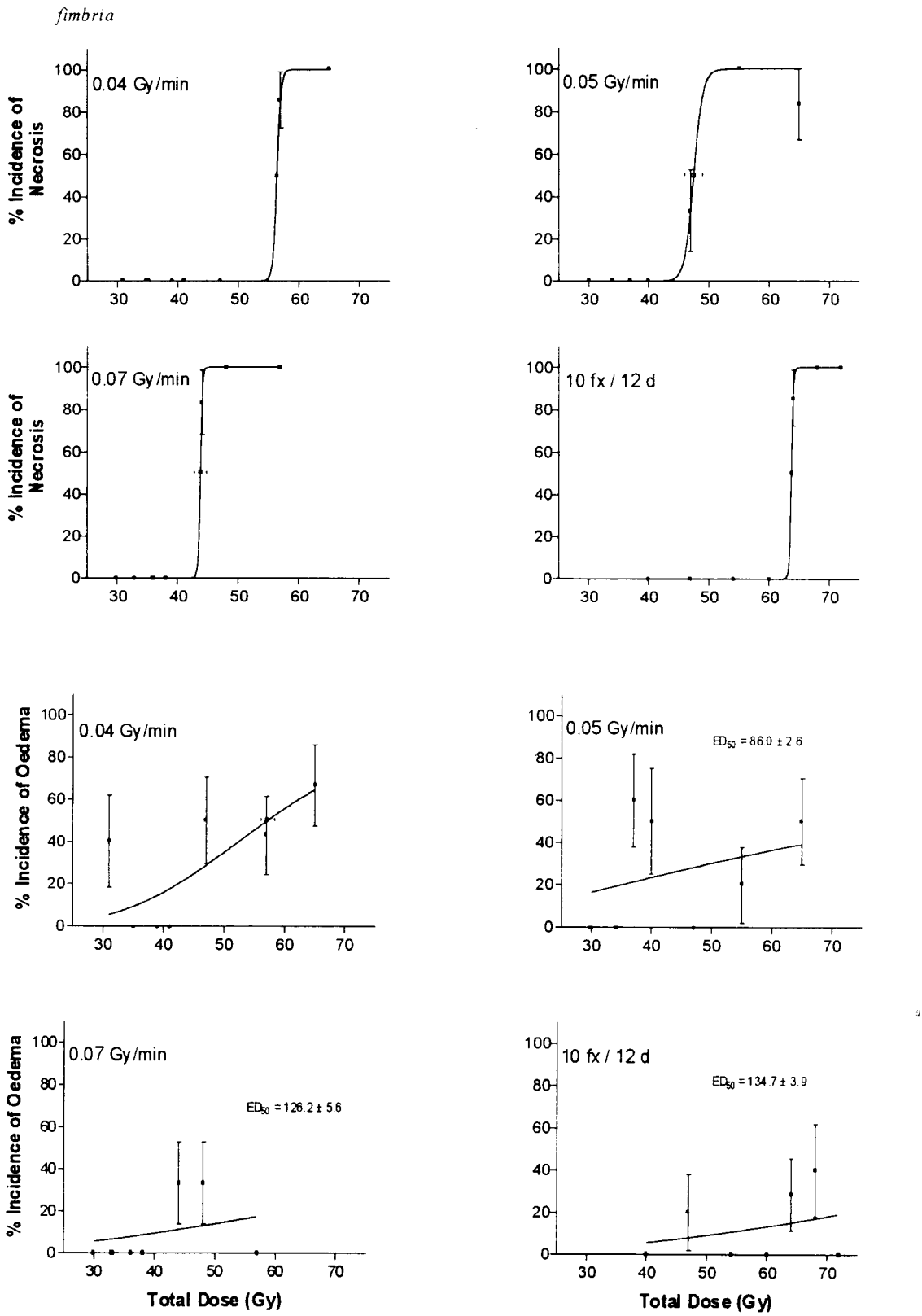

Figure 6.98 Dose related changes for incidence of necrosis and oedema in the *fimbria hipocampus* one year after irradiation with ^{60}Co γ-rays. Radiation was at 0.04, 0.05 and 0.07 Gy min^{-1} or 10 fractions over 12 days. Error bars indicate ± S.E.

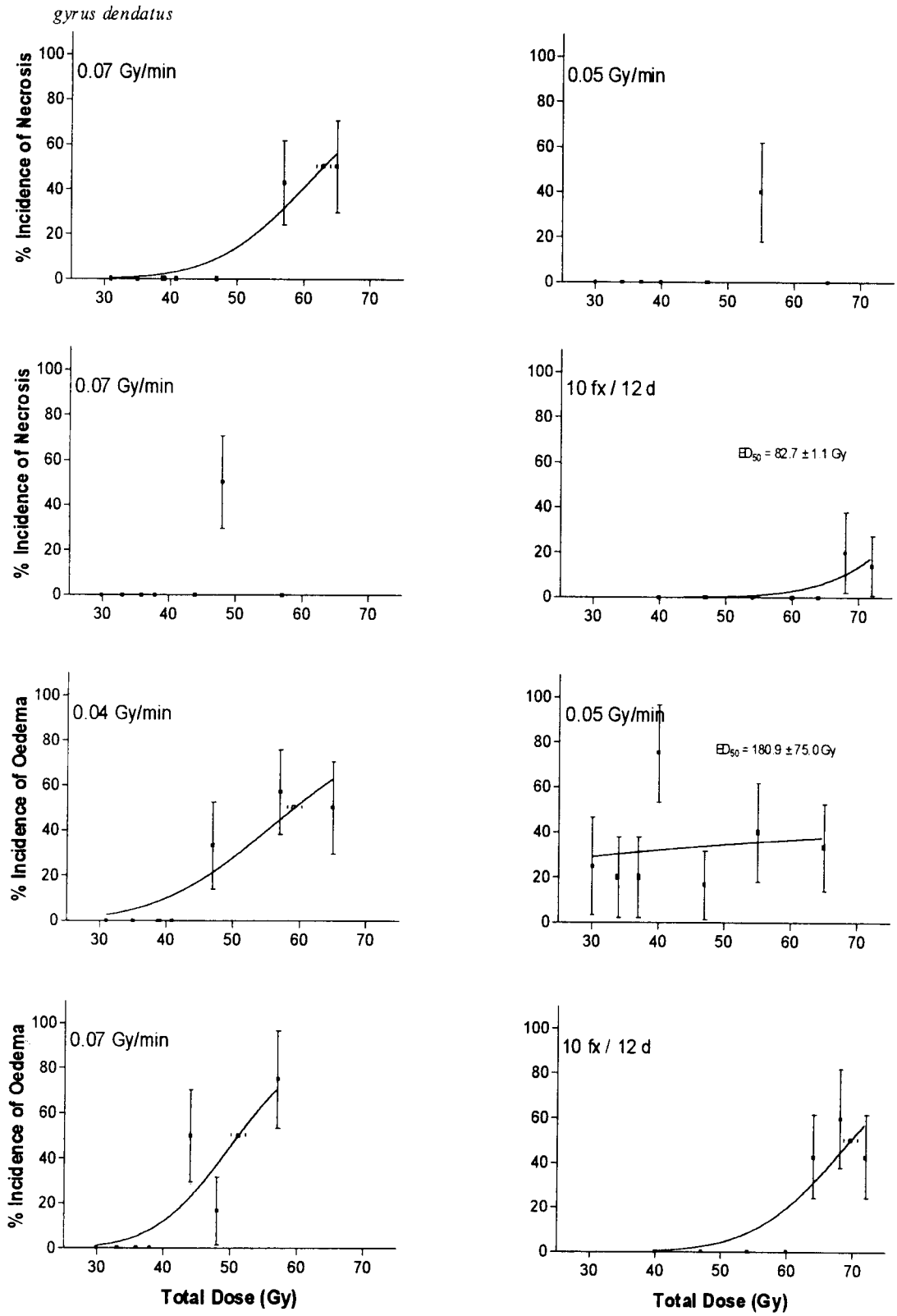

Figure 6.99 Dose related changes for incidence of necrosis and oedema in the *gyrus dentatus* one year after irradiation with ^{60}Co γ rays. Radiation was at 0.04, 0.05 and 0.07 Gy min^{-1} or 10 fractions over 12 days. Error bars indicate ± S.E.

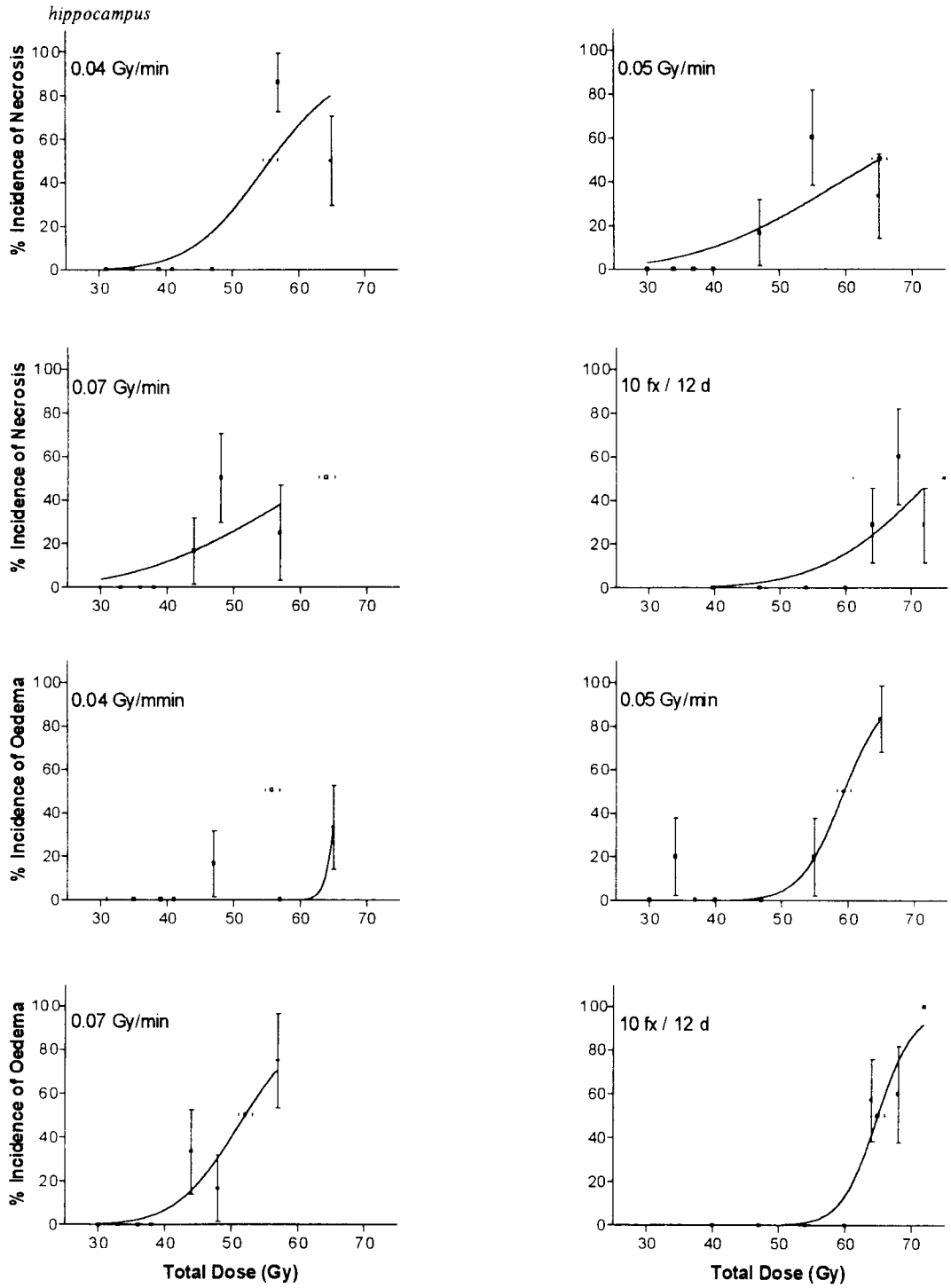

Figure 6.100 Dose related changes for incidence of necrosis and oedema in the *hipppocampus* one year after irradiation with ^{60}Co γ rays. Radiation was at 0.04, 0.05 and 0.07 Gy min^{-1} or 10 fractions over 12 days. Error bars indicate ± S.E.

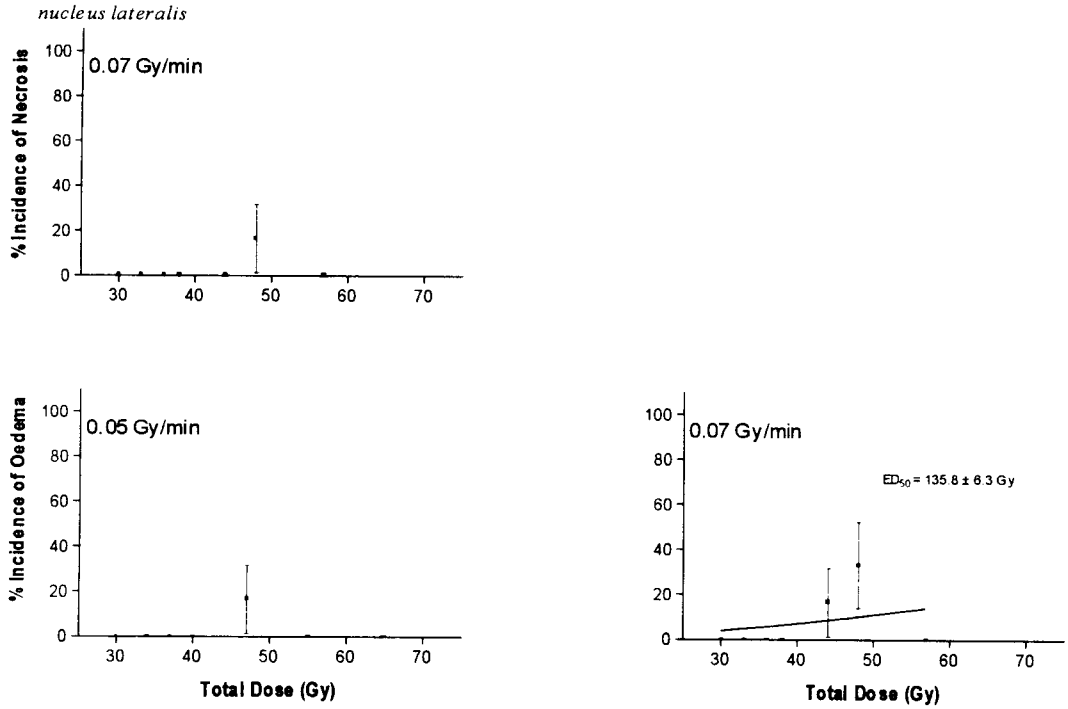

Figure 6.101 Dose related changes for incidence of necrosis and oedema in the *nucleus lateralis* one year after irradiation with ^{60}Co γ rays. Radiation was at 0.05 and 0.07 Gy min^{-1}. Error bars indicate ± S.E.

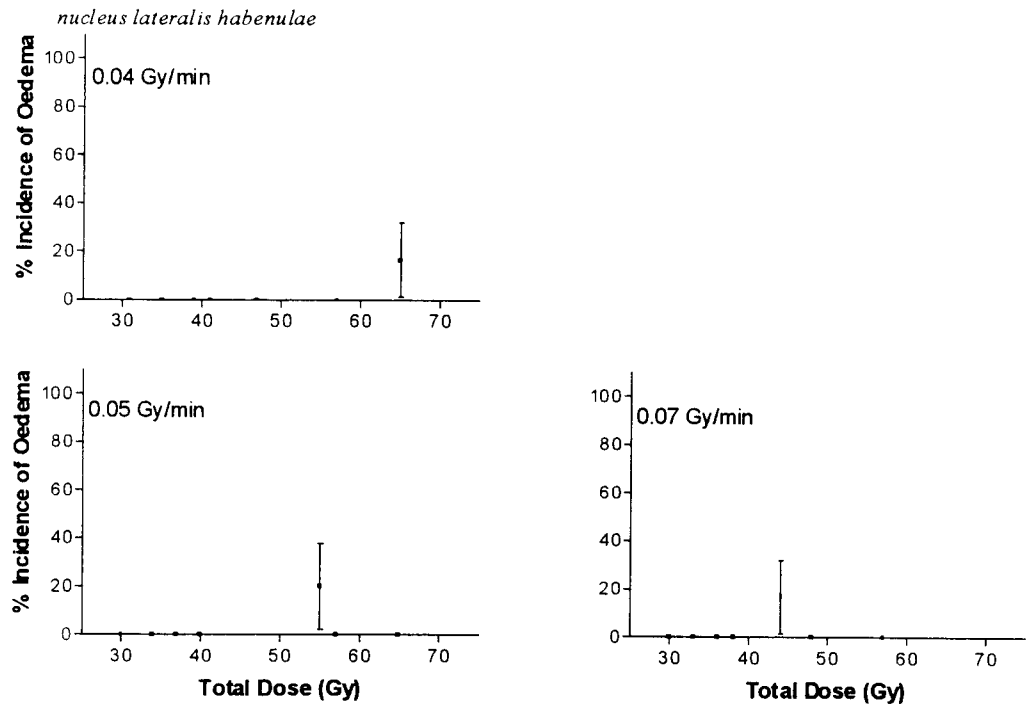

Figure 6.102 Dose related changes for incidence of oedema in the *nucleus lateralis habenulae* one year after irradiation with ^{60}Co γ rays. Radiation was at 0.04, 0.05 and 0.07 Gy min^{-1}. Error bars indicate ± S.E.

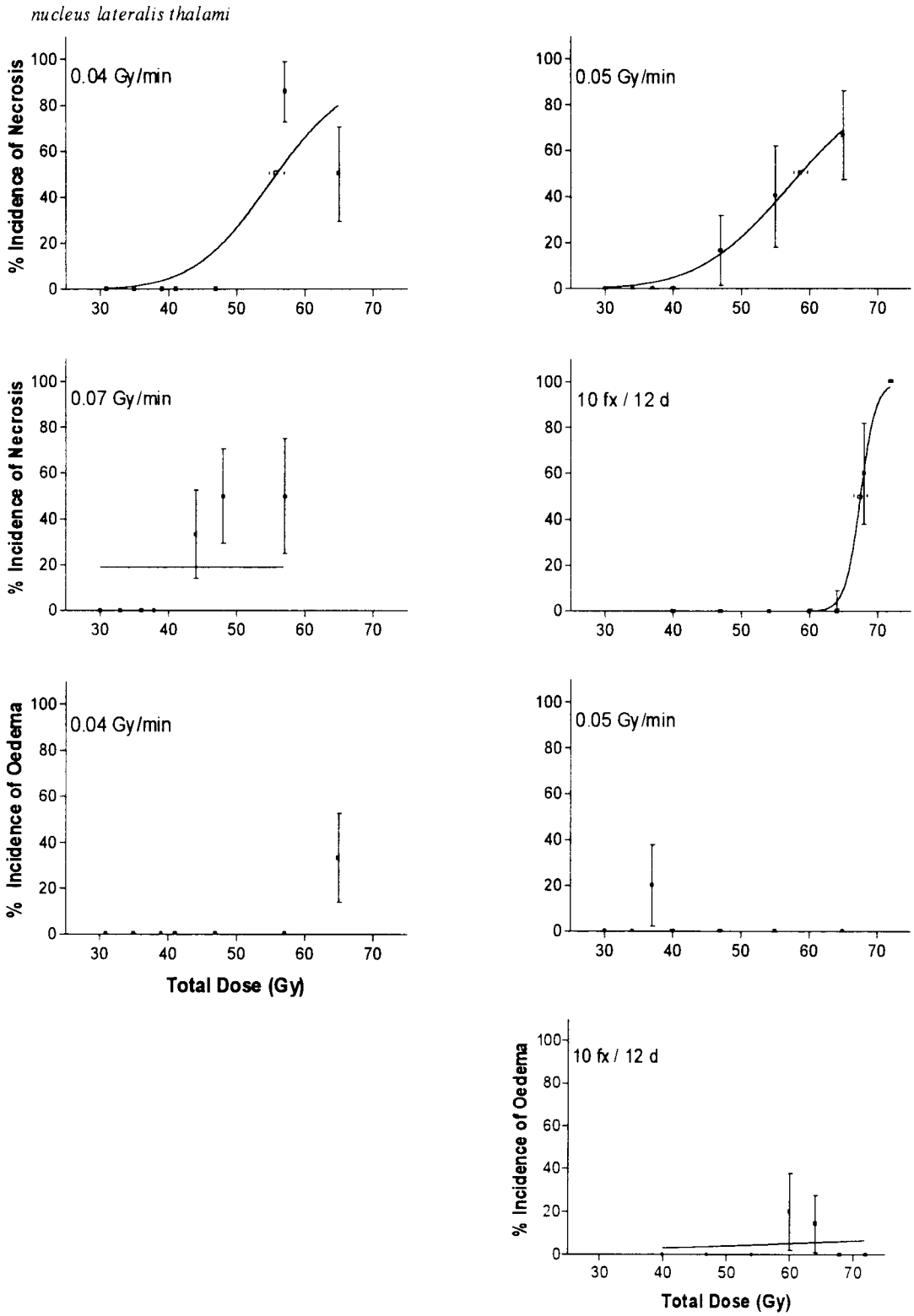

Figure 6.103 Dose related changes for incidence of necrosis and oedema in the *nucleus lateralis thalami* one year after irradiation with ^{60}Co γ rays. Radiation was at 0.04, 0.05 and 0.07 Gy min^{-1} or 10 fractions over 12 days. Error bars indicate ± S.E.

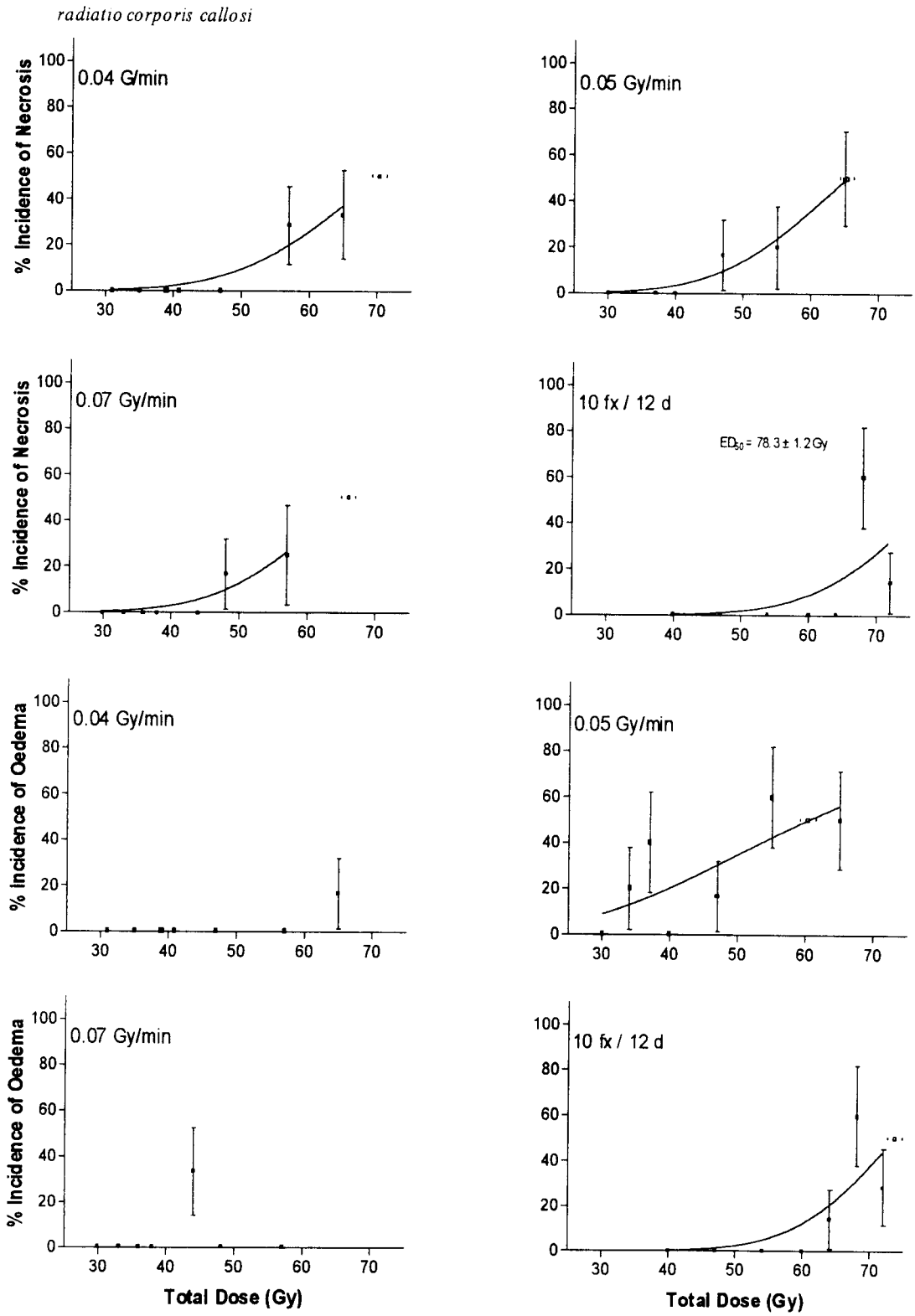

Figure 6.104 Dose related changes for incidence of necrosis and oedema in the *radiatio corporis callosi* one year after irradiation with ^{60}Co γ rays. Radiation was at 0.04, 0.05 and 0.07 Gy min^{-1} or 10 fractions over 12 days. Error bars indicate ± S.E.

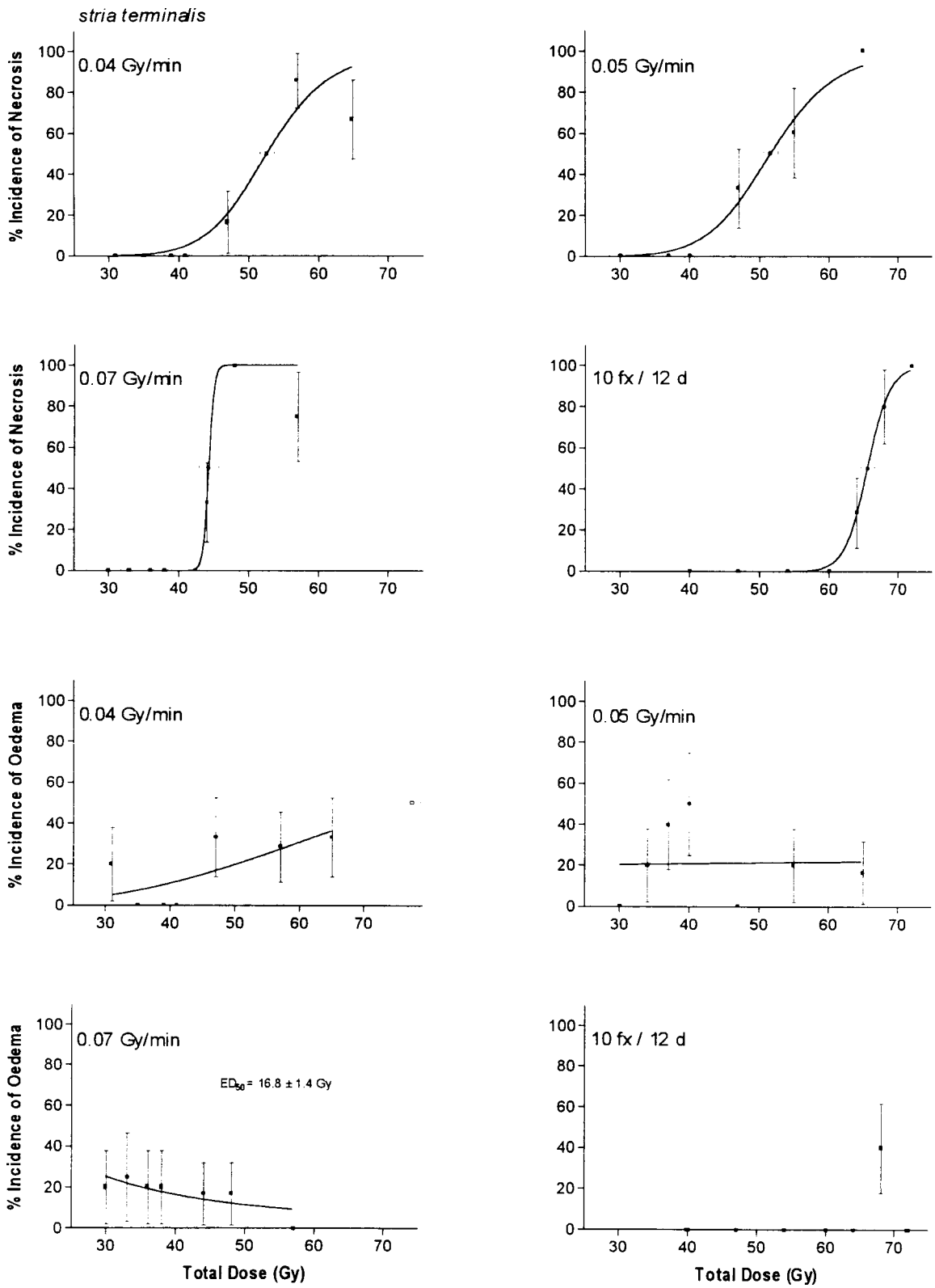

Figure 6.105 Dose related changes for incidence of necrosis and oedema in the *stria terminalis* one year after irradiation with ^{60}Co γ rays. Radiation was at 0.04, 0.05 and 0.07 Gy min^{-1} or 10 fractions over 12 days. Error bars indicate ± S.E.

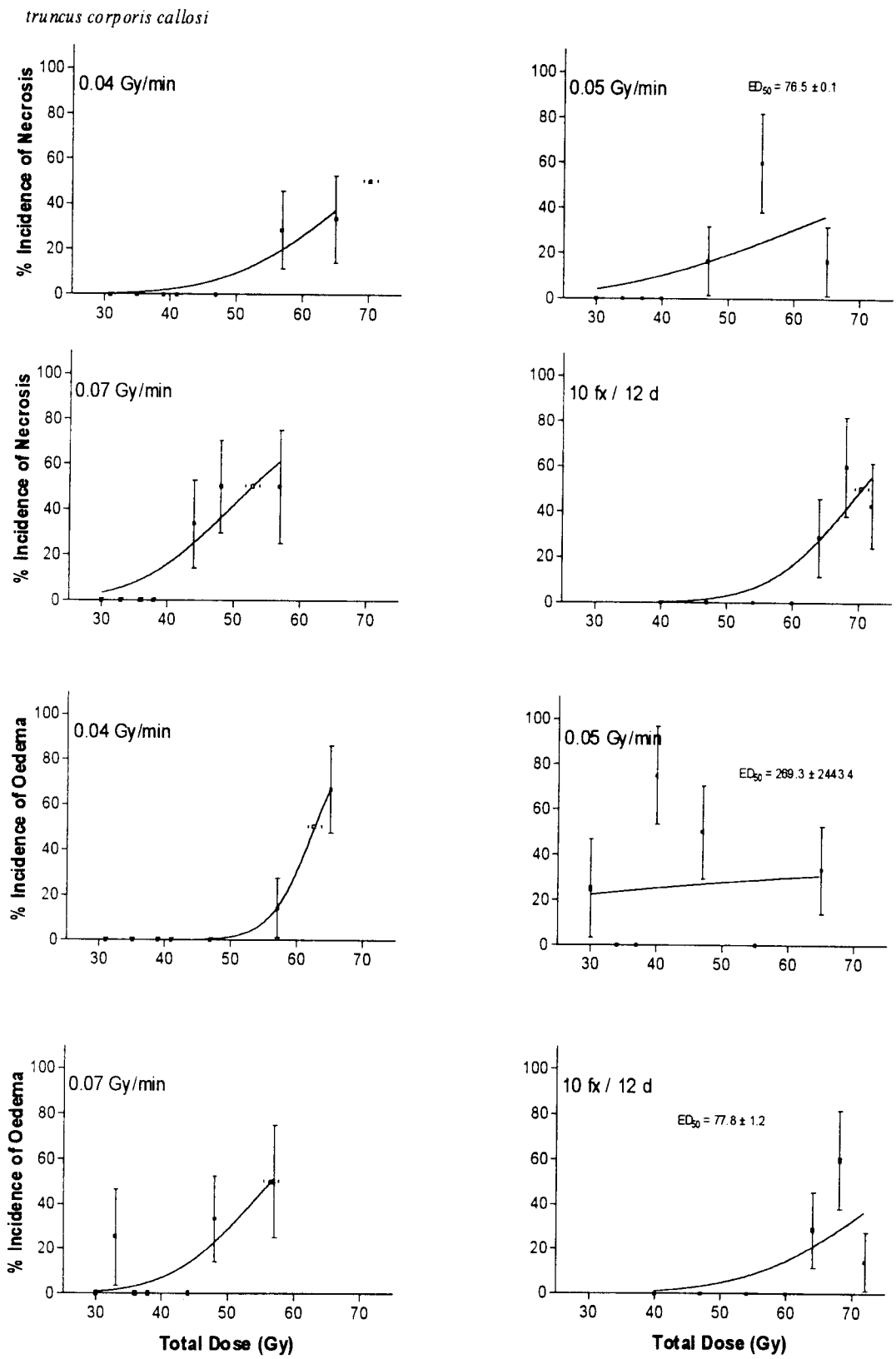

Figure 6.106 Dose related changes for incidence of necrosis and oedema in the *truncus corporis callosi* one year after irradiation with ^{60}Co γ rays. Radiation was at 0.04, 0.05 and 0.07 Gy min^{-1} or 10 fractions over 12 days. Error bars indicate ± S.E.

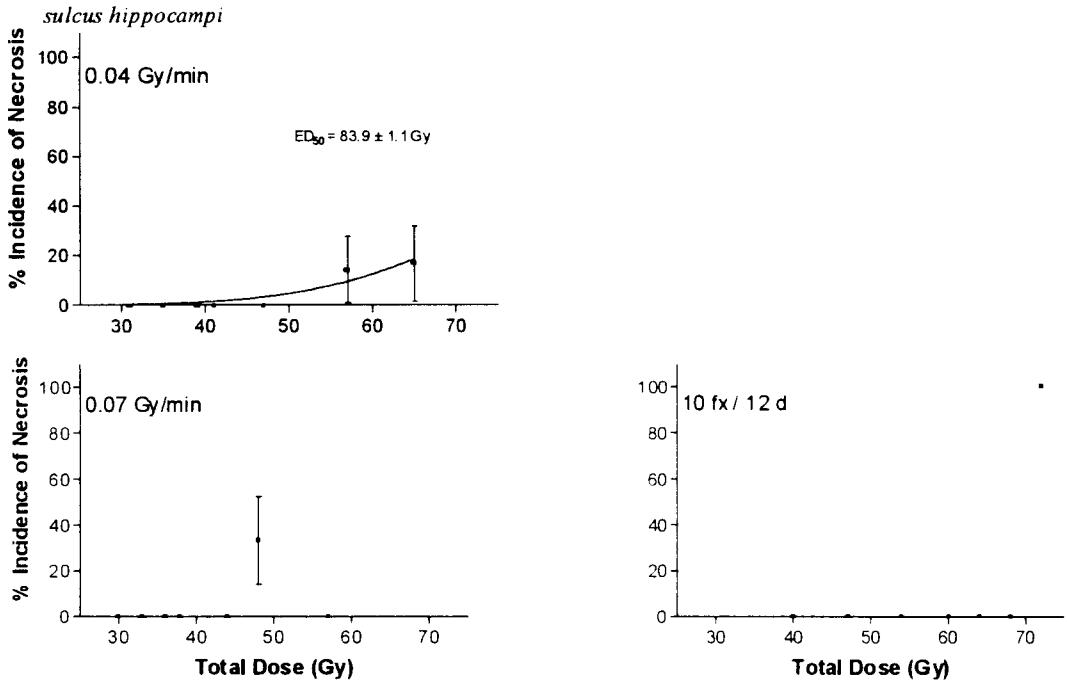

Figure 6.107 Dose related changes for incidence of necrosis in the *sulcus hippocampi* one year after irradiation with ^{60}Co γ rays. Radiation was at 0.04 and 0.07 Gy min^{-1} or 10 fractions over 12 days. Error bars indicate ± S.E.

Table 6.38 Isoeffect doses (ED_{50}) for necrosis and oedema in various sites of the rat brain one year after continuous protracted or fractionated ^{60}Co γ irradiation. (The ED_{50} is the dose required to produce a 50% incidence of the end point).

Site	Dose rate (Gy min^{-1})	Dose rate (Gy h^{-1})	Fractionated	ED_{50} (Gy) Necrosis	ED_{50} (Gy) Oedema
alveus hippocampi	0.04	2.4		55.9 ± 1.1	
	0.05	3.0		65.1 ± 1.1	
	0.07	4.2		52.8 ± 1.1	183.3 ± 25.1
			10 fx / 12 d	68.4 ± 1.0	73.3 ± 1.1
capsula interna	0.04	2.4		55.9 ± 1.1	
	0.05	3.0		54.1 ± 1.0	48.4 ± 1.0
	0.07	4.2		46.0 ± 1.0	
			10 fx / 12 d	70.9 ± 1.0	64.0 ± 1.0
capsula interna pars retrolenticularis	0.04	2.4			134.9 ± 3.5
	0.05	3.0			56.5 ± 1.0
	0.07	4.2		135.8 ± 6.3	
			10 fx / 12 d		245.7 ± 14.9
choroid plexus	0.04	2.4			
	0.05	3.0		62.7 ± 1.0	56.8 ± 1.0
	0.07	4.2		105.9 ± 4.0	42.2 ± 1.0
			10 fx / 12 d		72.6 ± 1.1
cingulum	0.04	2.4		70.3 ± 1.0	
	0.05	3.0		86.1 ± 1.4	17.7 ± 2.0
	0.07	4.2		126.2 ± 5.6	183.3 ± 25.1
			10 fx / 12 d	75.9 ± 1.1	84.4 ± 1.5
ependymal cells	0.04	2.4			
	0.05	3.0		59.4 ± 1.0	
	0.07	4.2		69.7 ± 1.1	
			10 fx / 12 d	67.2 ± 1.0	

Table 6.38 continued.

Site	Dose rate (Gy min^{-1})	Dose rate (Gy h^{-1})	Fractionated	ED_{50} (Gy) Necrosis	ED_{50} (Gy) Oedema
fasiculus medialis prosencephali	0.04	2.4			
	0.05	3.0			
	0.07	4.2			135.8 ± 6.3
			10 fx / 12 d		
fimbria hippocampus	0.04	2.4		56.4 ± 0.0	57.2 ± 1.1
	0.05	3.0		50.5 ± 1.5	86.0 ± 2.6
	0.07	4.2		43.4 ± 1.0	126.2 ± 5.6
			10 fx / 12 d	63.7 ± 0.0	134.7 ± 3.9
gyrus dentatus	0.04	2.4		62.9 ± 1.1	59.2 ± 1.1
	0.05	3.0			180.9 ± 1.1
	0.07	4.2			51.2 ± 1.1
			10 fx / 12 d	82.7 ± 1.1	69.7 ± 1.0
hippocampus	0.04	2.4		55.9 ± 1.1	65.6 ± 3.8
	0.05	3.0		65.1 ± 1.1	59.4 ± 1.0
	0.07	4.2		64.0 ± 1.2	52.1 ± 1.0
			10 fx / 12 d	75.0 ± 1.1	64.9 ± 1.0
nucleus lateralis	0.04	2.4			
	0.05	3.0			
	0.07	4.2			135.8 ± 6.3
			10 fx / 12 d		
nucleus lateralis habenulae	0.04	2.4			
	0.05	3			
	0.07	4.2			
			10 fx / 12 d		

Table 6.38 continued.

Site	Dose rate (Gy min^{-1})	Dose rate (Gy h^{-1})	Fractionated	ED_{50} (Gy) Necrosis	ED_{50} (Gy) Oedema
nucleus lateralis thalami	0.04	2.4		55.9 ± 0.0	
	0.05	3.0		58.7 ± 1.0	
	0.07	4.2			
			10 fx / 12 d	67.5 ± 1.0	
radiatio corporis callosi	0.04	2.4		66.9 ± 1.0	
	0.05	3.0		64.4 ± 1.0	60.4 ± 1.2
	0.07	4.2		61.3 ± 1.0	
			10 fx / 12 d	78.3 ± 1.2	73.7 ± 1.1
stria terminalis	0.04	2.4		52.7 ± 1.0	77.4 ± 1.2
	0.05	3.0		51.6 ± 0.0	
	0.07	4.2		44.3 ± 1.4	16.8 ± 1.4
			10 fx / 12 d	65.6 ± 1.0	
sulcus hippocampi	0.04	2.4		83.9 ± 1.1	
	0.05	3			
	0.07	4.2			
			10 fx / 12 d		
truncus corporis callosi	0.04	2.4		70.3 ± 1.1	62.7 1 1.0
	0.05	3		76.5 ± 1.4	
	0.07	4.2		52.9 ± 1.1	56.5 ± 1.1
			10 fx / 12 d	70.4 ± 1.0	77.8 ± 1.2

6.8 CALCULATION OF RADIOBIOLOGICAL PARAMETERS

Protracted Irradiation

Using incidences of necrosis as the end-point it is possible to calculate parameters of the linear quadratic model from ED_{50} values obtained from protracted radiation experiments using Dale's (1985) graphical method. This was done by plotting the reciprocal ED_{50} values at each dose rate against the factor KR as discussed in Chapter 4.

The method makes the assumption that repair is non-exponential. The best linear fit is obtained when the best approximation of the repair half-time is introduced.

The data from the various sites were subjected to the graphical analysis only when there was a trend for the ED_{50} values to steadily increase with decreasing dose rate. A study of Table 6.38 showed that only the *fimbria hippocampus*, *radiatio corporis callosi*, *stria terminalis* and the *capsula interna* would be likely candidates. The data were fitted using Graphpad software.

As shown by Dale (1985) small or low values of μ impart a concave shape to the $^1/_D$ *vs* KR curve, whereas higher values of μ impart a convex shape. With the data for the *stria terminalis* and *capsula interna* for values of μ up to 10 000, the curves remained concave.

For the *fimbria hippocampus* the best fit was obtained for $\mu = 0.36$ as shown in Figure 6.108. The *radiatio corporis callosi*'s best fit was for $\mu = 0.10$ and is shown in Figure 6.109.

For the data from both the *fimbria hippocampus* and *radiatio corporis callosi* it was possible to show that for μ values lower than 0.36 and 0.10, respectively, the shape of the curve was concave and for values greater than 0.36 and 0.10, the curve was convex.

The $^{\alpha}/_{\beta}$ values were obtained from the intercept on the KR axis, i.e., when $^1/_D = 0$.

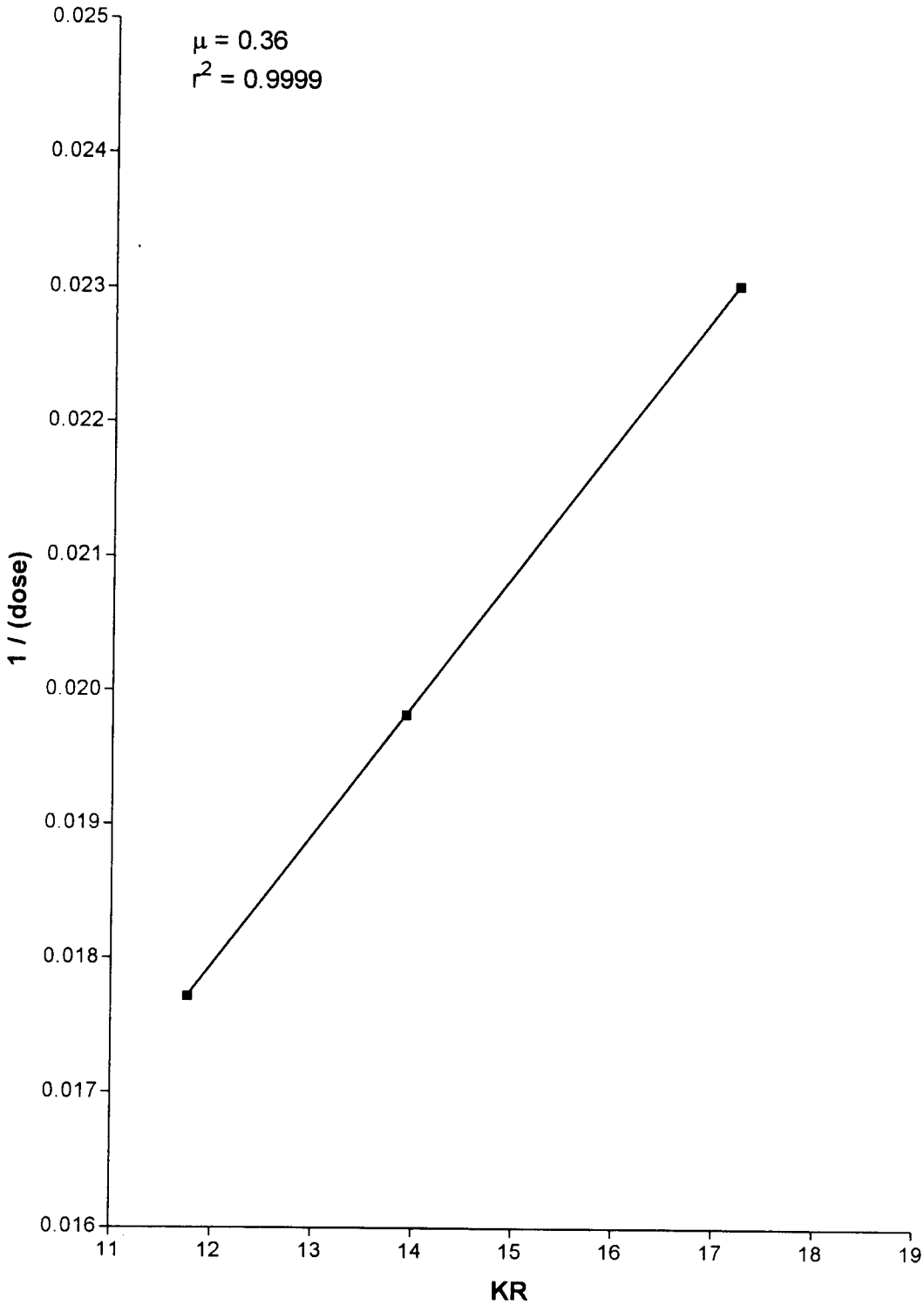

Figure 6.108 Plot of $^{1}/_{D}$ *vs* KR using data for necrosis of the *fimbria hippocampus*.

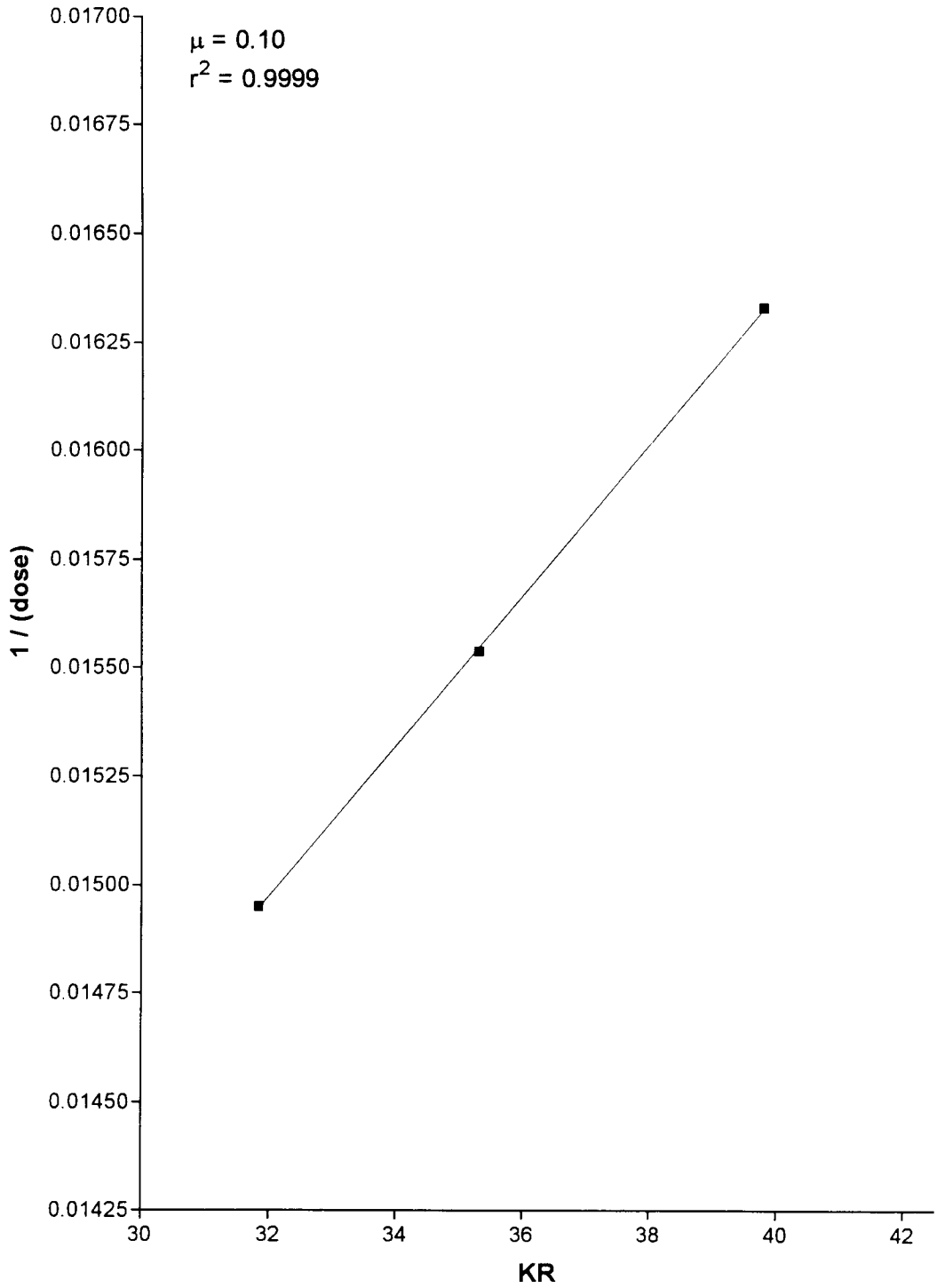

Figure 6.109 Plot of $^{1}/_{D}$ *vs* KR using data for necrosis of the *radiatio corporis callosi.*

The various calculated radiobiological parameters are presented in Table 6.39.

Table 6.39 Calculated radiobiological parameters.

Site	μ (h^{-1})	$^{\alpha}/_{\beta}$ (Gy)	$t_{1/2}$ (h)
fimbria hippocampus	0.36	6.2	1.92
radiatio corporis callosi	0.10	54.5	6.93

The biologically effective dose (BED) was calculated for necrosis induction in the *fimbria hippocampus* and the *radiatio corporis callosi* using Equation 11 in Chapter 4,

i.e., $$BED = D\left[1 + \frac{KR}{\left(\alpha/\beta\right)}\right]$$

where $$K = \frac{2}{\mu}\left\{1 - \frac{1}{\mu T}\left[1 - \exp(-\mu T)\right]\right\}$$

For large T, $$K = \frac{2}{\mu}\left\{1 - \frac{1}{\mu T}\right\}.$$

Then, for the *fimbria hippocampus* at a dose rate of 0.04 Gy min^{-1} (2.4 Gy h^{-1}), ED_{50} = 56.4 Gy (Table 6.38), μ=0.36 (Table 6.39), $^{\alpha}/_{\beta}$ = 6.2 Gy (Table 6.39), then,

$$BED = 56.4\left(1 + \frac{(2)(2.4)}{(0.36)(6.2)}\left[1 - \frac{1}{(0.36)(23.5)}\right]\right)$$

$$BED = 163.4\ Gy_L, \qquad \textbf{Equation 6.1}$$

where Gy_L indicates a late responding tissue.

BED's calculated for dose rates of 0.05 and 0.07 Gy min^{-1} (3.0 and 4.2 Gy h^{-1}) were the same.

For the *radiatio corporis callosi*, at a dose rate of 0.04 Gy min^{-1} (2.4 Gy h^{-1}) with ED_{50} = 66.9 Gy (Table 6.38), μ = 0.10 (Table 6.39), $^{\alpha}/_{\beta}$ = 54.5 Gy (Table 6.39),

$$BED = 66.9\left(1+\frac{(2)(2.4)}{(0.1)(54.5)}\left[1-\frac{1}{(0.1)(27.87)}\right]\right)$$

$$BED = 104.7\ Gy_L \qquad \textbf{Equation 6.2}$$

BED's calculated at dose rates of 0.05 and 0.07 Gy min^{-1} (3.0 and 4.2 Gy h^{-1}) were the same.

Fractionated Irradiation

The BED for the induction of necrosis resulting from protracted irradiation will equal the BED resulting from fractionated radiation. Therefore, for the *fimbria hippocampus*, for fractionated irradiation, where ED_{50} = 63.7 Gy and the dose per fraction is consequently 6.37 Gy (10 fractions), then by setting BED = 163.4 Gy_L from Equation 6.1 above, then from Equation 7, Chapter 4,

$$BED = D\left(1+\frac{d}{\alpha/\beta}\right)$$

$$163.4 = 63.7\left(1+\frac{6.37}{\alpha/\beta}\right)$$

Then, $^{\alpha}/_{\beta} = 4.1$ Gy **Equation 6.3**

Similarly, for the *radiatio corporis callosi*, where BED is set to 104.7 Gy_L, and ED_{50} = 78.3 Gy and dose per fraction = 7.83 Gy,

Then, $$104.7 = 78.3\left(1+\frac{7.83}{\alpha/\beta}\right)$$

Then $^{\alpha}/_{\beta} = 23.2$ Gy **Equation 6.4**

The $^{\alpha}/_{\beta}$ ratios obtained from the two analysis are given in Table 6.40.

Table 6.40 $^{\alpha}/_{\beta}$ ratios for protracted and fractionated irradiation for the *fimbria hippocampus* and the *radiatio corporis callosi.*

Site	$^{\alpha}/_{\beta}$ (Gy) Protracted irradiation	$^{\alpha}/_{\beta}$ (Gy) Fractionated irradiation
fimbria hippocampus	6.2	4.1
radiatio corporis callosi	54.5	23.2

It is noteworthy that the values obtained for $^{\alpha}/_{\beta}$ from analysis of the protracted irradiation data and fractionated irradiation data were substantially different.

Comment on Analysis

The method of analysis used in this work was a two-step process, and the $^{\alpha}/_{\beta}$ ratios and half-times of repair are calculated by indirect means.

Another method of calculation is by the direct method of Thames et al. (1986), but the computer programme was not available to perform the analysis in this way.

The incidence data for histological reactions other than necrosis and oedema, was random and not dose related. Examples of the histological reactions which are not dose related include the occurrence of dilated vessels (Tables 6.4 to 6.20), the calcification of vessel walls (Tables 6.5 and 6.6), red blood cell congested vessels (Tables 6.7 and 6.13), haemorrhage (Tables 6.4 and 6.8) and vacuolation (Table 6.7).

CHAPTER 7:

DISCUSSION

The literature pertaining to the experimental irradiation of the rat brain is limited. On the other hand, a considerable amount of experimental irradiation work has been done using the spinal cord to study the effects of radiation on the CNS. The brain and spinal cord are composed of the same cell types and are both part of the CNS. The reason for using the spinal cord in radiation experiments of the CNS, is that the damage is usually represented by gross physical changes in the animals when a particular part of the spinal cord is irradiated. Examples of these changes include changes in the gait of the animals or paralysis of either the fore- or hind-limbs. Irradiation of the brain does in general not result in the animals displaying any of the physical changes that are observed after spinal cord irradiation. Changes in the brain after irradiation are usually evident on histology and death of the irradiated animals may be considered a physical observation. The spinal cord does not have any cognitive functions as does the brain and therefore cannot be regarded the same as the brain even though the brain and spinal cord comprise the CNS. However, this should not preclude comparison of observations made in the spinal cord with those in the brain following irradiation.

7.1 ANIMAL WEIGHTS

No significant change in the relative weight of the irradiated rats was observed when they were compared to that of the control rats in this study. This observation was consistent for all the different dose rate experiments, including the fractionated study.

The area of the brain that was irradiated included the midbrain and the cerebral hemispheres [Calvo et al., 1987; Chauser et al., 1977; Hopewell and Wright, 1970; Hornsey et al., 1981a; Plotnikova et al., 1984; Reinhold and Hopewell, 1980; Rogers et al., 1982] and included the FH in the radiation field.

The classic late effect in the rat brain has been described as a localised necrotic lesion [Schultheiss et al., 1995]. Necrosis was observed in those rats receiving the higher doses of radiation in each of the dose rate experiments performed in this study, and even when complete destruction of the FH was noted, no difference in the weights of the irradiated rats was observed when compared to

that of the control rats. This may be because necrosis of the FH may not be life threatening to the rat as suggested by Calvo et al. (1988) and supported by this study, and indeed has no effect on the weights of the rats.

Care was taken to ensure shielding of the oropharynx because the structures contained therein are radiation sensitive [Calvo et al., 1987; van der Kogel, 1979]. If these structures were to be damaged as a result of radiation, the damage may affect the eating habits of the rats and in turn may affect their weights.

The findings regarding the effect of brain irradiation on animal weights can be contrasted with those studies where cervical and thoracic cord were irradiated and the rats subsequently exhibited weight loss. This weight loss, in the case of irradiation of the cervical cord, was attributed to radiation damage inflicted to the oropharynx, when the oropharynx was included in the radiation field. Likewise, weight loss displayed, when the thoracic cord was irradiated, was attributed to radiation damage inflicted to the oesophagus or gastrointestinal tract, when this structure was included in the radiation field. The importance of shielding of the oesophagus during spinal cord irradiation was highlighted in a study by Hopewell et al. (1987) where no weight loss was reported when the oesophagus was shielded.

In the studies presented in this thesis, the oesophagus and the gastrointestinal tract were not compromised.

7.2 RADIATION FIELD

The radiation field used in the current dose rate experiments included the area between the eye and the ear of the rat head, as detailed in Figure 5.1 The brain structures that were consequently irradiated included the mid-brain and cerebral hemispheres, as shown in Figure 5.2, where the arc labeled CD indicates the radiation field. The anatomical sites investigated in the current dose rate experiments are situated in the mid brain (Figure 3.1). Other investigators have also used the area between the eye and the ear of the rat as external markers for brain irradiation [Calvo et al., 1987; Chauser et al., 1977; Hornsey et al., 1981a; Plotnikova et al., 1984; Rogers et al., 1982].

The radiation apertures in the shielding that were used by some of these researchers had a range of diameters, namely, 2.0 cm [Calvo et al., 1987],

2.6 cm [Rogers et al., 1982], and 3.0 cm [Chauser et al., 1977]. Where the aperture diameter was greater than 2.0 cm, the cerebellum and the olfactory lobes were included in the radiation field. The work of Rogers et al. (1982) is of interest in that they stated that the radiosensitive oropharynx was not in their radiation field, but that they had experienced difficulty in lining up the rats consistently for irradiation as the rats were positioned without the aid of a jig. This variation in the degree of precision in lining up the rats resulted in some rats dying within one month after irradiation. Plotnikova et al. (1984) used a smaller field size (0.5 cm by 0.8 cm), the centre of which was positioned in the middle of the distance between the eye and the ear. The rats were observed for a total of 15 months but no mention was made of any changes in the weights of the irradiated rats.

7.3 DOSIMETRY

The rat brain is a relatively small organ and therefore the dosimetry is of critical importance, more so, since only the area between the eye and the ear was irradiated. The field size was therefore small. To ensure that the dose distribution across the brain irradiation field was uniform, the set-up of the irradiation field was done around the centre of the cobalt-60 beam. This positioning around the centre of the cobalt-60 beam reduced the effect of any beam divergence as is shown in Figure 6.2. Furthermore, dosimetry checks were performed with the aid of a wax rat phantom and a formalin-perfused rat, the results of which are presented in Table 6.1. The consistency of positioning the rats in the radiation field was also critical and this was facilitated by the use of the perspex restraining jigs (Figures 5.3 and 5.4). The importance of consistent positioning of the rats in the radiation field for brain irradiation is stressed by the work of Rogers et al. (1982). These researchers did not use a jig to aid with them in positioning the rats in the radiation field, which resulted in rats dying one month after irradiation of the brain. The use of jigs to aid in consistency of reproduction of the radiation field was also evident in the work of Hopewell et al. (1987) where the cervical spinal cord of the rats were irradiated.

There are limited data on CNS damage following ^{60}Co irradiation and no data on the low dose rate ^{60}Co irradiation of the CNS. Calvo et al. (1987) checked their dosimetry with the aid of TLD measurements using a frozen rat. These authors, using 250 kVp x-rays, observed a dose variation across the rat brain of

approximately 4%. In the current dose rate experiments, the rats were irradiated on either their left or right sides, but the histological scoring was performed only on that side of the brain which was closest to the radiation source. The rat brain lies approximately 0.5 cm below the skin surface [Albe-Fessard et al., 1966; de Groot, 1967; König and Klippel, 1963; Pellegrino et al., 1978], that is, at the position for the 100 % isodose curve, and is approximately 1.2 cm across. The dose variation across the 0.6 cm of brain that was scored for radiation damage was estimated from tables [Hering, 1999 – personal communication] to be 3.3 %.

7.4 ANAESTHETIC

Inhalation anaesthesia was used in all dose rate experiments performed in this study. This was done in preference to the use of intraperitoneal (IP) injections of anaesthetic which have been found by other investigators to have several limitations [Ang et al., 1982; van der Kogel, 1979]. These authors found that the IP injections were time consuming and could cause deaths, in addition the depth of anaesthesia was not easily controllable. With repeated IP injections of anaesthetic they also found that it caused respiratory arrest. Intraperitoneal anaesthesia was found to be of short duration, of the order of one to two hours [Ang et al., 1982]. With the low dose rate experiments of the current study, the irradiation times were much longer than two hours which would imply that if IP injections were used they would have to be repeated a number of times during the irradiation procedure. This would in turn disrupt the irradiation procedure and it would therefore not be continuous.

Ang et al. (1982) found that with their method for inhalation anaesthesia, no rats exhibited respiratory depression and no rats died during the six hour period of anaesthesia that they used. van der Kogel (1979) confirmed that Halothane and oxygen for the inhalation anaesthesia did not cause any respiratory depression, however, a possible disadvantage of this inhalation anaesthesia method may be the high serum level of inorganic fluoride which could cause nephrotoxicity [Mazze et al., 1977; van der Kogel, 1979].

van der Kogel (1979) who also used inhalation anaesthesia for his rat experiments, found that the use of Halothane and oxygen did not affect the latent period or the threshold dose for hind leg paralysis when the lumbar spinal cord was irradiated. However, a decrease in the threshold dose for myelopathy of the

cervical spinal cord was noted. This decrease was however slight and was not significant.

In each of the experiments conducted in the present study the duration and depth of anaesthesia were easily maintained and there were no anaesthetic deaths. After the prolonged anaesthesia for a low dose rate experiment the rats were found to awaken and start moving freely around their cages without impediment within two minutes after being removed from the radiation set-up area. Ang et al. (1982) stated that after the anaesthesia their rats recovered within one to five minutes and could eat and drink immediately.

Generally, concern is expressed about the effects of anaesthesia, namely, a decrease in the body temperature and a decrease in tissue oxygenation. Possibly the use of an humidifier as part of the inhalation anaesthesia set-up may have reduced the decrease in body temperature of the rats. The histology of the sham irradiated control rat brains and those of the control rat brains which were not sham irradiated, were found to be no different after one year of observation. Thus, if a decrease in tissue oxygenation occurred it did not manifest in a gross histological manner. In addition, prolonged anaesthesia did not appear to result in any visible physiological changes in the rats.

7.5 OXYGEN TOXICITY

Exposure to 100% oxygen for long periods of time, such as might be the case in the low dose rate experiments described here, may result in toxic reactions [Ahdab-Barmada et al., 1986]. In this regard, the levels of oxygen under the loose plastic drape covering the radiation set-up were measured and the recorded range was 55 to 80% (Table 6.3), which is comfortably below the 100% toxic level. The plastic drape was not fixed, sealed or taped down and therefore did not restrict the flow of air into or out of the radiation set-up area. Furthermore, a suction pump was used to extract the mixture of anaesthetic gas, air and oxygen from under the plastic drape and expel it into a ventilation duct, and a free standing fan allowed for the continuous circulation of air in the radiation room, thereby further preventing the build up of levels of anaesthetic and oxygen. Given these points it is most probable that there was no toxicity due to the use of oxygen for delivering the continuous anaesthesia. This would also account for our observations that the histological observations in the sham irradiated control

rats were not found to be different from those control rats which were not sham irradiated.

7.6 BEHAVIOURAL CHANGES

No observable changes in gait and behaviour were observed in any of the rats used in the present series of dose rate experiments. van der Kogel and Barendsen (1974) observed palpable muscle atrophy after irradiation of the rat spinal cord. Schultheiss et al. (1990) when studying the effects of radiation on the CNS by irradiating the cervical and thoracic spinal cord, observed exaggerated flexion, ataxia and loss of prehesion occurring as late reactions. These authors also stated that the early signs of neurologic deficit were changes in the animals behaviour patterns in that they became less active and less aggressive. Reinhold and Hopewell (1980) observing the effects of a 20 Gy single dose to the rat brain commented that all the animals in their study developed vascular abnormalities, however, these abnormalities did not affect the animals behaviour and condition. In a later study, Schultheiss et al. (1995) stated that the clinical signs associated with late radiation effects included the symptoms of a raised intracranial pressure. In the present series of dose rate experiments signs of increased intracranial pressure were not noted. Schultheiss et al. (1995) also stated that there was an impairment of the intellect in long term survivors of brain irradiation. Within this present series of dose rate experiments, no test was performed to measure the effect of radiation on the intelligence of the rats.

7.7 HISTOLOGICAL OBSERVATIONS

Necrosis

Areas of necrosis were characterised by a loss of cell structure and definition as observed in other studies [Asscher and Anson, 1962; Calvo et al., 1988; Cotran et al., 1989; Hopewell and Wright, 1970; Marks et al., 1981; Maisin, (1974); Remler et al., 1986; Safdari et al., 1985]. The expression of necrosis is the result of a combination of a vasogenic, cytotoxic and ischaemic insult of the brain. Radiation has the unique ability to inflict each of these three insults, namely, it will affect the endothelial cells of the blood vessels (vasogenic effect), it will kill

cells (cytotoxic effect), and it will induce ischaemia. Necrosis was also accompanied by calcium deposition. The presence of calcium deposition in and around areas of necrosis was confirmed in a selection of slides which were stained with the von Kossa stain. Where there was extensive necrosis, for example, the complete destruction of the FH, the necrosis invariably extended beyond the FH border and affected the surrounding structures as is evident in Figures 6.9, 6.10, 6.15 to 6.17, 6.23, 6.24, 6.30 and 6.31. The necrotic areas were found to be surrounded by areas of oedema which were not scored. Where the oedema was scored, it was foci of oedema which were not associated with any necrosis. This will be discussed in more detail below.

In the current study, the FH appeared to be the structure in the brain which showed the highest incidence of necrosis at all doses. This is also reflected by the lower ED_{50} values for incidence of necrosis in the FH at each dose rate compared with the ED_{50} values for other brain structures (Table 6.38). These findings are consistent with those of others [Calvo et al., 1988; Hopewell and Wright, 1970; Reinhold et al., 1990], which show that the FH was the first area to respond to a dose of radiation within approximately one year of observation. Calvo et al. (1988) put the earlier response of the FH, when compared to the other structures in the brain, down to an enhanced radioresponsiveness rather than an increased radiosensitivity. These authors also commented that necrosis of the FH alone did not appear to be life threatening to the rat. Leone and Ochs (1978) and Cotran et al. (1989) stated that the axons of the CNS are extremely sensitive to anoxia. In addition, they stated that it was significant that the regions of the spinal cord and the FH of the brain which were the first areas to exhibit signs of necrosis were both supplied from a terminal vascular network [Craigie, 1920; Lazorthes, 1972], which may predispose them to being more vulnerable to the ischaemic effects of radiation.

In the present study, no necrosis was scored in any of the examined structures for the lower doses of radiation, irrespective of the dose rate. However, at the higher doses of radiation, necrosis was observed in all the structures except for the NLH in all the dose rate experiments performed. However, necrosis of the CP and the ependymal cells lining the VL was by inference. In the case of the CP necrosis was scored when it was observed that the CP was continuous with the necrotic destruction. This was observed as a discontinuous CP, an example of which is shown in Figure 6.9. For the ependymal cells, necrosis was scored when there was a disruption in the continuity of the ependymal cells due to necrosis from the tissues adjacent to the VL as is also shown in Figure 6.9.

Calvo et al. (1988) observed demyelination and necrosis of the white matter of

the rat brain after single doses greater than or equal to 22.5 Gy x-rays (250 kV). However, their description of the necrosis was that it was focal. They did not observe instances of complete necrosis of the FH, CI or CC in their study as was observed in those rats who received the highest doses in each dose rate group in the present study.

The occurrence of necrosis was scored as being positive regardless of how small the area of involvement was. In general, a larger area of necrosis was observed for the higher radiation doses in each of the present dose rate experiments as is shown in Figures 6.4 to 6.31. These figures also show that the occurrence of extensive destruction of the tissue was accompanied by the presence of large cystic spaces as was observed by Hopewell and Wright (1970).

The incidence of necrosis in the white matter of the brain was found to be dose dependent as shown by the dose response curves in Figures 6.91 to 6.107. This dose dependence of the incidence of necrosis was also confirmed by the work of Calvo et al. (1988). These authors also demonstrated a time dependence for the development of necrosis. The ED_{50} values that were calculated for the FH at one year were observed to be lower than that for the other sites in the brain. The consistency of this observation of ED_{50} values for the FH and other sites in the brain was also confirmed by Calvo et al. (1988).

It is instructive to compare how necrosis as a result of radiation is distributed in the spinal cord and brain of the rat. In the case of the spinal cord, focal areas of necrosis have been reported to be distributed randomly throughout the white matter [Ruifrok et al., 1994]. On the other hand, as shown in the present study, necrosis induced by radiation in the brain was not randomly distributed, but confined to specific areas. This highlights the fact that brain and spinal cord must be regarded as different tissues in respect of response to radiation, in spite of the fact that both have the same types of cells and no major differences in vascularity [Craigie, 1920; Lazorthes, 1972].

Oedema

On histological examination of the brain sections, a finding throughout was that oedematous regions were commonly observed, that is, where there was a distinct separation between the fibres in the brain. When oedema was scored, the peripheral oedema surrounding the necrotic areas was not included in the count, thus only those foci of oedema not contiguous with necrosis were scored. Dose response curves (Figures 6. 91 to 6.95 and Figures 6.97 to 6.106) were constructed to examine the relationship between dose of radiation and oedema for each dose rate experiment. Examination of the dose response curves for

oedema did not show any consistent response with increasing dose.

Oedema is generally considered to be an early response to radiation [Calvo et al., 1987] occurring weeks after irradiation. Following irradiation, a number of events contribute to the production of oedema. These are: firstly, parenchymal cell damage and death; secondly, damage and eventual death of the endothelial cells lining the blood vessels which then leave the vessels permeable; and thirdly, an ischaemic insult [Cotran et al., 1989; Karlsson and Brady, 1987]. In addition, the lack of lymphatic drainage in the brain may contribute to the persistence of oedema during the early period after irradiation [Marks et al., 1981].

The oedema reported in this study is that which was present at one year. This may be representative of a second wave of oedema, support for which may come from the work of Calvo et al. (1987) where a second wave of oedema was observed in the CP of the brain after six months. The presence of oedema as a feature that occurs at a late stage after irradiation may simply be representative of the progressive manifestation of damage, that is, with more time more of the damaged slowly dividing cells in the brain die and this in turn contributes or results in oedema.

Dilated vessels

Dilated vessels, at varying degrees of dilation and number, were observed in each of the 17 sites examined in the rat brain after each dose point for each dose rate experiment. This response was a confirmation of Cotran et al.'s (1989) observation that vascular changes were found to be prominent in all irradiated tissues.

The reactions of the blood vessels were scored as being either large or small dilations which represents a subjective scoring system and are shown in Tables 6.4 to 6.20. No consistent pattern was observed in the occurrence of large or small dilated vessels after irradiation to suggest that there was a direct relationship of incidence with the dose of radiation. Figures 6.3 to 6.31 show that as the dose of radiation increased for a given dose rate experiment, the diameter of the dilated vessels also increased. In addition, an impression gained from Figures 6.3 to 6.31 is that the FH is the structure that has the greatest number of dilated vessels. Calvo et al. (1988) also observed a reduction in the number of blood vessels with time after irradiation in addition to an increase in the diameter of the blood vessels. These observations were also confirmed by Dimitrievich et al. (1984). Where there was complete destruction of the structure of interest, for example, the FH, due to necrosis, the scoring in terms of

the dilated vessels could not be done.

In the present study at the lower doses of radiation small dilated vessels were commonly seen in the various structures of the brain (Figures 6.4 to 6.7; Figures 6.11 to 6.14; Figures 6.18 to 6.21; Figures 6.25 to 6.28). This may be compared to the work of Plotnikova et al. (1988) where they also observed minor changes in the microvasculature of the rat brain after a low dose (single dose of 20 Gy) of radiation and an 18 month observation period. After a single dose of 25 Gy, Plotnikova et al. (1988) observed an increased incidence of vascular abnormalities.

In the present dose rate experiments, no quantification of the dilated vessels following radiation was performed for any of the anatomical sites in the rat brain. In many instances the occurrence of necrosis precluded the identification of structures. This in turn meant that due to the lack of high dose data, the construction of meaningful dose response curves was not possible.

Congested vessels

In this study congested blood vessels were observed in all areas of the rat brain with the exception of the ependymal cells. These congested vessels were not observed in all the rats for a given dose point for a particular dose rate experiment. Hopewell (1974) stated that endothelial cell damage repair may result in the occlusion of blood vessels. This observation was supported by the work of Calvo et al. (1987) who observed groups of endothelial cell nuclei which appeared to occlude the lumen of the blood vessels. Cotran et al. (1989) observed that in addition to endothelial cell proliferation, collagenous hyalinisation with the concomitant thickening of the tunica media may result in the narrowing of the affected vessels.

Haemorrhages

Haemorrhages were observed in all areas of the rat brain with the exception of the CP, EC and the NLH. These areas of haemorrhage were seen intermittently with no obvious relation to the dose of radiation in any particular dose rate experiment. Haemorrhage is usually associated with damage to the blood vessels which in turn become "leaky" [Cotran et al., 1989]. This is in keeping with the observations of White and Hornsey (1978) who had stated that areas of haemorrhage were indicative of vascular damage and with the earlier observations of Hopewell and Wright (1970) of haemorrhagic foci around small dilated blood vessels. The presence of red blood cells in the tissue surrounding a blood vessel was indicative of an area of haemorrhage. Extensive areas of

haemorrhage were observed in parts of the rat brain after the present dose rate experiments, and examples of these are shown in Figures 6.9, 6.42, and 6.54.

Iron deposits were indicative of haemorrhage that had occurred prior to killing of the rat and preparation of the histological sections. Where red blood cells were resorbed the intracellular iron was precipitated out and observed as brown-black dots (Figure 6.60).

Other vascular changes

No quantification of the endothelial cell nuclei was conducted in the present dose rate experiments. The reason for not attempting any quantification was that once complete necrosis was observed in a particular structure in the brain, no additional sub-structures could be identified within the necrotic debris, an example of which is shown in Figure 6.10. No enlargement of the endothelial cell nuclei were observed in the present dose rate experiments. Calvo et al. (1988) observed no changes in the numbers of endothelial cell nuclei with either the dose of radiation or the time after irradiation, however, endothelial cell nuclear enlargement was observed to precede the onset of necrosis by approximately 12 weeks.

Thickening of the blood vessel walls was not scored in the present dose rate experiments however, examples may be observed in Figures 6.34, 6.38, 6.67 and 6.74. Calvo et al. (1988) observed thickening of the blood vessel walls around areas of necrosis and found that these vascular changes were both time and dose dependent.

Development of radiation damage

In the present dose rate experiments vascular lesions were scored at one year after radiation generally without any necrosis being evident in the particular structure examined in the rat brain. This suggests that the latent period for the development of necrosis is longer than that for the development of vascular lesions. Support for this view, albeit in the spinal cord, may be the work of Myers et al. (1986) who observed that dilated blood vessels and the occurrence of perivascular oedema preceded necrosis of the white matter. Further support may come from the work of Maisin (1974) and Schultheiss et al. (1995) who observed that injury to the microvasculature resulted in the manifestation of focal necrosis. Reinhold and Hopewell (1980) stated that if the threshold dose for the rat brain was exceeded, radiation damage in the form of "gross vascular abnormalities" sometimes accompanied by necrosis, would become manifest. The current dose rate study did not seem to demonstrate the presence of a

vascular lesion threshold dose as the vascular lesions were observed even at the lowest doses of radiation (30 – 31 Gy for the low dose rate experiments and 40 Gy for the fractionated experiments), irrespective of the dose rate. If this threshold dose was calculated, it would however have to be considered with the degree of dilation of the vessels. However, there did appear to be some threshold dose with regards to the occurrence of necrosis in each of the dose rate experiments performed.

On the other hand, however, there were also instances in the current work where vascular lesions were also observed in the presence of necrosis. In this regard, the work of Calvo et al. (1988) may be supportive, in that they stated that the vascular abnormalities (dilated blood vessels, thickening of blood vessel walls, endothelial cell enlargement and astrocyte hypertrophy) observed in their study may be secondary to necrosis. This conclusion was made after Calvo et al. (1988) found that the latent period for vascular changes was longer than that for necrosis in the rat brain.

The dose of radiation appears to be the factor that determines whether there is the occurrence of only vascular lesions or whether there is the occurrence of necrosis and vascular lesions in the rat brain. Whether any additional vascular damage was to be expressed in the current dose rate experiments is unknown in that the interpretation was limited to the one year observation period.

What is interesting to note is the observation by Schultheiss et al. (1995) that after the administration of chemotherapy alone, similar occlusive vascular lesions and white matter necrosis was observed to that after irradiation. This observation leads to the question of the uniqueness of necrosis seen after radiation alone, that is, there is no difference to the necrosis that is induced by either a dose of radiation or the administration of chemotherapy.

Histiocytes

The histiocytes may be regarded as being part of the reticulo-endothelial system which implies that they have a role in the immune response of the body and are therefore important in the maintenance of normal tissues. Histiocytes, or macrophages, as they are also referred to, have the capacity to ingest debris of cellular origin and also to ingest dead cells [Copenhaver, 1964; Cruickshank et al., 1968; Fawcett, 1994]. In the CNS the microglial cells are the equivalent of the histiocytes. Given the above statement the assumption would therefore be that these cells should be evident in all the tissues where there is destruction or damage present. However, in the present study this was not evident. The reason for this could be that the response of the histiocytes may be an early one to

damage of the normal cells. As time progresses there may be the progression of the immune response which may involve other cell types coming to the fore. The observation of histiocytes at one year post irradiation may be associated with chronic granulomatous inflammation which can occur in response to radiation.

Calcification

The deposition of calcium salts in the presence of non-viable or dead tissues is termed dystrophic calcification [Cotran et al., 1989] and this is usually encountered in areas of necrosis [Cotran et al., 1989]. This deposition of calcium in areas of necrosis was confirmed in the current study with the staining of a selection of histological sections with the von Kossa stain and these are shown in Figures 6.83 and 6.84. Calcium deposition may also be indicative of some previous injury as indicated in Figures 6.52 and 6.53 for the CAIR where there is no necrosis present. In this regard, Schultheiss et al. (1990) observed small areas of demyelination which contained flecks of mineral. The mineral deposits were not specified, but may be indicative of calcium as there was the presence of demyelination which in turn implies the presence of dead nervous tissue. Sheline et al. (1980) stated that they observed areas of microcalcification in patients after CNS irradiation.

Disruption of myelin fibres

Necrosis was invariably accompanied by the disruption of the parenchymal fibres (demyelination) of the brain (Figures 6.9 and 6.10; Figures 6.15 to 6.17; Figures 6.23 and 6.24; Figures 6.29 to 6.31). This was in keeping with the observations of Sheline et al. (1980) who described the lesions in the brains of patients after CNS irradiation as plaques of demyelination with a central area of necrosis.

Astrocytosis and gliosis

In the present dose rate experiments the number of astrocytes in any particular area of the rat brain was not quantified. The presence of astrocytes (Figures 6.86 to 6.90) was confirmed in a limited number of histological sections with the GFAP stain in order to confirm the occurrence of astrocytosis and gliosis as opposed to fibrosis in the rat brain after CNS irradiation. Calvo et al. (1988) counted the nuclei of astrocytes in the FH after irradiation and found that the counts varied not only between the different animals but also between the different areas in the same specimen. Calvo et al. (1988) also observed that in areas surrounding the necrosis, there was hypertrophy and hyperplasia of the

astrocytes. These authors also found no significant difference in the counts of oligodendrocytes outside areas of necrosis, however, in areas that were necrotic and that displayed demyelination the oligodendrocytes were found to be reduced in number. Reinhold et al. (1990) stated that they found a high correlation between the "tissue injury unit" (TIU), which was comprised of astrocyte enlargement, endothelial enlargement, blood vessel wall thickening and blood vessel dilation, and demyelination. These authors concluded that the TIU may therefore be an indicator for demyelination.

Vacuolation and hyalinisation of the choroid plexus

The choroid plexus displayed vacuolation and hyalinisation at the higher doses of radiation irrespective of the dose rate that was used. Examples of these reactions are shown in Figures 6.67 and 6.68.

Apoptosis and quantification of nuclei

It was considered of interest to try to assess the effect of radiation of rat brain on apoptosis by determination of the presence of apoptotic cells. However, the attempt had to be abandoned because cells that had undergone apoptotic death could not be easily distinguished from those that had died as a result of necrosis, ischaemia, gliosis or any other mechanism.

In addition, in the present series of experiments, no quantification of astrocyte or endothelial cell nuclei following radiation was performed in any of the anatomical sites of the rat brain. At the higher doses within each dose rate group, in many instances the presence of necrosis precluded identification of structures. This meant that it would not have been possible to construct meaningful dose response curves because of the absence of the high dose data.

7.8 DOSE RESPONSE RELATIONSHIPS

It was possible to use only the data from the dose response curves for necrosis of the FH and RCC to calculate the radiobiological parameters of the linear quadratic model. For all the other sites examined, the ED_{50} values obtained from the dose response curves (Figures 6.91 to 6.107) for protracted irradiation were inconsistent and did not allow for the calculation of the parameters using the graphical method of analysis [Dale, 1985].

In general, the trend for the dose response curves for oedema observed at one year in the various sites in the rat brain was for the incidence of oedema to increase with dose for the low dose rate and fractionated studies. However, for some areas, namely the FH, ST and TCC, this trend was not evident and there was a lower incidence of oedema after higher doses compared with lower doses, as shown in Figures 6.105 and 6.106. In view of the inconsistencies noted in the data for the incidence of oedema, no further analysis was possible.

Steepness of the dose response curves

An examination of the dose response curves (Figures 6.91 to 6.107) for the incidence of necrosis in the various areas of the rat brain that were examined, revealed that the slopes of the dose response curves were the steepest for the FH. The other histological areas that were examined in the rat brain have slopes which were shallower. This observation appears to be in keeping with the observations of other authors [Ang et al., 1984; Fowler, 1989; Thames et al., 1989; Withers, 1986; Withers, 1988; Withers et al., 1986] who have stated that the dose response curves for late reacting tissues tend to be steep.

7.9 IMPORTANCE OF ACCURATE VALUES FOR α/β AND μ

In the linear quadratic (LQ) model, the α/β ratio and the damage repair rate constant (μ) are the most important parameters [Dale, 1985; Dale et al., 1988; Deehan and O'Donoghue, 1988]. For human tissues the α/β ratios are not as well defined as those for animal tissues [Deehan and O'Donoghue, 1988]. However, the LQ model has been used to answer clinical questions in relation to alterations in the number and size of radiation fractions [Dale, 1985, 1986a, 1986b, 1989; Dale et al., 1997; Deehan and O'Donoghue, 1988; Dische and Saunders, 1990; Fowler, 1983, 1984, 1989; Hendry et al., 1996; Lee et al., 1995; Mills and Wayte, 1993; Saunders et al., 1991; Scott, 1987; Thames et al., 1983; Yaes et al., 1991]. Fowler (1989) has stated that clinical data have been obtained that are consistent with the values of α/β obtained from animal experiments [Bentzen et al., 1988; Overgaard, 1985, 1988; Thomas et al., 1988; Turesson and Notter, 1984], thus allowing for the use of animal α/β ratios as a guide.

The above comments have implications for radiotherapy in the clinical situation, specifically when the clinicians try to exploit the "greater" tolerance of the late

reacting tissues to small doses per fraction [Thames et al., 1989; Withers, 1992; Yaes et al., 1989] in that the accuracy of the α/β ratio and the accuracy of the prescribed radiation dose should be greater for the late responding tissues than for the early responding tissues. Withers (1988) makes a similar comment by stating that the use of accurate α/β ratios for late reacting tissues is critical because the calculations using low values of α/β are more significant than when using large α/β values in terms of the calculated dosage. This view that the α/β ratio used in equivalence calculations is of critical importance is also shared by Fowler (1989) and Dale (1985). Similar comments about the importance of the value of μ for the different critical tissues when performing calculations for the equivalence of protracted and fractionated regimes were expressed by Dale et al. (1988).

The general distinction between α/β ratio values for the early reacting and late reacting tissues may be described as that of low α/β ratios for the late reacting tissues and high α/β ratios for the early reacting tissues, with little or no overlap between the values [Ang et al., 1985; Dale, 1985; Fowler, 1984, 1989; Pop et al., 1997; Thames et al., 1988; Turesson, 1990; van der Kogel, 1979; White and Hornsey, 1978]. An α/β ratio value of 3 Gy has been suggested by most authors for late effects when using the LQ equation [Fowler, 1987; Thames et al., 1982, 1983; Turesson, 1989]. However, there appears to be a range of α/β values for late reactions and the value of 3 Gy that is used in calculations is a generalisation. This range of α/β ratio values is evident even when looking at a particular tissue, for example, for the rat cervical spinal cord the following values for the α/β ratio were obtained, namely, 1.8 - 2.7 Gy [van der Kogel, 1979], 1.6 - 1.9 Gy [White and Hornsey, 1978], 1.5 - 2.0 Gy [Ang et al., 1983], 2.2 – 3.0 Gy [Thames et al., 1988], 1.14 – 2.17 [Pop et al., 1997], and 1.8 – 3.5 Gy [Pop et al., 1998]. Thus, although the importance of using the "correct" α/β ratio in the LQ equations is emphasized, particularly for late reacting tissue, there is clearly some uncertainty as to the "correct" value of α/β.

7.10 α/β RATIO IN THE RAT BRAIN

In the current work, the two stage analysis to calculate the α/β ratio from the incidence data of necrosis of the FH and the RCC following protracted radiation yielded values of 6.2 and 54.5 Gy respectively. When the biologically

equivalent doses for necrosis from the low dose rate studies were set equal to those for the fractionated study, the relationship held true only when the α/β ratios in the fractionated protocol were 4.1 Gy and 23.2 Gy for the FH and the RCC respectively. These values, from both the low dose rate and fractionated studies are higher than would be expected for late responding tissue. The results for the FH are similar to Hornsey et al's (1981a), where an α/β ratio of 6.0 Gy was calculated for brain damage in rats at one year and also similar to Barendsen's (1982) α/β ratio of 5.0 Gy for demyelination in the CNS. It is of interest that van der Schueren et al. (1988) calculated an α/β ratio of 4.0 Gy for the cervical spinal cord in rats after they were observed for one year.

In general, the α/β ratios that were calculated in the current dose rate experiments were higher than those reported by other researchers for late reacting tissues. These values for α/β were obtained for an observation period of one year. However, this assessment period of one year may not have been sufficiently long for the end point, namely necrosis, to have developed in all the potential responders. These potential responders may be those rats in the current dose rate experiments that displayed oedema in the histological structures of interest without any necrosis being observed in those same structures. As stated earlier, vascular injury and oedema, generally preceded necrosis [Maisin, 1974, Myers et al., 1986; Schultheiss et al., 1995]. Therefore, the presence of oedema at one year post irradiation may eventually lead to the development of necrosis if the rats are observed for a long enough period of time. Further support for the continued development of necrosis in the rat brain, if the observation period was extended, may come from the work of Calvo et al. (1988). These authors observed necrosis in the FH at about 36 weeks after a single dose of 25 Gy. However, when the rats were given a lower dose of 22.5 Gy, they observed necrosis in the FH at about 51 weeks, thus even their lower doses of radiation eventually lead to necrosis being observed in the brain. In other words, the latent period for the development of necrosis is dose dependent.

Thus, if a longer time (greater than one year) were to have been allowed to elapse before the histological assessment, and a greater incidence of necrosis at the lower doses occurs, the dose response curves would move to the left, although the steepness of the dose response curves may not necessarily be affected. The resultant changes in the ED_{50} may also change the value of the α/β ratio as calculated using Dale's (1985) graphical method. A similar explanation is applicable to the RCC, where the ED_{50}'s for necrosis are higher.

Also, the higher ED_{50} values for the RCC may be reflection of the variation in the latent time for necrosis in the RCC. Calvo et al. (1988) also stated that the reason for the higher ED_{50} values they observed for the CC and CI when compared to that for the FH may be indicative of the differences in time for the development of necrosis in these areas. Indeed, in the current dose rate experiments, all the histological structures have an ED_{50} value which is greater than or equal to that for the FH, as is evident in Table 6.38. Thus, if the period of observation had been longer, the incidence data for necrosis for all these histological structures of the rat brain would likely change, which would affect the ED_{50} values, which in turn may affect the calculated α/β ratios.

7.11 REPAIR RATE CONSTANT, μ, AND REPAIR HALF-TIME IN THE RAT BRAIN

The value of the repair constant is also considered to be of critical importance [Dale et al., 1988; Fowler, 1989] and an accurate knowledge of its value for different critical tissues is considered vital for the calculation when switching from low to high dose rate regimes [Dale et al., 1988; O'Donoghue, 1989; Thames et al., 1984]. Generally, it has been stated that those tissues with high α/β ratios tend to have a faster repair rate, however there are exceptions to this general statement [Dale et al., 1988; Down et al., 1986; Steel et al., 1987; Thames, 1984; Turesson, 1990; Wong et al., 1992].

Thames et al. (1989) state that the repair constant is assumed to be independent of dose, that is, independent of the number of repairable lesions that are induced by a dose of radiation. Furthermore, the repair rate constant is considered to be tissue specific [Thames, 1989; Thames et al, 1984]. On the other hand, there is evidence that the repair rate may be dependent on the dose rate and/or the dose per fraction [Ang et al., 1984; Dale, 1985; Dale et al., 1988; Iliakis and Pohlit, 1979]. If the different values of μ are associated with different tissue responses, then the use of a common value of μ for all the tissue responses is inappropriate.

There have been a substantial number of studies in the literature where the repair half-time following irradiation has been ascertained for rat spinal cord. However, information in respect of the repair half-time for rat brain is sparse. The following are values of the repair half-times that have been calculated for the rat spinal cord, namely, 1.76 h [Pop et al., 1997], 0.15 h and 2.44 h [Pop et al., 1998], 1.6 h [Wong et al., 1992], 1.55 h [Ang et al., 1985], 3.8 h [Ang et al.,

1992], 5.5 h [Ruifrok et al., 1992] and 0.25 h and 6.5 h [Landuyt et al., 1997]. Given that the spinal cord and the brain are both components of the CNS the repair half-times calculated for the present dose rate experiments for the FH and the RCC of 1.92 and 6.93 h, respectively, appear to be of a similar magnitude to those calculated by other authors for the spinal cord.

The different repair rates for the FH and the RCC may be surprising in that these structures are located adjacent to one another. However, they are different structures and the cellular architecture differs. Also, the observation period of one year that was used in this study may not have been long enough for the development of the end point in all the potential responders for both the FH and RCC. If the observation period had been longer, then the incidence data, the dose response curves and therefore the ED_{50} values may all have changed. This in turn could result in changes in the α/β ratios and in the repair rate constant. Therefore, the kinetic parameters that have been derived from the current protracted radiation experiments should be regarded as specific for the specific tissue (anatomical site) and for the observation period of one year.

7.12 MONO- AND BI-EXPONENTIAL REPAIR

The graphical method suggested by Dale (1985) allows for an indirect (two-step) analysis of the α/β ratio and the half time of repair. When using this graphical method of Dale's the assumption is made that repair is monoexponential with time. Thus, when the best estimate of the half-time of repair is used, the best linear fit is obtained. An alternative method for determining the α/β ratio and the half time of repair is the direct analysis of Thames et al. (1986) where all raw quantal response data are included in the analysis. Regrettably, a computer program for the direct analysis was not available and the data presented in this thesis could not be analysed in this way. Some researchers [Ang et al., 1984, 1985, 1992; Landuyt et al., 1997; O'Donoghue, 1989; Pop et al., 1998; Thames et al., 1988; van der Schueren et al., 1988] have shown that the repair kinetics in the spinal cord are biphasic, that is, there are two components for repair in the spinal cord, one a fast component and the other a slow component, with each component having a different repair rate constant. The data of Ang et al. (1984, 1985, 1992), Thames et al. (1988) and van der Schueren et al. (1988) may be summarised as being interpreted in terms of a two-component biexponential repair model in which the repair half time for the fast component was of the

order of 0.7 h and that for the slow component was 3.8 h. On the other hand, Pop et al. (1998) has calculated a repair half-time of 0.15 h for the fast component and 2.44 h for the slow component. Likewise, Landuyt et al. (1997) calculated repair half-times for the fast component ranging from 0.25 h to 0.37 h and 6.5 h for the slow component. However, in an earlier study of the rat spinal cord Pop et al. (1997) found a repair half time of 1.76 h and was unable to demonstrate a biphasic pattern for repair kinetics possibly because of limited dose rate data. The strong evidence for two components of repair in the spinal cord is highly suggestive that the same is true for the brain. The latter cannot be excluded based on the findings in the current dose rate experiments, where the analysis was performed assuming monoexponential repair [Dale, 1985].

7.13 THE EQUIVALENCE OF PROTRACTED AND FRACTIONATED RADIATION PROTOCOLS

The observation period of one year may not have been sufficient to allow all the potential responders to develop necrosis in the current dose rate experiments. However, if the LQ model is valid, then one should be able to compare different protocols with each other at one year. The assumption that has to be made for this statement to be valid is that the different protocols that were used did not affect the latent period for the development of the end point.

The LQ model allows for the calculations of equivalence doses thereby allowing, in theory, for the conversion between a fractionated and a protracted regime [Barendsen, 1982; Deehan and O'Donoghue, 1988]. This in turn would imply that the values of the α/β ratio and that of the repair rate constant that were derived from a particular protracted regime may be applied to the calculations for determining the equivalent fractionated regime. The α/β ratio should be equal for both the protracted and fractionated schedules as the end point was identical, implying that the α/β ratio is tissue specific.

In the present study these equivalence calculations for the protracted and fractionated schedules could only be applied to two of the seventeen histological sites examined in the rat brain, namely, the FH and the RCC. For the protracted experiments α/β ratios of 6.2 Gy and 54.5 Gy were calculated for the FH and RCC respectively. On performing the equivalence calculations a discrepancy was found in that the α/β ratios for the protracted and fractionated schedules were not equal for either of these two sites. The α/β ratios for the fractionated

schedule needed to be set at 4.1 and 23.2 Gy for the FH and RCC respectively for biological equivalence to be true. These discrepancies may be partly because of errors in the estimation of the repair constant μ from data provided by only three protracted irradiation studies. A second possibility for the discrepancy is that the kinetics of repair are radiation-schedule dependent and not dose rate independent, which is assumed by the incomplete repair model [Thames, 1989]. Indeed, faster repair has been determined to occur with fractionated low dose rate irradiation of the jejenum [Dale et al., 1988; Thames et al., 1984] or continuous lung irradiation [Down et al., 1986] compared with fractionated high dose rate experiments.

The results presented in this thesis indicate that the prediction of protracted schedules from fractionated schedules may not be straightforward, and in the clinical setting should be undertaken with extreme caution. An added complication to deriving biologically equivalent low dose rate continuous radiation protocols and fractionated protocols is that the brain comprises of a number of diverse anatomical structures which have differing radioresponsiveness, that is, the latent time for development of late radiation damage varies. Therefore, unless full development of the chosen endpoint has occurred in all structures, and it is shown that repair kinetics and α/β ratios are common to all the sites, it may be misleading to make use of a single α/β ratio as representing the entire brain in the calculation of equivalence schedules.

7.14 COMMENT ON EXPERIMENTAL DESIGN

There are some additional steps that could be taken to strengthen the results of the experiments reported in this thesis. Firstly, for the radiation dose response curves to be more reliable, more animals could be added to each dose group for all the protracted and fractionated protocols. Secondly, to obtain better estimates of the repair parameters from the low dose rate studies, further studies at dose rates other than 0.04, 0.05 and 0.07 Gy min^{-1} could be included. Thirdly, for purposes of testing the equivalence of low dose rate and fractionated radiation schedules, the inclusion of additional groups of animals receiving fractionated radiation, where different fractionation protocols to the 10 fractions in 12 days described here are used, would be useful.

In the current dose rate experiments an end point of one year post-irradiation

was used. This period may not have been sufficient to permit the calculation of "full" dose response curves for the chosen end point of necrosis. In addition, the various protocols were compared at one year with the assumption that the different protocols will not affect the latent periods for the development of the end points at the different doses. In order to obtain the "full" kinetic parameters for the rat brain one may use large numbers of animals for each dose point in each low dose rate experiment and fractionated experiment. Groups of animals may then be killed for example, each week after one year and assessed for the end point. Performing this type of serial killing may permit one to obtain the "true" response curves for necrosis in various histological sites in the brain, thus allowing the calculation of the true α/β ratios and repair rate constants. However, obtaining the repair kinetics for the rat brain may prove to be difficult as there is a limitation on the length of the observation period which is restricted by the life span of the rats. Additionally, as more damage is inflicted to the brain more animals may die thus making it impossible to obtain data on the least responsive structures in the brain.

7.15 CONCLUSION

In summary, the rat brain was used as a CNS model to determine an equivalence between protracted irradiation and fractionated irradiation. An assessment of the rat brain's reactions to radiation was made by an histological examination of 17 different structures in the rat brain. Necrosis was generally observed after the higher doses of radiation for any given dose rate with the FH being the histological structure which displayed the highest incidence of necrosis. The presence of oedema in the rat brain at one year after irradiation may represent a second wave of oedema that could occur in the CNS in response to radiation. Dilated vessels of varying diameter was the most common histological reaction observed. The general trend was that the diameter of the dilated vessels increased with increasing dose of radiation. Other histological reactions to radiation were observed in the rat brains which included the occurrence of congested vessels, haemorrhages, histiocytes, calcium deposition, iron deposition and the disruption of myelin fibres. Vacuolation and hyalinisation of the choroid plexus was also observed in this study.

Dose response curves for necrosis and oedema were constructed for each of the histological areas examined in the rat brain and ED_{50} values were calculated. Only the FH and the RCC were found to display an increasing ED_{50} as the experimental dose rate decreased for the incidence of necrosis. No such

relationship between ED_{50} and experimental dose rate was displayed for the occurrence of oedema. The radiobiological parameters of the linear quadratic model could therefore only be calculated from the dose response curves for necrosis of the FH and RCC. Different α/β ratios were derived for the FH and the RCC in the rats from the low dose rate and fractionated studies, which may suggest that the α/β ratios are radiation schedule dependent. This discrepancy in the α/β ratios also suggests that it may not be possible to predict low dose rate protocols for brain irradiation which are equivalent to fractionated protocols using the linear quadratic model.

Thus, the work presented in this study indicates that the prospect of achieving a better quality of life for patients with high grade astrocytomas by alteration of the conventional radiation protocols to that of a low dose rate protocol does not appear to be a straightforward matter.

APPENDIX A

TISSUE PREPARATION FOR HISTOLOGICAL EVALUATION

The following standard protocol was used for the preparation of brain tissue for cutting on the microtone. The brain tissue was transferred from the fixation solution (10% phosphate buffered formalin solution) to marked plastic processing trays.

Dehydration and wax impregnation of the tissues were performed with the aid of a Shandon Tissue Processing machine as follows:

Day 1	One hour in 30% alcohol (container I) One hour in 30% alcohol (container II) One hour in 50% alcohol (container I) One hour in 50% alcohol (container II) Overnight in 70% alcohol (container I)
Day 2	24 hours in 70% alcohol (container II)
Day 3	12 hours in 80% alcohol (container I) 12 hours in 80% alcohol (container II)
Day 4	12 hours in 90% alcohol (container I) 12 hours in 90% alcohol (container II)
Day 5	12 hours in absolute alcohol (container I) 12 hours in absolute alcohol (container II)
Day 6	12 hours in xylene (container I) 12 hours in xylene (container II)
Day 7	24 hours in xylene (container III)
Day 8	24 hours in molten wax
Day 9	Tissue specimens are fixed on marked plastic trays

APPENDIX B

LUXOL FAST BLUE AND CRESYL VIOLET STAIN

Technique for demonstrating myelin sheaths and myeloarchitecture.

Procedure:

1. Bring histological sections to 95% alcohol through xylene and absolute alcohol.
2. Place in luxol fast blue solution (luxol fast blue, 1 g; 95% ethanol, 1000 ml; 10% acetic acid, 5 ml) and leave in the 56°C incubator overnight (the staining dishes must be sealed to prevent evaporation of the alcohol and the drying up of the sections).
3. Drain off excess stain by dipping in 95% alcohol.
4. Rinse well in distilled water.
5. Differentiate in 0.05% lithium carbonate (0.05 g in 100 ml H_2O) until the white matter is bright blue and the grey matter is either almost colourless or pale blue.
6. Rinse twice or 3 times in distilled water.
7. Finish differentiation in 70% alcohol until the white and grey matter are clearly distinguishable (30-60 seconds), wash well and examine microscopically, nuclei should be decolourised.
8. Rinse well in distilled water.
9. Stain with 0.5 % cresyl violet acetate (Fluka; 0.5 g in 100 ml H_2O) for 10 to 20 minutes at room temperature.
10. Rinse off the stain in distilled water.
11. Differentiate carefully in 95% alcohol to which 1-3 drops of concentrated glacial acetic acid (Merck) has been added - until the difference between the gray and white matter is achieved. The white matter should be darker blue and the grey matter paler but violet tinted.
12. Dehydrate rapidly through 95% and 100% alcohol (2 changes) - clear in xylene, 3 changes and mount in Entellan (Merck).

Results:

Myelin sheaths and white matter stain royal blue.

Cell bodies and neurons stain mauve.

Nissl substance if coarse-grained stains purple.

Nissl substance if fine-grained stains violet.

Non-neural tissues stain with varying tints of blue and green.

Note: Acetic acid in the cresyl violet counterstain intensifies the myelin staining changing it from green to blue.

APPENDIX C

LUXOL FAST BLUE HAEMATOXYLIN AND EOSIN

The initial procedure is as for luxol fast blue cresyl violet (Appendix B) but with the following changes:

1. Sections to water.
2. Stain in Mayer's haematoxylin (haematoxylin, 1 g; distilled water, 1000 ml , potassium or ammonium allum, 50 g; citric acid, 1 g; chloral hydrate, 50 g; sodium iodate, 0.2 g) for 5 minutes.
3. Wash in tap water.
4. Blue in Scott's tap water (sodium bicarbonate, 3.5 g; magnesium sulphate, 20 g; distilled H_2O, 1000 ml) .
5. Rinse in water.
6. Counterstain in eosin-phloxine (1% eosin, 250 ml; 1% phloxine, 125 ml; distilled H_2O, 375 ml).
7. Rinse in water.
8. Dehydrate, clear and mount in Entellan (Merck).

Results:

White matter stain blue.

Cell bodies, neurons stain blue.

Grey matter stains pink / red.

APPENDIX D

MARTIUS SCARLET BLUE (M.S.B) STAIN FOR FIBRIN

Procedure:

1. Take sections to water.
2. Stain nuclei with stable iron haematoxylin (solution A: haematoxylin, 3 g; 95% alcohol, 300 ml; solution B: aluminium chloride hydrated, 30 g; ferrous sulphate, 10 g; distilled H_2O, 300 ml; combine solution A and B and add concentrated hydrochloric acid, 2 ml; aqueous sodium iodate, 2 ml) from fridge for 5 minutes.
3. Rinse in tap water.
4. Differentiate in 1% acid alcohol (concentrated hydrochloric acid, 20 ml; 70% alcohol, 2000 ml).
5. Wash well in tap water and rinse in 95% alcohol.
6. Stain in martius yellow (Sigma; 0.5% martius yellow in 95% alcohol containing 2% phosphotungstic acid) for 2 minutes.
7. Rinse in distilled water.
8. Stain in brilliant crystal scarlet (Sigma; 1% brilliant crystal scarlet in 2.5% acetic acid) for 10 minutes.
9. Rinse in distilled water.
10. Treat with 1% phosphotungstic acid (phosphotungstic acid, 1 ml; distilled H_2O, 100 ml) for approximately 5 minutes to fix and differentiate the red until no more red remains in collagen.
11. Rinse in distilled water.
12. Stain with soluble blue (Sigma; 0.5% soluble blue in 1% acetic acid) for 2-10 minutes (usually about 5 minutes).
13. Rinse in 1% acetic acid solution.
14. Dehydrate and clear.
15. Mount in Entellan (Merck).

Results:

Nuclei stain blue-black.

Erythrocytes stain yellow.

Fibrin stains red.

Muscle stains red.

Connective tissue stains blue.

APPENDIX E

von KOSSA'S STAIN FOR CALCIUM

Calcium deposits stain a dark blue-black with haematoxylin but the staining is due to traces of iron in the deposit and is not specific. von Kossa's method stains calcium black but here the reaction is due to the acid radical of the calcium deposits and is not strictly specific. It is, however, a very useful method.

1. Bring paraffin sections to distilled water.
2. Place in 10% aqueous silver nitrate (Merck; silver nitrate, 10 g; distilled H_2O, 100 ml) and leave in the light for one hour.
3. Wash in distilled water, then put in 5% sodium thiosulphate solution (Merck) for 5 minutes.
4. Counterstain in nuclear fast red (nuclear fast red - Kernechtrot, 1 g; aluminium sulphate, 50 g; distilled H_2O, 1000 ml).
5. Rinse in tap water.
6. Dehydrate up to xylene, clear and mount.

Results:

Calcium stains black.

Background stains pink.

APPENDIX F

GLIAL FIBRILLARY ACIDIC PROTEIN

Glial fibrillary acidic protein (GFAP) is an intermediate filament protein of 52 kD found in glial cells, for example, astrocytes and ependymal cells.

Procedure:

1. Dewax and hydrate sections.
2. Treat sections for antigen retrieval using citrate buffer (0.1 M citric acid; citric acid, 10.5 g; distilled H_2O, 500 ml).
3. Incubate slides in quenching solution (hydrogen peroxide, 3 ml; methanol, 97 ml) for 30 minutes.
4. Rinse well in phosphate buffered saline (PBS) (NaCl, 16 g; Na_2HPO_4, 3.5 g; KCl, 0.4 g; KH_2PO_4, 0.4 g; distilled H_2O, 2000 ml).
5. Incubate sections with appropriate normal serum for 20 minutes.
6. Drain slides and wipe around section. Do not rinse.
7. Incubate sections with primary antibody for 30 to 60 minutes.
8. Rinse well in PBS.
9. Apply secondary antibody for 30 minutes.
10. Rinse well in PBS.
11. Apply tertiary antibody for 30 to 45 minutes.
12. Rinse well in PBS.
13. Stain with 0.1% DAB solution (diaminobenzidine, 1 g; PBS, 100 ml) for 5 minutes.
14. Rinse well in tap water.
15. Counterstain lightly in Mayer's haematoxylin (haematoxylin, 1 g; distilled H_2O, 1000 ml; potassium or ammonium alum, 50 g; citric acid, 1 g; chloral hydrate, 50 g; sodium iodate, 0.2 g) as used in the routine haematoxyline and eosin stain for 30 seconds.

16. Dehydrate and mount in Entellan (Merck).

Results:

Postive signal – diaminobenzadine = brown (nuclear / cytoplasmic / membranous)

Background = blue.

REFERENCES

Ahdab-Barmada, M., Moossy, J., Nemoto, E.M. and Lin, M.R. (1986) Hyperoxia produces neuronal necrosis in the rat. *Journal of Neuropathology and Experimental Neurology*, **45**: 233-246.

Albe-Fessard, D., Stutinsky, F. and Libouban, S. (1966) *Atlas Stéréotaxique du diencéphale du rat blanc*. Editions du Centre National de la Recherche Scientifique, Paris.

Anderson, A.P. (1978) Postoperative irradiation of glioblastomas. Results in a randomised series. *Acta Radiologica Oncology*, **17** Fasc. 6: 475-484.

Ang, K.K., van der Kogel, A.J. and van der Schueren, E. (1982) Inhalation anesthesia in experimental radiotherapy: a reliable and time-saving system for the multifractionation studies in a clinical department. *International Journal Radiation Oncology Biology Physics*, **8**: 145-148.

Ang, K.K., van der Kogel, A.J. and van der Schueren, E. (1983) The effect of small radiation doses on the rat spinal cord: the concept of partial tolerance. *International Journal of Radiation Oncology Biology Physics*, **9**: 1487-1491.

Ang, K.K., van der Kogel, A.J., van Dam, J. and van der Schueren, E. (1984) The kinetics of repair of sublethal damage in the rat cervical spinal cord during fractionated irradiations. *Radiotherapy and Oncology*, **1**: 247-253.

Ang, K.K., van der Kogel, A.J. and van der Schueren, E. (1985) Lack of evidence for increased tolerance of rat spinal cord with decreasing fraction doses below 2 Gy. *International Journal of Radiation Oncology Biology Physics*, **11**: 105-110.

Ang, K.K., Jiang, G.L., Guttenberger, R., Thames, H.D., Stephens, L.C., Smith, C.D. and Feng, Y. (1992) Impact of spinal cord repair kinetics on the practice of altered fractionation schedules. *Radiotherapy and Oncology*, **25**: 287-294.

Asscher, A.W. and Anson, S.G. (1962) Arterial hypertension and irradiation damage to the nervous system. *The Lancet*, **2**: 1343-1346.

Barendsen, G.W. (1978) Fundamental aspects of cancer induction in relation to the effectiveness of small doses of radiation. In: *Late Biological Effects of Ionising Radiation*, vol. II. Vienna, International Atomic Energy Agency: 263-275.

Barendsen, G.W. (1979) Influence of radiation quality on the effectiveness of small doses for induction of reproductive death and chromosome aberrations in mammalian cells. *International Journal of Radiation Biology*, **36**: 49-63.

Barendsen, G.W. (1982) Dose fractionation, dose rate and iso-effect relationships for normal tissue responses. *International Journal Radiation Oncology Biology Physics*, **8**: 1981-1997.

Barr, M.L. (1979) *The human nervous system: An anatomical viewpoint.* 3rd edition, Harper & Row, Maryland, USA: 3-37.

Bentzen, S.M., Christensen, J.J., Overgaard, J. and Overgaard, M. (1988) Some methodological problems in estimating radiobiological parameters from clinical data. *Acta Oncologica*, **27**: 105-116.

Berry, R.J., Wiernik, G. and Patterson, T.J.S. (1974) Skin tolerance of fractionated x-irradiation in the pig - how good a predictor is the NSD formula for small fraction numbers? *British Journal of Radiology*, **47**: 185-190.

Brown, J.M. (1977) The shape of the dose-response curve for radiation carcinogenesis. Extrapolation to low doses. *Radiation Research*, **71**: 34-50.

Burger, P. and Boyko, O. (1991) Radiation injury to the nervous system. In: *The pathology of central nervous system radiation injury*, eds. Gutin, P., Leibel, S., Sheline, G. Raven Press, New York: 191-208.

Burger, P., Mahaley, M.S. and Dudka, L. (1979) The morphologic effects of radiation administered therapeutically for intracranial gliomas. *Cancer*, **44**: 1256-1272.

Calvo, W., Reinhold, H.S., Yeung, T.K. and Hopewell, J.W. (1986) Radiation-induced damage in the choroid plexus of the rat brain. CRC Normal tissue radiobiology research group, Oxford university, annual report 1985/6: 133-137.

Calvo, W., Hopewell, J.W., Reinhold, H.S., van den Berg, A.P. and Yeung, T.K. (1987) Dose-dependent and time-dependent changes in the choroid plexus of the irradiated rat brain. *British Journal of Radiology*, **60**: 1109-1117.

Calvo, W., Hopewell, J.W., Reinhold, H.S. and Yeung, T.K. (1988) Time- and dose-related changes in the white matter of the rat brain after single doses of x rays. *British Journal of Radiology*, **61**: 1043-1052.

Chang, C.H., Horton, J., Schoenfeld, D., Salazar, O., Perez-Tamayo, R., Kramer, S., Weinstein, A., Nelson, J.S. and Tsukada, Y. (1983) Comparison of postoperative radiotherapy and combined postoperative radiotherapy and chemotherapy in the multidisciplinary management of malignant gliomas: a joint Radiation Therapy Oncology Group and Eastern Cooperative Oncology Group study. *Cancer*, **52**: 997-1007.

Chauser, B., Morris, C., Field, S. and Lewis, P.D. (1977) The effects of fast neutrons and x-rays on the subependymal layer of the rat brain. *Radiology*, **122**: 821-823.

Cohen, L. and Creditor, M. (1981) An iso-effect table for radiation tolerance of the human spinal cord. *International Journal of Radiation Oncology Biology Physics*, 7: 961-966.

Cohen, L. and Creditor, M. (1983a) Iso-effect tables for tolerance of irradiated normal human tissues. *International Journal of Radiation Oncology Biology Physics*, **9**: 233-241.

Cohen, L. and Creditor, M. (1983b) Iso-effect tables and therapeutic ratios for epidermoid cancer and normal tissue stroma. *International Journal of Radiation Oncology Biology Physics*, **9**: 1065-1071.

Copenhaver, W.M. (1964) *Bailey's textbook of histology*. 15th edition, Williams and Wilkins, Baltimore.

Cotran, R.S., Kumar, V. and Robbins, S.L. (1989) *Pathologic basis of disease*. 4th edition. WB Saunders Co., Philadelphia.

Cox, R., Thacker, J. and Goodhead, D.T. (1977) Inactivation and mutation of cultured mammalian cells by alluminium characteristic ultrasoft x-rays. II. Dose-response of Chinese hamster and human diploid cells to alluminium x-rays and radiation of different LET. *International Journal of Radiation Biology*, **31**: 561-576.

Craigie, E.H. (1920) On the relative vascularity of various parts of the central nervous system of the albino rat. *Journal of Comparative Neurology*, **31**: 429-464.

Cruickshank, B., Dodds, T.C. and Gardner, D.L. (1968) *Human histology*. 2nd edition, E and S Livingstone Ltd., Edinburgh: 42.

Dale, R.G. (1985) The application of the linear-quadratic dose-effect equation to fractionated and protracted radiotherapy. *British Journal of Radiology*, **58**: 515-528.

Dale, R.G. (1986a) The application of the linear-quadratic model to fractionated radiotherapy when there is incomplete normal tissue recovery between fractions, and possible implications for treatments involving multiple fractions per day. *British Journal of Radiology*, **59**: 919-927.

Dale, R.G. (1986b) Agreement of quadratic and CRE models in predicting the late effects of continuous low dose rate radiotherapy. *British Journal of Radiology*, **59**: 194-195.

Dale, R.G. (1989) Time-dependent tumour repopulation factors in linear-quadratic equations – implications for treatment strategies. *Radiotherapy and Oncology*, **15**: 371-382.

Dale, R.G., Huczkowski, J. and Trott, K.R. (1988) Possible dose rate dependence of recovery kinetics as deduced from a preliminary analysis of the effects of fractionated irradiations at varying dose rates. *British Journal of Radiology*, **61**: 153-157.

Dale, R.G., Coles, I.P., Deehan, C. and O'Donoghue, J.A. (1997) Calculation of integrated biological response in brachytherapy. *International Journal of Radiation Oncology Biology Physics*, **38**: 633-642.

Davis, L.W. (1989) Presidential address: Malignant glioma - a nemesis which requires clinical and basic investigations in radiation oncology. *International Journal of Radiation Oncology Biology Physics*, **16**: 1355-1366.

de Groot, J. (1967) *The rat forebrain in stereotaxic coordinates*. 3rd edition, N.V. Noord-Hollansche Uitgevers Maatschappij, Amsterdam.

Deehan, C. and O'Donoghue, J.A. (1988) Biological equivalence between fractionated radiotherapy treatments using the linear-quadratic model. *British Journal of Radiology*, **61**: 1187-1188.

Dimitrievich, G.S., Fischer-Dzoga, K. and Griem, M.L. (1984) Radiosensitivity of vascular tissue. I. Differential radiosensitivity of capillaries: a quantitative *in vivo* study. *Radiation Research*, **99**: 511-534.

Dische, S. and Saunders, M.I. (1990) The rationale for continuous, hyperfractionated, accelerated radiotherapy (CHART). *International Journal of Radiation Oncology Biology Physics*, **19**: 1317-1320.

Down, J.D., Easton, D.F. and Steel, G.G. (1986) Repair in the mouse lung during low dose-rate irradiation. *Radiotherapy and Oncology*, **6**: 29-42.

Dumas-Duport, C., Scheithauer, B., O'Fallan, J. and Kelly, P. (1988) Grading astrocytomas. A simple and reproducible method. *Cancer*, **15**: 2152-2165.

Ellis, F. (1968) The relationship of biological effect to dose-time-fractionation factors in radiotherpy. In: *Current Topics in Radiation Research*, Vol. IV, Eds. Ebert and Howard, Amsterdam, North Holland: 357-397.

Ellis, F. (1969) Dose, time and fractionation: A clinical hypothesis. *Clinical Radiology*, **20**: 1-8.

Fawcett, D.W. (1994) *A textbook of histology*. 12th edition, Chapman and Hall, New York: 1150-151.

Fertil, B. and Malaise, E.P. (1981) Inherent cellular radiosensitivity as a basic concept for human tumour radiotherapy. *International Journal of Radiation Oncology Biology Physics*, 7: 621-629.

Fike, J.R., Cann, C.E., Truowski, K., Higgins, R.J., Chan, A.S.L., Phillips, T.L. and Davis, R.L. (1988) Radiation dose response of normal brain. *International Journal of Radiation Oncology Biology Physics*, **14**: 63-70.

Fowler, J.F. (1971) Experimental animals results relating to time-dose relationships in radiotherapy and the 'ret' concept. *British Journal of Radiology*, **44**: 81-90.

Fowler, J.F. (1983) Fractionation and therapeutic gain. In: *The biological basis of radiotherapy*, eds. Steel, G.G., Adams, G.E. and Peckham, M.J., Elsevier, Amsterdam: 81-90.

Fowler, J.F. (1984) What next in fractionated radiotherapy? *British Journal of Cancer*, **49** (Suppl. VI): 285-300.

Fowler, J.F. (1987) Short and long fractionated schedules in radiotherapy and a proposed improvement. *British Journal of Radiology*, **60**: 777-779.

Fowler, J.F. (1989) The linear-quadratic formula and progress in fractionated radiotherapy. *British Journal of Radiology*, **62**: 679-394.

Fowler, J.F., Morgan, R.I., Silvester, J.A., Bewley, D.K. and Turner, B.A. (1963) Experiments with fractionated x-ray treatment of the skin of pigs. I. Fractionation up to 28 days. *British Journal of Radiology*, **36**: 188-196.

Garcia, J.H. (1991) Chapter 2: Classification of Brain Tumours, In: *Neurobiology of brain tumours Volume 4: Concepts in Neurosurgery.*, ed. M. Salcman, Williams and Wilkins, Baltimore: 19-32.

Gehan, E.A. and Walker, M.D. (1977) Prognostic factors for patients with brain tumours. In: Modern Concepts in Brain tumour therapy: Laboratory and Clinical investigations, ed. by JC Bailar and EK Weisberger. *National Cancer Institute Monograph*, **46**: 189-195.

Green, S.B., Byar, D.P., Walker, M.D., Pistenmaa, D.A., Alexander, E., Batzdorf, U., Brooks, W.H., Hunt, W.E., Mealey, J., Odom, G.L., Paoletti, P., Ranshoff, J., Robertson, J.T., Selker, R.G., Shapiro, W.R., Smith, K.R., Wilson, C.B. and Strike, T.A. (1983) Comparisons of Carmustine, procarbazine, and high-dose methylprednisolone as additions to surgery and radiotherapy for the treatment of malignant gliomas. *Cancer Treatment Reports*, **67**: 121-132.

Hall, E.J. (1988) *Radiobiology for the radiologist*, 3rd edition, JB Lippencott, Philadelphia: 107-136.

Hall, E.J. (1994) *Radiobiology for the radiologist*. 4th edition. JB Lippincott, Philadelphia: 29-44.

Hendry, J.H., Bentzen, S.M., Dale, R.G., Fowler, J.F., Wheldon, T.E., Jones, B., Munro, A.J., Slevin, N.J. and Robertson, A.G. (1996) A modelled comparison of the effects of using different ways to compensate for missed treatment days in radiotherapy. *Clinical Oncology*, **8**: 297-307.

Hopewell, J.W. (1974) The late vascular effects of radiation. *British Journal of Radiology*, **47**: 157-158.

Hopewell, J.W. (1983) Experimental studies of early and late responses in normal tissues. In: *The biological basis of radiotherapy*. eds. Steel, Adams and Peckham, Elsevier Science Publishers: 157-166.

Hopewell, J.W. (1987) The role of the vasculature in normal tissue responses. In: *Proceedings of the 8th International Congress of Radiation Research*, Edinburgh, July 1987. Eds. E.M. Fieldman, J.F. Fowler, J.H. Hendry and D. Scott, Taylor and Francis, London: 789-794.

Hopewell, J.W. and Wright, E.A. (1970) The nature of latent cerebral irradiation damage and its modification by hypertension. *British Journal of Radiology*, **43**: 161-167.

Hopewell, J.W. and Cavanagh, J.B. (1972) Effects of x-irradiation on the mitotic activity of the subependymal plate of rats. *British Journal of Radiology*, **45**: 461-465.

Hopewell, J.W., Reinhold, H.S., Wilkinson, J. and Blackiewicz, B. (1978) Changes in the architecture of blood vessels in the rat brain after local irradiation. *British Journal of Radiology*, **51**: 561.

Hopewell, J.W., Campling, D., Calvo, W., Reinhold, H.S., Wilkinson, J.H. and Yeung, T.K. (1986) Vascular irradiation damage: its cellular basis and likely consequences. *British Journal of Cancer*, **53**(Suppl. VII): 181-191.

Hopewell, J.W., Morris, A.D. and Dixon-Brown, A. (1987) The influence of field size on the late tolerance of the rat spinal cord to single doses of x-rays. *British Journal of Radiology*, **60**: 1099-1108.

Hornsey, S., Morris, C.C. and Myers, R. (1981a) The relationship between fractionation and total dose for x-ray induced brain damage. *International Journal of Radiation Oncology Biology Physics*, 7: 393-396.

Hornsey, S., Myers, R., Coultas, P.C., Rogers, M.S. and White, A. (1981b) Turnover of proliferative cells in the spinal cord after x-irradiation and its relation to time-dependent repair of radiation damage. *British Journal of Radiology*, **54**: 1081-1085.

Hornsey, S., Myers, R. and Jenkinson, T. (1990) The reduction of radiation damage to the spinal cord by post-irradiation administration of vasoactive drugs. *International Journal of Radiation Oncology Biology Physics*, **18**: 1437-1442.

Hubbard, B.M. and Hopewell, J.W. (1979) Changes in neuroglial cell populations of the rat spinal cord after local x-irradiation. *British Journal of Radiology*, **52**: 816-821.

Iliakis, G. and Pohlit, W. (1979) Quantitative aspects of repair of potentially lethal damage in mammalian cells. *International Journal of Radiation Biology*, **36**: 649-658.

Johns, H.E. and Cunningham, J.R. (1969) *The physics of radiology*. 3rd edition, Charles Thomas, Illinois USA: 277.

Junqueira, L.C. and Carneiro, J. (1980) *Basic Histology*. 3rd edition, Lange Medical Publishers, California, USA: 152-185.

Karlsson, U.L. and Brady, L.W. (1987) Chapter 20: Primary intracranial neoplasms. In: *Principles and practice of radiation oncology*. eds. Perez, C.A. and Brady, L.W., J.B. Lippincott Co., Philadelphia: 408-436.

Karnofsky, D.A., Abelmann, W.H., Craver, L.F. and Burchenal, J.H. (1948) The use of the nitrogen mustards in the palliative treatment of carcinoma; with particular reference to bronchogenic carcinoma. *Cancer*, **1**: 634-656.

Kim, Y.H. and Fayos, J.V. (1981) Radiation tolerance of the cervical spinal cord. *Radiology*, **139**: 473-478.

Kirk, J., Gray, W.M. and Watson, E.R. (1971) Cumulative radiation effect. Part I: Fractionated treatment regimes. *Clinical Radiology*, **22**: 145-155.

Kirk, J., Gray, W.M. and Watson, E.R. (1972) Cumulative radiation effect. Part II: Continuous radiation therapy – Long-lived sources. *Clinical Radiology*, **23**: 93-105.

König, J.F.R. and Klippel, R.A. (1963) *The rat brain – a stereotaxic atlas*. Williams and Wilkins, Baltimore.

Kristiansen, K., Hagen, S., Kollevold, T., Torvic, A., Holme, I., Nesbakken, R., Hatlevoll, R., Lindgren, M., Brun, A., Lindgren, S., Notter, G., Anderson, A.P. and Elgen, K. (1981) Combined modality therapy of operated astrocytomas Grade III and IV. Confirmation of the value of postoperative irradiation and lack of potentiation of Bleomycin on survival time: A prospective multicentre trial of the Scandinavian Glioblastoma Study Group. *Cancer* **47**: 649-652.

Landuyt, W., Fowler, J., Ruifrok, A., Stuben, G., van der Kogel, A.J. and van der Schueren, E. (1997) Kinetics of repair in the spinal cord of the rat. *Radiotherapy and Oncology*, **45**: 55-62.

Lazorthes, G. (1972) Pathology, classification and clinical aspects of vascular diseases of the spinal cord. *Handbook of Clinical Neurology*, **12**: 492-503.

Lee, Y., Wikstrand, C.J., Humphrey, P.A., Bigner, S.H., Friedman, H.S., Vrionis, F.D. and Bigner, D.B. (1991) Chapter 10: In vitro growth of brain tumours. In: *Neurobiology of brain tumours Volume 4: Concepts in Neurosurgery*, ed. M. Salcman, Williams and Wilkins, Baltimore: 163-183.

Lee, S.P., Leu, M.Y., Smathers, J.B., McBride, W.H., Parker, R.G. and Withers, H.R. (1995) Biologically effective dose distribution based on the linear quadratic model and its clinical relevance. *International Journal of Radiation Oncology Biology Physics*, **33**: 375-389.

Leone, J. and Ochs, S. (1978) Anoxic block and recovery of axoplasmic transport and electrical excitability of nerve. *Journal of Neurobiology*, **9**: 229-245.

Levin, V.A., Sheline, G.E. and Gutin, P.H. (1989) Neoplasms of the Central Nervous System. In: *Cancer: Principles and Practice of Oncology*, eds. DeVita, V.T., Hellman, S. and Rosenberg, S.A., 3rd edition. Philadelphia; JB Lippincott Co.: 1557-1611.

Levin, V.A., Leibel, S.A. and Gutin, P.H. (1997) Neoplasms of the Central Nervous System. In: *Cancer: Principles and Practice of Oncology*, eds. DeVita, V.T., Hellman, S. and Rosenberg, S.A., 5th edition. Philadelphia, Lippincott-Raven: 2022-2082.

Lloyd, D.C., Purrott, R.J., Dosphin, G.W. and Edwards, A.A. (1976) Chromosome aberrations induced in human lymphocytes by neutron irradiation. *International Journal of Radiation Biology*, **29**: 169-182.

Maisin, J.R. (1974) Chapter III: Ultrastructure of the vessel wall. In: *Current topics in radiation research quarterly*, **10**: 29-57.

Marks, J.E., Baglan, R.J., Prassad, S.C. and Blank W.F. (1981) Cerebral radionecrosis: incidence and risk in relation to dose, time, fractionation and volume. *International Journal of Radiation Oncology Biology Physics*, **7**: 243-252.

Marks, J.E. (1991) Chapter 17: Ionising radiation. In: *Neurobiology of brain tumours Volume 4: Concepts in Neurosurgery,*. ed. M. Salcman, Williams and Wilkins, Baltimore: 299-309.

Mazze, R.I., Calverley, R.K. and Smith, N.T. (1977) Inorganic fluoride nephrotoxicity: prolonged enflurane and halothane anaesthesia in volunteers. *Anaesthesiology*, **46**: 265-271.

McCunniff, A.J. and Liang, M.J. (1989) Radiation tolerance of the cervical spinal cord. *International Journal of Radiation Oncology Biology Physics*, **16**: 675-678.

McDonald, J.V., Salazar, O.M., Rubin, P., Lapham, L.W. and Bakemeier, R.F. (1983) Chapter 20: Central Nervous System Tumours. In: *Clinical Oncology - A multidisciplinary approach*, ed. Rubin, P., 6th edition, American Cancer Society, New York: 262-279.

Mills, J.A. and Wayte, S.C. (1993) Use of the linear quadratic model in order to accommodate a small reduction in the number of fractions of a standard radiotherapy treatment regime. *British Journal of Radiology*, **66**: 447-451.

Moustafa, H.F. and Hopewell, J.W. (1980) Late functional changes in the vasculature of the rat brain after local x-irradiation. *British Journal of Radiology*, **53**: 21-25.

Myers, R., Rogers, M.A. and Hornsey, S. (1986) A reappraisal of the roles of glial and vascular elements in the development of white matter necrosis in irradiated rat spinal cord. *British Journal of Cancer*, **53**, Suppl. VII: 221-223.

Nelson, D.F., Nelson, J.S., Davis, D.R., Chang, C.H., Griffin, T.W. and Pajak, T.F. (1985) Survival and prognosis of patients with astrocytoma with atypical or anaplastic features. *Journal of Neuro-oncology*, **3**: 99-103.

Nelson, D.F., Diener-West, M., Weinstein, A.S., Schoenfeld, D., Nelson, J.S., Sause, W.T., Chang, C.H., Goodman, R. and Carabell, S.A. (1986) A randomised comparison of misonidazole sensitised radiotherapy plus BCNU and radiotherapy plus BCNU for treatment of malignant glioma after surgery: final report of an RTOG study. *International Journal of Radiation Oncology Biology Physics*, **12**: 1793-1800.

Nelson, D.F., Diener-West, M., Horton, J., Chang, C.H., Shoenfeld, D. and Nelson, J.S. (1988) Combined modality approach to treatment of malignant gliomas. Re-evaluation of RTOG 7401/ECOG 1374 with long-term follow-up: a joint study of the Radiation Therapy Oncology Group and the Eastern Cooperative Oncology Group, National Cancer Institute. *National Cancer Institute Monograph*, **6**: 279-284.

Nelson, D.F., McDonald, J.V., Lapham, L.W., Qazi, R. and Rubin, P. (1993) Chapter 30: Central Nervous System Tumours. In: *Clinical Oncology A Multidisciplinary Approach for Physicians and Students*. ed. Rubin, P. 7th edition, W.B. Saunders Co., Philadelphia, U.S.A.: 617-644.

Norman, M.G. and O'Kusky, J.R. (1986) The growth and development of microvasculature in human cerebral cortex. *Journal of Neuropathology and Experimental Neurology*, **45**: 222-232.

O'Donoghue, J.A. (1989) Comparison of the predictions of the LQ and CRE models for normal tissue damage due to biologically targeted radiotherapy with exponentially decaying dose rates. *Radiotherapy and Oncology*, **15**: 359-362.

Orton, C.G. (1974) Time-dose factors (TDFs) in brachytherapy. *British Journal of Radiology*, **47**: 603-607.

Orton, C.G. and Ellis, F. (1973) A simplification in the use of the NSD concept in practical radiotherapy. *British Journal of Radiology*, **46**: 529-537.

Overgaard, M. (1985) The clinical implication of non-standard fractionation. *International Journal of Radiation Oncology Biology Physics*, **11**: 1225-1229.

Overgaard, M. (1988) Spontaneous radiation-induced rib fractures in breast cancer patients treated with postmastectomy irradiation. A clinical radiobiological analysis of the influence of fraction size and dose-response relationships on late bone damage. *Acta Oncologica*, **27**: 117-122.

Packer, R.J. (1991) Chapter 16: Prognostic factors in patients with brain tumours, In: *Neurobiology of brain tumours Volume 4: Concepts in Neurosurgery*, ed. M. Salcman, Williams and Wilkins, Baltimore: 275-295.

Pellegrino, L.J., Pellegrino, A.S. and Crushman, A.J. (1978) *A stereotaxic atlas of the rat brain*. Plenum Press, New York.

Pezner, R.D. and Archameau, J.O. (1981) Brain tolerance unit: a method to estimate risk of radiation brain injury for various dose schedules. *International Journal of Radiation Oncology Biology Physics*, **7**: 397-402.

Peters, L.J. and Withers, H.R. (1980) Morbidity from large dose fractions in radiotherapy. *British Journal of Radiology*, **53**: 170-171.

Plotnikova, E.D., Levitman, M.K., Shaposhnikova, V.V., Koshevoy, J.V. and Eidus, L.K. (1984) Protection of microcirculation in rat brain against late radiation injury by Gammaphos. *International Journal Radiation Oncology Biology Physics*, **10**: 365-368.

Plotnikova, E.D., Levitman, M.K., Shaposhnikova, V.V., Koshevoj, J.V. and Eidus, L.K. (1988) Protection of microvasculature in rat brain against late radiation injury by gammaphos. *International Journal Radiation Oncology Biology Physics*, **15**: 1197-1201.

Pop, L.A.M., van der Plas, M., Skwarchuk, M.W., Hanssen, A.E.J. and van der Kogel, A.J. (1997) High dose rate (HDR) and low dose rate (LDR) interstitial irradiation (IRT) of the rat spinal cord. *Radiotherapy and Oncology*, **42**: 59-67.

Pop, L.A.M., van der Plas, M., Ruifrok, A.C.C., Schalkwijk, L.J.M., Hanssen, A.E.J. and van der Kogel, A.J. (1998) Tolerance of rat spinal cord to continuous interstitial irradiation. *International Journal of Radiation Oncology Biology Physics*, **40**: 681-689.

Ransohoff, J., Koslow, M. and Cooper, P.R. (1991) Chapter 24: Cancer of the Central Nervous System and Pituitary. In: *American Cancer Society Textbook of Clinical Oncology*. eds. Holleb, A.I., Fink, D.J. and Murphy, G.P.: 329-337.

Reinhold, H.S. and Hopewell, J.W. (1980) Late changes in the architecture of blood vessels of the rat brain after irradiation. *British Journal of Radiology*, **53**: 693-696.

Reinhold, H.S., van Putten, W.L.J., Hopewell, J.W. and van der Kogel, A.J. (1984) The latent period in clinical radiation myelopathy. *International Journal of Radiation Oncology Biology Physics*, **10**: 2385-2387.

Reinhold, H.S., Calvo, W., Hopewell, J.W. and van den Berg, A.P. (1990) Development of blood vessel-related radiation damage in the fimbria of the central nervous system. *International Journal Radiation Oncology Biology Physics*, **18**: 37-42.

Remler, M.P., Marcussen, W.H. and Tiller-Borsich, J. (1986) The late effects of radiation on the blood brain barrier. *International Journal of Radiation Oncology Biology Physics*, **12**: 1965-1969.

Rogers, M., Myers, R., Jenkinson, T. and Hornsey, S. (1982) Histology of the irradiated rat brain in the first post-irradiation year. *British Journal of Radiology*, **55**: 208-212.

Ruifrok, A.C.C., Kleiboer, B.J. and van der Kogel, A.J. (1992) Radiation tolerance and fractionation sensitivity of the developing rat cervical spinal cord. *International Journal of Radiation Oncology Biology Physics*, **24**: 505-510.

Ruifrok, A.C.C., Stephens, L.C. and van der Kogel, A.J. (1994) Radiation response of the rat cervical spinal cord after irradiation at different ages: tolerance, latency and pathology. *International Journal Radiation Oncology Biology Physics*, **29**: 73-79.

Rubin, P., Gash, D.M., Hausen, J.T., Nelson, D.F. and Williams, J.P. (1994) Disruption of the blood-brain barrier as the primary effect of CNS irradiation. *Radiotherapy and Oncology*, **31**: 51-60.

Safdari, H., Fuentes, J.M., Dubois, J.B., Alirezai, M.., Castan, P. and Vlahovitch, B. (1985) Radiation necrosis of the brain: time of onset and incidence related to total dose and fractionation of radiation. *Neuroradiology*, **27**: 44-47.

Salazar, O.M., Rubin, P., Feldstein, M.L. and Pizzutiello, R. (1979) High dose radiation therapy in the treatment of malignant gliomas: final report. *International Journal of Radiation Oncology Biology Physics*, **5**: 1733-1740.

Saunders, M.I., Dische, S., Grosch, E.J., Fermont, D.C., Ashford, R.F., Maher, E.J. and Makepeace, A.R. (1991) Experience with CHART. *International Journal of Radiation Oncology Biology Physics*, **21**: 871-878.

Schoenberg, B.S. (1991) Chapter 1: Epidemiology of primary intracranial neoplasms: Disease distributions and risk factors. In: *Neurobiology of brain tumours Volume 4: Concepts in Neurosurgery*, ed. M. Salcman, Williams and Wilkins, Baltimore: 3-18.

Schultheiss, T.E., Higgins, E.M. and El-Mahdi, A.M. (1984) Extrinsic versus intrinsic dose dependency of latency in radiation myelopathy. *International Journal of Radiation Oncology Biology Physics*, **10**: 2389.

Schultheiss, T.E., Stevens, L.C. and Maor, M.H. (1988) Analysis of the histopathology of radiation myelopathy. *International Journal of Radiation Oncology Biology Physics*, **14**: 27-32.

Schultheiss, T.E., Stevens, L.C., Jiang, G.L., Ang, K.K. and Peters, L.J. (1990) Radiation myelopathy in primates treated with conventional fractionation. *International Journal of Radiation Oncology Biology Physics*, **19**: 935-940.

Schultheiss, T.E., Kun, L.E., Ang, K.K. and Stephens, L.C. (1995) Radiation response of the central nervous system. *International Journal of Radiation Oncology Biology Physics*, **31**: 1093-1112.

Scott, O.C.A. (1987) Divergence of opinion over the linear-quadratic model. *British Journal of Radiology*, **60**: 1042-1043.

Sheline, G.E. (1977) Radiation therapy of brain tumours. *Cancer*, **39**: 873-881.

Sheline, G.E., Wara, W.M. and Smith, V. (1980) Therapeutic irradiation and brain injury. *International Journal of Radiation Oncology Biology Physics*, **6**: 1215-1228.

Sheline, G.E. (1990) Radiotherapy for high grade gliomas. *International Journal of Radiation Oncology Biology Physics*, **18**: 793-804.

Steel, G.G., Down, D.J., Peacock, J.H. and Stephens, T.C. (1987) The dose-rate effect in human tumour cells. *Radiotherapy and Oncology*, **9**: 299-310.

Strandqvist, M. (1944) Studien über die kumulative Wirkung der Röntgenstrahlen bei Franktionierung. Erfahrungen aus dem Radiumhemmet an 280 Haut und Lippenkarzinomen. *Acta Radiologica* (Suppl.55): 1-300.

Thames, H.D. (1984) Effect-independent measures of tissue responses to fractionated irradiation. *International Journal of Radiation Biology*, **45**: 1-10.

Thames, H.D. (1989) Repair kinetics in tissues: alternative models. *Radiotherapy and Oncology*, **14**: 321-327.

Thames, H.D. and Hendry, J.H. (1987) *Fractionation in radiotherapy*. Taylor and Francis, London: 221.

Thames, H.D., Withers, H.R., Peters, L.J. and Fletcher, G.J. (1982) Changes in early and late radiation responses with altered dose fractionation: implications for dose-survival relationships. *International Journal of Radiation Oncology Biology Physics*, **8**: 219-226.

Thames, H.D., Peters, L.J., Withers, H.R. and Fletcher, G.H. (1983) Accelerated fractionation vs. hyperfractionation: rationales for several treatments per day. *International Journal of Radiation Oncology Biology Physics*, **9**: 127-138.

Thames, H.D., Withers, H.R. and Peters, L.J. (1984) Tissue repair capacity and repair kinetics deduced from multifractionated or continuous irradiation regimens with incomplete repair. *British Journal of Cancer*, **49** (Suppl. VI): 263-269.

Thames, H.D., Rozell, M.E., Tucker, S.L., Ang, K.K., Fisher, D.R. and Travis, E.L. (1986) Direct analysis of quantal radiation response data. *International Journal of Radiation Biology*, **49**: 999-1009.

Thames, H.D., Ang, K.K., Stewart, F. and van der Schueren, E. (1988) Does incomplete repair explain the apparent failure of the basic LQ model to predict spinal cord and kidney responses to low doses per fraction? *International Journal of Radiation Biology*, **54**: 13-19.

Thames, H.D., Hendry, J.H., Moore, J.V., Ang, K.K. and Travis, E.L. (1989) The high steepness of dose-response curves for late-responding normal tissues. *Radiotherapy and Oncology*, **15**: 49-53.

Thomas, F., Ozanne, F., Mamelle, G., Wilbault, P. and Eschwege, F. (1988) Radiotherapy alone for oropharyngeal carcinomas: the role of fraction size (2 Gy vs 2.5 Gy) on local control and early and late complications. *International Journal of Radiation Oncology Biology Physics*, **15**: 1097-1102.

Travis, E.L. and Tucker, S.L. (1987) Iso-effect models and fractionated radiation therapy. *International Journal of Radiation Oncology Biology Physics*, **13**: 283-287.

Turesson, I. (1989) The progression rate of late radiation effects in normal tissue and its impact on dose-response relationships. *Radiotherapy and Oncology*, **15**: 217-226.

Turesson, I. (1990) Radiobiological aspects of continuous low dose-rate irradiation and fractionated high dose-rate irradiation. *Radiotherapy and Oncology*, **19**: 1-16.

Turesson, I. and Notter, G. (1979a) The response of pig skin to single and fractionated high dose-rate and continuous low dose-rate ^{137}Cs-irradiation - I. Experimental Design and Results. *International Journal of Radiation Oncology Biology Physics*, **5**: 835-844.

Turesson, I. and Notter, G. (1979b) The response of pig skin to single and fractionated high dose-rate and continuous low dose-rate ,^{137}Cs-irradiation - II. Theoretical considerations of the results. *International Journal of Radiation Oncology Biology Physics*, **5**(7): 955-963.

Turesson, I. and Notter, G. (1979c) The response of pig skin to single and fractionated high dose-rate and continuous low dose-rate ^{137}Cs-irradiation - III. Re-evaluation of the CRE system and the TDF system according to the present findings. *International Journal of Radiation Oncology Biology Physics*, **5**(10): 1773-1779.

Turesson, I. and Notter, G. (1984) The influence of fraction size in radiotherapy on the late normal tissue reaction. I. Comparison of the effects of daily and once-a-week fractionation on human skin. *International Journal of Radiation Oncology Biology Physics*, **10**: 593-598.

van der Kogel, A.J. (1979) *Late effects of radiation on the spinal cord: dose effect relationships and pathogenesis*. Radiobiological Institute of the Organisation for Health Research TNO, Rijswiijk, The Netherlands.

van der Kogel, A.J. (1986) Radiation-induced damage in the central nervous system: An interpretation of target cell response. *British Journal of Cancer*, **54**: 207-217.

van der Kogel, A.J. and Barendsen, G.W. (1974) Late effects of spinal cord irradiation with 300 kV x-rays and 15 MeV neutrons. *British Journal of Radiology*, 47: 393-398.

van der Kogel, A.J., Sissingh, H.A. and Zoetelief, J. (1982) Effects of x-rays and neutrons on repair and regeneration in the rat spinal cord. *International Journal of Radiation Oncology Biology Physics*, **8**: 2095-2097.

van der Kogel, A.J., Kleiboer, B.J., Verhagen, I., Morris, G.M., Hopewell, J.W. and Coderre, J.A. (1995) White matter necrosis of the spinal cord: studies on glial progenitor survival and selective vascular irradiation. In: *Proceedings of the 10th International Congress of Radiation Research*, Wurzburg, Germany. Eds. U. Hagen, D. Harder, H. Jung and C. Streffer. Universitatsdruckerei H. Sturtz, Germany: 769-772.

van der Schueren, E., Landuyt, W., Ang, K.K. and van der Kogel, A.J. (1988) From 2 Gy to 1 Gy per fraction: sparing effect in rat spinal cord, lung and rectum. *Radiation Research*, **104 S**: 208-216.

Walker, M.D., Alexander, E., Hunt, W.E., MacCarthy, C.S., Mahaley, M.S., Mealey, J., Norrell, H.A., Owens, G., Ransohoff, J., Wilson, C.B., Gehan, E.A. and Strike, T.A. (1978) Evaluation of BCNU and/or radiotherapy in the treatment of anaplastic gliomas. A cooperative clinical trial. *Journal of Neurosurgery*, **49**: 333-343.

Walker, M.D., Strike, A. and Sheline, G.E. (1979) An analysis of dose-effect relationship in the radiotherapy of malignant gliomas. *International Journal of Radiation Oncology Biology Physics*, **5**: 1725-1731.

White, A. and Hornsey, S. (1978) Radiation damage to the rat spinal cord: the effect of single and fractionated doses of x-rays. *British Journal of Radiology*, **51**: 515-523.

Wilkinson, J.H., Hopewell, J.W. and Reinhold, H.S. (1986) A quantitative study of the effects of local x-irradiation on the vasculature of the rat cerebral cortex. CRC Normal tissue radiobiology research group, Oxford university, annual report 1985/6: 138-143.

Withers, H.R. (1986) Predicting late normal tissue responses. *International Journal of Radiation Oncology Biology Physics*, **12**: 693-698.

Withers, H.R. (1988) The linear-quadratic model. *British Journal of Radiology*, **61**: 705-707.

Withers, H.R. (1992) Chapter 2: Biologic basis of radiation therapy. In: *Principles and Practice of Radiation Oncology*, 2nd edition, eds. Perez, C.A. and Brady, L.W., J.B. Lipponcott Co., Philadelphia: 64-96.

Withers, H.R., Peters, L.J. and Kogelnik, H.D. (1980) The pathobiology of late effects of irradiation. In: *Radiation biology in cancer research*, Eds. R.E. Meyn and H.R. Withers, Raven Press, New York: 439-447.

Withers, H.R., Mason, K.A. and Thames, H.D. (1986) Late radiation response of kidney assayed by tubule-cell survival. *British Journal of Radiology*, **59**: 587-595.

Wong, C.S., Minkin, S. and Hill, R.P. (1992) Linear-quadratic model underestimates sparing effect of small doses per fraction in rat spinal cord. *Radiotherapy and Oncology*, **23**: 176-184.

Yaes, R.J. and Kalend, A. (1988) Local stem cell depletion model for radiation myelitis. *International Journal of Radiation Oncology Biology Physics*, **14**: 1247-1259.

Yaes, R.J., Feola, J., Wierzbicki, J., Urano, M. and Maruyama, Y. (1989) Biological equivalence between fractionated radiotherapy treatments using the linear-quadratic model. *British Journal of Radiology*, **62**: 873-874.

Yaes, R.J., Patel, P. and Maruyama, Y. (1991) On using the linear-quadratic model in daily clinical practice. *International Journal of Radiation Oncology Biology Physics*, **20**: 1353-1362.

Young, H.F., Merchant, R.E. and Apuzzo, M.J. (1991) Chapter 12: Immunocompetence of patients with malignant glioma. In: *Neurobiology of brain tumours Volume 4: Concepts in Neurosurgery*, ed. M. Salcman, Williams and Wilkins, Baltimore: 211-227.